

AD-A015 541

THEORY AND APPLICATION OF X-RAY AND GAMMA-RAY BACKSCATTER  
TO LANDMINE DETECTION

Frederick L. Roder, et al

Army Mobility Equipment Research and Development  
Center  
Fort Belvoir, Virginia

March 1975

DISTRIBUTED BY:

**NTIS**

National Technical Information Service  
U. S. DEPARTMENT OF COMMERCE

AD A015541

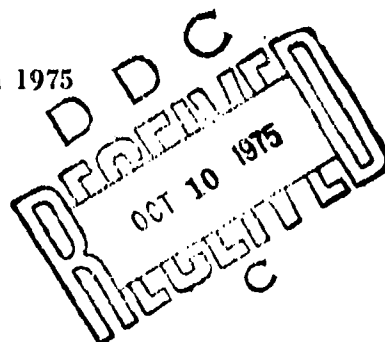
289109

AD

Report 2134

THEORY AND APPLICATION OF X-RAY AND GAMMA-RAY  
BACKSCATTER TO LANDMINE DETECTION

March 1975



Approved for public release; distribution unlimited.



U. S. ARMY MOBILITY EQUIPMENT RESEARCH AND DEVELOPMENT CENTER  
FORT BELVOIR, VIRGINIA

Reproduced by  
NATIONAL TECHNICAL  
INFORMATION SERVICE  
US Department of Commerce  
Springfield, VA 22151

ACCESSION BY	
NTIS	PRIMA SECTION <input checked="" type="checkbox"/>
D/C	UNIT SECTION <input type="checkbox"/>
UNCLASSIFIED	<input type="checkbox"/>
JULIATION	
BY	
RESTRICTION/AVAILABILITY CODES	
DISC	ALL INFORMATION CONTAINED HEREIN IS UNCLASSIFIED

**A**

Destroy this report when no longer needed.  
Do not return it to the originator.

The citation in this report of trade names of commercially available products does not constitute official endorsement or approval of the use of such products.

1a

UNCLASSIFIED

SECURITY CLASSIFICATION OF THIS PAGE (When Data Entered)

REPORT DOCUMENTATION PAGE		READ INSTRUCTIONS BEFORE COMPLETING FORM
1. REPORT NUMBER 2134	2. GOVT ACCESSION NO.	3. RECIPIENT'S CATALOG NUMBER
4. TITLE (and Subtitle) THEORY AND APPLICATION OF X-RAY AND GAMMA- RAY BACKSCATTER TO LANDMINE DETECTION		5. TYPE OF REPORT & PERIOD COVERED Research; 1968 through 1973
7. AUTHOR(s) Fredrick L. Reder Cpt Richard A. Van Konynenburg *		6. PERFORMING ORG. REPORT NUMBER
9. PERFORMING ORGANIZATION NAME AND ADDRESS Mine Detection Division, Laboratory 1000 U.S. Army Mobility Equipment Research and Development Center, Fort Belvoir, Virginia 22060		8. CONTRACT OR GRANT NUMBER(s)
11. CONTROLLING OFFICE NAME AND ADDRESS Mine Detection Division, Laboratory 1000 U.S. Army Mobility Equipment Research and Development Center, Fort Belvoir, Virginia 22060		10. PROGRAM ELEMENT, PROJECT, TASK AREA & WORK UNIT NUMBERS  Project: 1W663619D606-02
14. MONITORING AGENCY NAME & ADDRESS (if different from Controlling Office)		12. REPORT DATE March 1975
		13. NUMBER OF PAGES 125
		15. SECURITY CLASS. (of this report)  Unclassified
		15a. DECLASSIFICATION/DOWNGRADING SCHEDULE
16. DISTRIBUTION STATEMENT (of this Report)  Approved for public release; distribution unlimited.		
17. DISTRIBUTION STATEMENT (of the abstract entered in Block 20, if different from Report)		
18. SUPPLEMENTARY NOTES		
19. KEY WORDS (Continue on reverse side if necessary and identify by block number) Backscatter energy spectra      Nuclear radiation detector applications Compton scattering              X-ray backscatter Gamma-ray backscatter Nonmetallic mine detection		
20. ABSTRACT (Continue on reverse side if necessary and identify by block number)  This report discusses the theory and application of X-ray and gamma-ray backscatter to the problem of nonmetallic landmine detection. The fundamental interactions of X and gamma radiation with matter, including photoelectric absorption, Compton scattering, and pair production, are reviewed. The backscatter spectrum is analyzed in terms of the components due to single and multiple scattering. The variation of the backscatter spectrum with changes in the average atomic number of the scattering material and with changes in source energy is explained. (Continued)		

DD FORM 1473  
1 JAN 73

EDITION OF 1 NOV 65 IS OBSOLETE

UNCLASSIFIED

SECURITY CLASSIFICATION OF THIS PAGE (When Data Entered)

UNCLASSIFIED

SECURITY CLASSIFICATION OF THIS PAGE(When Data Entered)

(Block 20 Cont'd)

Four different source/detector geometries are compared in terms of count rate for a given source strength, target-present-to-target-absent ratio, sensitivity to height variations above the scatterer, and sensitivity to scatterer density. Theoretical and practical factors in the selection of sources and detectors are considered. Three techniques for compensating for height variations are discussed, the most promising of which is a K-edge-filter method. Backscatter mine detection is shown to be based on the fact that explosives have a lower average atomic number than the surrounding soil medium and, therefore, a lower photoelectric absorption cross section. As a consequence, more photons are backscattered from explosives than from soil in the energy region below about 200 keV. An account is given of the history of research in backscatter mine detection spanning 5 years of effort, including basic soil-box studies, parameter optimization, computer simulation, development of equipment, and field testing. It is concluded that the limitations of the backscatter approach outweigh its capabilities when viewed from a practical military standpoint. Nevertheless, the work described did provide considerable insight into the mechanism of the photon-backscatter process which may be of interest to other researchers in the field.

\*Present address:

Radiation Chemistry Division, L-233  
Lawrence Livermore Laboratory  
P.O. Box 808  
Livermore, CA 94550

UNCLASSIFIED

SECURITY CLASSIFICATION OF THIS PAGE(When Data Entered)

## SUMMARY

At the present time, detection of nonmetallic landmines, of both the antipersonnel and antivehicular varieties, is an important technological problem facing the U.S. Army. Because of the great differences found among nonmetallic mines produced throughout the world (including a host of field-expedient devices recently employed in Southeast Asia), and because of the wide variation in soil types and conditions found in even a limited theater of operations, identification of a unique mine signature has proven to be a most difficult task. Perhaps the only attribute which all nonmetallic mines may be said to possess in common is an explosive charge. A detection technique that senses this charge is, therefore, to be considered quite desirable.

Since the interaction of ionizing radiation within a solid medium depends on the elemental and isotopic composition of that medium, the potential of nuclear research in the area of mine detection was recognized soon after the dawn of the nuclear era.

At present, the known types of ionizing radiation which are available from either isotopic sources or machines of reasonable size are  $\alpha$ ,  $\beta^-$ ,  $\beta^+$ ,  $\gamma$ , X, and neutron. Of these, only  $\gamma$ , X, and neutron radiation are uncharged and may, therefore, penetrate appreciable distances into a solid medium (on the order of inches at available energies).

Although mine-detection techniques involving both neutrons and gamma and X photons have been investigated extensively over the past several years, the scope of this report is limited to gamma- and X-ray backscatter methods.<sup>1</sup>

Because of the rather circuitous and evolutionary development of the photon-backscatter mine-detection program, we have chosen to present the results, not in the usual chronological order, but in a form which can be understood most easily. As a result, we sometimes have found it necessary to present conclusions prior to recounting the detailed work which led to them. It also should be noted that, as of the time of writing, effort on the backscatter mine-detection approach has been terminated, in the belief that the limitations of this approach outweigh its capabilities when viewed from a practical military standpoint. As a result, some questions have remained unresolved. Nevertheless, we believe that this report not only presents a thorough account of the mine-detection research effort, but also offers new insights into the photon-backscatter process itself. (Shortly before publication of this report, we learned that an Israeli report has been written independently on the same topic.<sup>2</sup>)

<sup>1</sup> An account of nonmetallic landmine detection research involving the utilization of neutrons may be found in W. A. Coleman, R. O. Guayven, and G. M. Reynolds, *Nuclear Methods of Mine Detection* Vol. III, Final Report, Contract DAAK02-73-C-0139 (May 1974), AD 919475L.

<sup>2</sup> K. Preiss and R. Livant, "Detection of Plastic Mines by Gamma Ray Backscattering" *Trans. Israel Nuclear Soc.* 1, 30 (1973).

Section I (Interaction of X and Gamma Radiation with Matter) is essentially a review of basic processes which have been understood for some time by workers in the field. As such, it should be of interest to readers who are unfamiliar with the nature of these interactions and who are interested in the fundamentals upon which backscatter mine detection is based.

Section II (The Backscatter Spectrum) presents in some detail the dependence of the backscatter spectrum on various parameters and, therefore, should be of particular interest to individuals involved in nuclear-gauge design. The conclusions presented in this section rest in part on the work discussed in section III and on the basic theory in section I.

Section III (History) is a chronological account of developmental efforts from 1968 through 1973. Section IV (Delivered Hardware) briefly describes the end items delivered to USAMERDC under this program by its contractors and, in an unclassified context, discusses the capabilities and limitations of each.

## PREFACE

The information contained in this report has been derived from many sources, including experiments and computations performed in-house, by contractors, and by other government organizations; personal communications; and published literature. Every effort has been made to reference those cases where the efforts of others have been relied upon.

Dr. Karl H. Steinbach and MM. Charles N. Johnson, Jr. and Robert Brooke, of USAMERDC, provided direction and support.

MM. Charles Jones and Douglas G. Conley, of USAMERDC, provided technical assistance for the in-house experiments and aided in the testing of prototypes.

MM. Samuel Helf and James McCahill, of the Feitman Research Laboratories, Picatinny Arsenal, collaborated in the early experiments and aided in developing an understanding of the basic processes.

Dr. Wayne Coleman, of the Ballistic Research Laboratories, performed the calculations reported in Appendix A.

Drs. John Ashe, Emmett Hudspeth, and William E. Tucker, and Mr. Wendell Miller, of Texas Nuclear Division, Nuclear-Chicago Corporation, initially proposed the gamma-ray-backscatter approach; Mr. Miller performed much of the experimental work described herein.

Drs. Harold Kurstedt, Jr., Robert Pfeifer, Boong Che, and Mason Thompson, and Mr. Ward Perley, of the Industrial Nucleonics Corporation, performed a portion of experimental effort on the man-portable detector.



## CONTENTS

Section	Title	Page
	SUMMARY	iii
	PREFACE	v
	ILLUSTRATIONS	vii
I	INTERACTION OF X AND GAMMA RADIATION WITH MATTER	
	1. General	1
	2. Pair Production	1
	3. Photoelectric Absorption	3
	4. Compton Scattering	6
	5. Attenuation Coefficients and Mean Free Path	8
II	THE BACKSCATTER SPECTRUM	
	6. General	8
	7. Components of the Backscatter Energy Spectrum	8
	8. Principle of Backscatter Mine Detection	14
	9. Selection of Source/Detector Geometry	16
	10. Source and Detector Selection	22
	11. Compensation for Height Variations	28
III	HISTORY	
	12. Background	38
	13. Contract DAAK02-68-C-0229	39
	14. Contract DAAK02-69-C-0263	43
	15. Contract DAAK02-70-C-0105	57
	16. Contract DAAK02-71-C-0359	59
	17. Contract DAAK02-72-C-0619	69
IV	DELIVERED HARDWARE	
	18. Experimental Vehicle-Mounted X-Ray Backscatter Detector of Antivehicular Mines	79
	19. Experimental Man-Portable Detector of Antipersonnel Mines (Coaxial Geometry)	97
	20. Breadboard Searchhead: Man-Portable Detector of Antipersonnel Mines (Geometry (b))	105
	21. Breadboard Searchhead: Man-Portable Detector of Antipersonnel Mines (Geometry (c))	111
V	SUMMARY AND CONCLUSIONS	
	22. Summary and Conclusions	118
	APPENDIXES	
	A. Monte Carlo Calculations	119
	B. Statistical Analysis of Backscatter Mine Detection	136

## ILLUSTRATIONS

Figure	Title	Page
1	Regions of Dominance for Photon-Interaction Mechanisms	2
2	Photoelectric Cross Section as a Function of Energy for $Z = 4$ to 20	4
3	Photoelectric Cross Section as a Function of Atomic Number for Energies from $1 \times 10^{-2}$ to $5 \times 10^{-1}$ Mev	5
4	Dependence of Compton-Scattered Photon Energy on Initial Energy and Scattering Angle	7
5	Klein-Nishina Differential Cross Section for the Number of Photons Scattered per Unit Solid Angle in the Direction $\theta$	7
6	Mass Attenuation Coefficients for Soils and Explosives	9
7	Detection Geometries	10
8	Pulse-Height Spectrum of $^{60}\text{Co}$ Photons Backscattered from Aluminum	12
9	Pulse-Height Spectrum of $^{137}\text{Cs}$ Photons Backscattered from Aluminum	13
10	Comparison of Pulse-Height Spectra of $^{60}\text{Co}$ Photons Backscattered from Graphite and Aluminum	15
11	Uncollimated-Source -- Collimated-Detector Backscatter Spectra	19
12	Change in Backscatter with Height Above Scatterer	20
13	High-Energy Gamma-Ray Backscatter Experimental Setup	21
14	Comparison of Pulse-Height Spectra of $^{137}\text{Cs}$ Photons Backscattered from Soil With and Without the Presence of a Dinitrobenzene (DNB) Block	25
15	Comparison of Pulse-Height Spectra of $^{241}\text{Am}$ Photons Backscattered from Soil With and Without the Presence of a Dinitrobenzene (DNB) Block	26
16	Two Detectors at Different Heights Viewing the Same Area	29
17	Variation of Backscatter Flux with Height (Data from Contract DAAK02-72-C-0619)	30
18	Geometries for Two-Signal Height-Compensation Technique	31

Figure	Title	Page
19	Pulse-Height Spectrum of $^{137}\text{Cs}$ Photons Backscattered from Lucite and Concrete for Two Values of $h$	33
20	Geometry for K-Edge Filter Height-Compensation Technique	35
21	Computed Shift of Single-Scatter Peak with Variation in Height	36
22	Variation of Count of Filtered and Unfiltered Detectors as a Function of Height (Data from Contract DAAK02-72-C-0619)	37
23	Initial Experimental Setup	40
24	Model for Single Scatter Computation	44
25	Results of Single-Scatter Computation	45
26	Experimental Values of $R$ for the Geometry Shown in Figure 24	46
27	Experimental Values of $R$ Obtained with X-Ray Source	47
28	Geometry for "Iron Curtain" Experiments	49
29	Results of "Iron Curtain" Experiments	50
30	Geometry Used for Parametric Studies	51
31	$R$ Versus Emplacement Depth in Red Clay for Different X-Ray Tube Potentials	53
32	$R$ Versus Emplacement Depth in Sand for Different X-Ray Tube Potentials	54
33	Initial Geometry for Man-Portable Detector Experiments	56
34	First Man-Portable Searchhead	58
35	M-14 Mine Sketch	60
36	Geometry for Man-Portable Detector Parametric Experiments	61
37	Gamma-Backscatter Height-Compensation Data	64
38	Combined Height and Mine Sensor	66
39	Beta-Sensor Output as a Function of Height	67
40	Height-Compensated Searchhead Performance in the Laboratory	68
41	Industrial Nucleonics Experimental Setup	70
42	$R$ as a Function of Height for Different Half-Angles	71

Figure	Title	Page
43	Sensor Performance with Single-Aperture Collimator as a Function of Position Over Mine	72
44	Sensor Performance with Multiaperture Collimator as a Function of Position Over Mine	74
45	Dependence of Countrate on Height and Soil Type for $^{241}\text{Am}$ Gamma Source	75
46	Dependence of Countrate on Height and Soil Type for $^{90}\text{Sr}$ Beta Source	76
47	Dependence of Countrate on Height and Soil Type for $^{85}\text{Kr}$ Beta Source	77
48	Dependence of Countrate on Height and Soil Type for $^{241}\text{Am}$ Source and Uncollimated Gamma Detector	78
49	Dependence of Countrate on Height Using Sm Filter	80
50	Dependence of Countrate on Height Using Eu Filter	81
51	Dependence of Countrate on Height Using Gd Filter	82
52	Dependence of Countrate of Height Using Eu Filter (Humic)	83
53	Dependence of Countrate on Height Using Eu Filter (Roadbed)	84
54	Dependence of Countrate on Height Using Eu Filter (Grass-Covered Humic)	85
55	Vehicle-Mounted Detector	87
56	Closeup of Searchhead	88
57	Service Control Section	89
58	Jefferson Proving Ground Results	91
59	Fort Hood Results	92
60	Mississippi Test Facility Results	93
61	Eglin Air Force Base Results	94
62	Fort Belvoir Results	95
63	Experimental Man-Portable Detector	98
64	Experimental Man-Portable Detector in Use at Fort Belvoir	99
65	Simulated Foreign Mines	101
66	Sample Test Run	103

Figure	Title	Page
67	Effects of Varying the Ratemeter Time Constant	104
68	Effects of Varying Detector Height	106
69	Effects of Centerline Offset	107
70	Sketch of Beta-Gamma Breadboard Searchhead	109
71	Test Results for Beta-Gamma Breadboard Searchhead	110
72	Test Results Over Gravel When the Searchhead is Calibrated for Grass	112
73	Performance of Filter Height-Compensated Searchhead (Sand)	114
74	Performance of Filter Height-Compensated Searchhead (Roadbed)	115
75	Performance of Filter Height-Compensated Searchhead (Humic)	116
76	Performance of Filter Height-Compensated Searchhead (Grass-Covered Humic)	117
A-1	Model for Monte Carlo Calculations	120
A-2	Results for $E_0 = 130$ keV and $d = 2$ Inches	122
A-3	Results for $E_0 = 200$ keV and $d = 4$ Inches	123
A-4	Percent Increase in $\phi$ for $E_0 = 70$ keV and $d = 2$ Inches	125
A-5	Percent Increase in $\phi$ for $E_0 = 130$ keV and $d = 2$ Inches	126
A-6	Percent Increase in $\phi$ for $E_0 = 200$ keV and $d = 4$ Inches	127
A-7	No Detector Collimation, $R = 0$ to 2 Centimeters	128
A-8	No Detector Collimation, $R = 2$ to 4 Centimeters	129
A-9	No Detector Collimation, $R = 4$ to 6 Centimeters	130
A-10	No Detector Collimation, $R = 6$ to 8 Centimeters	131
A-11	No Detector Collimation, $R = 8$ to 12 Centimeters	132
A-12	No Detector Collimation, $R = 12$ to 17 Centimeters	133
A-13	No Detector Collimation, $R = 17$ to 22 Centimeters	134
A-14	No Detector Collimation $R = 22$ to 28 Centimeters	135
B-1	Probability Distributions of Count with Mine Present and Mine Absent for the Case: $N = 100$ , $R = 1.5$	137
B-2	Required Mean Count as a Function of the Mine-Present – Mine-Absent Count Ratio for Various Degrees of Certainty	139

# THEORY AND APPLICATION OF X-RAY AND GAMMA-RAY BACKSCATTER TO LANDMINE DETECTION

## I. INTERACTION OF X AND GAMMA RADIATION WITH MATTER

1. **General.** Both gamma and X radiation consist of photons (quanta of electromagnetic energy) which may be characterized by a wavelength  $\lambda$  or an energy  $E$ . The factors  $\lambda$  and  $E$  are related by  $\lambda \approx 12.4/E$ , where  $\lambda$  is in angstroms ( $1 \text{ \AA} = 10^{-8} \text{ cm}$ ) and  $E$  is in kiloelectron volts (keV). For purposes of the present discussion, gamma- and X-ray photons of a given energy may be said to react identically with matter; they differ only in their method of production.<sup>3</sup> Gamma photons are emitted by nuclei undergoing a transition from a higher to a lower energy state; X-ray photons are emitted either by electrons undergoing a transition from one atomic energy level to another or by high-energy electrons being slowed down by coulombic interactions (predominantly with nuclei) in a material medium. This second type of X-ray photon is the most prevalent one produced by X-ray generators and often is referred to as bremsstrahlung, or "braking radiation." For convenience, then, the term "photon" will be used to denote a quantum of either X or gamma radiation unless one or the other is specifically intended.

When a photon impinges on a region containing matter, there are three main interactions which may occur: photoelectric absorption, pair production, and Compton scattering. The relative probabilities of occurrence of these processes depend on the energy of the photon and the atomic number ( $Z$ ) of the medium. Figure 1 shows the conditions under which each of these effects is dominant.<sup>4</sup> The two lines separating the regions of dominance denote the conditions of equal probability. (Photonuclear reactions and Rayleigh scattering will not be considered in this report, since the threshold for the former, for all stable isotopes except the very lightest ones, is  $\sim 8 \text{ MeV}$ , and since the latter is of importance only for photons of energies too low to be of interest.)

2. **Pair Production.** Pair production is the creation of an electron/positron pair by the conversion of photon energy to matter, usually in the neighborhood of the nucleus. Because the electron and positron rest masses are each equal to  $0.511 \text{ MeV}/c^2$ , the minimum photon energy required for this process is  $1.022 \text{ MeV}$ . Incident photon energy in excess of  $1.022 \text{ MeV}$  appears as kinetic energy of the electron and positron, and, to a negligible extent, of the nucleus. The atomic cross section for pair production ( $\sigma_{\text{pp}}$ ) increases with atomic number squared ( $Z^2$ ) and with incident photon energy in a rather

<sup>3</sup> Strictly speaking, this is true in the present case only because we may neglect polarization (i.e., we shall not be concerned with gamma radiation from nuclei aligned in an external field or with thin-target bremsstrahlung).

<sup>4</sup> R. D. Evans, *The Atomic Nucleus*, New York, McGraw-Hill (1955), p. 712.

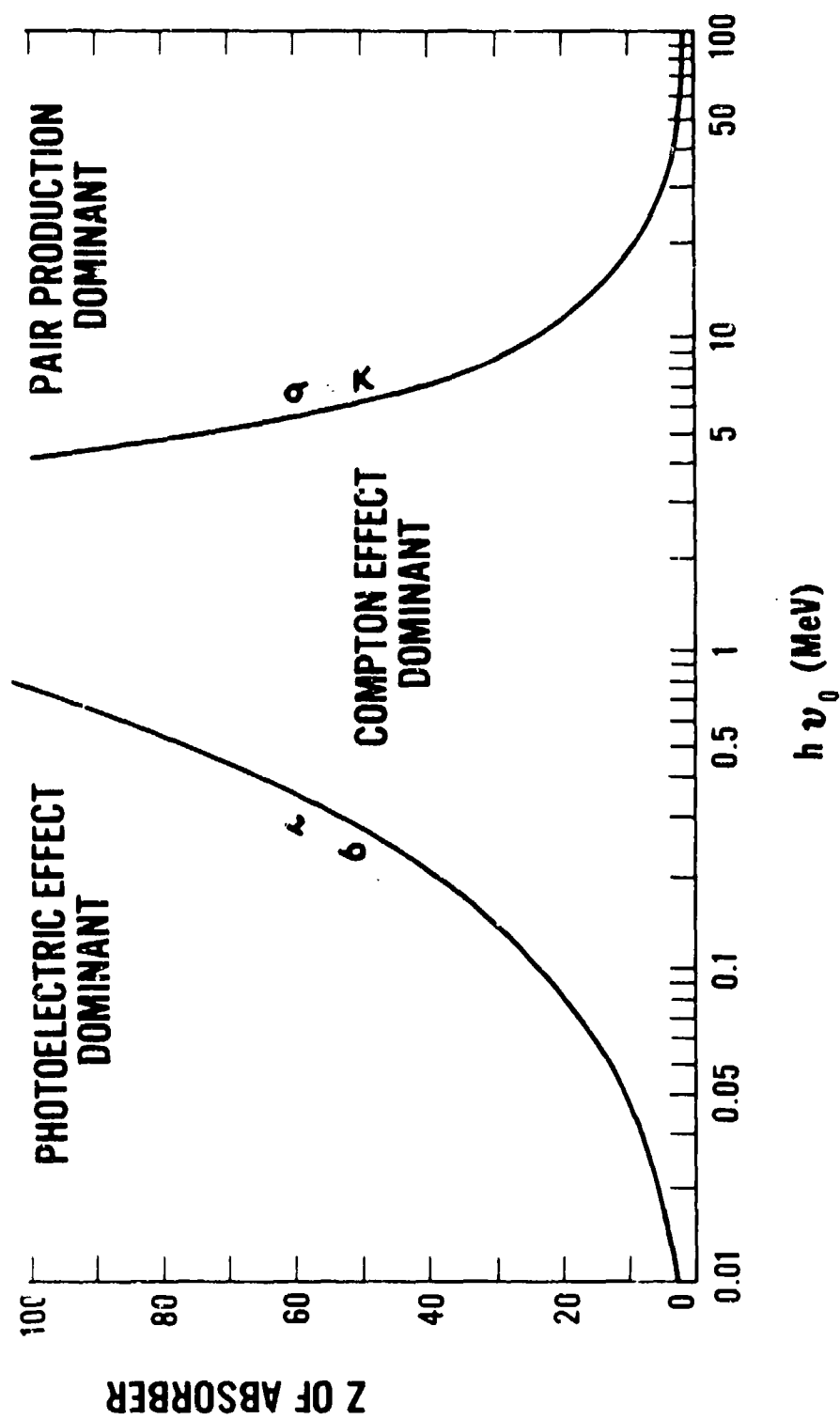


Figure 1. Regions of dominance for photon-interaction mechanisms. (After Evans)

more complex manner. It should be noted, however, that pair production does not become a major mode of interaction for low-Z materials (including soils and explosives) for photon energies below  $\sim 10$  MeV. Since available radioisotopes do not emit gamma rays of energies greater than  $\sim 2$  MeV, and since bremsstrahlung sources in the MeV range are too bulky and heavy to consider for field use, mine-detection techniques based on pair production are not considered promising, and pair production will not be considered further.

**3. Photoelectric Absorption.** Unlike pair production, photoelectric absorption occurs primarily at low photon energies. In a photoelectric event the incident photon is absorbed, in this case giving up all its energy to a bound atomic electron, which in turn is ejected from the atom. In solid materials, these ejected electrons are readily absorbed, thus precluding direct observation of the number of photoabsorptions occurring. No first-principles derivation exists for the atomic photoelectric cross section ( $\tau_a$ ). In the energy region below 200 keV, the best estimates rely on high-precision, total-attenuation-coefficient measurements and on subtraction of theoretical estimates of the attenuation due to scattering.<sup>5 6</sup> The dependence of  $\tau_a$  on Z and E in the ranges of interest is shown in Figures 2 and 3.<sup>7</sup> Note the approximate dependence  $\tau_a \propto Z^5/E^3$  in this range. If the energy of an incident photon is below the binding energy of a given electron, then photoabsorption by that electron is absolutely forbidden. Together with the energy dependence described above, this means that, as the energy of the incident photon decreases,  $\tau_a$  increases, reaching a maximum at the electron binding energy. Any further decrease in photon energy results in a sudden drop in the photoelectric cross section. Thus a plot of  $\tau_a$  versus photon energy contains a series of discontinuities, or "edges." These edges can be utilized to form the equivalent of low-pass filters: a photon beam passing through such a filter is greatly attenuated if it is of energy just above an edge, and far less attenuated if it is of energy just below an edge. This technique was utilized to effect one of the height-compensation methods discussed later (paragraph 11).

For materials with  $2 \leq Z \leq 20$ , atomic weight  $A \cong 2Z$ ; for  $Z > 20$ ,  $2Z \leq A \leq 2.6Z$ . Thus, roughly, the number of electrons per unit mass is independent of atomic number. However, since for photon energies above the K-edge  $\sim 80$  percent of all photoabsorptions involve one of the K electrons (two of which are present in all atoms with  $Z > 1$ ), the portion of the electron density which is of importance for photoabsorption is inversely proportional to Z. As a result, the macroscopic photoelectric cross section ( $\tau$ ) which is defined on a per-unit-mass basis, has the approximate functional dependence

<sup>5</sup> R. D. Evans, *The Atomic Nucleus*, New York, McGraw-Hill (1955).

<sup>6</sup> J. H. Hubbell and M. J. Berger, "Photon Atomic Cross Sections," in *Engineering Compendium on Radiation Shielding*, Vol. I, R. G. Jaeger et al., Ed., New York, Springer-Verlag (1968), p. 185.

<sup>7</sup> E. F. Plechaty and J. R. Terrall, *Photon Cross Sections -- 1 keV to 100 MeV*, Lawrence Livermore Laboratory Report UCRL-50406, Vol. VI (1966).



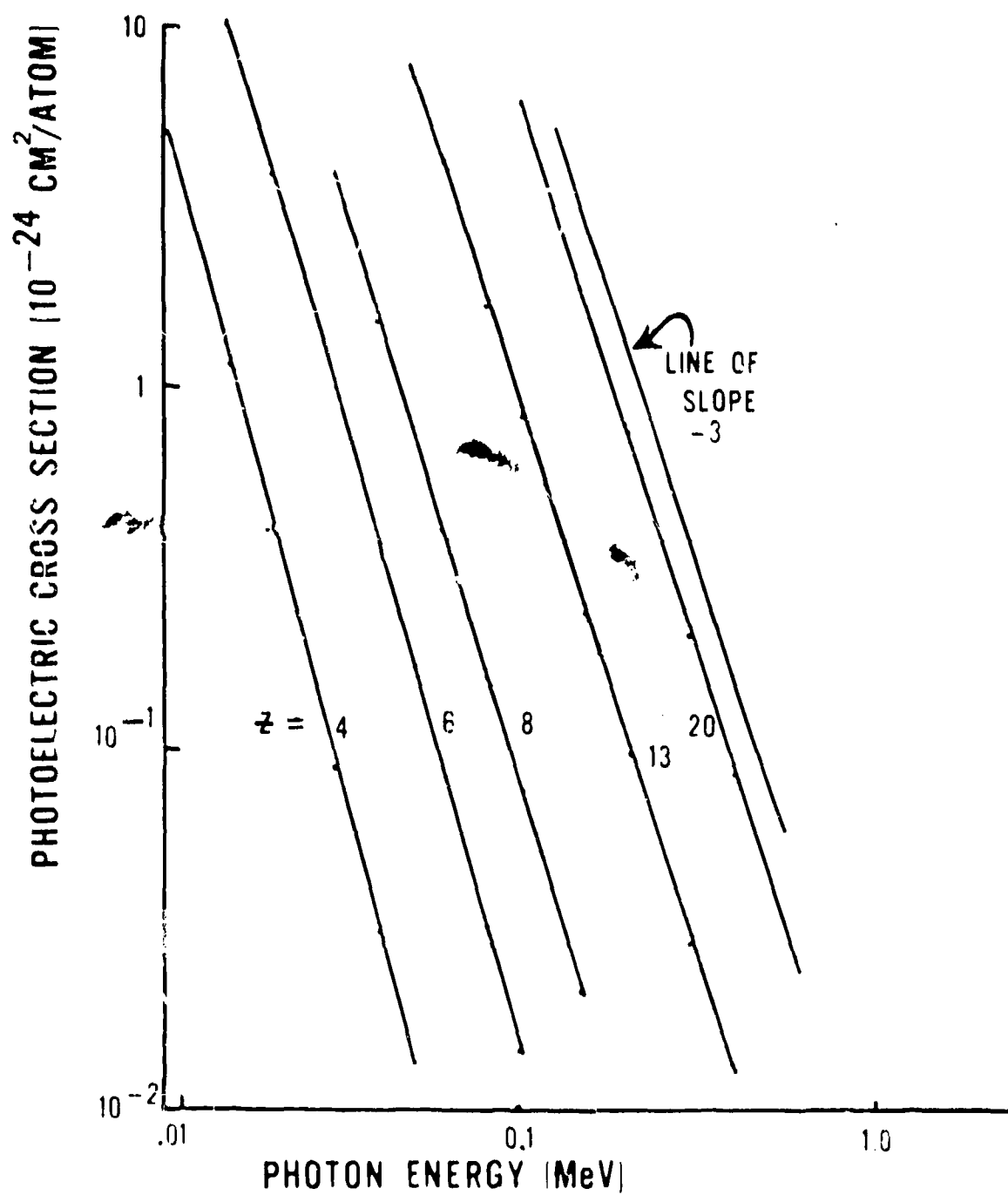


Figure 2. Photoelectric cross section as a function of energy for  $Z = 4$  to 20.  
(After Plechaty and Terrall)

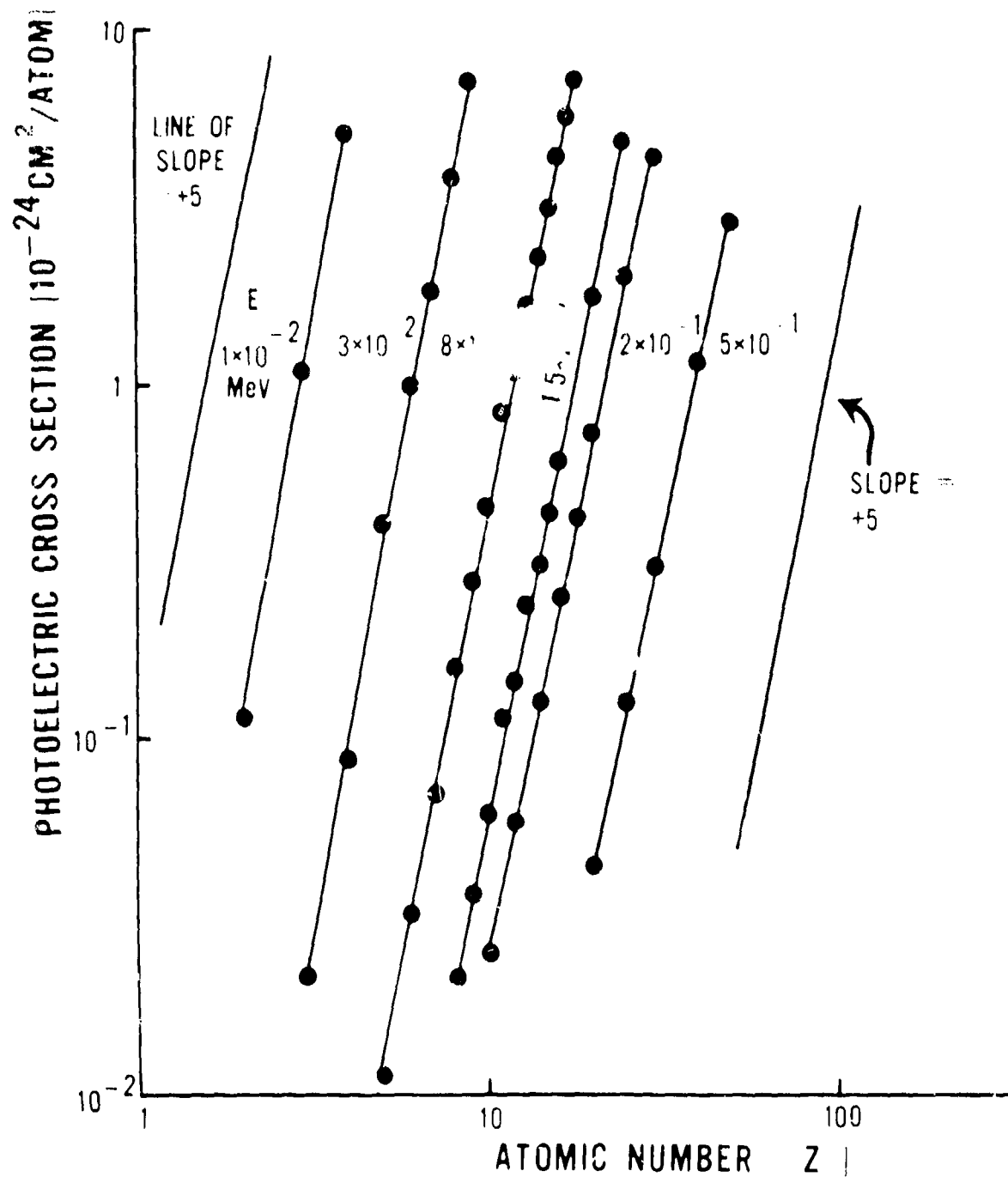


Figure 3. Photoelectric cross section as a function of atomic number for energies from  $1 \times 10^{-2}$  to  $5 \times 10^{-1}$  MeV. (After Plechaty and Terrall)

$\tau \propto Z^4/E^3$  for  $E \gg I_K$ , where  $\tau \equiv \tau_a N/A$ ,  $I_K$  is the binding energy of the K electrons, and  $N$  is Avogadro's number.

**4. Compton Scattering.** Unlike pair production and photoabsorption, Compton scattering does not result in the demise of the incident photon. The relative probability of occurrence of the Compton process is a maximum at intermediate energies, and its effect is to alter the trajectory of the photon, leaving it at a lower energy. In this process, the photon interacts with a single electron, the electron being considered unbound. (This is a valid assumption provided that  $E \gg I$  for the interacting electron.) Part of the initial photon energy is transferred to the electron, leaving the photon with energy  $E_1$  which depends on the scattering angle  $\theta$  as follows:

$$E_1 = E/[1 + \alpha(1 - \cos \theta)],$$

where  $\alpha = E/m_0 c^2$  is the incident photon energy expressed in multiples of the electron rest-mass energy. Figure 4 is a plot of this equation for various values of  $E$  and  $\theta$ .<sup>8</sup> The relative probability of scattering through a given angle is given by the Klein-Nishina differential scattering cross section (see Figure 5):<sup>9</sup>

$$\frac{d_e \sigma_c}{d\Omega} = r_0^2 \frac{(1 + \cos^2 \theta)}{2} \frac{1}{[1 + \alpha(1 + \cos \theta)]} \left\{ 1 + \frac{\alpha^2 (1 - \cos \theta)^2}{(1 + \cos^2 \theta)[1 - \alpha(1 - \cos \theta)]} \right\}.$$

The total probability of interaction is given by the integral of this equation over all scattering angles:

$$\sigma_c = 2\pi r_0^2 \left\{ \frac{(1 + \alpha)}{\alpha^3} \left[ \frac{2\alpha(1 + \alpha)}{(1 + 2\alpha)} - \ln(1 + 2\alpha) \right] + \frac{1}{2\alpha} \ln(1 + 2\alpha) - \frac{1 + 3\alpha}{(1 + 2\alpha)^2} \right\},$$

where  $r_0$  is the classical radius of the electron ( $\equiv e^2/m_0 c^2$ ). Since the Compton effect is an interaction with a single electron, the atomic cross section ( $\sigma_a$ ) is obtained by multiplying the electronic cross section by the atomic number  $Z$  and is, therefore, proportional to the first power of atomic number. However, since electron density is approximately independent of  $Z$ , the macroscopic Compton cross section [ $\sigma_c \equiv \sigma_a N/A$  ( $\text{cm}^2/\text{g}$ )] is approximately a function of energy alone. The Klein-Nishina cross section has the following characteristics which will be of interest: As the incident photon energy increases, (1) the average scattering angle decreases (i.e., the scattered-photon distribution becomes more forward-peaked), and (2) the total scattering cross section decreases.

<sup>8</sup> R. D. Evans, "Compton Effect," in *Handbuch der Physik*, Vol. 34, S. Flügge, Ed., Berlin, Springer-Verlag (1958), pp. 218-298.

<sup>9</sup> *Ibid.*

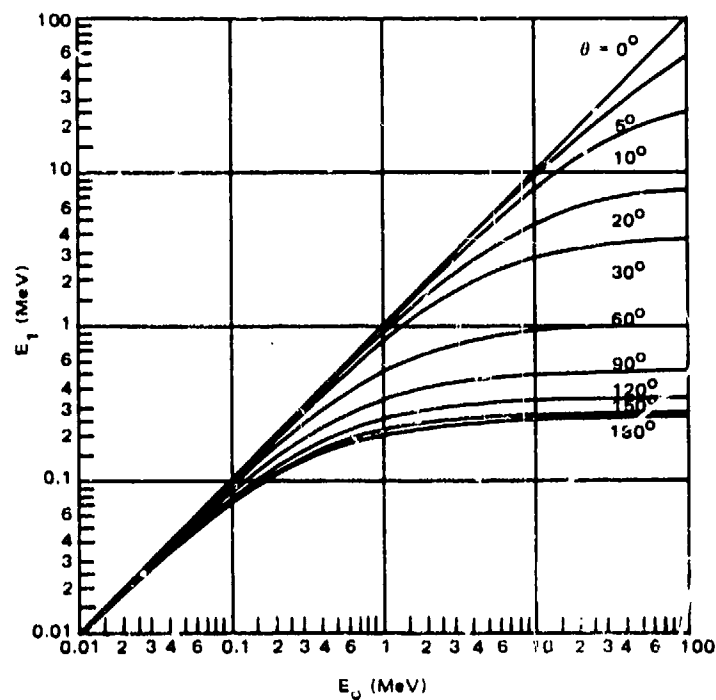


Figure 4. Dependence of Compton-scattered photon energy on initial energy and scattering angle. (After Evans)

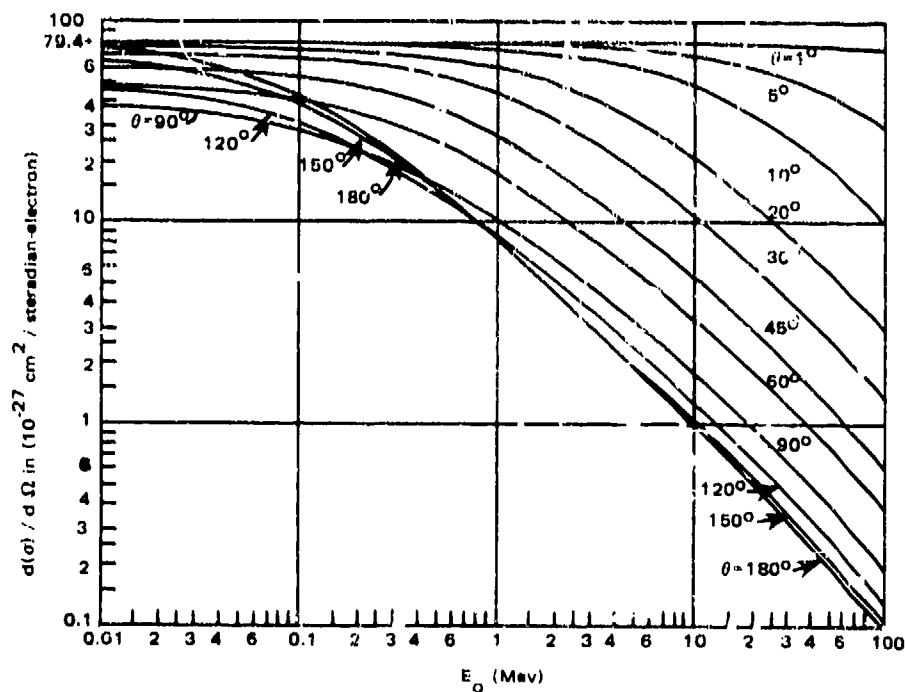


Figure 5. Klein-Nishina differential cross section for the number of photons scattered per unit solid angle in the direction  $\theta$ . (After Evans)

5. **Attenuation Coefficients and Mean Free Path.** The sum of the pair-production, photoelectric, and Compton macroscopic cross sections of a medium ( $\kappa + \tau + \sigma_c$ ) is defined as the mass attenuation coefficient [ $\mu/\rho$  ( $\text{cm}^2/\text{g}$ )]. Typical density ( $\rho$ ) values for soils are in the range of 1 to 2  $\text{g}/\text{cm}^3$ . Figure 6 shows approximate values of  $\kappa$ ,  $\tau$ ,  $\sigma_c$ , and  $\mu/\rho$  for typical soils and explosives. The linear-attenuation coefficient  $\mu$  ( $\text{cm}^{-1}$ ) for  $0.02 \leq E \leq 1.0$  MeV may be approximated by  $(\tau + \sigma_c) \rho$  and has the distinction of being readily measurable. If the medium is in the form of a slab, then

$$\phi = \phi_0 \exp(-\mu x),$$

where  $\phi$  is the narrow-beam photon flux normally incident on the slab,  $\phi_0$  is the undeflected photon beam emerging from the slab, and  $x$  is the thickness of the slab. The term  $1/\mu$  is referred to as the photon mean free path.

## II. THE BACKSCATTER SPECTRUM

6. **General.** Since the nature of the mine-detection problem permits access to only one side of the scattering medium, only backscattered radiation is useful in this context. Just how the spectrum of backscattered radiation changes as a function of both detector design parameters (source type, system geometry, and detector type) and environmental parameters (soil composition and density, variations in soil microrelief, and, of course, the presence or absence of a mine) is, therefore, of principal importance and will be discussed in detail in the present section. We initially will consider how systems of differing geometries respond to variations in (1) the average atomic number of the scattering material ( $\langle Z \rangle$ ), (2) density ( $\rho$ ), and (3) operating height ( $h$ ). (For convenience,  $\langle Z \rangle$  is defined on a weight-percent basis.)

For purposes of this discussion, four system geometries will be considered. As depicted in Figure 7, these geometries are: (a) collimated source and detector with the axes of collimation focused on the center of a spherical scattering medium; (b) vertically collimated source and detector with the axes of collimation separated by some distance  $q$ ; (c) isotropic source and vertically collimated detector; and (d) coaxially mounted, vertically collimated source and detector. The scattering medium for geometries (b), (c), and (d) will be considered first as semi-infinite (i.e., as an infinite half-space) of uniform composition and density.

7. **Components of the Backscatter Energy Spectrum.** In order to gain a basic familiarity with the backscatter spectrum, we initially will restrict our considerations to geometry (a). Figure 8 is a pulse-height spectrum obtained by utilizing a  $^{60}\text{Co}$  source ( $E_\gamma = 1.17$  and 1.33 MeV), a NaI (Tl) detector, and a spherical aluminum scattering

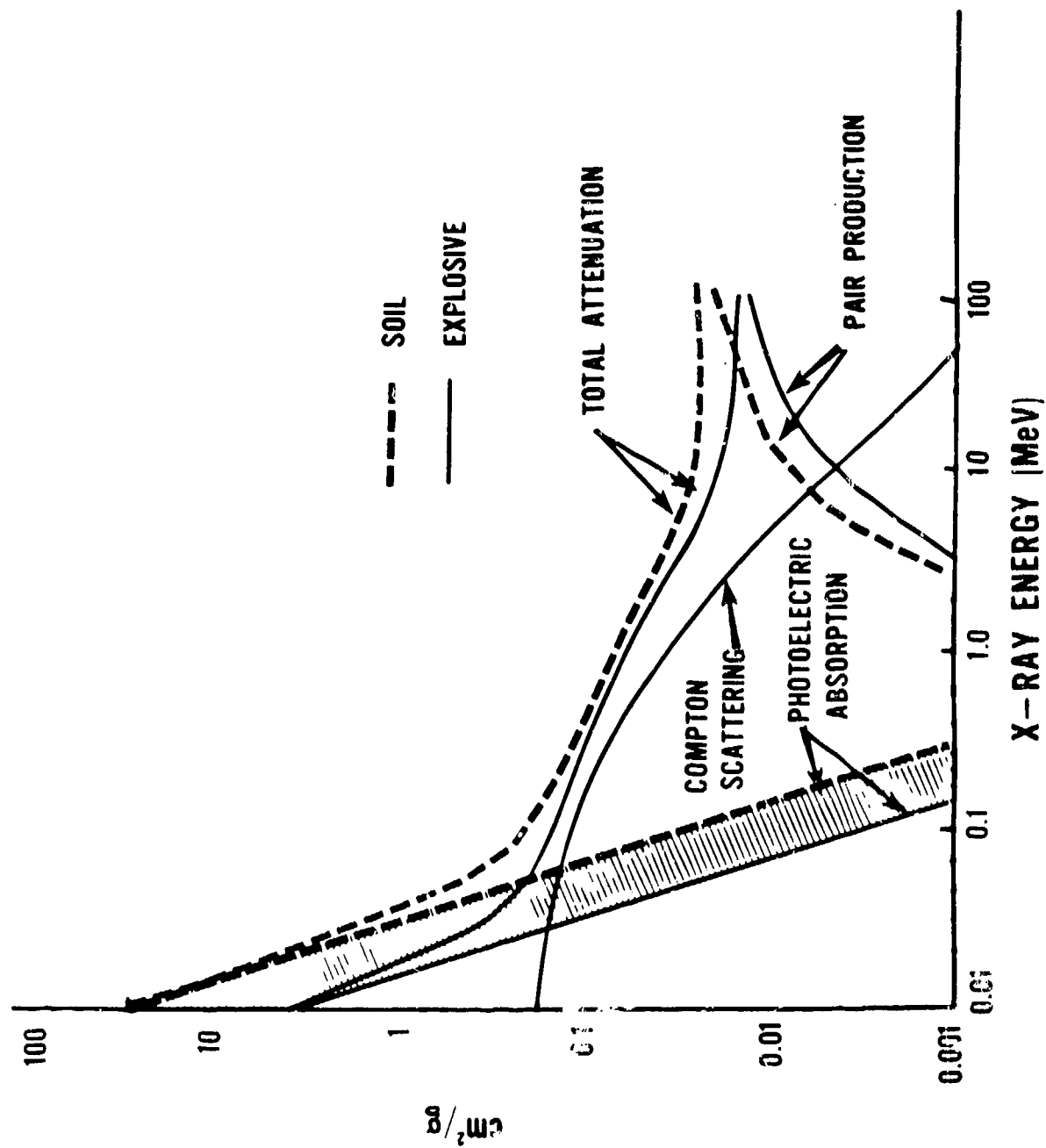


Figure 6. Mass attenuation coefficients for soils and explosives.

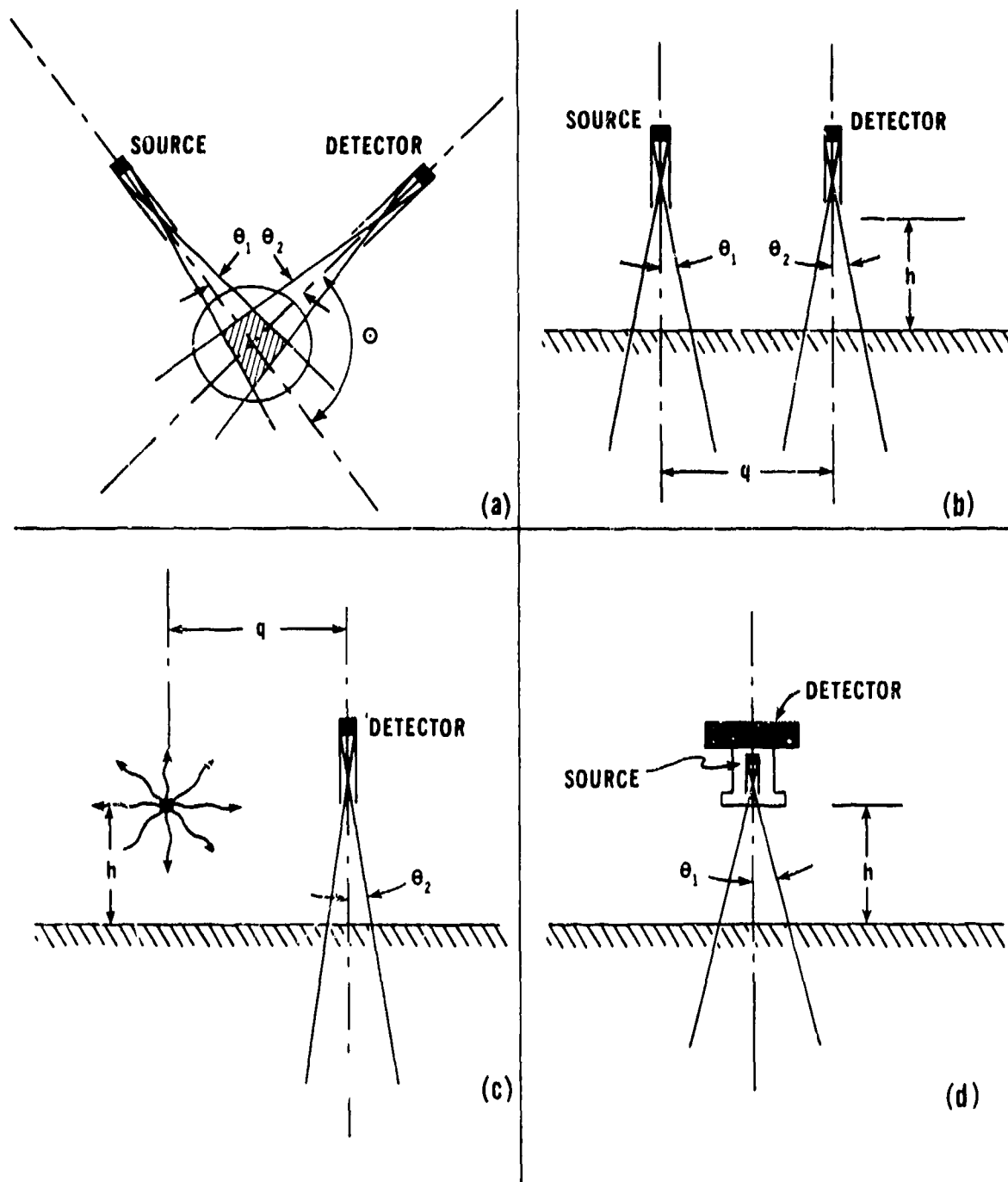


Figure 7. Detection geometries.

medium, and by setting the single-scatter angle  $\Theta = 90^\circ$ .<sup>10</sup> Note that there are two broad maxima, one centered at  $\sim 360$  keV and the other at  $\sim 110$  keV.<sup>11</sup> The higher energy maximum is a single-scatter peak and is predominantly due to gamma photons which penetrate without energy loss to the crossover (shaded) region of the scatterer, scatter once in this region through an angle of approximately  $90^\circ$ , and exit the scatterer without a second interaction. The energy of these photons is, therefore, determined by the Compton scattering equation. The observed breadth of the single-scatter peak can be explained by (1) the finite half angles ( $\theta_1$  and  $\theta_2$ ) of the source and detector collimators and by (2) the finite energy resolution of the NaI (Tl) detector (typically 8 percent FWHM).

The lower energy, broader maximum is due to the presence of multiply scattered photons. (The discussion in MERDC Report 2097 indicates that doubly scattered photons do not contribute significantly to this maximum under the specified experimental conditions.<sup>12</sup>) The presence of this maximum results from the interplay of two phenomena.<sup>13</sup> First, the energy lost per collision by a photon undergoing successive collisions decreases, both relatively and in absolute terms, as the photon's energy is diminished. For example, a 1.33-MeV gamma, scattered through  $180^\circ$ , loses 84 percent of its initial energy; a 50-keV gamma, scattered through the same angle, loses only 16 percent of its initial energy. Thus, a photon will lose the bulk of its energy in the first few collisions in a medium, after which it may scatter several more times, without losing appreciably more energy, before it is either scattered out of the medium or photoabsorbed. Second, there is a rapid increase in the photoelectric cross section as the photon energy decreases ( $\tau \propto E^{-3}$ ). Thus, as the photon energy decreases, the absorption-to-scatter ratio increases rapidly, resulting in the abrupt truncation of the energy spectrum which may be noted in Figure 8.

As a consequence of the above, it is to be expected that the shape and energy of the multiple-scatter "peak" should be virtually independent of the source energy, as, indeed, may be seen to be the case from the spectrum shown in Figure 9.<sup>14</sup> The only difference between Figures 8 and 9 is that for the latter a  $^{137}\text{Cs}$  source has replaced the  $^{60}\text{Co}$  source. Note that although there is a corresponding change in the single-scatter

<sup>10</sup> Texas Nuclear Corporation, Final Report, Subcontract 1023-1 to Dikewood Corporation; Prime Contract AF29(601) - 4569 (1962).

<sup>11</sup> E. Hayward and J. H. Hubble, J. Appl. Phys. 25, 506 (1954).

<sup>12</sup> F. L. Roder and D. G. Conley, *Computed Energy Distribution of Double-Scattered Photons, Obtained for Purposes of Mine Detector Design Analysis*, USAMERDC Report 2097 (1974).

<sup>13</sup> V. E. Wechselberger, Atomkernenergie 16, 64 (1970).

<sup>14</sup> Texas Nuclear Corporation, Final Report, Subcontract 1023-1 to Dikewood Corporation; Prime Contract AF29(601) - 4569 (1962).



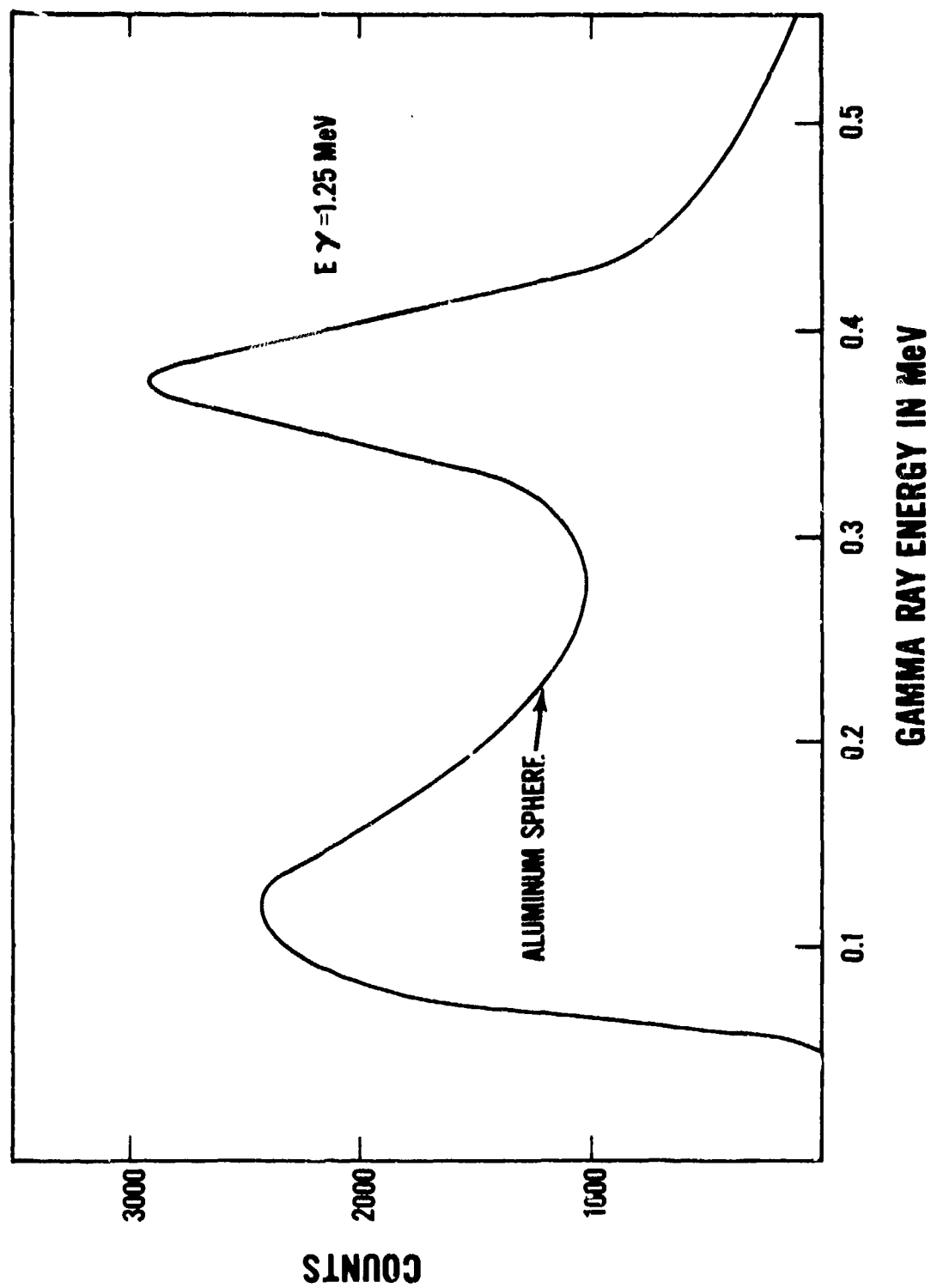


Figure 8. Pulse-height spectrum of  $^{60}\text{Co}$  photons backscattered from aluminum.  
(After Texas Nuclear Corporation, Final Report)

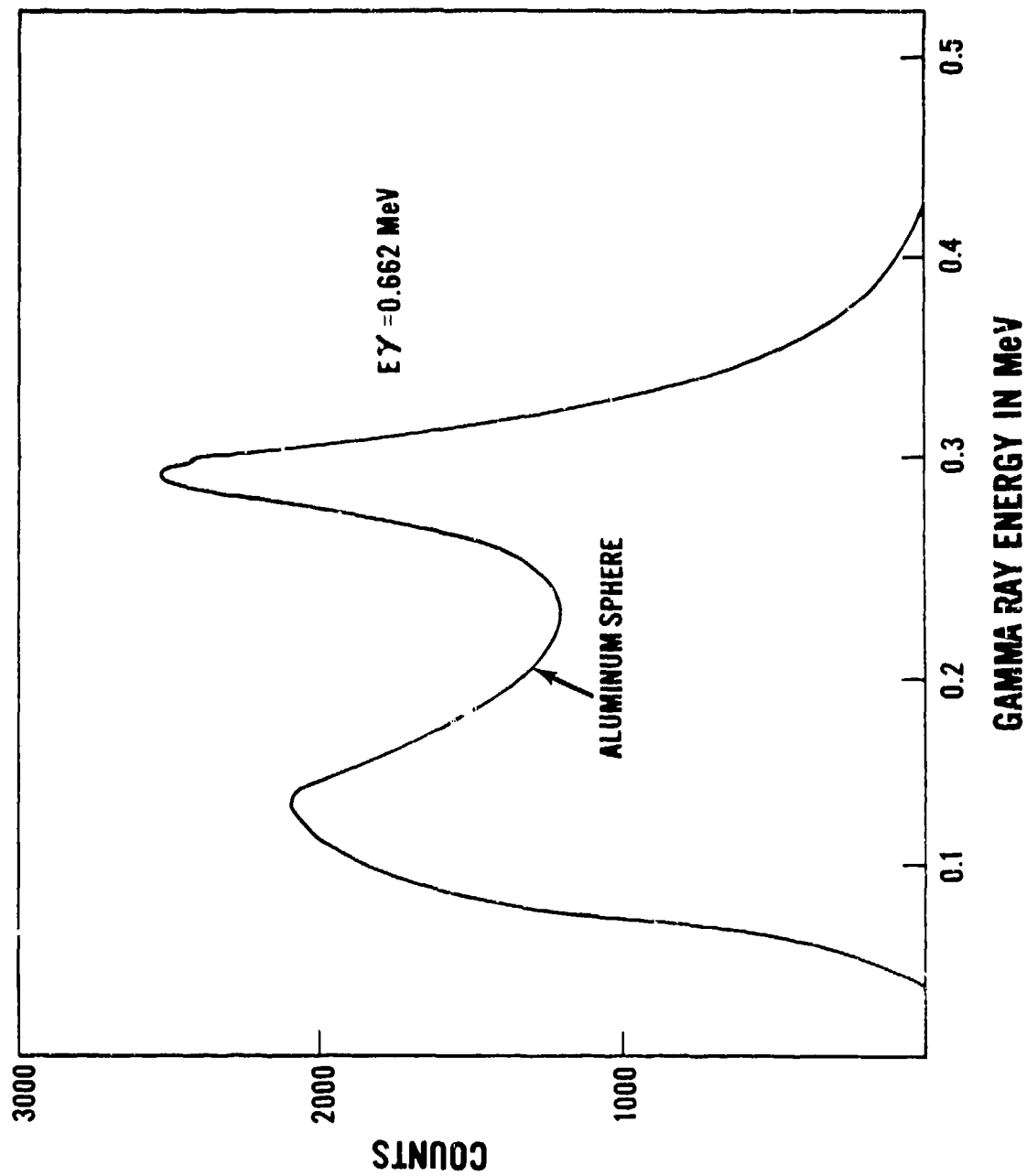


Figure 9. Pulse-height spectrum of  $^{137}\text{Cs}$  photons backscattered from aluminum.  
(After Texas Nuclear Corporation Final Report)

energy (290 keV versus 360 keV), there is virtually no change in the multiple-scatter "peak."<sup>15</sup>

The relative amplitude of the single- and multiple-scatter peaks is a function of the crossover depth of the acceptance cones defined by the source and detector collimators. The shallower this depth (the fewer the number of mean free paths), the greater the relative single-scatter contribution.

**8. Principle of Backscatter Mine Detection.** Before leaving geometry (a), one crucial experiment remains to be considered. Let us substitute a graphite sphere for the aluminum sphere used previously. By so doing, we have altered two parameters: the density and the atomic number of the scattering medium. Figure 10 shows the spectrum obtained after making this substitution.<sup>16</sup> In order to facilitate comparison, we also have retraced the spectrum of Figure 8. Two things should be noted. First, the single-scatter peak for the graphite scatterer occurs at the same energy as does that for the aluminum (as required by the Compton scattering equation) but is of greater amplitude. Second, the multiple-scatter peak for graphite is both of greater amplitude and extends to lower energies than for aluminum. The first effect is due to the change in scatterer density.<sup>17</sup> The second is due to the decrease of both the density and the atomic number (and, consequently, of the photo-electric cross section) of the scattering material ( $\tau \propto Z^4$ ). As a result of a decrease in  $\langle Z \rangle$ , each photon will, on average, undergo more collisions and survive to lower energies.<sup>18</sup> This effect is of primary importance in utilizing backscattered radiation for the detection of nonmetallic landmines. Since the average atomic number of most soils (on a weight-percent basis) is  $\sim 12$  (O, Si, Al, Fe, etc.), whereas that of plastics and high explosives is  $\sim 7$  (H, C, N, O), more photons will be backscattered from a mine than from soil in the low-energy range, where the photoelectric cross section is appreciable. In addition, since the probability of survival is  $\sigma_c/(\tau + \sigma_c)$  per collision, the change in the backscatter will vary roughly as  $[\sigma_c/(\tau + \sigma_c)]^N$ , where  $N$  is the average number of collisions per photon history. (It should be remembered, of

<sup>15</sup> This effect has been noted by S. Minato, Nucl. Sci. Engrg. 51, 32 (1973).

<sup>16</sup> Texas Nuclear Corporation, Final Report, Subcontract 1023-1 to Dikewood Corporation; Prime Contract AF29 (601) - 4569 (1962).

<sup>17</sup> In general, the effect of density changes on the magnitude of a single-scatter peak for geometries similar to geometry (a) is as follows: As the mass density and, consequently, the number of electrons in scattering volume increases from zero, so does the number of scattering events occurring in that volume. However, a maximum exists at which point further increases in density will result in a decrease in the observed single scatter due to attenuation of the incident radiation before reaching the scattering volume and of the scattered radiation before reaching the detector. Consequently, if the amplitude of the single-scatter peak falls within a certain range (this range depending on gamma-ray energy and system geometry), it may denote either of two densities. R.D. Gardner and R.L. Ely, Jr., *Radioisotope Measurement Applications in Engineering*, New York, Reinhold (1967), pp. 345 ff.

<sup>18</sup> In practice, the finite dimensions of a scattering medium tend to rob the multiple-scatter portion of the spectrum of its lowest energy components. Consequently, the low-energy truncation observed in these experiments is at a somewhat higher energy than is predicted by moments computations, which necessarily assume an infinite medium. L. V. Spencer, National Bureau of Standards (private communication).

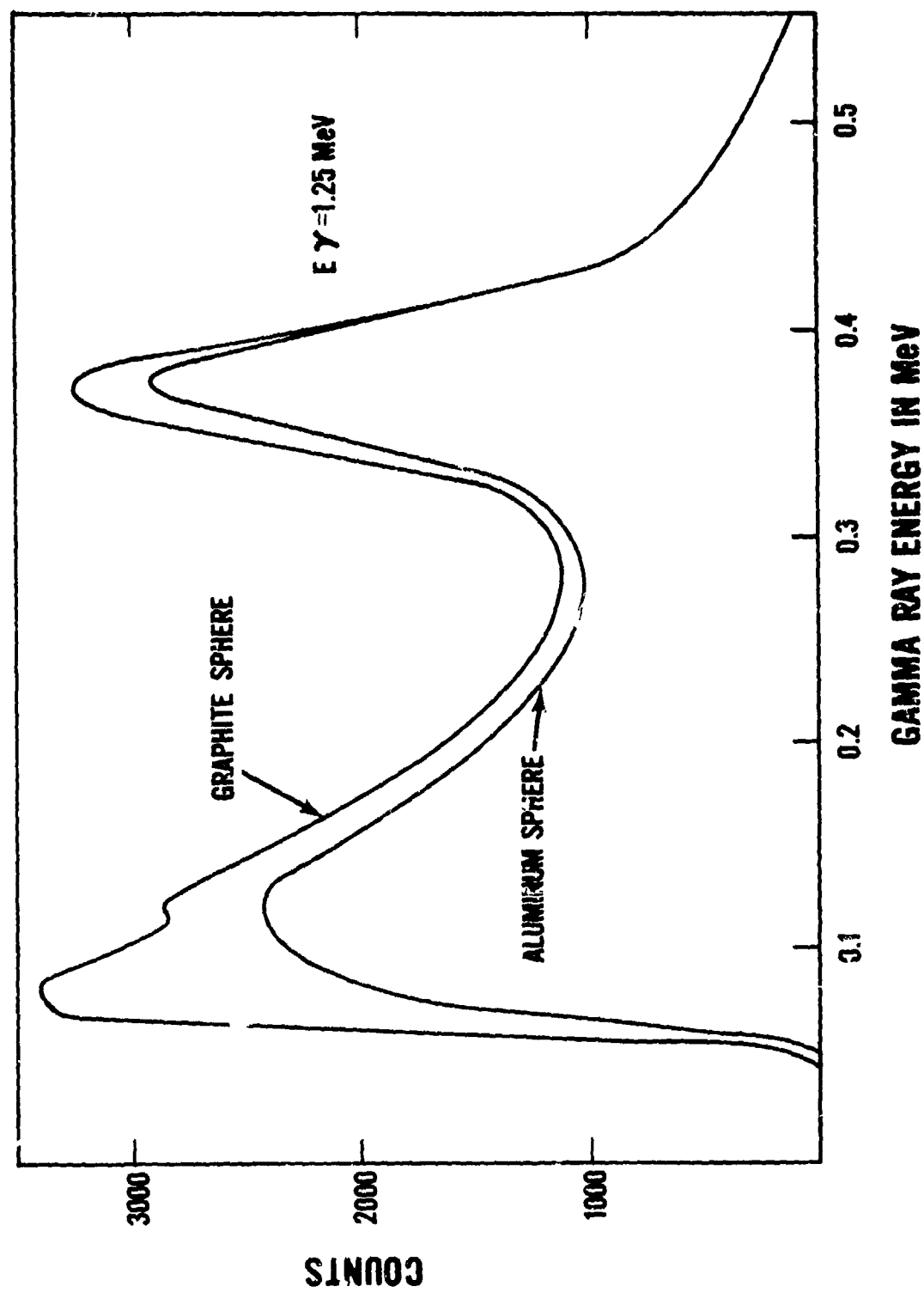


Figure 10. Comparison of pulse-height spectra of  $^{60}\text{Co}$  photons backscattered from graphite and aluminum.  
(After Texas Nuclear Corporation Final Report)

course, that both  $\tau$  and  $\sigma_c$  are functions of photon energy and, therefore, change with each scatter.)

Thus far we have considered only relatively high-energy isotopic sources and a relatively small scattering angle ( $90^\circ$ ). By doing so, we have been able to energy-resolve the single- and multiple-scatter peaks and, thereby, simplify the analytical discussion. For reasons to be shown, for the remainder of the report it will be necessary to consider larger scattering angles and lower source energies. As a result, it no longer will be possible to distinguish between single- and multiple-scatter contributions on the basis of energy, although both types of radiation may be known to be present.

**9. Selection of Source/Detector Geometry.** It is now appropriate to consider the three remaining geometries and to see how the backscatter spectrum changes as a function of  $\langle Z \rangle$  for each, still considering only semi-infinite scattering media.

As noted for geometry (a), the relative contribution of single and multiple scatter depends on the composition of the medium and on the depth of the crossover region. In the limit of an infinite crossover depth, there would be no single-scatter contribution — only multiple scatter. This will occur if the source- and detector-collimator axes are parallel (geometry (b)). Further, with this idealized geometry, the separation between the point illuminated by the source and the point viewed by the detector would be independent of height above the scattering medium. Thus, the magnitude of the backscatter flux density  $\theta$  would be independent of height, clearly a major advantage in terms of an operational detector traversing a less-than-ideal surface.

In practice, even if the source- and detector-collimator axes are parallel, there will be some angular dispersion of the incident and backscattered fluxes due to the finite acceptance angles of the collimators. The smaller the acceptance angles, the less dispersion will be present, and the less height-sensitive the system will be. However, as the acceptance angle decreases, so does  $\phi$ . Consequently, a trade-off must be made between achieving height-independence and obtaining the maximum possible value of  $\phi$ . Nevertheless, the assumption of parallel incidence and return represents a good approximation for this geometry as implemented.

Now, let us consider what happens when the source/detector separation  $q$  is varied for this geometry. As  $q$  is increased, the lateral distance a photon must traverse in the medium before its backscatter can be observed by the detector also increases. As a result, there is an approximately exponential decrease in  $\phi$  as  $q$  is increased, which is a disadvantage in that the count rate is lowered.<sup>19</sup> (See Appendix A.) However, the

<sup>19</sup> K. Preiss and R. Livant, Nucl. Engrg. and Design 24, 258 (1973); M. Leimdörfer, "The Backscattering of Photons," Sec. 4.4 in *Engineering Compendium on Radiation Shielding*, Vol. 1, R. G. Jaeger et al., Ed., New York, Springer-Verlag (1968).

average number of scatters ( $N$ ) undergone by the photons which are detected also increases as  $q$  is increased, since  $q$  becomes large compared to the mean free path of the photons. This is an advantage, since, as noted above, the ability to discriminate between media having differing values of  $\langle Z \rangle$  varies approximately as  $(\text{constant})^N$  (for low incident-photon energies). Thus, we have arrived at another trade-off:  $q$  should be set at the maximum possible value consistent with an acceptably high value of  $\phi$  at the detector for the case of semi-infinite media.

In the case of the mine-detection geometry (a low- $Z$  inclusion of finite size imbedded in a higher  $Z$  semi-infinite medium), this conclusion must be modified, since there is then a disadvantage to the use of a  $q$  value much greater than the lateral dimensions of the inclusion. (See Appendix A.) At this point, it should be noted that, for scatterer densities above some minimal value,  $N$  also will vary in direct proportion to  $\rho$ . Thus, a decrease in the density of the scattering medium without a change in composition will result in a positive change in the backscatter flux  $\Delta\phi$ . Since this is a linear effect, however, it is small compared to that observed for the  $Z$ -change due to the presence of a mine in the energy region where the photoelectric effect is important.

The advantages of geometry (b) are height independence and maximal values of  $\Delta\phi/\phi$ . However, both these advantages are achieved at the expense of  $\phi$ . Consequently, geometry (b) is of little value if only limited source activities are available. In this latter case, we must consider the advantages offered by geometries (c) and (d).

In geometry (c), the radiation source is an isotropic emitter and the detector is vertically collimated. In this case,  $\phi$  decreases comparatively slowly as  $q$  increases. ( $\phi \cong \frac{1}{2} \phi_{\text{max}}$  for  $q = h$ .) It also should be noted that single scatter is no longer geometrically excluded, and that the single-to-multiple-scatter ratio should be large compared to that for geometry (b) (and, as we shall see, for geometry (d)). The average number of scatters per photon history  $N$  also will be smaller than for geometry (b) and will be roughly independent of  $q$ . Thus, while  $\phi$  may be expected to be much larger for geometry (c) than for geometry (b) (for comparable detector collimation),  $\Delta\phi/\phi$  will be much lower. In addition,  $\phi$  no longer will be height-independent, but will vary rapidly with  $h$ . One advantage to geometry (c), however, is its minimal sensitivity to density changes. This may be seen to follow from the Theorem of Plane Density Variations, which states that "In an infinite medium in which the material is everywhere the same except for plane density variations, if there is a source of radiation which is likewise constant along planes of constant density, the radiation flux equals that in a corresponding problem with constant density."<sup>20</sup> In this case, the source condition can be satisfied by an isotropic source if it is employed at distances large compared to the mean free path of the

<sup>20</sup> Office of Civil Defense and Kansas State University, *Radiation Shielding*, William R. Kunel, Ed., U.S. Government Printing Office, Washington, D.C. 20402 (1966), p. 1-62.


photons in the medium.<sup>21</sup> See Figure 11. The principal advantage of geometry (c), however, is that it maximizes  $\phi$ . We will see later, in considering finite media, that geometry (c) has a second advantage: unlike geometry (b), the detector response is dependent on the material properties in a well-defined volume.

Geometry (d) consists of a vertically collimated source coaxially mounted with a vertically collimated detector. The collimation in this case, however, is intentionally "loose." The net result is something of a compromise between geometries (b) and (c). For small values of  $h$ , the detector is shielded from single scatter occurring near the surface of the scattering medium by a lip surrounding the source collimator. As  $h$  increases, the diameter of the spot directly illuminated by the source increases more rapidly than does the diameter of the shadow imposed by the collimator lip. As a result, as  $h$  increases, more single scatter is seen by the detector. (Of course, there is a maximum beyond which the single scatter begins to decrease.) The multiple scatter behaves in very much the same way except that it reaches its maximum value at a lower value of  $h$  than does the single scatter. The net result is that a compensated region is found to exist wherein the increase in the single scatter just compensates for the decrease in the multiple scatter. Thus,  $\phi$  for a detector operated in this range will be roughly independent of height. Figure 12 illustrates this effect. (Single- and multiple-scatter contributions were separated by visual examination of the data.) The geometry used to obtain the data shown was actually similar to geometry (b) with "loose" collimation and, as such, might be considered one radial element of geometry (d). (See Figure 13.) The source used was  $^{137}\text{Cs}$  in order to facilitate energy resolution of the single- and multiple-scatter contributions.<sup>22</sup>

The advantages of geometry (d) over geometry (c) are (1) height independence and (2) higher values of  $\Delta\phi/\phi$  as the composition of the scattering medium changes (due to the geometrical exclusion of some single scatter). The disadvantages are (1) a somewhat lower  $\phi$  and (2) a  $\Delta\phi/\phi$  which depends on height (since the single-to-multiple-scatter ratio changes with height). It should be recognized that, although not a disadvantage for semi-infinite media, the sensitive volume for geometry (d) is doughnut shaped. This proved to be a rather severe handicap in some cases of practical importance.

<sup>21</sup> It is difficult to change appreciably the density of a scattering medium without also changing its chemical composition. In experiments conducted in cooperation with personnel of the Explosives Laboratory, Picatinny Arsenal, sand and gravel of varying sieve size, obtained from the same quarry (therefore, presumably of similar composition), were placed in thin, aluminum trays approximately 11 by 16 by 2 inches deep. The trays were set flush with the surface of a semi-infinite, sand scattering medium. The extreme densities for the trays were 1.7 g/cm<sup>3</sup> (sand) and 1.5 g/cm<sup>3</sup> (1.5-inch-sieve gravel). Since the gravel was closely packed, it was assumed to represent a homogeneous scattering medium. (The air gap between stones was much less than the mean free path in stone of the  $^{137}\text{Cs}$  gamma rays employed.) System geometry was similar to that shown in Figure 13, except that the source was lowered to the bottom of the lead collimator ( $h = 15$  inches;  $q = 11$  inches). Integral counts obtained for the two density extremes showed less than a 1 percent difference. The pulse-height spectra obtained are depicted in Figure 11.

<sup>22</sup> Data obtained in collaboration with J. McCahill and S. Helf of the Feltman Research Laboratories, Picatinny Arsenal (1970).

UNCOLLIMATED  $^{137}\text{Cs}$  SOURCE  
 2" x 2" NaI (TI)  
 DETECTOR ( $22^\circ \frac{1}{2}$  )

SOURCE-DETECTOR  
 SEPARATION ( $q$ ) = 11 IN.  
 $h = 15$  IN.

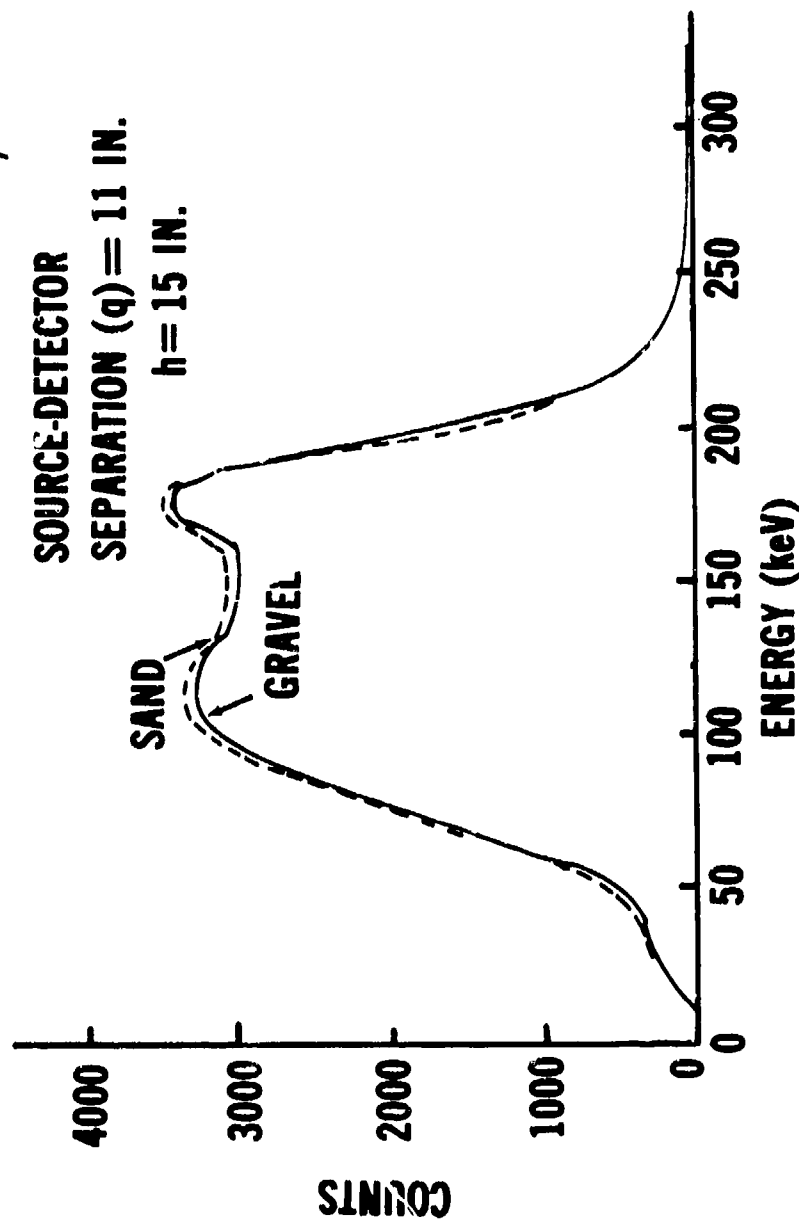


Figure 11. Uncollimated-source — collimated-detector backscatter spectra.



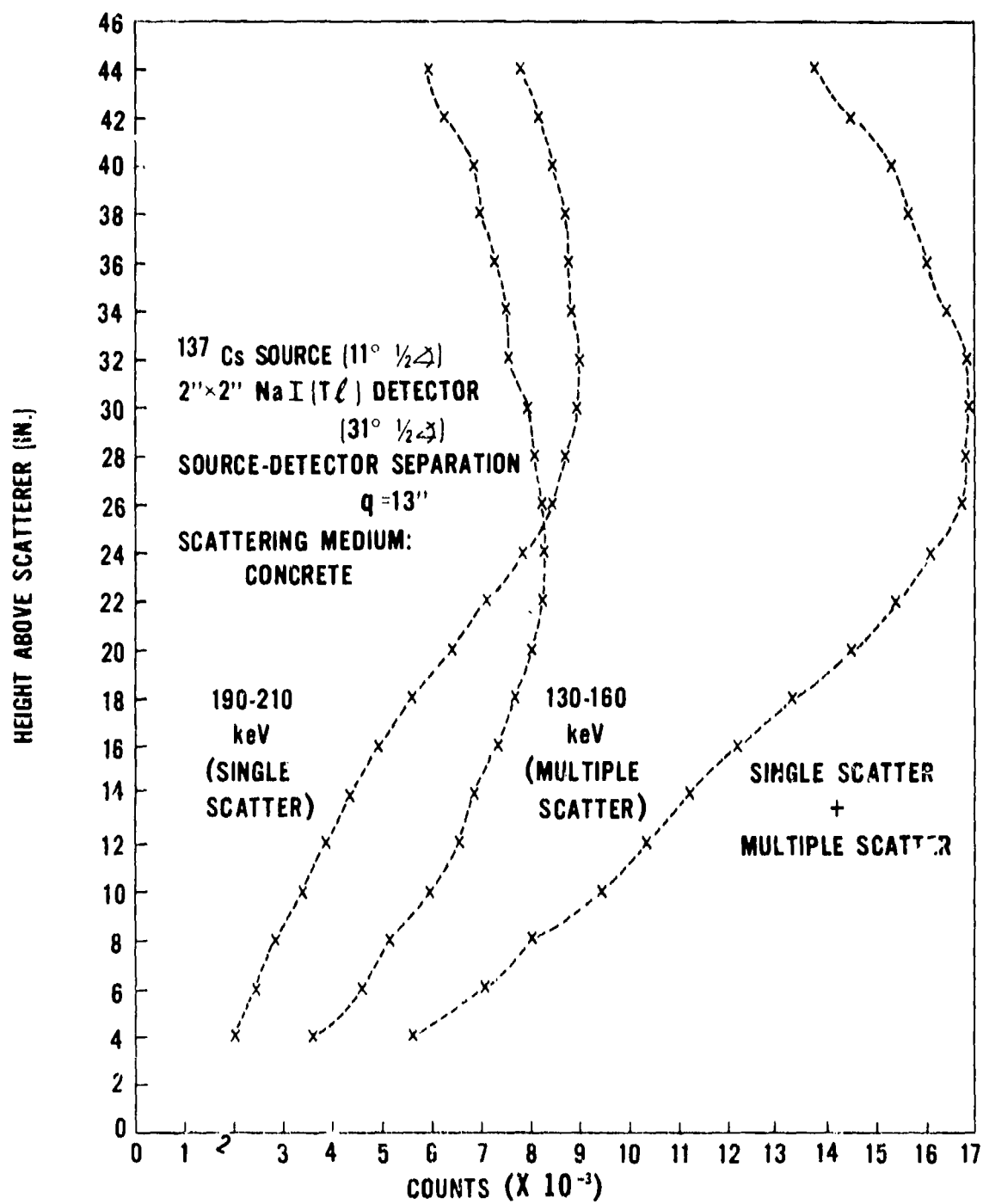


Figure 12. Change in backscatter with height above scatterer. (After McCahill and Helf)

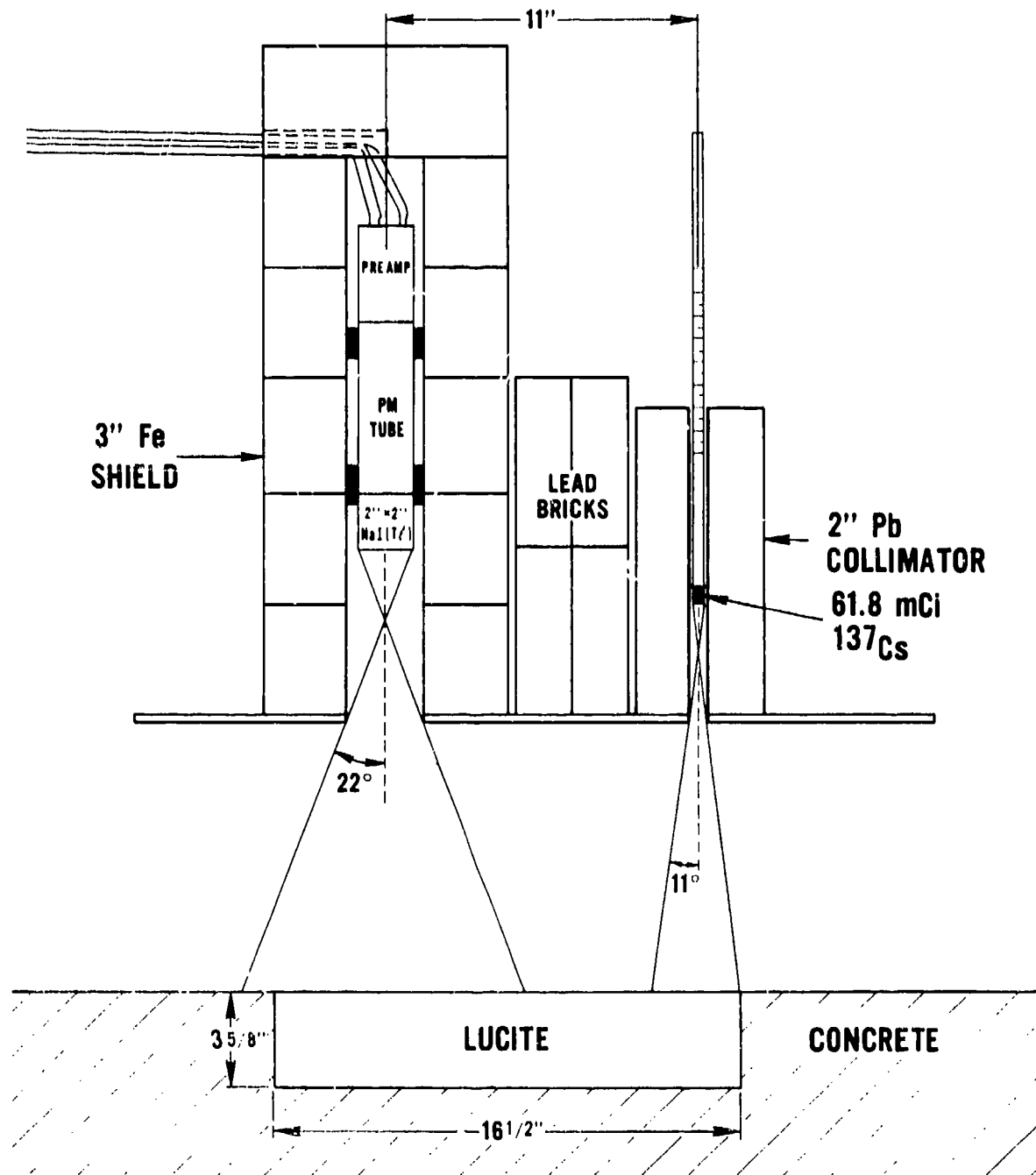


Figure 13. High-energy gamma-ray backscatter experimental setup. (After McCahill and Helf)

The results of this section are summarized in Table 1.

Table 1. Summary of System Characteristics as a Function of Geometry

Characteristic	Geometry Description			
	(a) Collimated Source; Collimated Detector; Defined Crossover	(b) Vertically Collimated Source and Detector	(c) Uncollimated Source; Vertically Collimated Detector	(d) Coaxial Source and Detector
Relative $\phi$	medium	low	high	medium
Relative $\Delta\phi/\phi$	medium	high	low	medium
Height Sensitivity	high	low	high	low
Density Sensitivity	high	high	low	medium

## 10. Source and Detector Selection.

a. **General.** The two remaining parameters which affect detector design are source and detector type. Since these parameters are determined more by the practical requirements of mine detection than by theoretical considerations, it will be necessary at this point to abandon the assumptions of semi-infinite scattering media of uniform composition and of point detectors and consider the problem as it presents itself in the real world.

Two broad classifications of mines need to be considered: antivehicular and antipersonnel. Antivehicular (AV) mines generally contain upward of 20 pounds of high explosives and may be buried under soil overburdens of up to a foot. For detection purposes, this is a very different class of targets from the antipersonnel (AP) mines which generally contain anywhere from 1/2 to 8 ounces of explosive and rarely are employed at depths exceeding an inch.

Since AP and AV mines pose very different detection problems, it was decided that two separate detection systems should be developed. The AP-mine detector was of necessity to be man-portable (because AP mines do not pose a major threat to vehicles). Thus, it was necessary to minimize the searchhead weight (since holding even 5 pounds at the end of a long handle is very fatiguing) while maintaining an acceptable rate of radiation exposure to the operator. Although it is obviously desirable to conduct mine-detection operations as rapidly as possible, it was recognized that, by keeping within the weight constraints of man-portability, the source size and, therefore, the count rate would have to be limited. As a result, it was envisioned that the detector could be employed only in suspect areas; therefore, relatively slow search speeds were considered to be acceptable (say, 0.1 mi/h clearing a path 4 feet wide). (See Appendix B.) The detector also was intended to be capable of functioning in a variety of terrains, under adverse weather conditions, and over a reasonable range of operating heights.

The AV detector was to be mounted on a boom attached to the front of a vehicle (for experimental purposes, a ¼-ton truck was employed). Because the metal of the vehicle would provide shielding for the operator, the exposure rate in the vicinity of the searchhead was not considered to be of overriding importance. It was, however, necessary that the searchhead clear a path at least equal to the width of the vehicle and be capable of operating at forward speeds in the neighborhood of 5 mi/h. (Speeds much greater than 5 mi/h would result in braking distances in excess of reasonable boom lengths.) Again, the detector was to be capable of operating in a variety of terrains, under adverse weather conditions, and over a reasonable range of heights.

b. **Source Selection.** Secondary high explosives consist entirely of light elements (H, O, N, C) yielding an average  $Z$  of approximately 7. Soils, on the other hand, consist of somewhat heavier elements (O, Al, Si, Fe, etc.) yielding an average  $Z$  in the neighborhood of 12. Both soils and explosives have specific gravities in the range  $1.3 \leq \rho \leq 2$ . It should be remembered that, since photoelectric absorption per unit mass is proportional to  $\langle Z^4 \rangle$ , inorganic clay, for example, will photoabsorb some 27 times the number of gamma rays per unit mass as will explosive at the same photon energy per unit flux (see Table 2). However, the percentage of gamma photons whose scattering histories are terminated by photoabsorption (as opposed to backscatter) depends on the incident gamma energy ( $\tau \propto E^{-3}$ ). Thus, the backscatter spectrum from a relatively high-energy gamma source (say,  $^{137}\text{Cs}$ ;  $E = 0.662$  MeV) will be relatively insensitive to changes in the atomic number of the scattering medium except for the lowest energy portion of the multiple-scatter component (see Figure 14). On the other hand, if a relatively low-energy gamma source is employed (say,  $^{241}\text{Am}$ ;  $E_\gamma = 0.060$  MeV), the amplitude of the entire backscatter spectrum increases as the atomic number of the scattering medium decreases<sup>23 24</sup> (see Figure 15). (The lower energy peak shown is the iodine X-ray escape peak.) Integrating over the entire spectrum, we have found that this change may be as great as several hundred percent in going from a semi-infinite soil medium to a semi-infinite explosive medium. On this basis, it would appear desirable for purposes of mine detection to utilize the lowest energy possible, consistent with an acceptable return rate. (The lower the incident energy, the lower the percentage of gammas backscattered for energies below about 250 keV.<sup>25</sup>) This, indeed, would be

<sup>23</sup> W. D. Miller, W. E. Tucker, and E. L. Hudspeth, *The Detection of Concealed Explosives by the Use of Gamma-Ray Scattering and Transmission Techniques*, Confidential Final Report, Contract DAAK02-68-C-0229 (October 1969), AD 506-081L.

<sup>24</sup> In the case of semi-infinite scattering media, there is a downward spectral shift in the backscatter spectrum as  $Z$  decreases, even when an  $^{241}\text{Am}$  source is utilized. However, in the case of mine detection, since there is an intervening soil overburden, the lowest energy portion of the backscatter from the target is severely attenuated. As a result, no spectral shift is evident. Note that Figure 15 refers to a target under a 1-inch soil overburden. See also F. L. Roder and D. G. Conley, *Computed Energy Distribution of Double-Scattered Photons, Obtained for Purposes of Mine Detector Design Analysis*, USAMERDC Report 2097 (1974).

<sup>25</sup> M. Leimdörfer, "The Backscattering of Photons," Sec. 4.4 in *Engineering Compendium on Radiation Shielding*, Vol. 1, R. G. Jaeger, Ed., New York, Springer-Verlag (1968).

Table 2. Composition of TNT and Sample Soils

Chemical Composition (Pet by Weight)	Chemical Formula	Average Z Values	Chemical Composition (Pet by Weight)	Element
TNT				
100	$C_7H_5(NO_2)_3$	$\langle Z \rangle \cong 7$	37	C
		$\langle Z^4 \rangle_{\text{eff}} \cong 2,600^{(a)}$	2	H
			19	N
			42	O
Inorganic Clay <sup>(b)</sup>				
72	$SiO_2$	$\langle Z \rangle \cong 12$	50	O
20	$Fe_2O_3$		34	Si
5	Organic	$\langle Z^4 \rangle_{\text{eff}} \cong 72,000^{(a)}$	14	Fe
3	$H_2O$		2	C
			0.6	H
Grass-Covered Soil <sup>(c)</sup>				
59	$SiO_2$	$\langle Z \rangle \cong 11$	61	O
10	$Fe_2O_3$		28	Si
7	Organic	$\langle Z^4 \rangle_{\text{eff}} \cong 40,000^{(a)}$	7	Fe
24	$H_2O$		1	C
			3	H

(a) Since  $\tau \propto Z^4$  is an approximation for  $\tau \propto Z^3/A$ , the values given for  $\langle Z^4 \rangle_{\text{eff}}$  were computed as  $\langle 2Z^3/A \rangle$ .

(b) Soil from Mine Lanes Test Facility.

(c) Soil from Fort Belvoir, Virginia.

NOTE: Soil samples analyzed at MERDC.

true if all mines were emplaced flush with the surface. In practice, however, mines are buried under soil overburdens ranging from a light dusting for small antipersonnel mines to as much as a foot for large antivehicular mines. Although the percentage of the backscatter spectrum originating in a particular depth interval depends to some extent on the source/detector geometry employed, it is generally valid to state that backscatter as a function of depth decreases exponentially: the lower the gamma energy, the higher the exponent of the exponential. Therefore, lower incident energies result in shallower sampled volumes. As an example, the mean free path of 60-keV gamma rays in typical soils is about 1 inch. A final consideration in the selection of source energy is the thickness of the explosive charge of the mine being sought. An antivehicular mine generally will have an explosive charge on the order of 3 inches thick. An antipersonnel mine, on the other hand, may have a charge less than 1/2-inch thick. Thus, an antivehicular mine may be considered nearly semi-infinite for the range of gamma energies where photoabsorption is of importance (i.e.,  $\lesssim 200$  keV); whereas, the backscatter reaching a detector focused on an antipersonnel mine might well arise from the soil beneath the mine

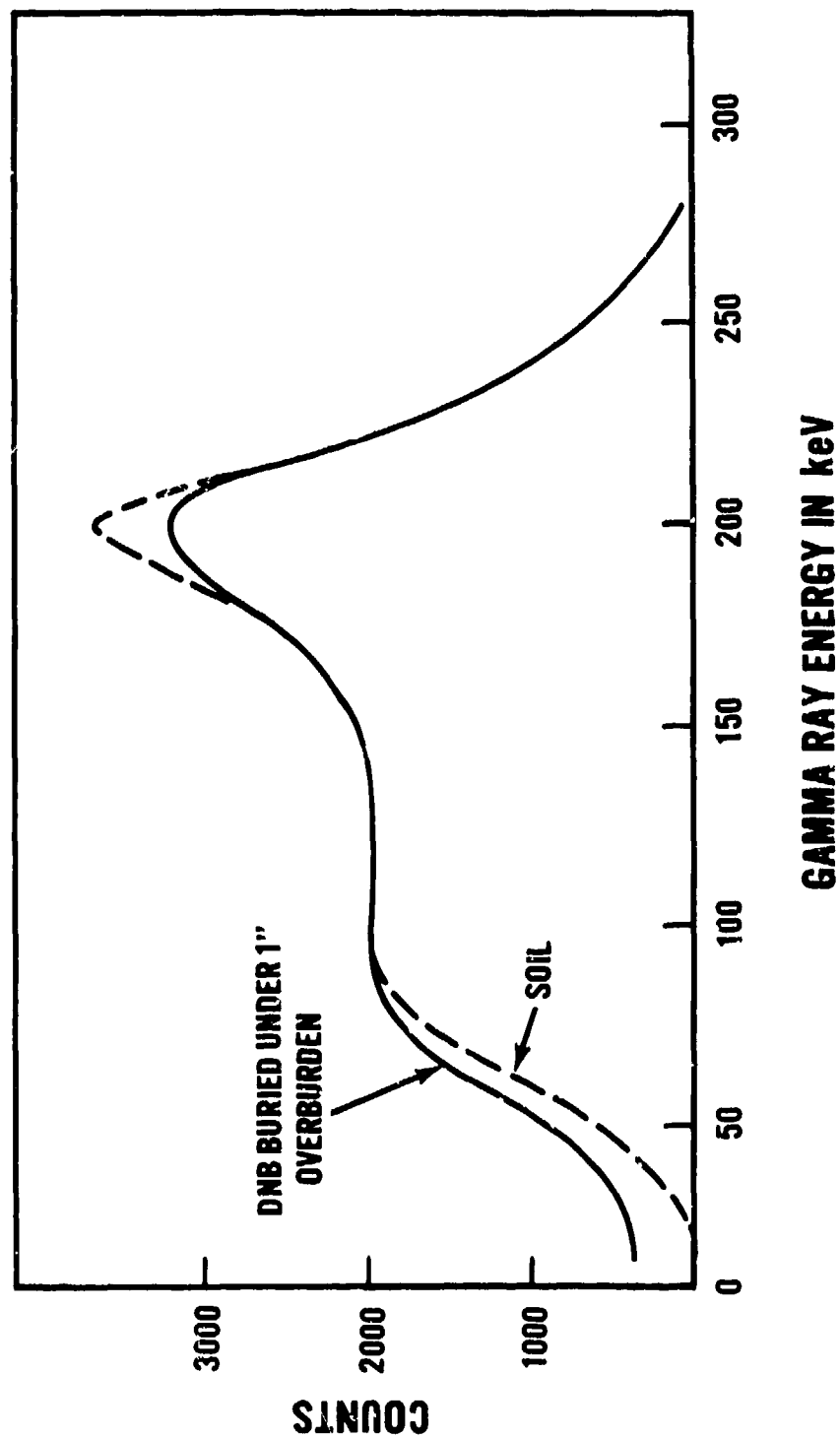


Figure 14. Comparison of pulse-height spectra of  $^{137}\text{Cs}$  photons backscattered from soil with and without the presence of a dinitrobenzene (DNB) block. (After Miller, Tucker, and Hudspeth; Contract DAAK02-68-C-0229)

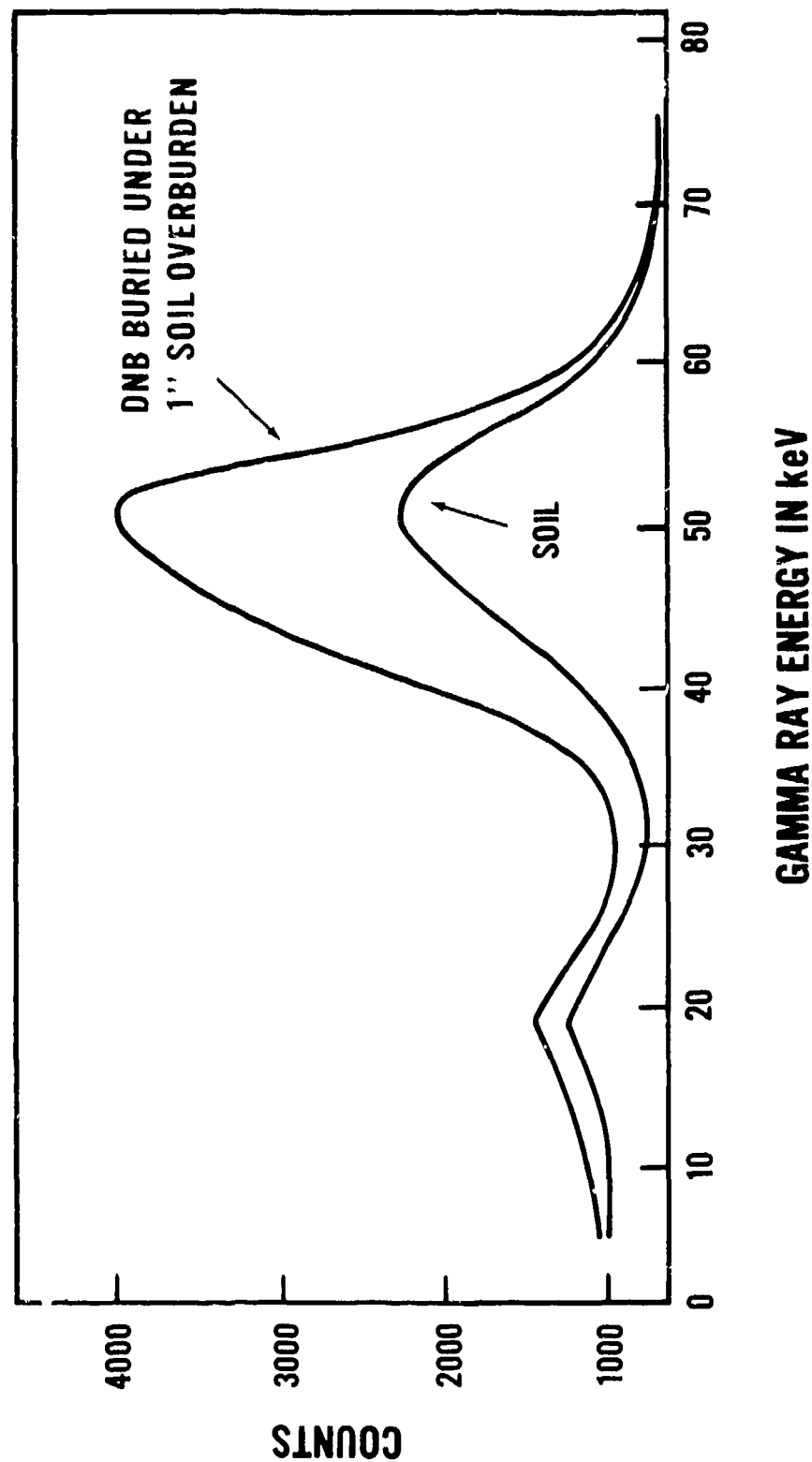


Figure 15. Comparison of pulse-height spectra of  $^{241}\text{Am}$  photons backscattered from soil with and without the presence of a dinitrobenzene (DNB) block. (After Miller, Tucker, and Hudspeth; Contract DAAK-02-068-C-0229)

as well as from the mine itself and its soil overburden. Thus, a lower energy (and, thus, less penetrating) radiation might be desirable for this application.

In addition to the above three theoretical considerations, we are also faced with the more practical problem of what source energies are available. In the realm of low-energy gamma sources of practical half-life, we have  $^{241}\text{Am}$  at 60 keV,  $^{109}\text{Cd}$  at 88 keV, and  $^{57}\text{Co}$  at 122 and 136 keV.  $^{57}\text{Co}$  and  $^{109}\text{Cd}$  both are an order of magnitude more expensive than  $^{241}\text{Am}$  and have half-lives two orders of magnitude shorter (271 and 453 days, respectively). For these reasons,  $^{241}\text{Am}$  was selected as the most promising radioisotope for mine-detection applications. However, because of its low specific activity and the low energy of the gamma ray produced, self-absorption limits the maximum usable activity of an  $^{241}\text{Am}$  disk source to approximately 1 Ci/in.<sup>2</sup>,<sup>26</sup> (1 Ci =  $3.7 \times 10^{10}$  disintegrations/s.) Thus, for geometries where source collimation is required, the gamma flux attainable on the soil surface from an  $^{241}\text{Am}$  source is rather limited. In order to produce a more intense directional photon source, it was, therefore, necessary to utilize an X-ray generator.

X-ray tubes currently are available which are sufficiently rugged to consider for field use. However, only the smallest of these do not require a circulating-oil bath for cooling. (Only a few percent of the energy of the electron beam is converted to X-rays; the remainder is converted to heat in the anode.) However, the added burdens of an X-ray generator (oil bath, pump, regulated high-voltage supply, and kilowatt-size power supply) are offset by two prime advantages: (1) The unit may be shut off and, therefore, will not pose a radiation hazard when not in use; and (2) an X-ray generator, when compared to  $^{241}\text{Am}$ , will supply an almost unlimited photon flux in the requisite energy range. For example, a tube operated in a continuous mode at 120 kV with a tungsten anode will have a conversion efficiency  $\epsilon$  of about 1.1 percent.<sup>27</sup> Of the X-rays produced by bremsstrahlung (i.e., neglecting the characteristic spectrum), ~45 percent will fall in the 40- to 120-keV range, which we might consider realistically to be the range of interest. This translates to  $5.5 \times 10^{13}$  useful photons/s, or about 4,500 equivalent curies per milhamp of beam current, taking into account the 36-percent yield of the 60-keV gamma ray in  $^{241}\text{Am}$ . In addition, the distribution of X-rays is not isotropic (as is the case for  $^{241}\text{Am}$ ), but is peaked at right angles to the electron beam, in the direction of the port. (This is true only for nonrelativistic electrons: i.e.,  $E \ll 511$  keV.) For these reasons, it was decided that an X-ray generator would be the photon source of choice for the vehicular application.

c. **Detector Selection.** In selecting  $^{241}\text{Am}$  and an X-ray generator for the

<sup>26</sup> Wendell Miller, Nuclear-Chicago Corporation, Private communication (1970).

<sup>27</sup> E. U. Condon, "X Rays," in *Handbook of Physics*, Second Ed., E. U. Condon and H. Odishaw, Eds., New York, McGraw-Hill (1967), p. 7-126.



man-portable and vehicle-mounted applications, respectively, the requirement that the detectors employed be capable of energy-resolving the backscattered flux was eliminated (since the presence of a low-Z inclusion is manifested over the entire energy spectrum). Nevertheless, scintillation detectors were employed in all experimental searchheads, primarily to capitalize on their virtual 100-percent efficiency for photons in the requisite energy range. CsI(Na) scintillators were employed in place of the more conventional NaI(Tl) primarily because the former are less subject to damage from mechanical shock. (The possibility of utilizing other detectors was considered and will be discussed in Section III.)

**11. Compensation for Height Variations.** As noted in paragraph 9, geometries (a) and (c) are extremely height-dependent. However, since, of the two, only geometry (c) (uncollimated source - collimated detector) is of practical importance for the present application, discussion will be limited to that geometry.

Since the criterion for detection is simply an increase in the backscattered flux  $\phi$ , variations in  $\phi$  with height (resulting from either a change in searchhead height or surface irregularity) can be disastrous. In practice, a  $\Delta\phi/\phi$  value of 10 percent may be indicative of a mine; whereas, for geometry (c), a change in  $\phi$  of 25 pct/in. of height is typical for the geometrical parameters employed.

Several techniques of compensating for height changes were considered, and two were instrumented.

**a. Two Detectors at Different Heights Viewing the Same Area (See Figure 16).** In principle, this technique is very simple: If  $h_1$  and  $h_2$  are the distances from the lower and upper detectors, respectively, to the soil surface, with corresponding fluxes  $\phi_1$  and  $\phi_2$ , then a change in searchhead height  $\Delta h$  should result in different values of  $\Delta\phi_1$  and  $\Delta\phi_2$ , provided that  $\phi_1$  and  $\phi_2$  do not change linearly with height. For example, if  $\phi_1$  and  $\phi_2$  vary as  $1/h^2$ , then

$$\frac{(\Delta\phi_1 - \Delta\phi_2)}{\Delta h} \propto 2(h_2^{-3} - h_1^{-3}).$$

Unfortunately, experimentally obtained results utilizing geometry (c) reveal a  $\phi(h)$  dependence nearly linear for the small values of  $h$  which are of practical importance (see Figure 17). For this reason, this approach was not pursued further.

**b. Two Backscatter Signals (See Figure 18).** In this technique, use is made of the fact that only low-energy photons are sensitive to the presence of landmines. In principle, then, there are two possible methods of achieving height compensation: either using a high-energy gamma source (say,  $^{137}\text{Cs}$ ) or using a beta source (say,  $^{90}\text{Sr}$ ) together with an  $^{241}\text{Am}$  gamma source.

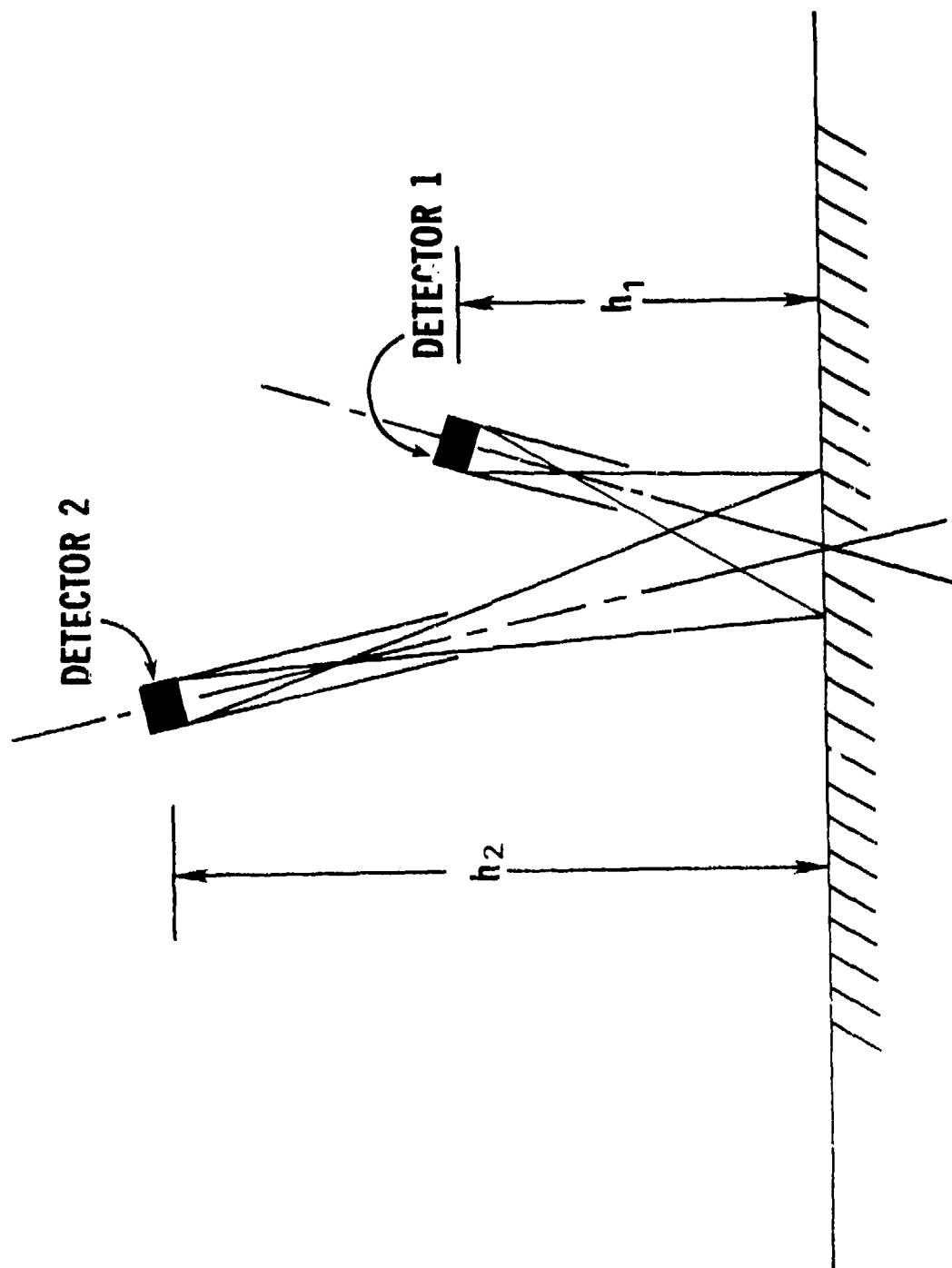


Figure 16. Two detectors at different heights viewing the same area.

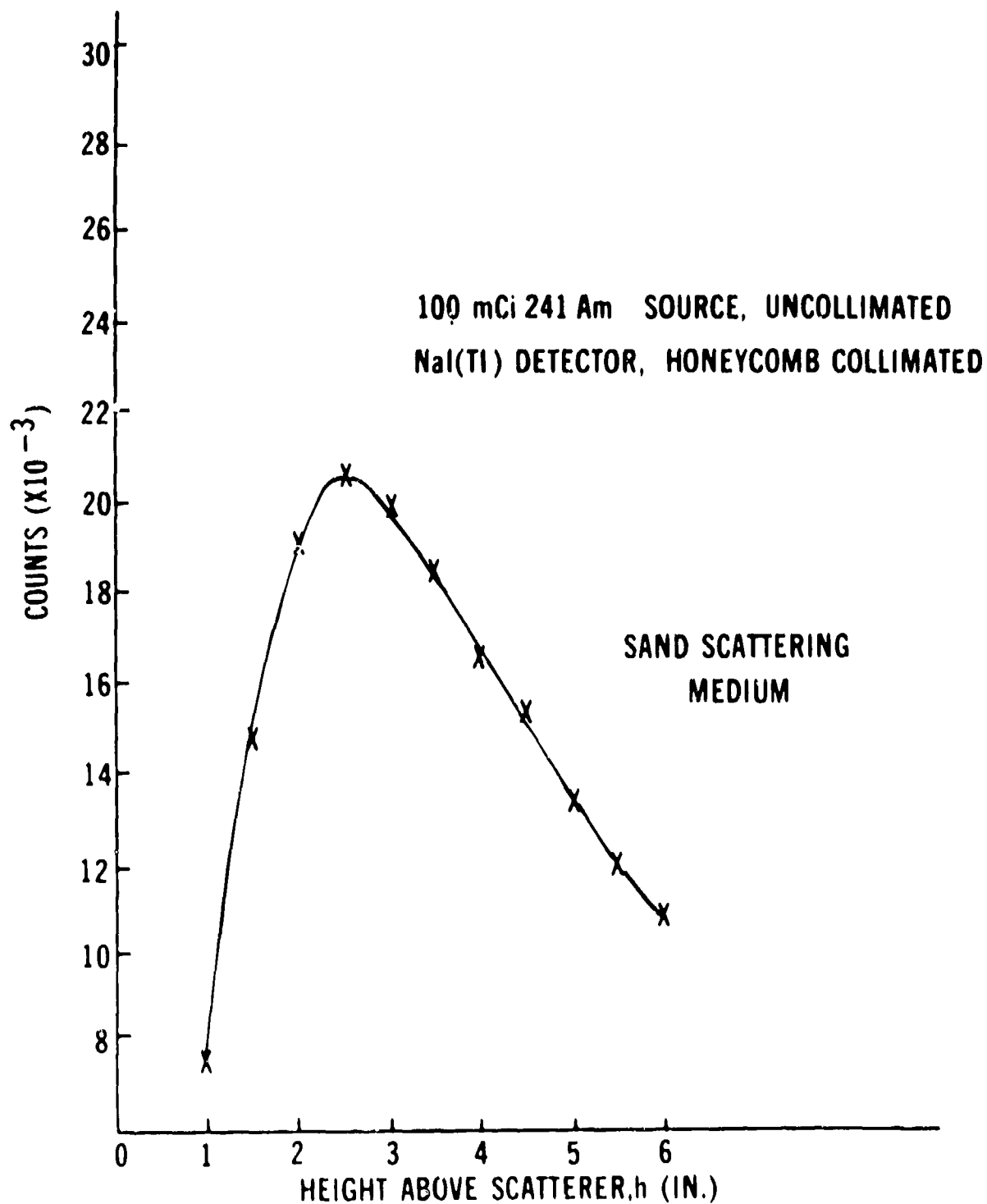


Figure 17. Variation of backscatter flux with height. (Data from Contract DAAK02-72-C-0619)

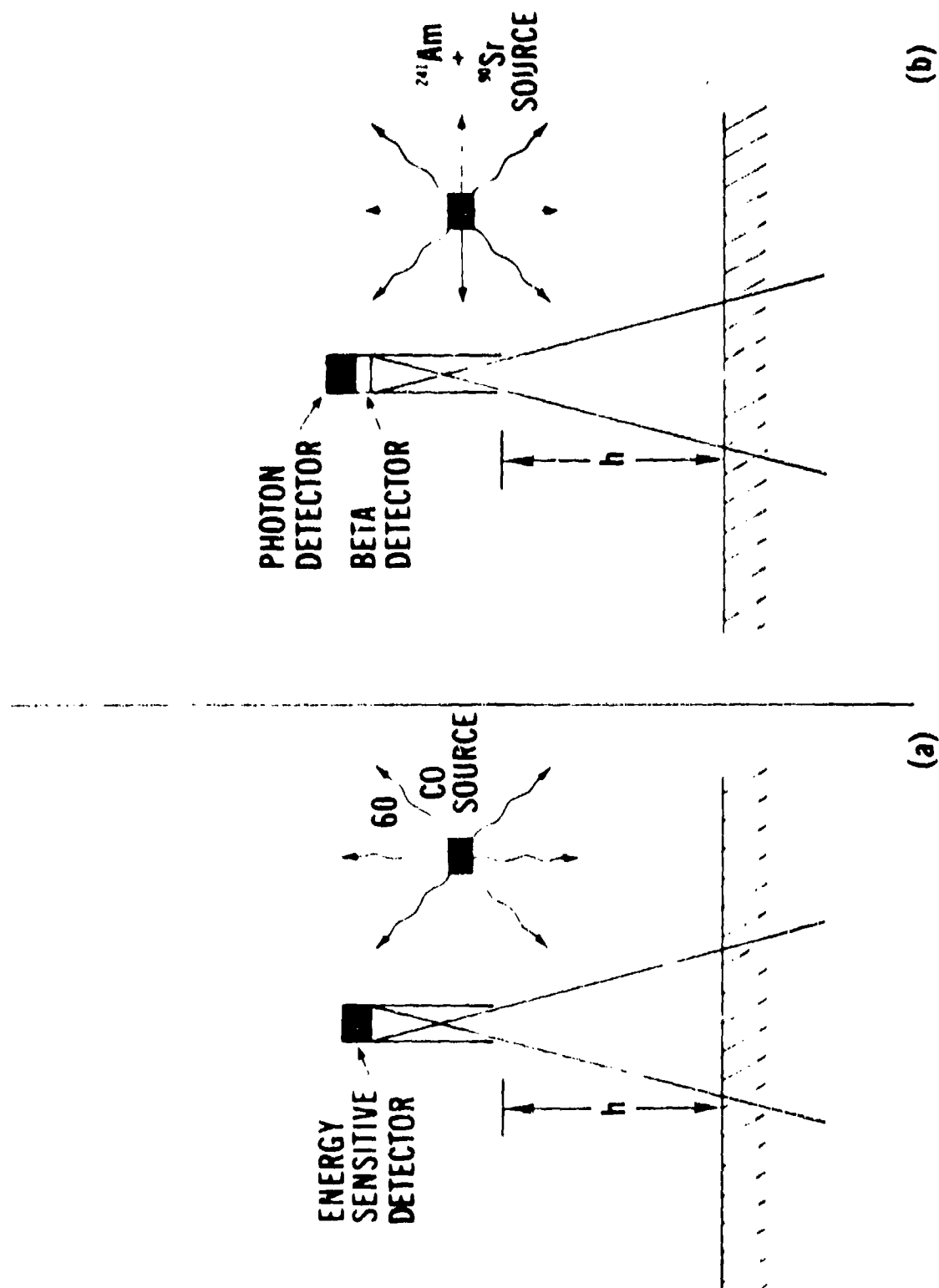


Figure 18. Geometries for two-signal height-compensation technique.

If  $^{137}\text{Cs}$  is employed, the backscatter spectrum will contain single- and multiple-scatter peaks resolvable in energy. The amplitude of the single-scatter peak is largely insensitive to  $\langle Z \rangle$  changes and is primarily a function of  $h$ . The amplitude of the multiple-scatter peak is a function of both  $\langle Z \rangle$  and  $h$  (and, to a lesser extent, of density)<sup>28</sup> (see Figure 19). Clearly, Figure 19 contains sufficient information to compute both  $\langle Z \rangle$  and  $h$ . Unfortunately, this method has two practical limitations which preclude its incorporation in a mine detector. First, only a small fraction of the gammas emitted are of use in actually determining whether a mine is present or absent. Thus, the source utilization is far lower than is the case for  $^{241}\text{Am}$ . Second, as previously noted, geometry (c) is of primary interest for implementation in a man-portable device. Thus, the increase in shielding weight required (for operator protection and to prevent direct feedthrough to the detectors) is a substantial handicap.

The second method, using a beta source in conjunction with an  $^{241}\text{Am}$  source, avoids the practical limitations inherent in the use of  $^{60}\text{Co}$ . A beta source placed in the same housing as the  $^{241}\text{Am}$  requires no additional shielding (although the bremsstrahlung produced will introduce a slight additional background in the scintillator). A small, gas-filled detector placed in front of the scintillator then will respond to backscattered betas while remaining virtually transparent to backscattered gammas. Thus, although two detectors (and associated electronics) must be employed instead of one, the size and weight of the searchhead need not be increased appreciably. On the debit side, it should be noted that, since betas have essentially no penetration relative to the gamma rays, the number of betas backscattered is a function of height over the first solid scatterer, even if this scatterer is a blade of grass or a dry leaf (items essentially transparent to 60-keV gammas). Further, beta backscatter is itself  $Z$ -sensitive. Thus, the backscatter will change as a function of soil type.<sup>29</sup>

As a consequence of the above, beta backscatter can be used only for height compensation if the device is (1) recalibrated for each soil type encountered, and (2) used in nonvegetative areas or in areas with relatively uniform vegetative ground cover. Since, in any case, the gamma-backscatter technique cannot be used in areas with excessive vegetation (because the  $\langle Z \rangle$  of the scattering medium is then too close to the  $\langle Z \rangle$  of an explosive), beta backscatter was instrumented and used as the height-compensation technique for one of the detectors described in Section IV.

c. **Filters.** In geometry (c), a large number of singly scattered photons and a somewhat smaller number of multiply scattered photons are incident on the detector.

<sup>28</sup> Modeling a vertically-collimated source-uncollimated-detector geometry by Monte Carlo techniques, S. Minato; [Nucl. Sci. Engng. 51, 32 (1973)] has found the energy of the peak of the multiple-scatter distribution to fit the empirical equation  $E(\text{keV}) = 6.8 \langle Z \rangle^{0.29}$ . Note the dependence of  $E$  on the  $Z$  of the scattering medium and the absence of dependence of  $E$  on the energy of the incident photon.

<sup>29</sup> H. H. Seliger, *Phys. Rev.*, **103**, 103 (1952).

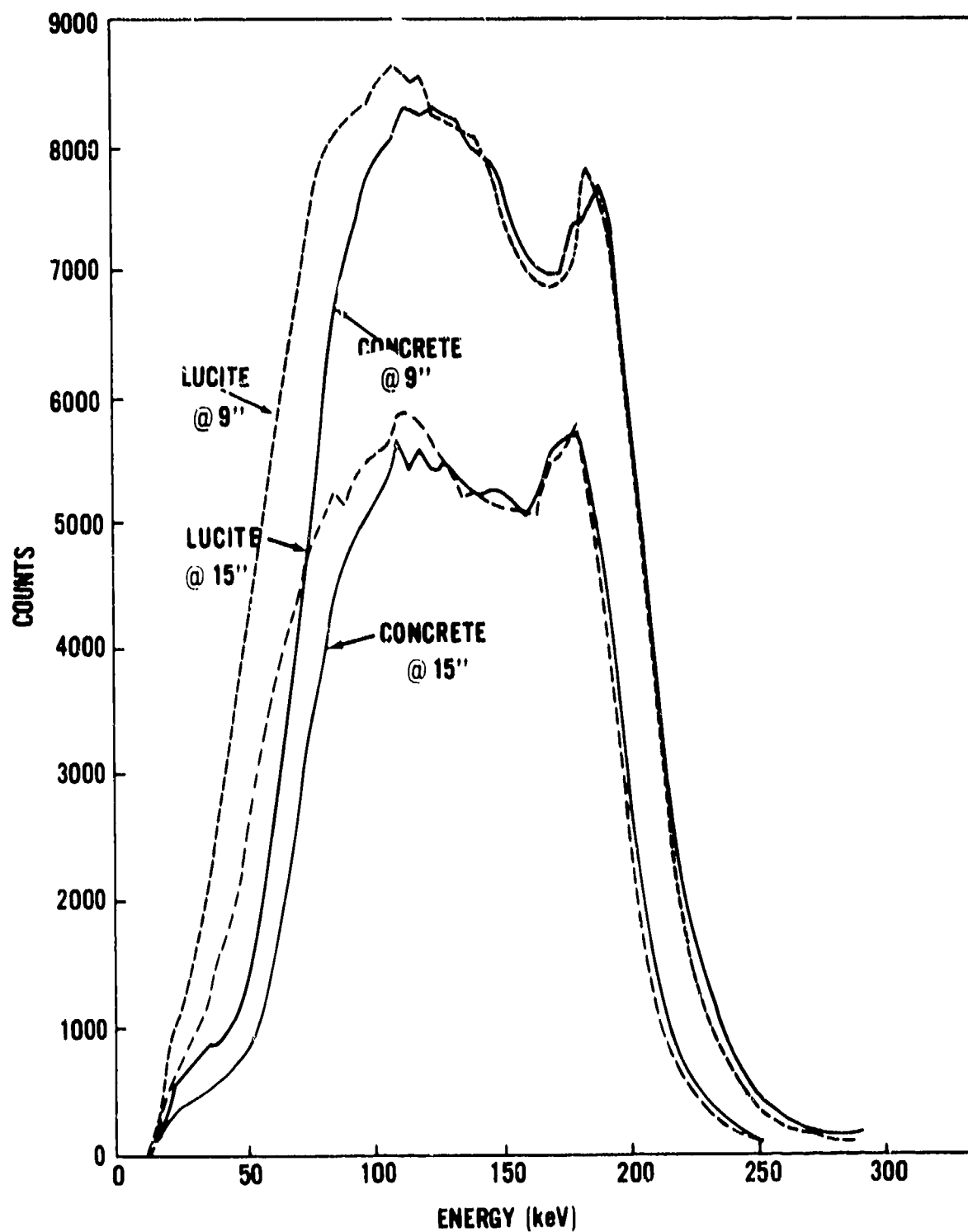


Figure 19. Pulse-height spectrum of  $^{137}\text{Cs}$  photons backscattered from Lucite and concrete for two values of  $h$ . (After McCahill and Helf)

although utilizing an  $^{241}\text{Am}$  source precludes the energy resolution of these two components by conventional scintillation detectors.<sup>30</sup> Filters provide a means of crudely resolving these components.

Let us consider a particular example: assume a source/detector separation of 2 inches center-to-center, a 1-inch-diameter  $^{241}\text{Am}$  source, and a 1-inch-diameter scintillation detector with a honeycomb collimator. Allow the system to vary in height over the range from 2 to 5 inches. (See Figure 20.) Since the single-scatter angle varies with detector height, so will the energy of the single-scatter radiation ( $E_{\text{ss}}$ ). In this case,  $E_{\text{ss}} = 49.62$  keV for  $h = 2$  inches, and  $E_{\text{ss}} = 48.87$  keV for  $h = 5$  inches, a variation of 0.75 keV (assuming a photon produced at the center of the source, absorbed at the center of the scintillator, and scattering  $\frac{1}{2}$  inch below the surface of the scattering medium). The given geometrical parameters permit an energy spread in the single-scatter radiation of from 48.83 to 50.24 keV at  $h = 2$  inches (assuming a maximum scattering depth of 1 inch). Thus, the shift in the approximate centroid of the single-scatter peak with height is an appreciable fraction of the peak width. See Figure 21. (It should be emphasized that Figure 21 is an idealized spectrum, possibly realizable with a Ge (Li) detector, but not otherwise.) Multiple scatter, on the other hand, is distributed over a broad energy spectrum both above and below the single-scatter energy. As a result, even if the centroid of this spectrum does shift as  $h$  is varied (a question which at present is unresolved) the shift would not constitute an appreciable fraction of the width of the multiple-scatter energy distribution.

Let us now interpose a filter in front of the detector which has a K-edge in the vicinity of the energy of the backscattered radiation. In this case, europium, with a K-edge at 48.515 keV, is most appropriate. At  $h = 2$  inches, essentially all single-scattered photons are at an energy just above the K-edge and, consequently, are greatly attenuated. As  $h$  increases, progressively more single scatter falls below the K-edge and passes through the filter. There is no equivalent change in the transmission of multiply scattered photons because of the energy spread of this portion of the spectrum. (This technique has the advantage of being independent of soil conditions because the energy distribution of singly scattered photons is a function of geometry alone.)

If two detectors, one filtered and one unfiltered, are used to view the same spot on the soil surface, then the ratio of single to multiple scatter will vary as a function of  $h$ . The result of this effect is shown in Figure 22. If the detector then passes over a mine, there is an increase in the countrate of both detectors, but there is no change (once background is subtracted) in the ratio of countrates. Thus, sufficient information is present to detect a mine without incurring false signals due to small

<sup>30</sup> A recently developed technique, utilizing Xe as the scintillating medium, may enable resolution of the single- and multiple-scatter components of a backscatter spectrum without the use of a Ge(Li) detector. Robert Moler, Science Applications, Inc., private communication (1974).

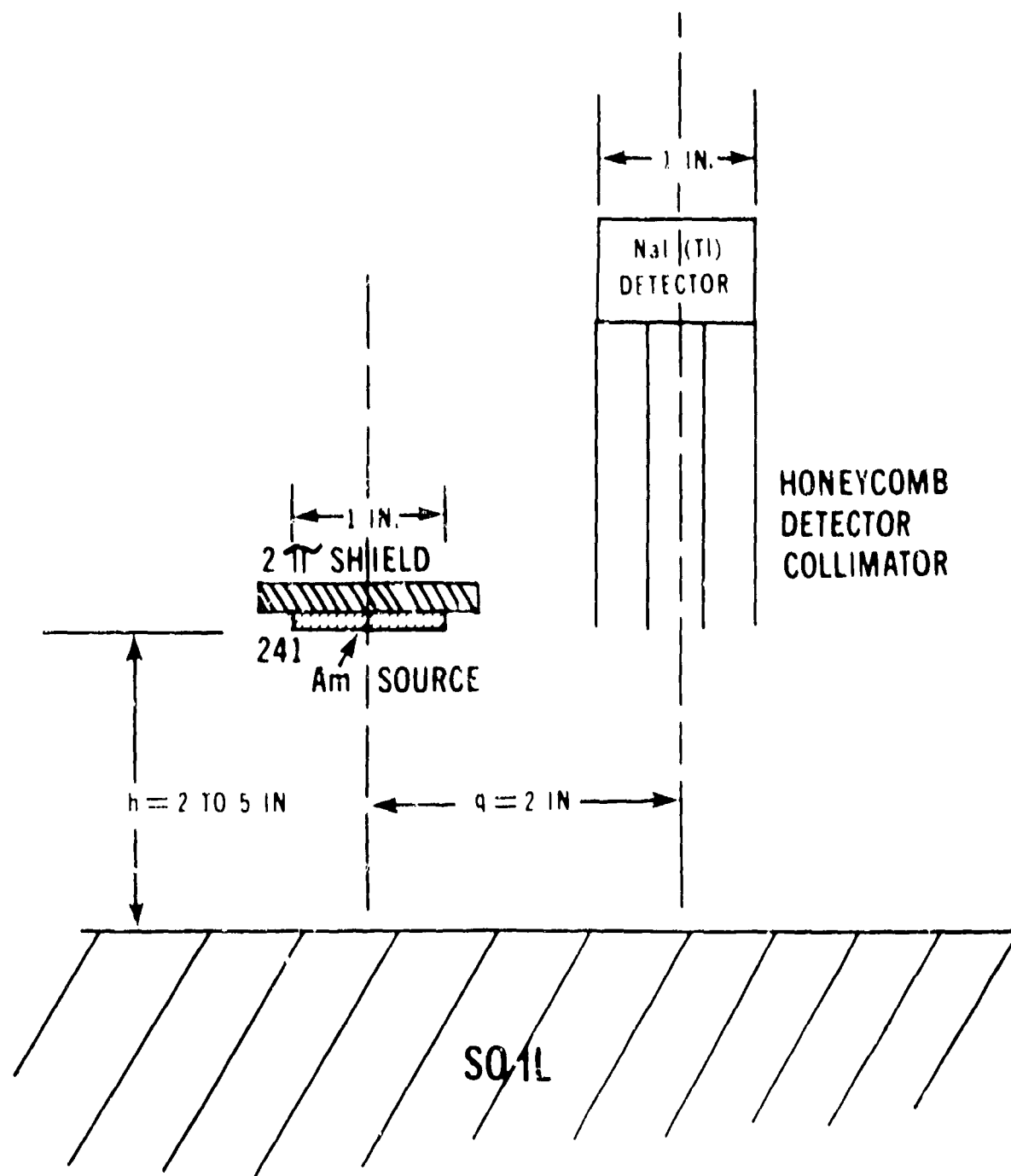


Figure 20. Geometry for K-edge filter height-compensation technique.



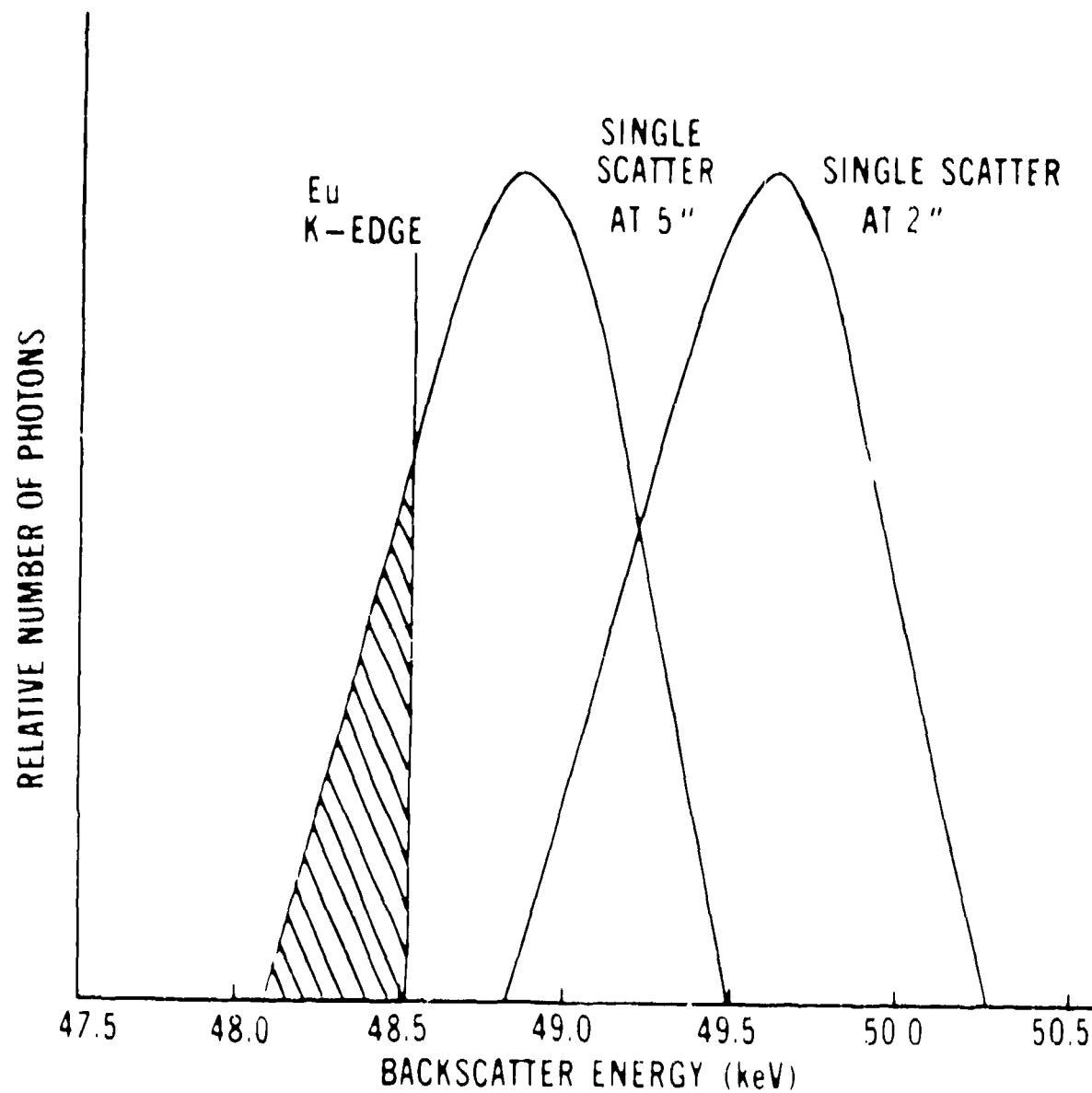


Figure 21. Computed shift of single-scatter peak with variation in height.

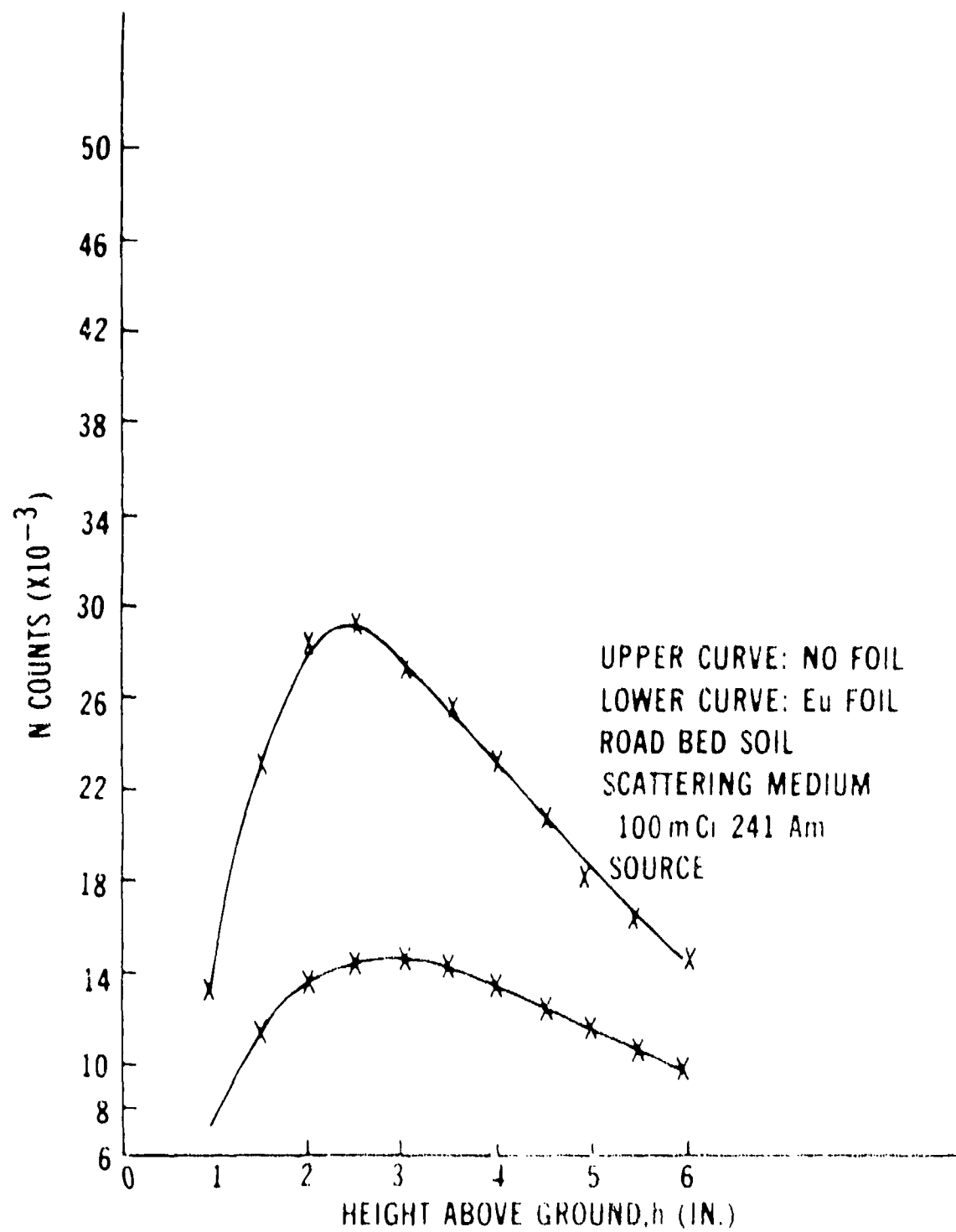


Figure 22. Variation in count of filtered and unfiltered detectors as a function of height.  
 (Data from Contract DAAK02-72-C 0619)

variations in h. This technique was instrumented in a breadboard detector which will be discussed in section IV.

### III. HISTORY

**12. Background.** In 1967, representatives of Texas Nuclear Corporation proposed the development of a mine detector based on the backscatter of gamma rays.<sup>31</sup> This proposal was based on an earlier observation made in the course of other defense research that the spectrum of backscattered radiation differs for materials of differing atomic number.<sup>32</sup> Texas Nuclear personnel reasoned that the elements found in explosives would yield a backscatter spectrum which differed from that obtained from the higher atomic number (higher Z) elements commonly found in soils. If these differences could be exploited, a mine detector based on measurement of the average atomic number might be developed.

This proposal was funded on 26 February 1968 by the U.S. Army Mobility Equipment Research and Development Center (USAMERDC), Fort Belvoir, Virginia. Contractual effort on backscatter mine-detection research was continued until June 1973. In addition to the work at the Texas Nuclear Corporation (later a division of Nuclear-Chicago Corporation), detector development was carried out by Industrial Nucleonics Corporation. Experiments were also conducted in cooperation with personnel at the Explosives Laboratory at Picatinny Arsenal, and computer simulations were performed by personnel at the Nuclear Effects Laboratory, Edgewood Arsenal (later part of the Ballistic Research Laboratories, Aberdeen Research and Development Center). As noted earlier, effort in this area now has been terminated as a result of the appraisal that the limitations of the backscatter approach outweigh its capabilities when viewed from a practical military standpoint.

Results of importance to the present discussion stemming from studies carried out at Picatinny Arsenal already have been presented in Section II. Results of the computations carried out at Edgewood Arsenal are presented in Appendix A. The purpose of the present section, then, is to recount the experimental procedures followed and the salient results obtained under contracts DAAK02-68-C-0229, DAAK02-69-C-0263, DAAK02-70-C-0105, and DAAK02-71-C-0359 with the Nuclear-Chicago Corporation and under contract DAAK02-72-C-0619 with the Industrial Nucleonics Corporation. Although more detailed accounts of these contractual efforts may be found in the final reports of the above contracts, the reader should be aware that in many instances the theoretical explanations presented in these reports for the experimental results have

<sup>31</sup> Texas Nuclear Corporation., *Investigation of Gamma Ray Backscattering for the Detection of Buried Land Mines - An Unsolicited Proposal*, 8 August 1967.

<sup>32</sup> Texas Nuclear Corporation, Final Report, Subcontract 1023-1 to Dikewood Corporation; Prime Contract AF29 (601) - 4569 (1962).

been found to be in error.<sup>33-37</sup>

**13. Contract DAAK02-68-C-0229.** The principal purpose of this contract was to explore the feasibility of photon-backscatter mine detection in a laboratory environment. To this end, the following experimental setup was employed:

A soil box, 18 by 36 by 14 inches deep, was prepared and filled with red clay ( $\sim 85 \text{ lb/ft}^3$ ,  $\sim 3$  percent  $\text{H}_2\text{O}$ , no organic content, and  $\sim 6.5$  percent Fe). The top 6 inches of the soil box consisted of four 1-inch-deep trays and one 2-inch-deep tray. This latter tray contained the target, usually a 1-pound block of dinitrobenzene (DNB), 2.5 by 3 by 1.75 inches thick. The bottom of each tray consisted of thin aluminum screening covered with 1-mil polyethylene. The purpose of the trays was to establish a reproducible geometry for various target burial depths. The sources employed were  $^{241}\text{Am}$  and  $^{137}\text{Cs}$ ; the detector was usually NaI (Tl), although others were investigated. Backscatter spectra were recorded on a 400-channel multichannel analyzer.

The experimental setup is depicted in Figure 23. With this arrangement, the following parameters could be varied:

- a. The angle of incidence of radiation from the collimated source.
- b. The angle of incidence of the detector-collimator axis.
- c. The acceptance half-angles of the source and detector collimators.
- d. The source/detector separation ( $q$ ).
- e. The height above the soil surface ( $h$ ).

---

<sup>33</sup> W. D. Miller, W. E. Tucker, and E. L. Hudspeth, *The Detection of Concealed Explosives by the Use of Gamma-Ray Scattering and Transmission Techniques*, Confidential Final Report, Contract DAAK02-68-C-0229 (October 1969), AD 506-081L.

<sup>34</sup> W. E. Tucker, W. D. Miller, and E. L. Hudspeth, *The Development of Experimental Explosives Sensors Using X-Ray and Gamma-Ray Backscatter Techniques*, Confidential Final Report, Contract DAAK02-69-C-0263 (June 1971), AD 402-9106.

<sup>35</sup> W. E. Tucker and W. D. Miller, *Design and Construction of a Man-Portable Gamma-Ray Explosives Sensor*, Confidential Final Report, Contract DAAK02-70-C-0105 (January 1972), AD 519-617L.

<sup>36</sup> W. D. Miller, M. N. Anastasi, and W. E. Tucker, *The Design, Construction, and Testing of an Advanced Experimental Model Portable AP Mine Detector (Gamma-Ray)*, Confidential Final Report, Contract DAAK02-71-C-0359 (March 1973), AD 403-0097.

<sup>37</sup> Mason L. Thompson, *Advanced Experimental Model AP Detector (Gamma Ray)*, Confidential Final Report, Contract DAAK02-72-C-0619 (August 1973), AD 526-7422.

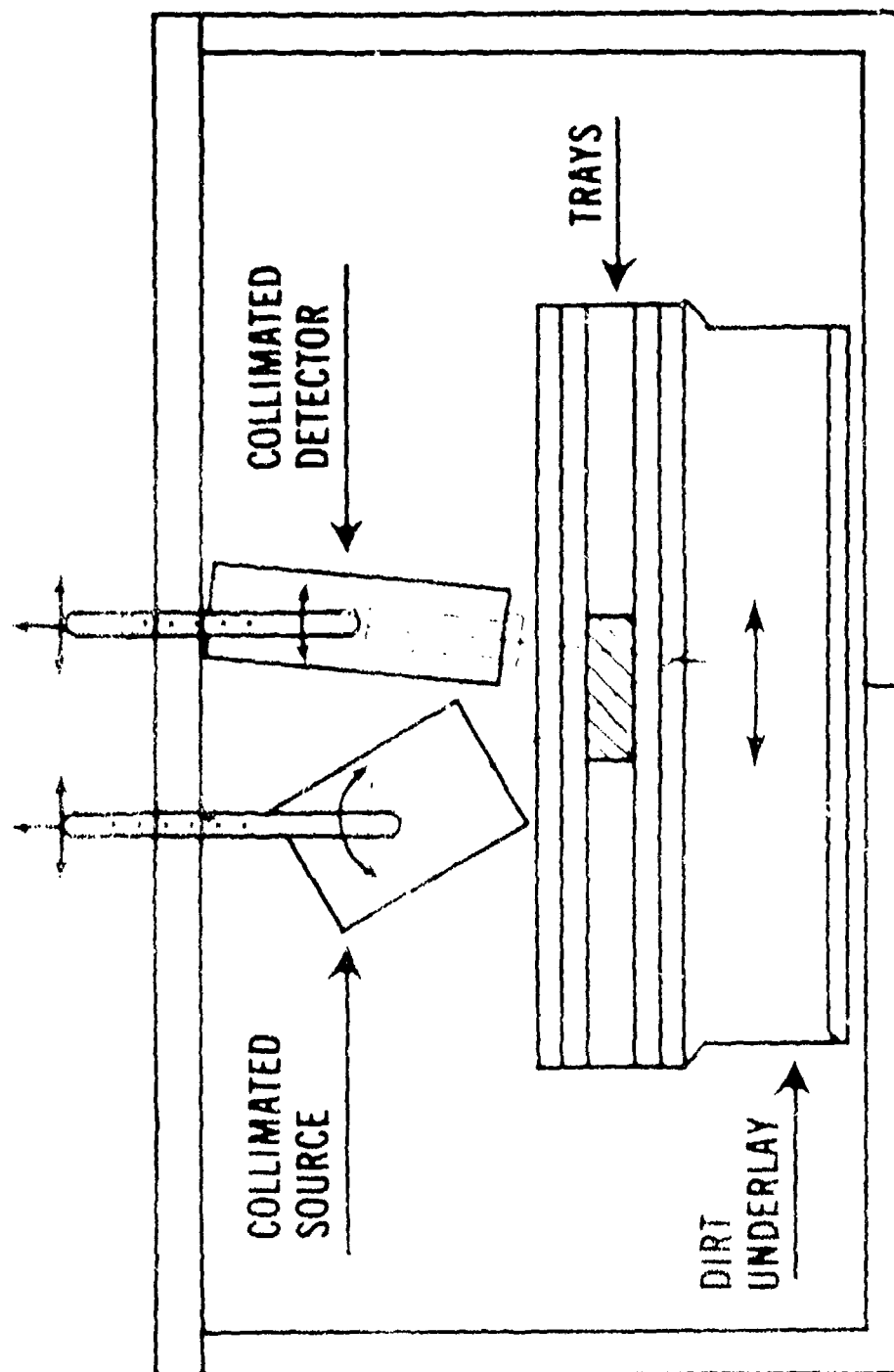


Figure 23. Initial experimental setup. (After Miller, Tucker, and Hudgorth; Contract DAK 02-68-C-6229)

The first series of experiments performed with this apparatus concerned the selection of source type and the establishment of criteria for mine detection. As noted in Section II, both the amplitude and shape of a backscatter spectrum will change as the  $\langle Z \rangle$  of the scattering medium is varied. However, use of a  $^{137}\text{Cs}$  (662-keV) source under the more realistic condition of a finite DNB target buried under a soil overburden revealed that only a small change in the lowest energy portion of the spectrum could be observed. (See Figure 14.) (Note that the variation at  $\sim 200$  keV is due to a density change rather than to a  $\langle Z \rangle$  change.) By utilizing an  $^{241}\text{Am}$  (60-keV) source, however, the target was manifested as a general increase in amplitude over the entire spectrum. See Figure 15. The lack of a shift in the energy distribution of backscattered photons was ascribed to the severe attenuation of the lowest energy photons by the soil overburden. On this basis, it was decided that: (a) the criterion for mine detection should be a percentage increase ( $\Delta\phi/\phi$ ) in the integrated countrate above some lower level set to exclude only photomultiplier dark current, and (b), in order to maximize this percentage increase, the source energy should be as low as possible consistent with an acceptable countrate. In general, photons of energies from 50 to 200 keV were considered to possess the greatest promise for mine detection. Consequently, further effort under this contract was performed with an  $^{241}\text{Am}$  source, and an X-ray generator ( $\sim 140$  kVp) was ordered for use in future studies.

The second series of experiments conducted concerned the selection of source/detector geometry. Since the experimental setup consisted of a collimated source (in this case, 1 Ci  $^{241}\text{Am}$ ) and a collimated detector, experiments were limited to variations of this arrangement. By varying the included angle between source- and detector-collimator axes ( $\theta$ ), it was determined that (a)  $\Delta\phi/\phi$  increased as the depth of intersection of the axes increased, (b)  $\Delta\phi/\phi$  greatly decreased whenever the detector "saw" an appreciable amount of single-scatter radiation, and (c)  $\Delta\phi/\phi$  increased as  $q$  decreased. This last result, which appears to contradict statements made in Section II, may be seen to follow from the limitations of the experimental setup:  $q$ , in all cases, exceeded the linear dimensions of the target. Further, by varying  $h$ , it was determined that the change in  $\phi$  as  $h$  was varied ( $\Delta\phi/\Delta h$ ) was minimized by minimizing  $\theta$ . By varying the half-angle at the source collimator, it was observed that  $\Delta\phi/\Delta h$  could be reduced further by tightly collimating the source (although, on the negative side, this also greatly reduced  $\phi$ ).

On the basis of the above, it was determined that the optimal system for mine detection would consist of a tightly collimated source and detector, as close as possible to each other, with a small angle included between the source and detector collimator axes.

The purpose of the third series of experiments was to determine the type of response to be expected from a variety of artifacts which might be encountered in the

soil. For these experiments, the included angle  $\theta$  was set at  $35^\circ$ . The artifacts were: blocks of wood, aluminum, granite, and limestone, each 2 by 8 by 2 inches deep; and a container of water of similar dimensions. A DNB block was, in each case, used for comparison. The artifacts were emplaced at depths of 0 inch (flush), 1 inch, 2 inches, and 4 inches. Two soil conditions were considered: dry ( $\sim 3$  percent  $H_2O$ ) and moist ( $\sim 20$  percent  $H_2O$ ). Table 3 shows the results of these experiments in terms of the ratio  $R$  of the countrate obtained over an artifact to the countrate obtained over soil. In general, it was found that  $R$  was greater than unity for wood and water, as well as for DNB, and was less than unity for the aluminum, granite, and limestone. (Difficulty was encountered in repacking the soil trays to uniform density, resulting in certain instances in  $R$  values less than unity for wood, water, and DNB.) From the data shown in Table 3, it may be observed that: (a) smaller values of  $R$  obtain under identical circumstances when appreciable soil moisture is present; and (b), with the geometry employed, increases in the backscatter countrate are observable for low- $Z$  inclusions buried at depths of up to 2 inches in dry soil and 1 inch in moist soil.

Table 3. Backscatter Information From DNB and Other Artifacts Emplaced in Moist and Dry Soil

Artifact	Emplacement Depth (In.)			
	0 (Flush)	1	2	4
Ratio (R) in Dry Soil				
DNB	7.14	2.17	1.08	0.89
Wood	10.98	2.70	1.08	0.88
Water	8.33	2.63	1.15	0.92
Aluminum	0.14	0.55	0.87	0.87
Granite	0.29	0.71	0.95	0.95
Limestone	0.14	0.58	0.87	0.94
Ratio (R) in Moist Soil				
DNB	6.25	1.68	0.91	0.78
Wood	10.40	1.81	0.85	0.80
Water	7.14	1.64	0.85	0.73
Aluminum	0.13	0.64	0.79	0.79
Granite	0.31	0.63	0.72	0.72
Limestone	0.13	0.50	0.72	0.71

Finally, some attention was given to the selection of detectors for the mine-detection application. Geiger tubes, ionization chambers, and Si(Li) and Ge(Li) solid-state detectors were considered; some experiments were conducted with plastic scintillators (NE 102 and 10 percent lead-loaded Pilot B). These demonstrated that the

count rate obtained with plastic scintillators is excessively sensitive to small gain changes and, thus, would not be stable enough for field application. Geiger tubes were dismissed because they are not capable of operating at more than a few thousand cps. Since energy resolution of the backscattered flux was not required, Ge(Li) and Si(Li) were not considered promising; however, the possibility of using Si(Li) in the future was left open because Si(Li) detectors of large enough volume (high enough efficiency) may be obtained at some time in the future [Si(Li), unlike Ge(Li), does not require cryogenic cooling]. The possibility of using ionization chambers in a vehicle-mounted system also was left open, since a large-volume detector was considered feasible for that application. Ionization chambers were not considered feasible for a man-portable device since, in order to achieve reasonable efficiency, a high-pressure chamber would have to be employed. Such a chamber necessarily must have a thick window, which, in turn, would severely attenuate the backscatter flux.

**14. Contract DAAK02-69-C-0263.** Contract 0229 (paragraph 13) established the feasibility of utilizing photon backscatter to detect explosives buried under soil overburdens. The initial phase of Contract 0263 sought to determine the nature of the underlying phenomena which made this technique feasible. Later phases of this contract concerned the establishment of design parameters for man-portable and vehicular mine detectors. Finally, an experimental, vehicle-mounted detector was fabricated, and limited field tests were performed. (Discussion of this final phase of Contract 0263 will be deferred to section IV.)

At the outset of Contract 0263 it was assumed that the interaction mode of primary importance for mine detection was single scatter. According to this model, the increase in backscatter observed over the target was due to the decrease in attenuation of the incident and return beams as they passed through the target. See Figure 24. A computer program simulating this model was executed, assuming an  $^{241}\text{Am}$  source and various target thicknesses and emplacement depths. Some of the results thereby obtained are shown in Figure 25. Note that R remains constant as emplacement depth increases until the target enters the crossover region; beyond this point, R decreases rapidly as emplacement depth increases.

In order to test these results, an experiment was performed which simulated as closely as possible the configuration shown in Figure 24. The results, shown in Figure 26, revealed a roughly exponential decrease in R as emplacement depth was increased, in complete contradiction to the computer results. It was, therefore, concluded that single scatter could not be the mode of interaction of greatest import for mine detection. Further studies were performed using this geometry, replacing the 60-keV  $^{241}\text{Am}$  source with an X-ray generator operated at 80, 110, and 130 kVp. Results of these experiments are shown in Figure 27. (It should be noted that, since error bars are not shown, there is some question as to whether or not the curves shown cross as emplacement depth



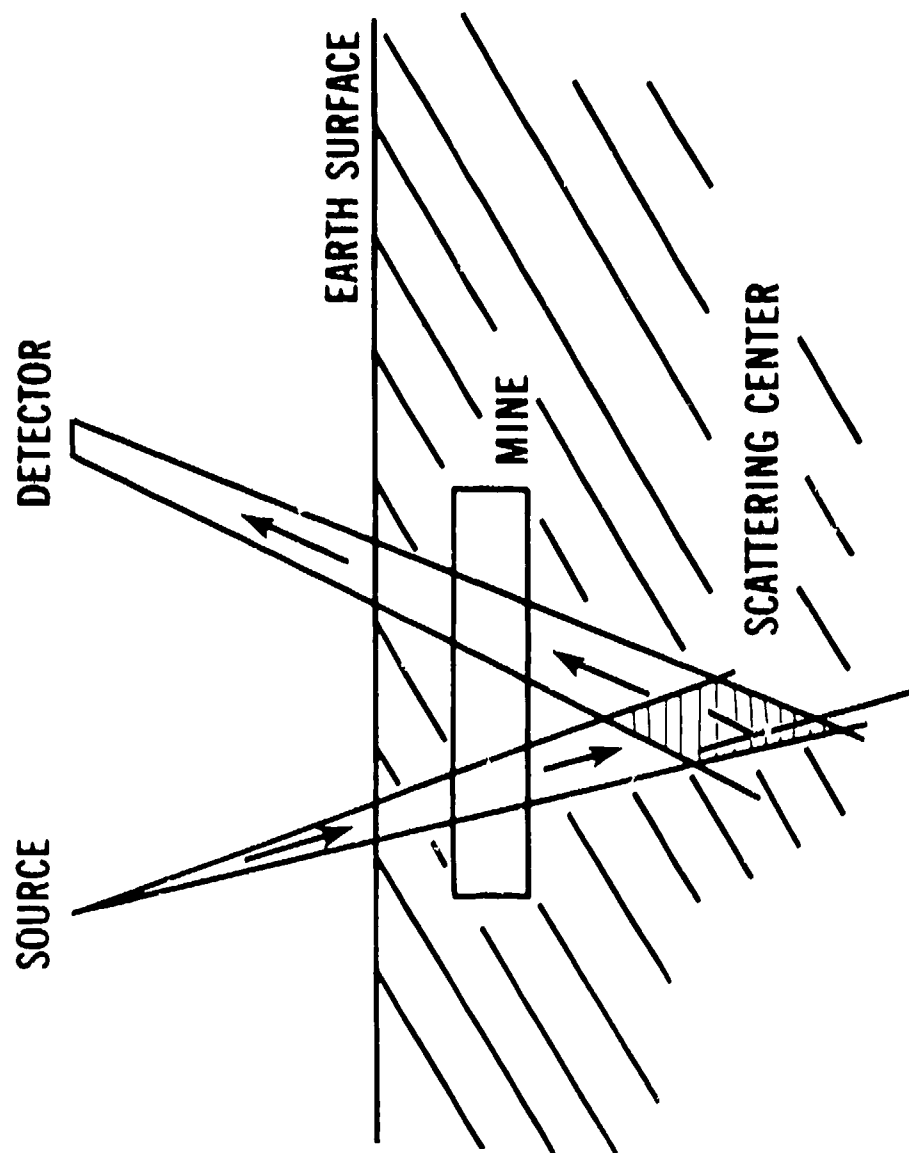


Figure 24. Model for single-scatter computation. (After Tucker, Miller, and Hudspeth: Contract DAAK02-69-C-0263)

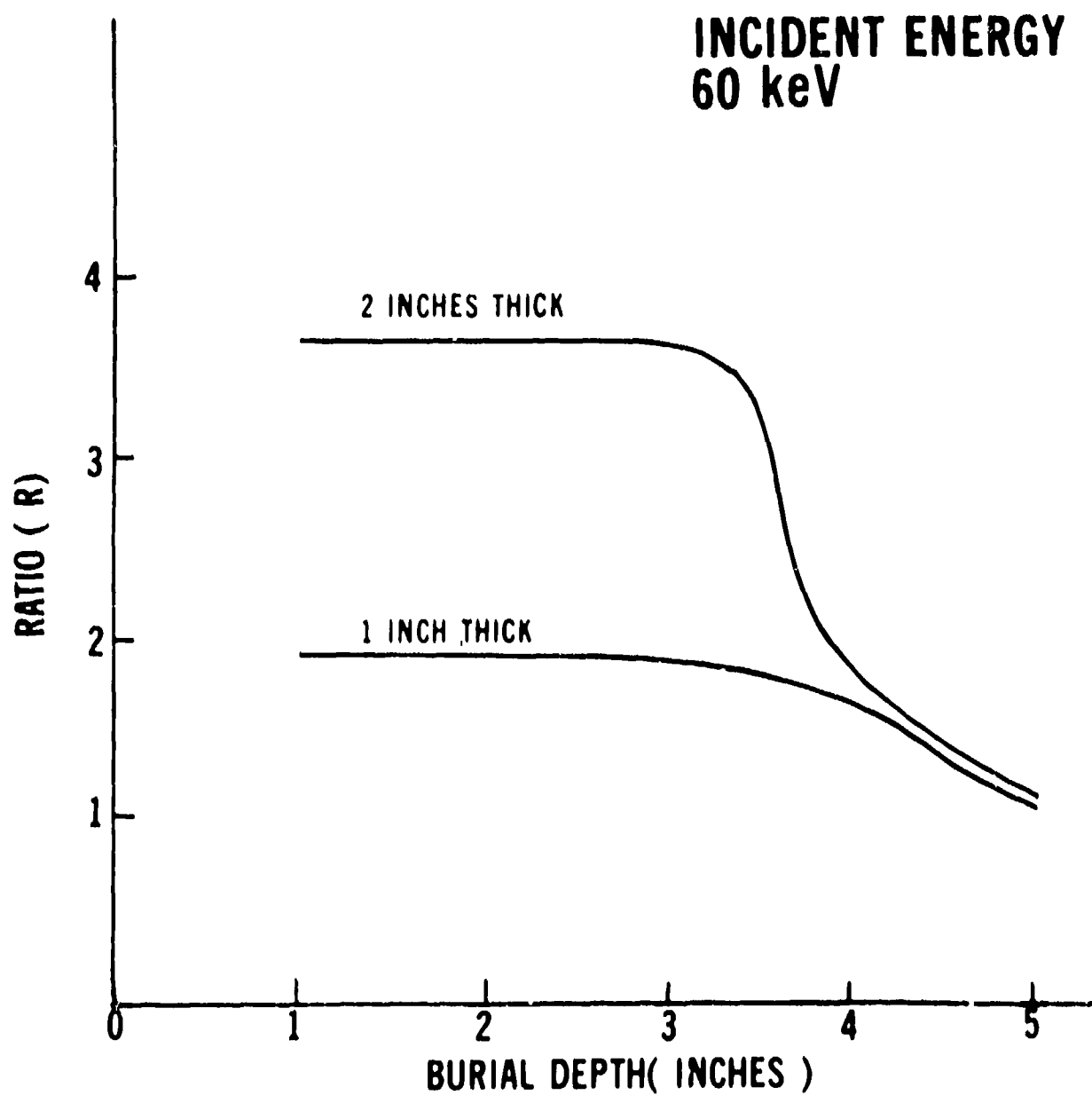


Figure 25. Results of single-scatter computation. (After Tucker, Miller, and Hudspeth; Contract DAAK02-69-C-0263)

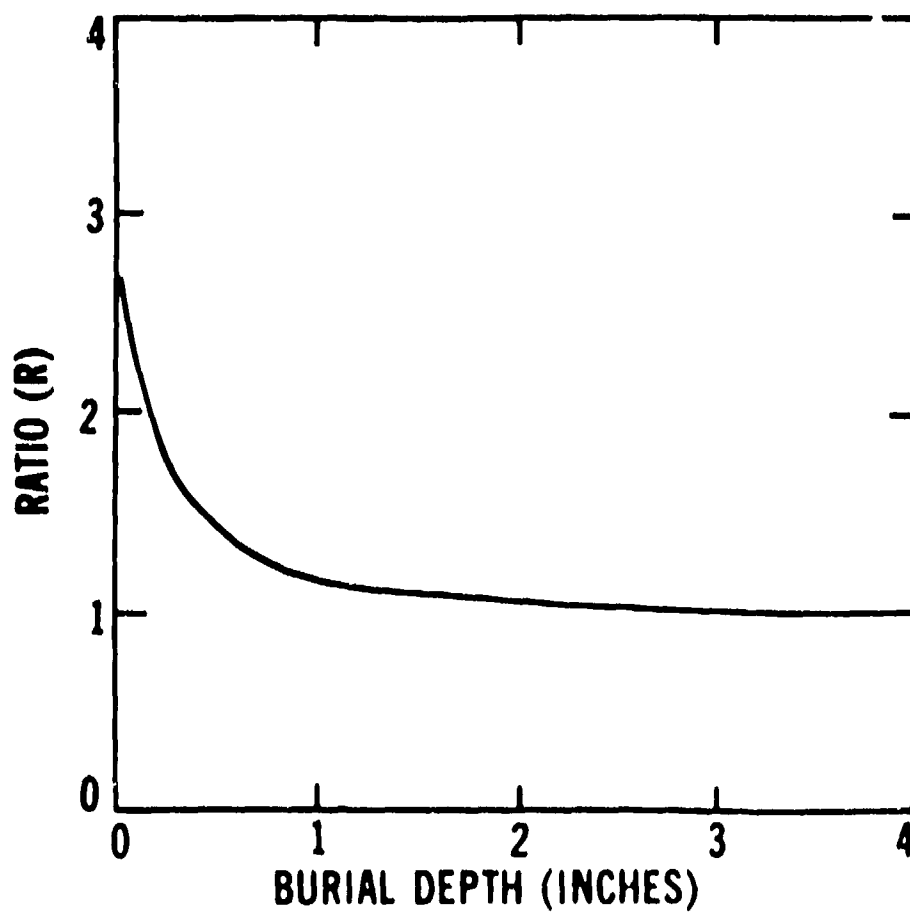


Figure 26. Experimental values of R for the geometry shown in Figure 24. (After Tucker, Miller, and Hudspeth; Contract DAAK02-69-C-0263)

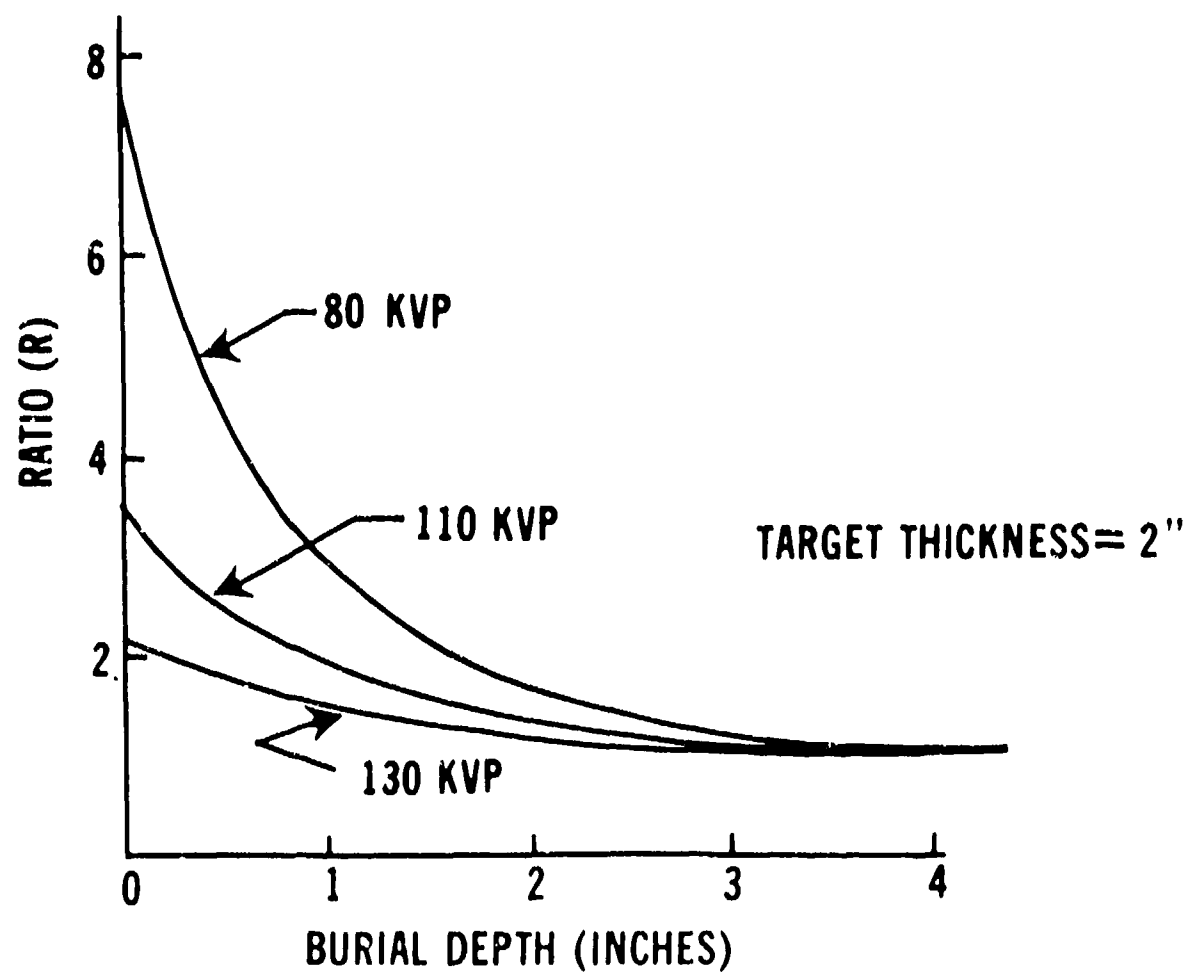


Figure 27. Experimental values of R obtained with X-ray source. (After Tucker, Miller, and Hudspeth; Contract DAAK02-69-C-0263)

increases. This question, at present, is still unresolved.)

Since a single-scatter model clearly did not satisfy the experimental results, another model had to be developed. To this end, a series of experiments, known as "iron curtain" experiments, was performed.

A 3/8-inch-thick iron sheet, perpendicular to the plane of the source and detector collimator axes, was inserted in the middle of a DNB target. See Figure 28. The effect of this "iron curtain" was to prevent the horizontal flow of photons from one half of the target into the other. An X-ray generator, operated at 80, 110, and 130 kVp, was used as the source. The emplacement depth of the target then was varied from 0 to 4 inches. The result (Figure 29) was that, instead of the usual decrease in backscatter flux as target depth increased, there was a gradual increase in backscatter flux. On the basis of this experiment, it was concluded that the target itself furnished a low-attenuation path for photons to pass from source to detector. Geometrically, for photons to follow such a path, they must be scattered two or more times. Consequently, it was concluded that multiple scatter was the interaction mode of principal importance for mine detection.

The second phase of this contract concerned the establishment of design parameters for a vehicle-mounted detector through the parametric variation of source energy and certain geometric variables. To this end, the soil box constructed for contract 0229 was employed. The source was a Norelco PG-140 X-ray generator, continuously variable from 20 to 140 kVp and from 0 to 5 mA. The X radiation generated was vertically incident on the soil surface and had a beamspread half-angle of  $3^\circ$ . The detector was a Harshaw NaI(Tl) scintillator, 1.5 inches in diameter by 1 inch thick, with an  $8^\circ$  half-angle collimator. The target for these experiments was a 2 by 8 by 2-inch-thick DNB block aligned with its long axis in the source/detector plane. See Figure 30. The geometrical parameters varied in these experiments were  $h$ ,  $q$ , mine emplacement depth ( $d$ ), and angle of incidence of the detector-collimator axis ( $\theta$ ). The range of variation for each of the variables is shown below.

#### Range of Variables for Parametric Study (Vehicular)

<u>Variable</u>	<u>Values</u>
E (kVp)	90; 110; 130
$\theta$ (Deg)	0; 5; 10; 15; 20
h (In.)	13.5-19.5 (1-inch Increments)
q (In.)	8.75; 9.25; 9.75; 10.25
d (In.)	0; 1; 2; 3; 4

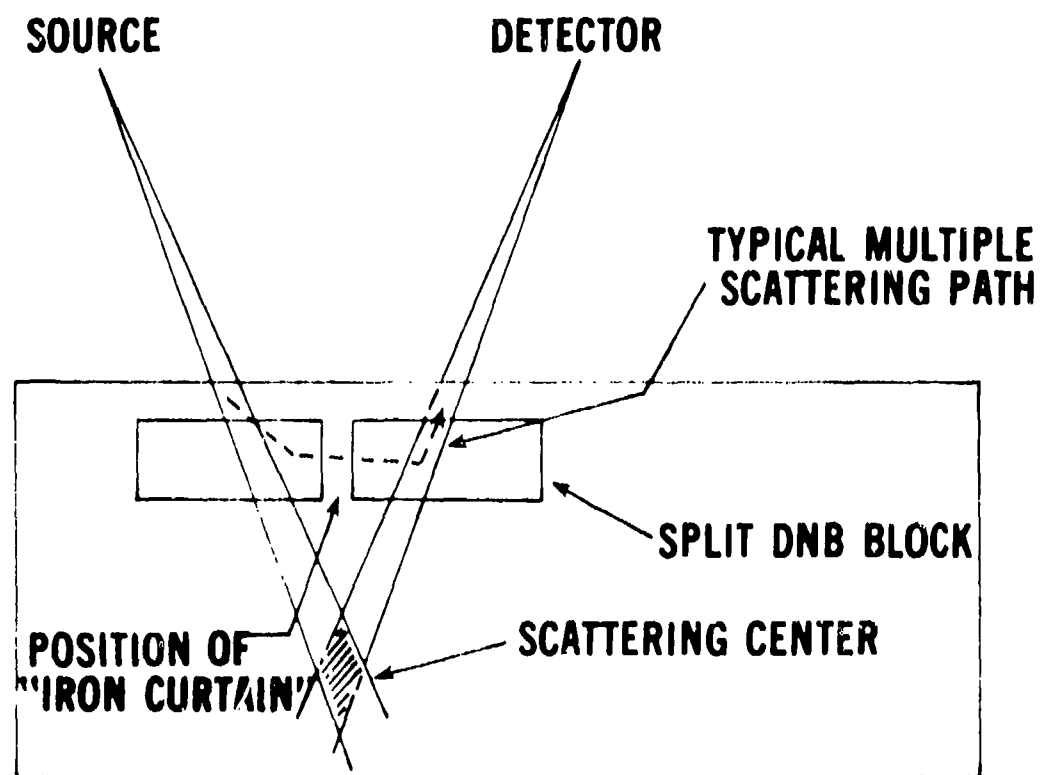


Figure 28. Geometry for "iron curtain" experiments. (After Tucker, Miller, and Hudspeth; Contract DAAK02-69-C-0263)

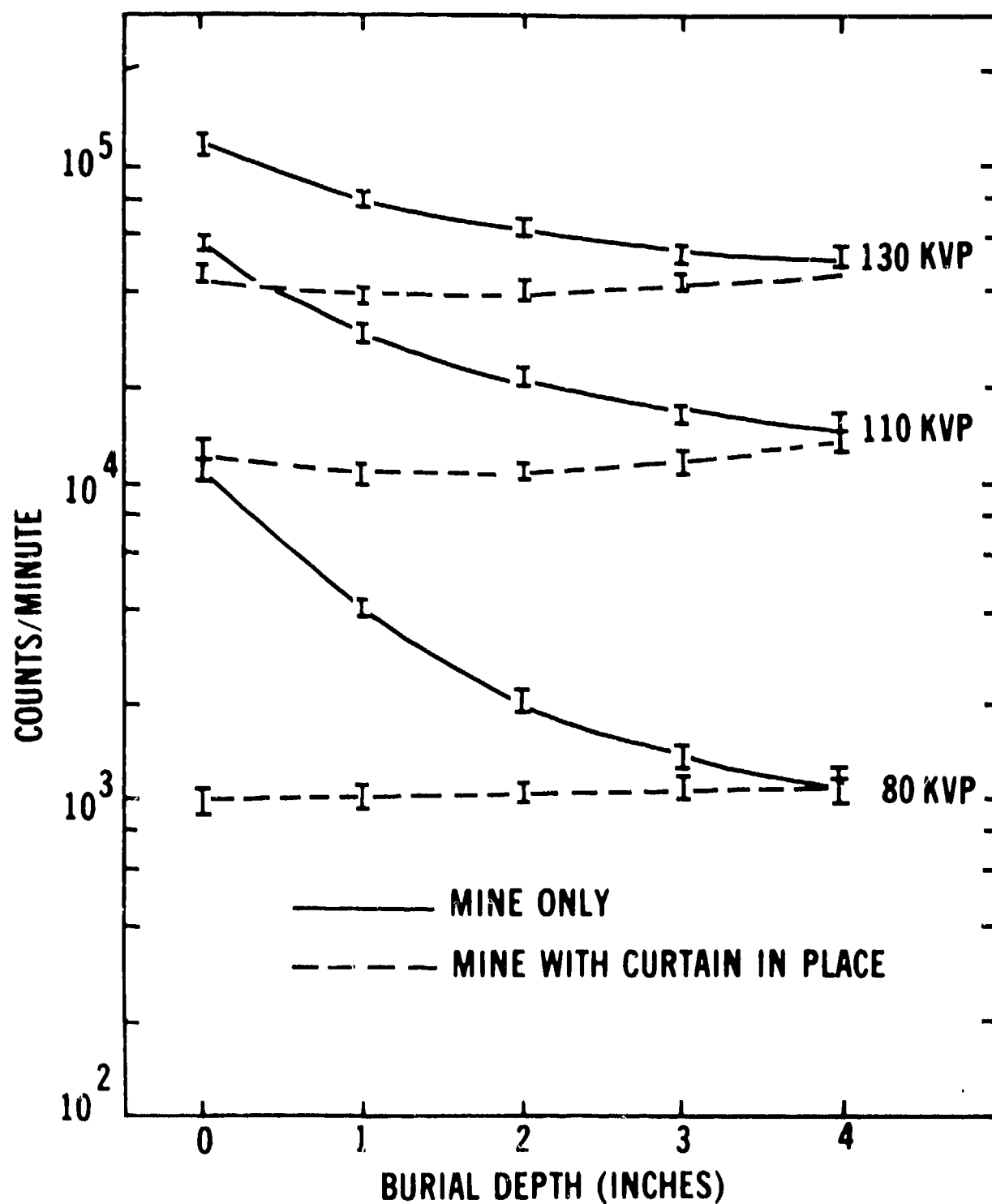


Figure 29. Results of "iron curtain" experiments. (After Tucker, Miller, and Hudspeth; Contract DAAK02-69-C-0263)

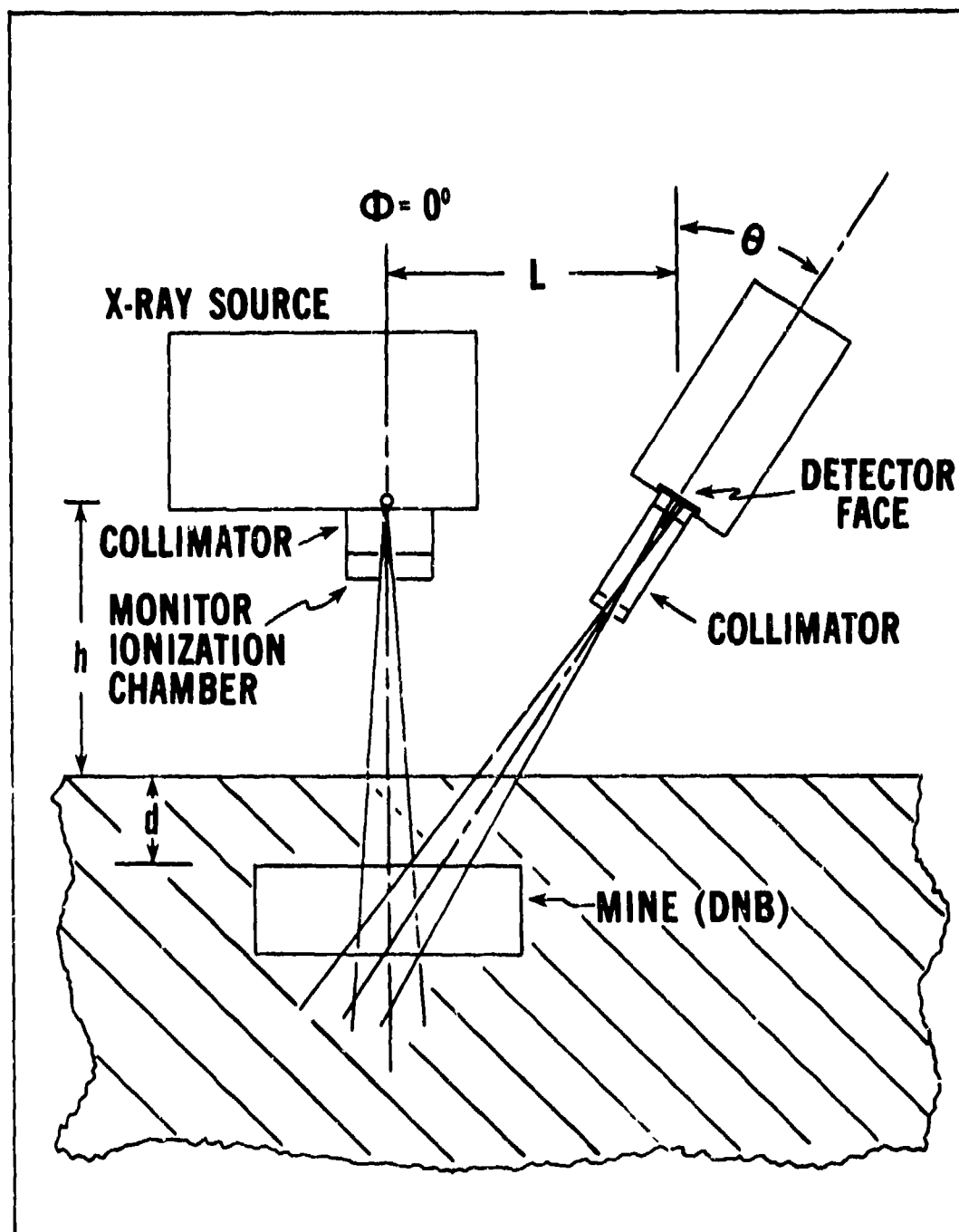


Figure 30. Geometry used for parametric studies. (After Tucker, Miller, and Hudspeth; Contract DAAK02-69-C-0263)



As a result of this study, values for the geometric and energy variables were selected for incorporation in a vehicular detector which (a) maximized  $R$ , (b) minimized  $\Delta\phi/\Delta h$ , and (c) maximized  $\phi$ .

By varying  $\theta$  and  $q$ , test personnel observed that the  $\theta$ -value at which maximum- $R$  obtained decreased as  $q$  decreased. Further, it was observed that the maximum  $R$  value increased as  $q$  decreased. By extrapolation, then, it was inferred that the highest  $R$  value would obtain for  $\theta=0$  and  $q \cong 7$  inches (i.e.,  $q$  slightly less than the length of the target).

By varying  $E$  and the target emplacement depth ( $d$ ), it was determined that: (a) for  $d < 2$  inches,  $R$  increased as  $E$  decreased; (b) for  $d = 2$  inches,  $R$  was roughly independent of  $E$ ; and (c) for  $2 < d < 4$  inches,  $R$  increased as  $E$  increased. The value of  $R$  was essentially unity (no detection) for  $d > 4$  inches. See Figure 31. In all cases,  $\phi$  increased as  $E$  increased. (It should be noted that for this part of the study the target was a 9.5-inch-diameter by 3.5-inch-thick block of DNB.)

By varying  $E$ ,  $h$ ,  $q$ , and  $\theta$ , it was determined that: (a) for constant  $q$  and  $\theta$ ,  $R$  was independent of  $h$  (and, for  $d = 2$  inches, independent of  $E$ ); (b) for constant  $E$  and  $q$ ,  $\Delta\phi/\Delta h$  was a minimum for  $\theta=0$  and increased as  $\theta$  increased; and (c) no unambiguous dependence of  $\Delta\phi/\Delta h$  on either  $q$  or  $E$  was found.

Based on the above, it was decided that the optimal parameters for a vehicle-mounted, photon-backscatter mine detector would be  $\theta=0$ ,  $q \cong$  expected target diameter, and  $E > 130$  kVp for an X-ray source. No upper bound was determined for  $E$  since the maximum operating potential for the X-ray generator employed was 140 kilovolts. It also should be noted that the optimal  $E$  value for an X-ray source is not necessarily that for a gamma source; an X-ray target produces a spectrum of energies, the number of photons per unit energy interval decreasing as energy increases, with essentially no photons being produced at the operating potential of the tube.

In addition to the parametric studies, the above experimental setup was used to determine the effects of soil-density variations and of disturbed soil. The red clay first was replaced with sand, the latter having a density of  $1.8 \text{ g/cm}^3$ , as opposed to  $1.36 \text{ g/cm}^3$  for the former. The results, obtained for different values of  $E$  and  $d$ , are shown in Figure 32. Note that, for flush emplacement,  $R$  values are higher for sand than for clay. However, the slopes of the  $R$ -versus- $d$  curves for sand are steeper, with an energy crossover at 1 inch (instead of at 2 inches) and with the point of zero detection occurring at  $\sim 3$  inches (as opposed to  $\sim 4$  inches).

Next, a soil box of uniform density ( $1.7 \text{ g/cm}^3$ ) was prepared. A volume at the surface of the soil, 12 inches in diameter and 4 inches deep, was removed and

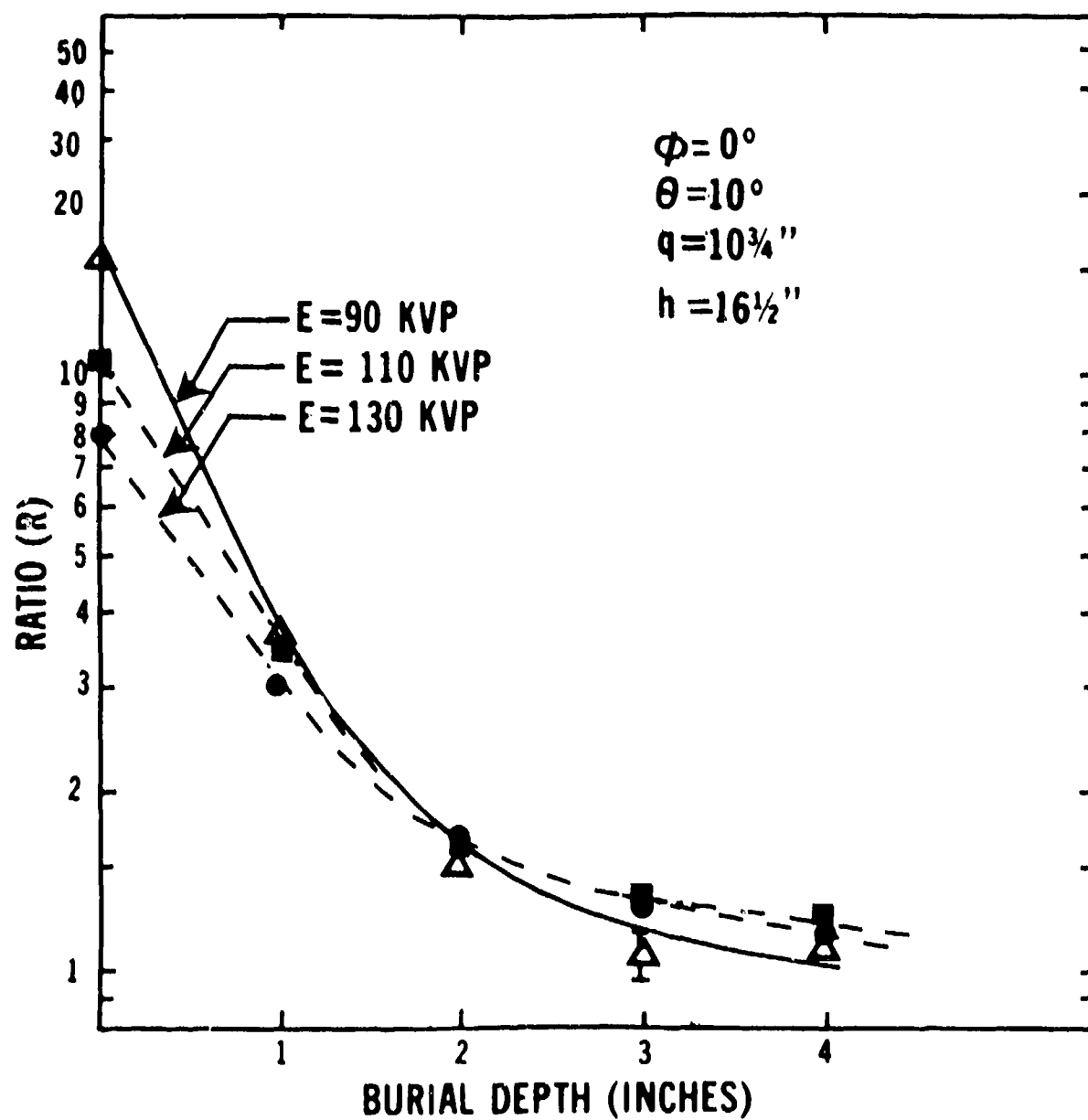


Figure 31. R versus emplacement depth in red clay for different X-ray tube potentials.  
 (After Tucker, Miller, and Hudspeth; Contract DAAK02-69-C-0263)

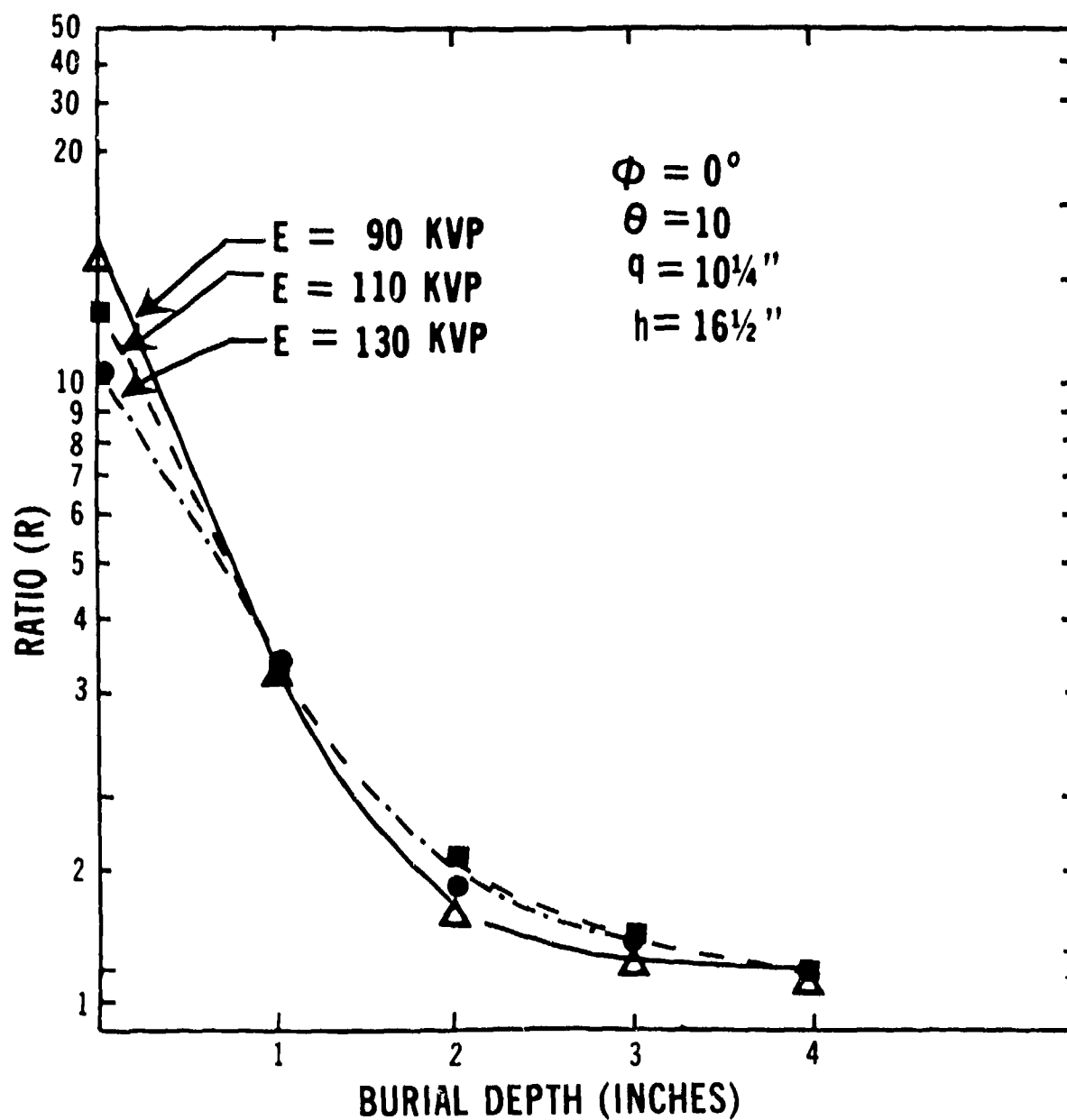


Figure 32. R versus emplacement depth in sand for different X-ray tube potentials.  
 (After Tucker, Miller, and Hudspeth; Contract DAAK02-69-C-9263)

replaced with some of the same soil but with a different air-void fraction. Surface density was varied in this manner from 1.0 to 1.7 g/cm<sup>3</sup>. Backscatter measurements made over this area showed values of R greater than unity, decreasing from 2.2 to 1.0 over the designated density range.

Whether or not this sensitivity to disturbed soil is desirable in a mine detector is debatable. On the positive side, the soil over a freshly emplaced mine is not likely to be as well compacted as the soil in the surrounding area. Thus, a mine, no matter how deeply buried, might be sensed by detecting the disturbed soil above it. On the negative side, any naturally occurring soil-density variation of appropriate spatial frequency would produce a false alarm. In addition, once the mode of detection became known to the enemy, he could generate false alarms (i.e., refilled holes) at will for purposes of harassment.

The third research phase of Contract 0263 consisted of an attempt to establish design parameters for a man-portable mine detector. To that end, a 1 Ci<sup>241</sup>Am source was employed. (At that time, X-ray sources light enough to be considered for the man-portable application were beyond the state of the art.) The detector was 1-inch-diameter by 1-inch-thick NaI (Tl). The principal difference between this and the preceding phase of the work was that, in this latter case, the source and detector collimators were quite "loose." A source half-angle of ~40° and a detector half-angle of ~50° were utilized in order to achieve reasonable countrates. As a result, there was considerable overlap of source and detector collimator cones. See Figure 33.

The targets for this study were 2- by 2- by 4-inch blocks of DNB emplaced in a red-clay soil medium at depths of ½ and 1 inch. As before, h, q, and d were parametrically varied. However, in this case,  $\varphi$  (the angle of incidence of the source collimator axis) was varied, and  $\theta$  was held constant at 0°. The range of variation for each parameter is shown below.

#### Range of Variables for Parametric Study (Man-Portable)

<u>Variable</u>	<u>Values</u>
$\varphi$ (deg)	-10° to 35° (5° increments)*
h (in.)	2.75; 3.75; 4.75
q (in.)	3 to 5 (0.5-inch increments)
d (in.)	0.5 and 1.0

\* Negative values of  $\varphi$  refer to the source collimator axis sloping away from the detector.

Results of this study demonstrated, once again, that optimal values for R occur for  $\varphi = \theta = 0^\circ$  and for  $q \cong$  target diameter. However, the R-values obtained in this

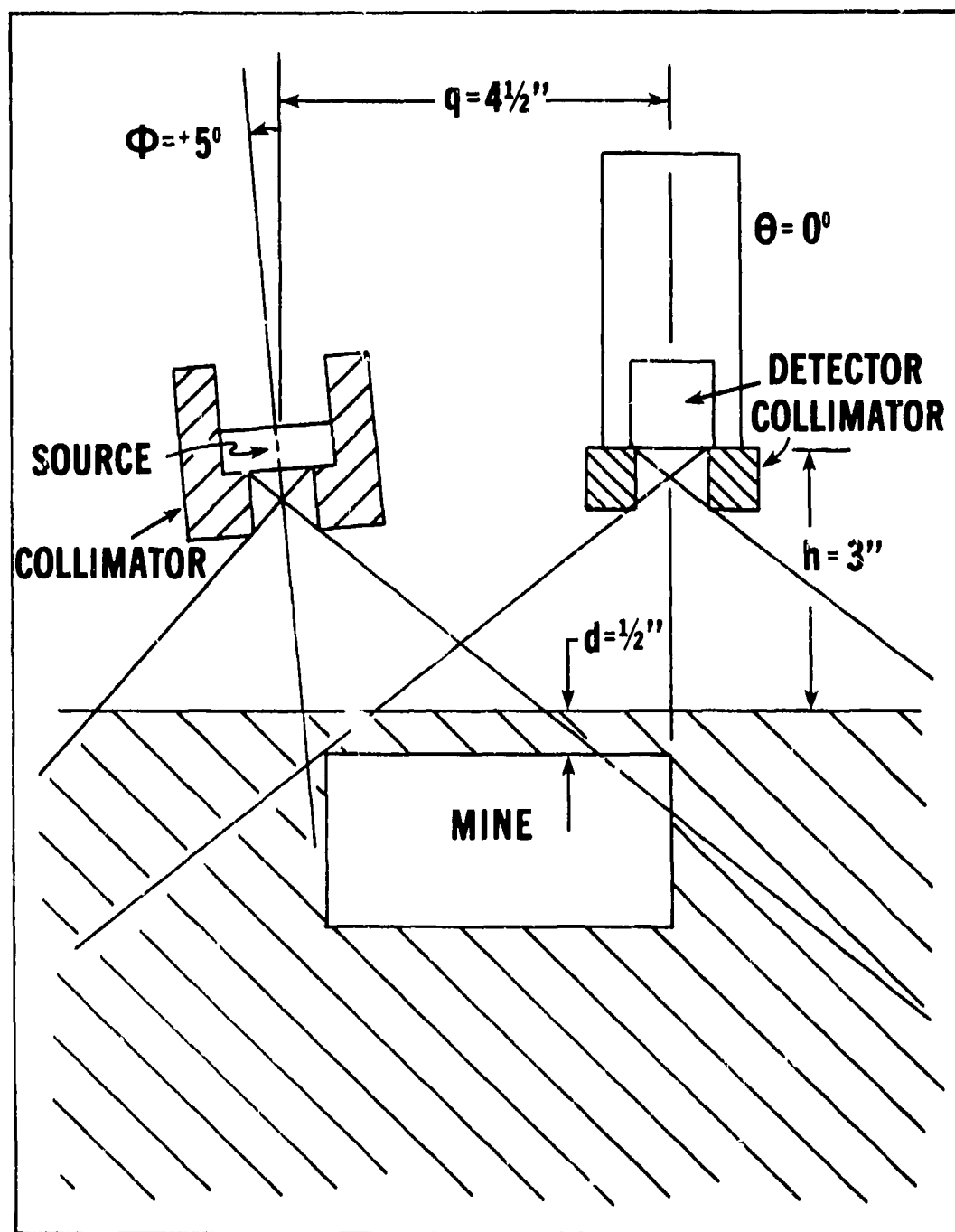


Figure 33. Initial geometry for man-portable detector experiments. (After Tucker, Miller, and Hudspeth; Contract DAAK02-69-C-0263)

case were considerably lower than those obtained previously, primarily because single scatter near the surface was not geometrically excluded. In addition,  $R$  was found to decrease as  $h$  increased (due to the loose collimation, the target-volume/soil-volume ratio decreased as  $h$  increased), and  $\phi$  decreased rapidly as  $h$  increased. For these reasons, it was concluded that no collimated-source-collimated-detector geometry utilizing an isotropic source could be employed in a practical man-portable mine detector.

Effort on developing a man-portable detector would have been terminated after Contract 0263 had not a radically different geometrical approach, conceived by Wendell Miller of the Nuclear-Chicago Corporation, been instrumented in a breadboard detector without benefit of prior laboratory studies. This device, depicted in Figure 34, was demonstrated at Fort Belvoir during the 4th quarter of Fiscal Year 1969. The device consisted of a 14 mCi  $^{241}\text{Am}$  source coaxially mounted with a NaI (Tl) detector. The source was housed in a "stepped" collimator, tapered toward the scintillator surface, and flared about the radiation exit port. Total searchhead weight was  $\sim 3$  pounds. Signal-processing and alarm electronics were rack-mounted. This device demonstrated the capability of detecting 1-pound blocks of DNB emplaced at depths of up to  $\sim 1$  inch in a homogeneous, inorganic soil medium. The device had to be held at a relatively constant distance ( $\sim 1.5 \text{ inch} \pm 1 \text{ inch}$ ) from the soil surface and scanned very slowly; but, the capability it demonstrated had been unattained previously by any mine-detection technique. In view of the encouraging performance of this breadboard device and of the pressing need to field a device capable of locating small, shallowly buried, nonmetallic mines, it was decided to forgo the usual research phase of development and to attempt to fabricate prototype detectors capable of field evaluation. This effort was funded in December 1969.

15. Contract DAAK02-70-C-0105. The primary objective of this contract was to design, develop, fabricate, test, and deliver two experimental, man-portable, gamma-ray backscatter mine detectors utilizing the coaxial source/detector geometry discussed above.<sup>38</sup> The decision to proceed immediately with the construction of experimental models, without first performing extensive laboratory studies, resulted from two factors: (a) The success of the breadboard detector which had been demonstrated the previous spring, and (b) the need to field a detector capable of locating small, near-surface anti-personnel mines as expeditiously as possible. In retrospect, this decision was a mistake. The detector searchheads delivered under the contract, while principally differing from the breadboard model in containing two detecting elements rather than one (each incorporating a 100-mCi, rather than 14-mCi  $^{241}\text{Am}$  source), also contained some rather minor geometrical changes. The results of these minor changes, however, proved to be rather major. The experimental detectors were capable of locating only large blocks of

<sup>38</sup> Normally, discussion of Contract DAAK02-70-C-0105 would be deferred to section IV, since this contract was concerned primarily with hardware development. Its inclusion in section III is necessary, however, in order to achieve chronological clarity.

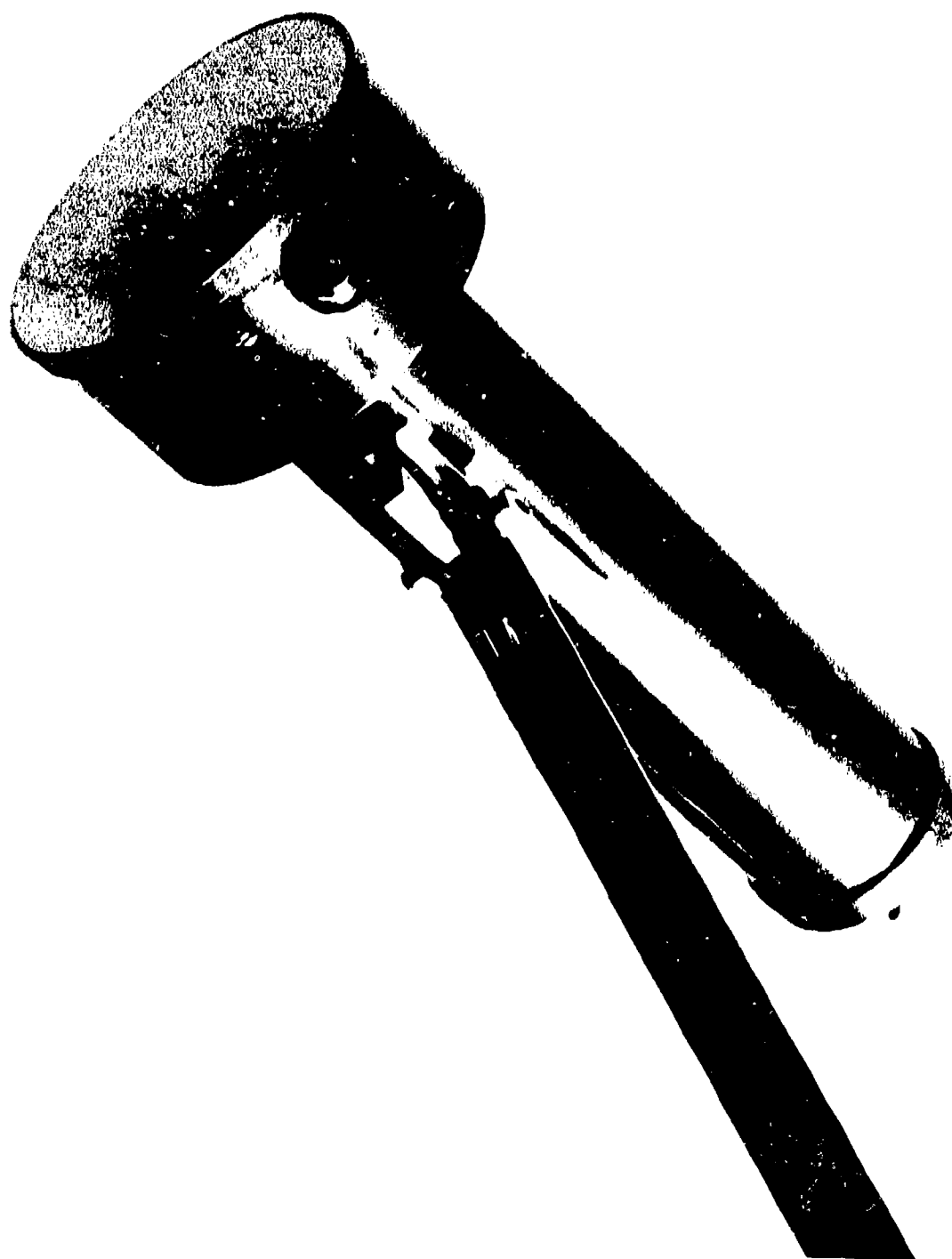


Figure 34. First man-portable searchhead.

S9044

explosives (~ 20 pounds) which were essentially flush with the surface. With the recognition of the dangers inherent in attempting to implement a technique not fully understood, a new contract was awarded which required performance of the type of laboratory investigations previously neglected.

**16. Contract DAAK02-1-C-0359.** The initial objective of this contract was to gain an understanding of the design criteria for a coaxial backscatter sensor by means of an extensive parametric investigation of the geometrical variables involved. For purposes of this investigation, the U.S. M-14 nonmetallic antipersonnel mine was designated as the target of principal interest, replacing the ~ 0.5-pound blocks of DNB and DNT that had been employed previously.

The M-14 mine consists of a cylindrical plastic body, 2-3/16 inches in diameter by 1-9/16 inches deep. The main charge consists of 1 ounce of tetryl located in the lower half of the mine case, below a partition that separates the charge from the firing mechanism. The detonator is located at the center of the tetryl charge. Total weight of the mine is ~ 3-1/3 ounces. See Figure 35. For purposes of this investigation 1 ounce of DNT was cast into the bottom of empty M-14 mine cases with the detonator removed.

The experimental sensor used for these studies is sketched in Figure 36. The source was 100-mCi  $^{241}\text{Am}$ , the detector a 1.75-inch-diameter by 0.25-inch-thick NaI (Tl) crystal coupled to a 2-inch-diameter, RCA 6342 photomultiplier tube. The primary source shield, mounted below the scintillator, was a 0.75-inch-diameter by 1.5-inch-long lead cylinder. The M-14 targets were emplaced at depths of from 0 to 2 inches in a homogeneous red-clay soil medium. Reproducible, three-dimensional positioning of the experimental sensor over the soil was achieved by installing the sensor between the motor-support forks of a radial-arm saw.

The dimensions labeled A, B, C, h, and d in Figure 36 were varied parametrically over the range of values specified in Table 4. The resulting data are contained in the final report and will not be reproduced here. The design parameters selected from this data field to implement in an advanced experimental searchhead represented a trade-off which maximized R over the target while maintaining a low value for  $\Delta\phi/\Delta h$ , and a high value for  $\phi$ . The parameters selected were A = 0.25 inch, B = 1.25 inches, and C = 1.50 inches. As a result of varying A, B, and C in 0.06-inch increments about these values, it was decided that A = 0.25 inch, B = 1.12 inches, and C = 1.50 inches represented the optimal configuration for incorporation in a coaxial searchhead designed to detect M-14 mines. The resulting backscatter count rate was ~10<sup>5</sup> cpm over soil, the change in count rate with sensor height was less than ±5 percent for 1.5 ≤ h ≤ 3.5 inches, and R was 1.24 for d = 0.5 inch and h = 2.0 inches. By displacing the axis of the sensor relative to the axis of the target in 0.5-inch increments, it was found that R decreased from ~1.24 to ~1.18 at



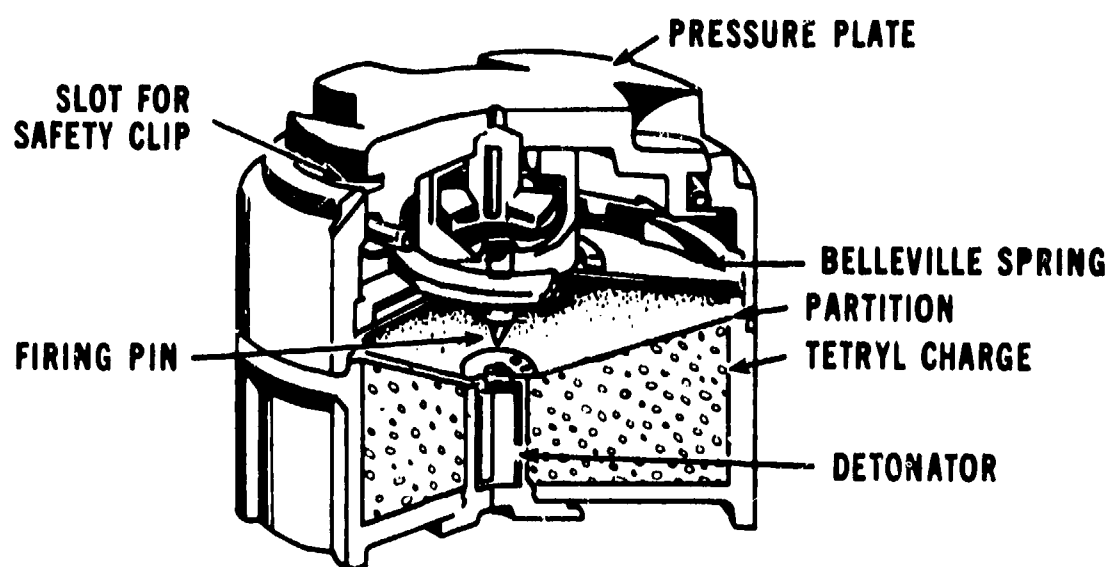


Figure 35. M-14 mine sketch.

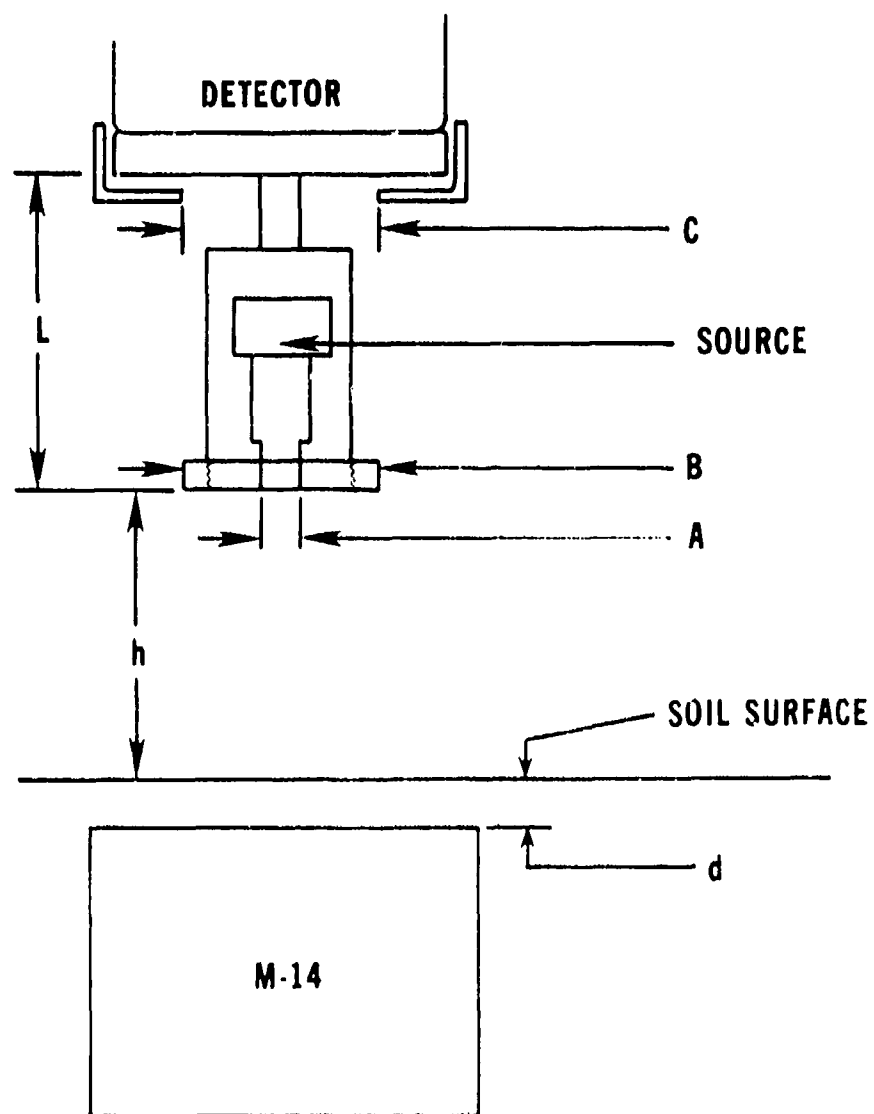


Figure 36. Geometry for man-portable detector parametric experiments.  
(After Miller, Anastasi, and Tucker)

Table 4. Range of Variables for Parametric Study (Coaxial Man-Portable)

Symbol	Parameter	Range of Variation (In.)	Increments (In.)
d	Burial Depth	0-2.0	0.5
h	Height	1.0-3.0	0.5
A	Collimator Aperture	0.05-0.25	0.005
B	Scatter-Shield Diameter	0.75-1.50	0.25
C	Detector Aperture	1.00-1.75	0.25
N	Lateral Displacement	0-2.0	0.5
V	Scan Velocity	0-3 ft/s	1 ft/s

1 inch off-axis and to  $\sim 1.10$  at 1.5 inches off-axis. As a compromise, it was, therefore, decided that each sensor element effectively could cover 2 inches laterally (i.e., the target could be detected if it passed beneath the sensor at a maximum of 1 inch off-axis). This, in turn, necessitated that three sensor elements be employed to achieve the design goal of 6-inch lateral coverage for the entire searchhead.

A total of three advanced experimental mine detectors, each employing a searchhead with three sensor elements conforming to the optimal geometry specified above, were fabricated and shipped to Fort Belvoir for test and evaluation. A more detailed account of these detectors and a summary of the performance data obtained with them will be found in section IV. For the present, it is sufficient to state that, while these detectors were capable of detecting M-14 mines buried at depths of up to 0.5 inch in a homogeneous soil medium at lateral search speeds of  $\sim 1$  ft/s, it was believed that the sensitivity of these detectors to vegetative ground cover was such that the detectors would not be acceptable in the field. It was, therefore, decided that the coaxial sensor design would not be pursued further and that every effort would be made to improve detector performance against the M-14 mine emplaced in soil with appreciable organic content.

The decision to continue effort on the development of a man-portable gamma-backscatter AP-mine detector was based on the results of a limited, in-house program which demonstrated that detection of an M-14 could be effected utilizing an uncollimated-source-collimated-detector geometry (geometry (c)) in certain instances when the same mine could not be detected by a coaxial sensor. It was recognized that, in abandoning the coaxial geometry, the principal advantage of that geometry (insensitivity of the countrate to small changes in sensor height) also would have to be relinquished. In addition, it was recognized that only limited improvement in detector performance in vegetative areas could be expected (due to the detection principle employed) and that substantial variations in the amount of vegetation present would result in continual false alarms.

In order to obtain the greatest probability of success in a limited time frame, parallel efforts were initiated. Contract DA-K02-71-C-0359 with the Nuclear-Chicago Corporation was modified, and that effort was redirected to investigate the possibility of utilizing a collimated-source-collimated-detector geometry (similar to that employed in the vehicle-mounted detector developed under Contract DAAK02-69-C-0263) in a man-portable configuration. At the same time, a contract was awarded on a competitive basis to the Industrial Nucleonics Corporation to investigate the possibility of utilizing an uncollimated-source-collimated-detector geometry in a man-portable system. Effort under both contracts was to include investigations of potential height-compensation techniques.

Since extensive investigations of geometry (b) were conducted by Nuclear-Chicago Corporation under Contract DAAK02-69-C-0263, the performance characteristics of a man-portable detector utilizing this geometry were fully anticipated. Consequently, only limited laboratory studies were performed to verify that: (a) maximal R values obtained for  $q \cong$  mine diameter (2 inches in this case); (b) R decreased rapidly as h increased; (c)  $\phi$  increased rapidly and, for the chosen geometrical parameters, nearly linearly as h increased; and (d)  $\phi$  was appreciably lower for this geometry than geometry (d) for comparable source activity. These characteristics necessitated that, by utilizing geometry (b), the resultant detector would have to operate closer to the ground and more slowly than the coaxial detectors fabricated previously. However, it also would be possible to attain appreciably higher values of R than were previously possible. In fact, for an M-14 in red clay and for h = 2 inches, it was found that R = 1.88 for d = 0 inch and R = 1.26 for d = 0.5 inch for this new geometry; whereas, for the coaxial design, R = 1.49 for d = 0 inch and R = 1.14 for d = 0.5 inch. By moving the new sensor even closer to the surface, R values were found to increase dramatically: for h = 0.5 inch, R = 4.35 for d = 0, and R = 2.60 for d = 0.5 inch. Since these large R values only would be of use if a means could be found to compensate for the changes in  $\phi$  resulting from small h-variations ( $\phi$  was found to decrease by a factor of three as h was increased from 0.25 to 2.0 inches), the primary R&D effort under this phase of the contract was directed toward this end.

Several techniques were tried in order to obtain this desired result. The first technique considered consisted of placing a small, uncollimated Geiger-Mueller (GM) tube midway between the source and detector at the bottom of the sensor. Thus placed, the GM tube primarily "viewed" photons singly scattered from the soil volume directly below the collimated source. As a result, the count rate obtained from the GM tube decreased as h increased. It was empirically determined that the slopes of the  $\phi$  versus h curves for the GM (height) and scintillation (mine) sensors were essentially constant over the range  $0.25 \leq h \leq 2.0$  inches, although the magnitude of  $\phi$  was found to be a different function of soil composition for the two sensors. (See Figure 37.) By adding the outputs from the two sensors ( $\phi_1 + m\phi_2$ , where m is a multiplicative constant built

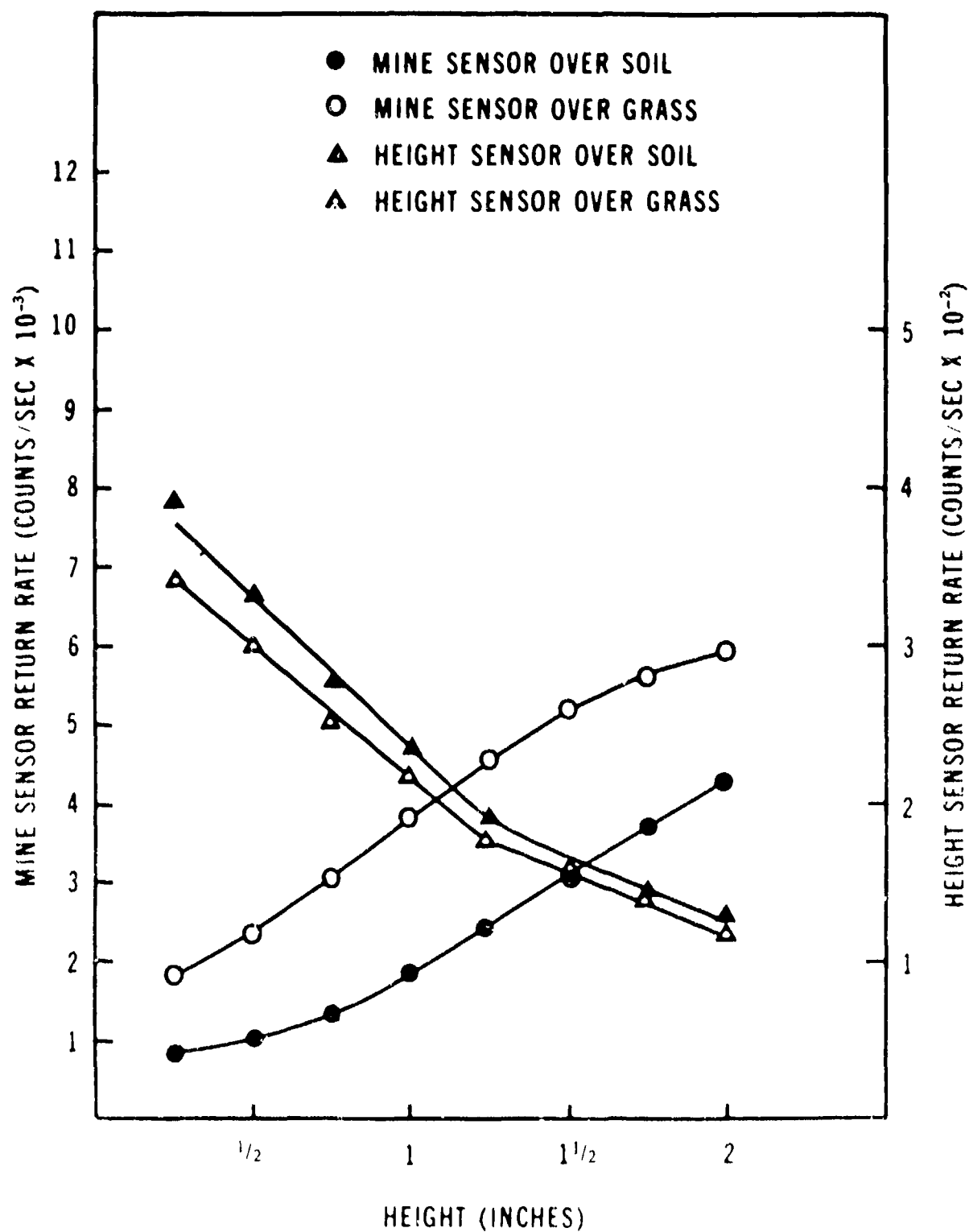


Figure 37. Gamma-back-scatter height compensation data. (After Miller, Anastasi, and Tucker)

into the system), the resultant signal was found to be only moderately sensitive to height variations ( $\sim \pm 4.5$  percent over grass and  $\sim \pm 18$  percent over inorganic soil). The  $\sim \pm 18$  percent variation found over inorganic soil was not considered critical because of the large R values attainable over this type of soil by the mine sensor. The primary disadvantage of this technique was its sensitivity to small changes in soil microrelief. The mine sensor was found to be primarily sensitive to variations in h between the scintillation detector and the soil surface; whereas, the height sensor was found to be primarily sensitive to variations in h between the source and the soil surface.

In order to overcome this deficiency, it was decided that it was essential that the height sensor view the same area on the soil surface as did the mine sensor. To this end, a GM tube was placed inside the mine-sensor collimator, just in front of the scintillator. In order to generate a noninterfering height-sensor signal, an uncollimated  $^{90}\text{Sr}/^{90}\text{Y}$   $\beta^-$  source ( $\beta^-_{\text{max}} = 0.546$  and 2.27 MeV) was employed. See Figure 38. The GM tube employed, while only 1 to 2 percent efficient for backscattered  $\gamma$  radiation, was virtually 100 percent efficient for  $\beta^-$  radiation.

On the other hand, the aluminum window on the scintillator, while almost transparent to  $\gamma$  radiation, was virtually opaque to backscattered  $\beta^-$ 's. Some slight contribution from the  $^{90}\text{Sr}/^{90}\text{Y}$  source to the mine-sensor signal resulted from  $\beta^-$  bremsstrahlung, but this contribution was found to be negligible when both upper- and lower-level discriminators were employed to delimit the energy bandwidth of the accepted photomultiplier pulses. The output of the height-sensor channel was found to decrease nearly exponentially as h increased from 1 to 4 inches (Figure 39). Specifically,  $\phi_2 = \exp(-ah-b)$ , where a is a constant of the system and b is a constant that depends on soil type; consequently, by summing  $\phi_1$  and  $\phi_2$  it was possible to obtain a nearly constant signal level as h was varied from 1 to 3 inches. This resulted in an increase in the signal level as the sensor passed over the target. See Figure 40. The principal disadvantage of this approach was that, since  $\beta^-$ 's in this energy range have a range which is negligible compared to the mean free path of 60-keV gammas, the height sensor monitored h from the mine sensor to the nearest solid material, be that material the true soil surface or be it a dried leaf or blade of grass above the surface. This approach also required that a calibration procedure be carried out before the detector could be utilized for any one soil type.

An experimental searchhead and electronics package incorporating this height-compensation technique was fabricated and shipped to Fort Belvoir for testing. A description of this system and the results of testing will be found in section IV.

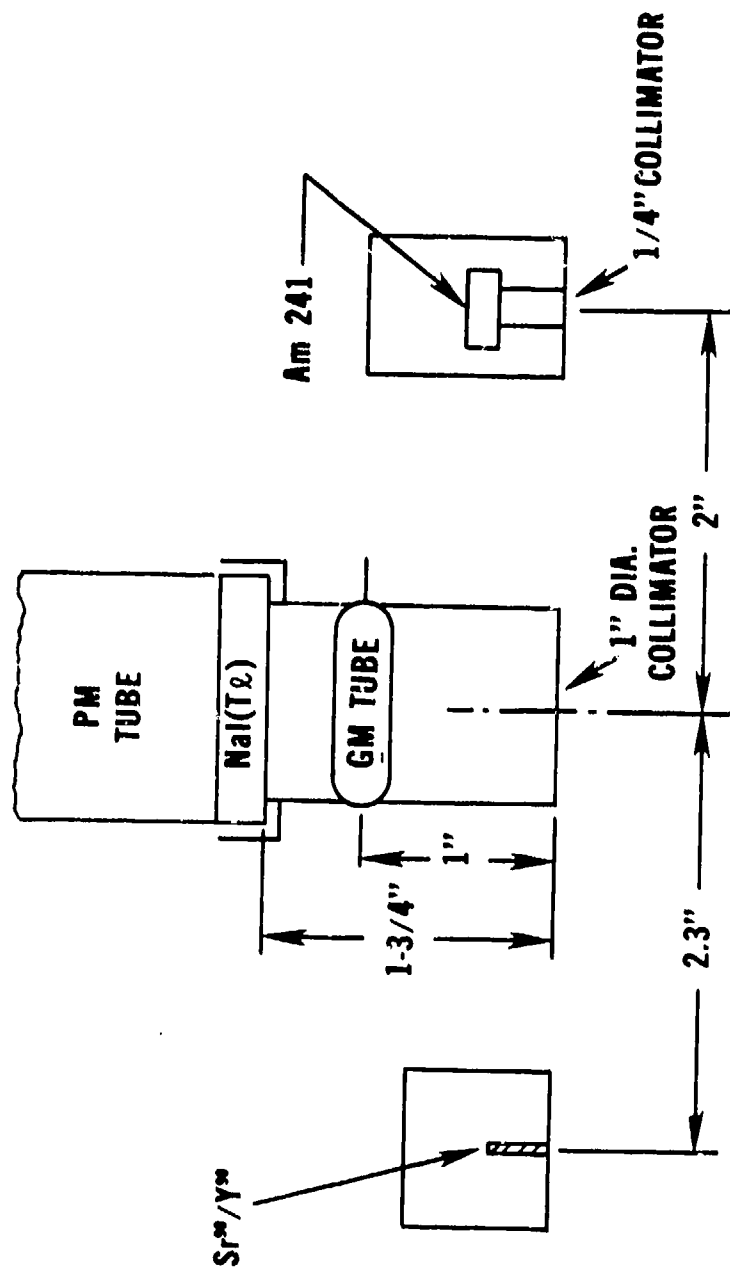


Figure 38. Combined height and mine sensor. (After Miller, Anastasi, and Tucker)

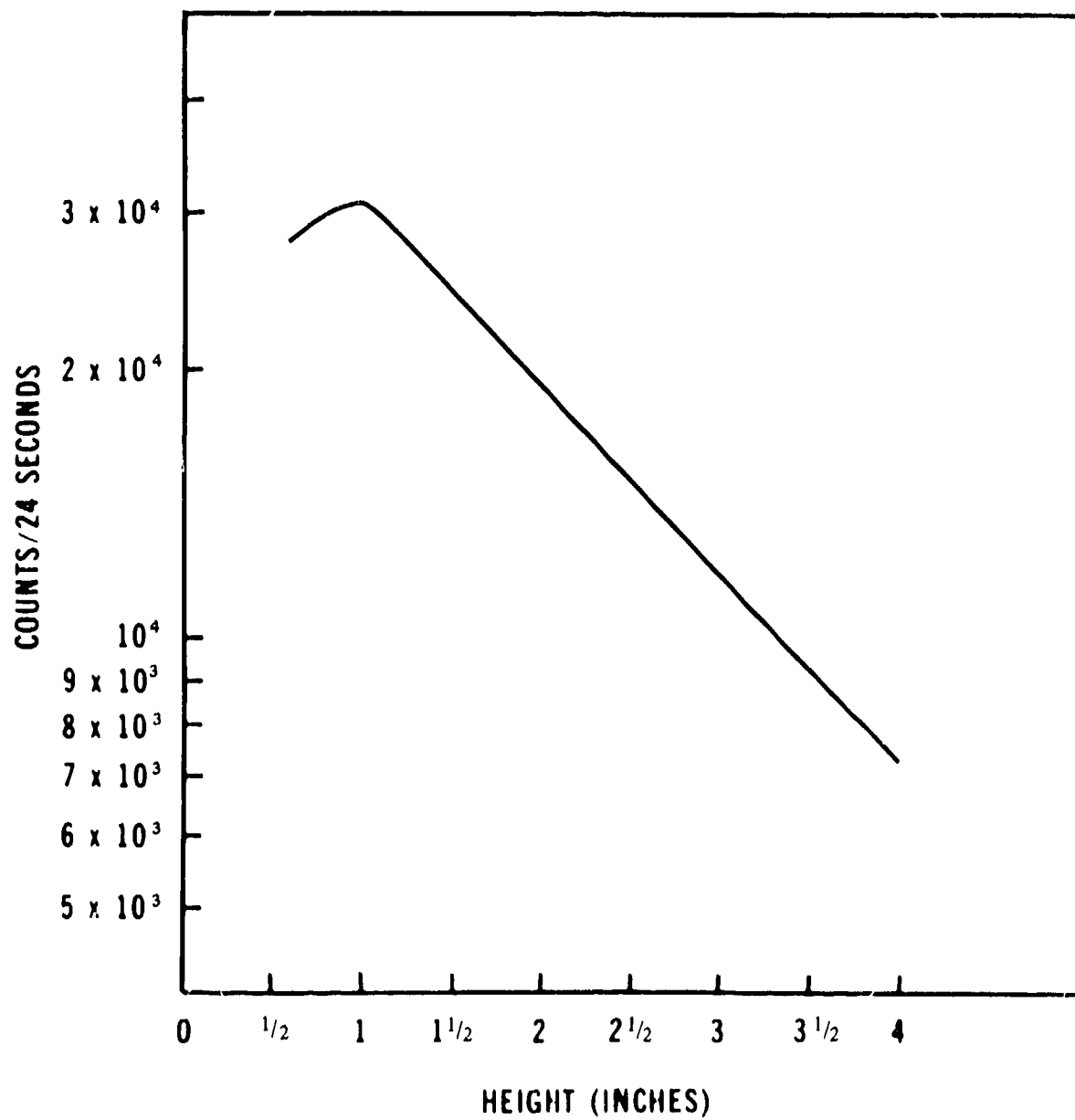


Figure 39. Beta-sensor output as a function of height. (After Miller, Anastasi, and Tucker)



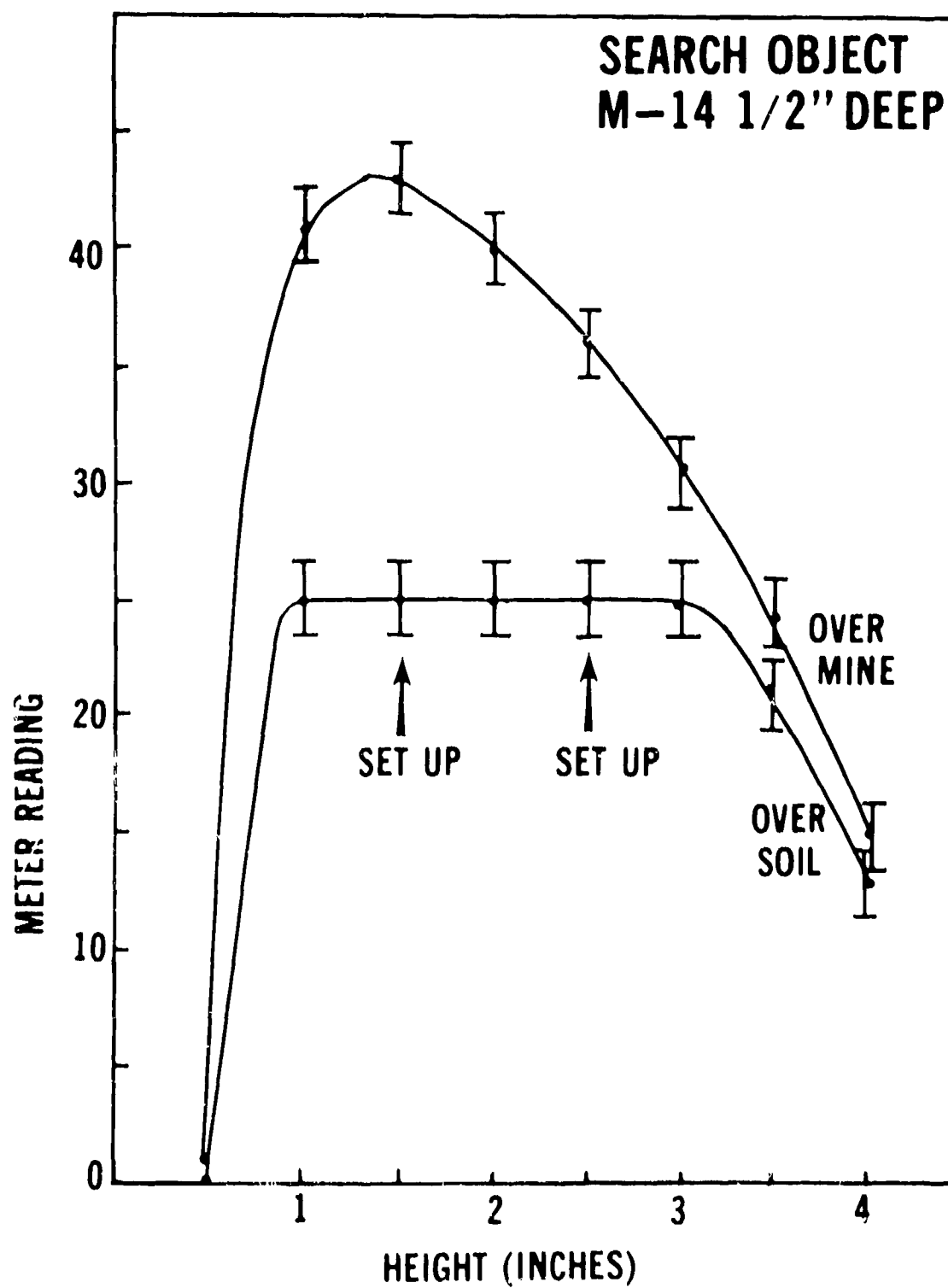


Figure 40. Height-compensated searchhead performance in the laboratory. (After Miller, Anastasi, and Tucker)

**17. Contract DAAK02-72-C-0619.** The purpose of this contract was to develop an experimental mine sensor capable of locating M-14, nonmetallic, antipersonnel mines buried at operational depths in reasonably organic soil media. To this end, the contractor, the Industrial Nucleonics Corporation, was constrained to utilize an uncollimated source and a collimated detector. Effort under this contract centered on two problems: (1) developing a detector collimator which would maximize the target signal, and (2) devising a height-compensation technique which would enable field utilization of the otherwise extremely height-sensitive uncollimated-source - collimated-detector geometry.

The test setup utilized for this contract consisted of a wooden box, 6 feet by 8 feet by 8 inches deep, which was partitioned into four compartments. Each compartment contained a different soil type: sand, roadbed (rock and clay), humic, and grass-covered humic. None of these soils had appreciable iron content (i.e., the Z contrast between the soil and the mine was not unusually high), and all were watered periodically to assure normal moisture content (10 to 30 percent by weight). The humic soil contained 12.6 percent organic material (combustion loss, dry weight); the grass, in the grass-covered humic section, was never cut, resulting in an extremely lush ground cover. A metal frame surrounding the soil box supported the transport mechanism. This mechanism permitted the sensor to be reproducibly positioned ( $\pm 1/16$  inch) anywhere above the soil box in all three dimensions. See Figure 41.

In order that the detection characteristics of the mine sensor remain stable over a usable range of operating heights, initial effort under this contract concerned the development of a detector collimator which would enable the maintenance of maximum R values for an M-14 mine as the sensor height was varied from 2 to 5 inches above the soil surface. This was accomplished by fabricating a breadboard sensor utilizing the uncollimated-source - collimated detector geometry ( $q = 2.3$  inches) and by using simple right-cylindrical collimators of variable length (half-angle). Figure 42 shows R values obtained with this arrangement as a function of sensor height. On the basis of these data, it was determined that a half-angle of  $5.1^\circ$  both maximized R and maintained a relatively constant value of R over a 2- to 5 inch operating range. Experiments also were performed wherein R values were obtained at various positions over the target as the sensor moved along a diameter. Results of one such experiment, for the  $5.1^\circ$  half-angle collimator, are shown in Figure 43. Distance measurements are from the center of the mine to the center of the collimator. Note that maximum R occurs when the target is slightly offset toward the source.

Knowing that a  $5.1^\circ$  half-angle collimator will function well in a mine sensor is of little value in itself, since, for a 1-inch-diameter detector, this would mean using a collimator almost a foot long. However, the performance characteristics of this collimator can be used as reasonable performance criteria in the design of more compact

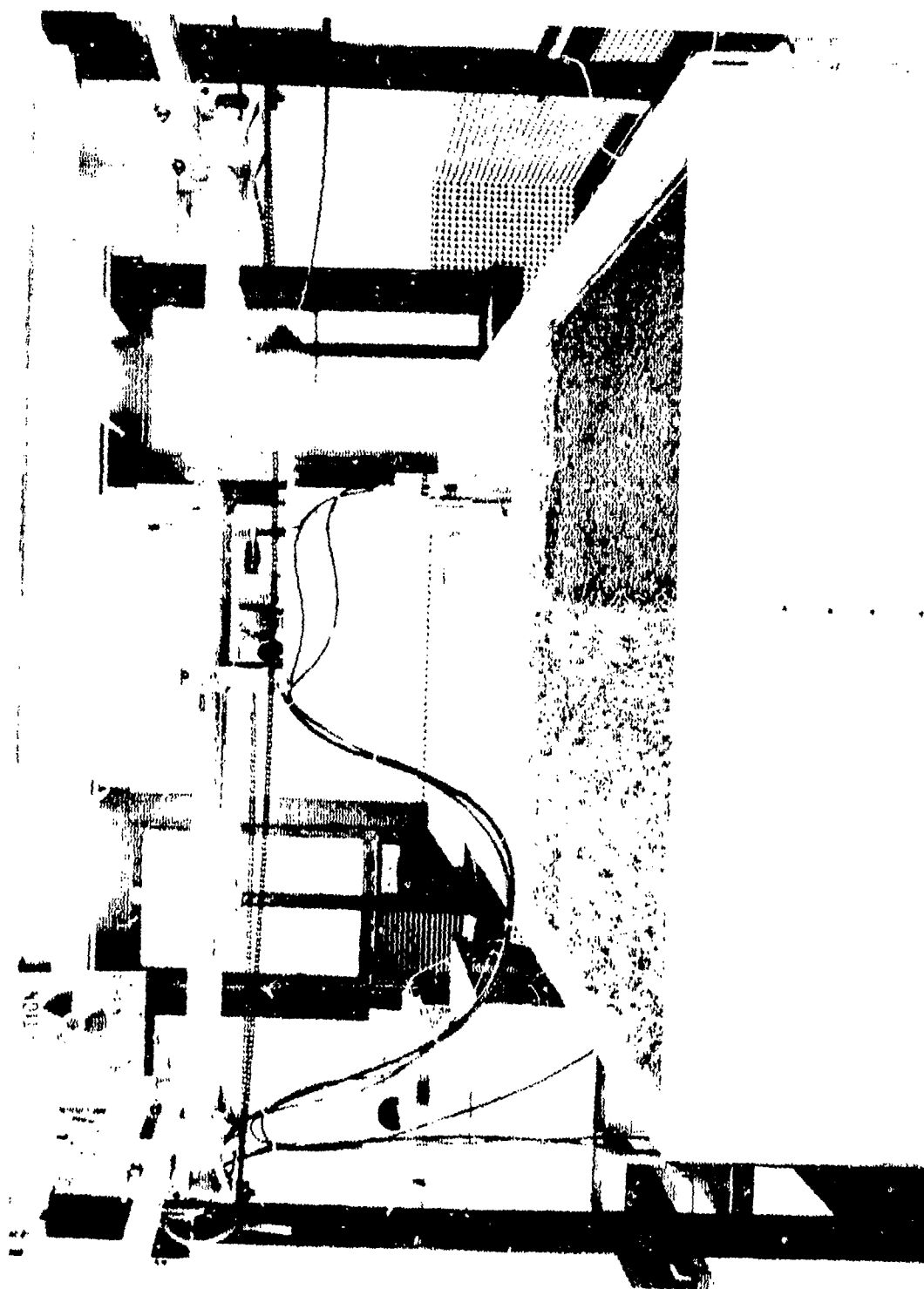


Figure 41. Industrial Nucleonics experimental setup. (After Thompson)

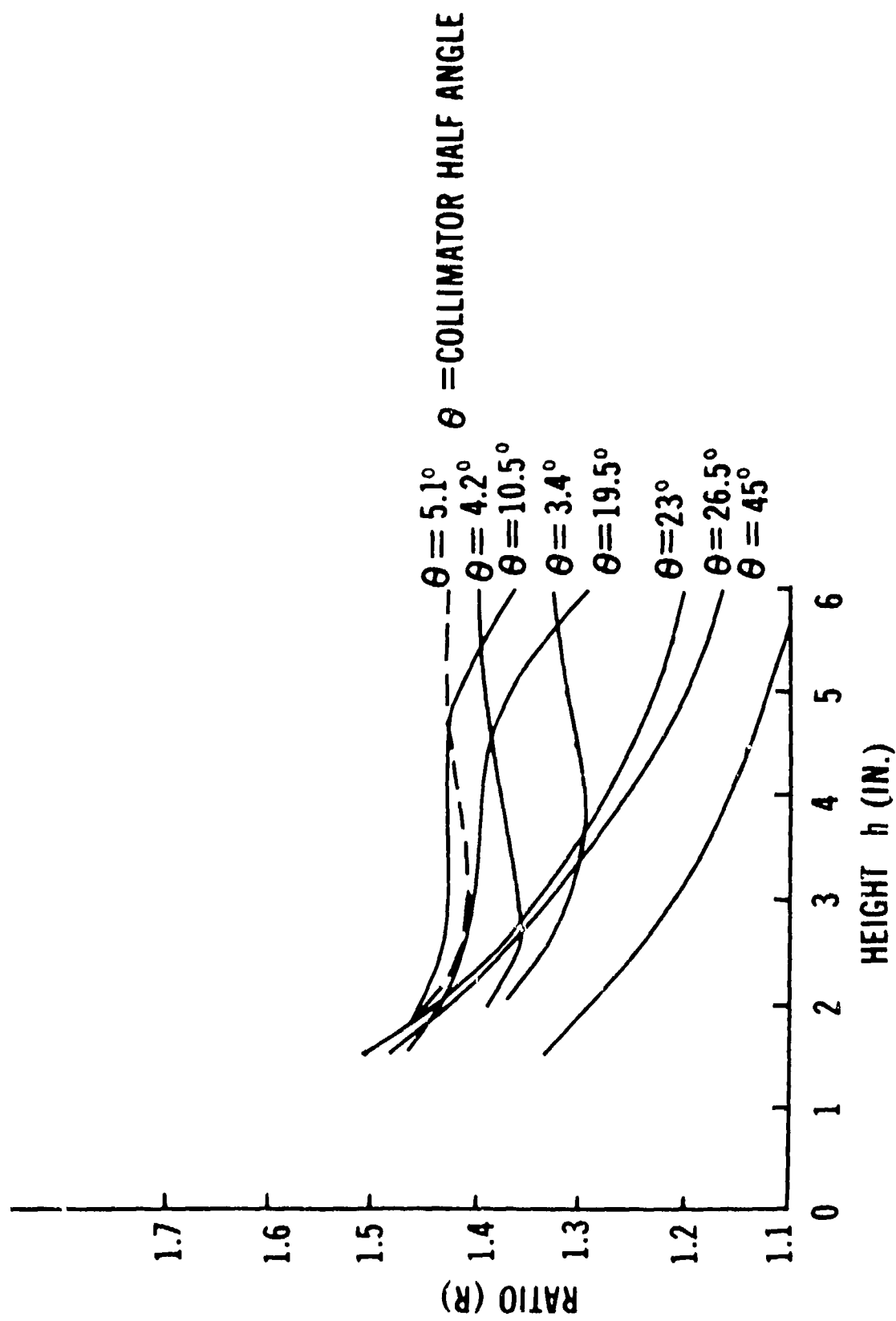


Figure 42. R as a function of height for different half-angles. (After Thompson)

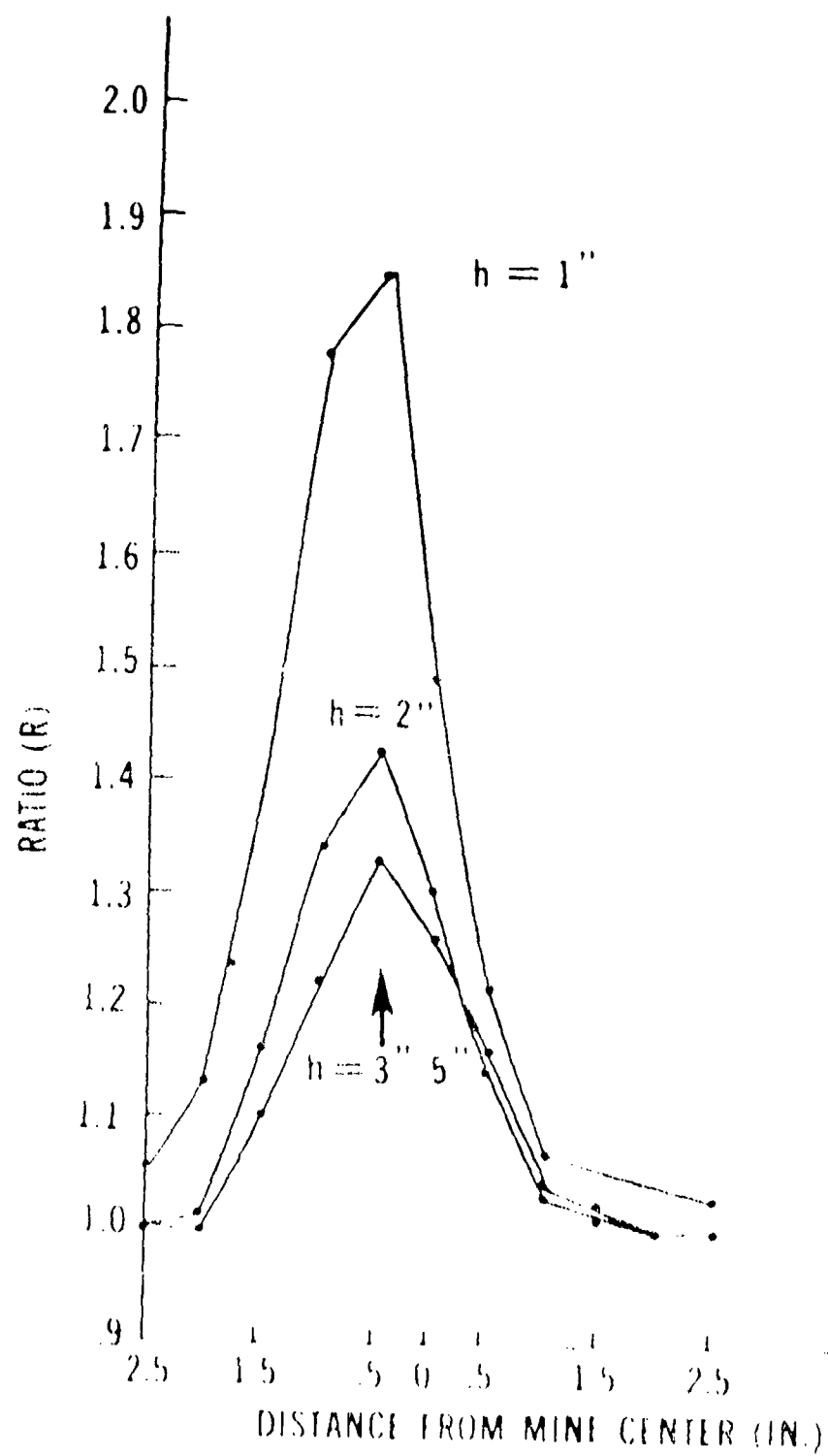


Figure 13. Sensitivity of performance of wide angle aperture collimator as a function of position over mine. (After Thompson)

collimators. These criteria were satisfied (and, indeed, slightly surpassed) by a 1.5-inch-long multiaperture collimator with holes of different diameters. See Figure 44.

It should be emphasized that the development of a mine sensor for which  $R$  is independent of  $h$  does not imply that  $\phi$  will be independent of  $h$  or of soil type. Figure 45 shows the  $h$  and soil-type dependence of  $\phi$  for an uncollimated-source - collimated-detector sensor utilizing a slightly less ideal honeycomb collimator. Since  $\phi$  is seen to be a strong function of soil type, the abrupt increase in  $\phi$  resulting from traversing a grassy patch of ground must induce a false alarm. Further, unless some means can be found to compensate for  $\phi$  changes due to small  $h$  fluctuations, no viable mine sensor can result. This brings us to the second major problem undertaken in this contract: devising a realistic height-compensation technique.

Like TND (Texas Nuclear Division), IN (Industrial Nucleonics) undertook to investigate several height-detection techniques, namely: beta backscatter, gamma backscatter using an uncollimated source and an uncollimated detector, and K-edge filtration of the gamma backscatter into a collimated detector.

The beta-backscatter study was conducted first using uncollimated  $^{90}\text{Sr}/^{90}\text{Y}$  and  $^{85}\text{Kr}$  sources and a collimated NaI (Tl) detector. Count rate as a function of sensor height was determined for each of the four soil types. Results of these measurements are shown in Figures 46 and 47. Note that, for each soil condition, the count rate is found to reach a maximum for  $h \approx 1.5$  inches and then to fall off rapidly as  $h$  increases further. These results are in qualitative agreement with those obtained by TND, and, like those of TND, could be used as a basis for a height-compensated detector, provided that we are willing to accept the requirement that the detector be recalibrated for each soil type encountered. (Note the change in count rate with soil type in Figures 46 and 47.)

Utilizing an uncollimated gamma detector proved to afford a simple means of height compensation, provided we are concerned only with changes in detector elevation above a level soil plane. Figure 48 shows the results of this phase of the effort. Note that although count rate may be seen to be a function of soil type as well as of sensor height, this was considered an advantage in this case, since the count rate of the mine sensor varies as a function of the same soil variables (i.e.,  $\rho$  and  $\langle Z \rangle$ ). However, for this technique, the height sensor reads the average height above a large area of the surface. Since the count rate of the mine sensor depends on its height above a small (mine-size) patch on the surface, a small mound of soil would yield a false signal, and a mine depressed below the surface would not be detected. For these reasons, no further effort was expended on this technique.

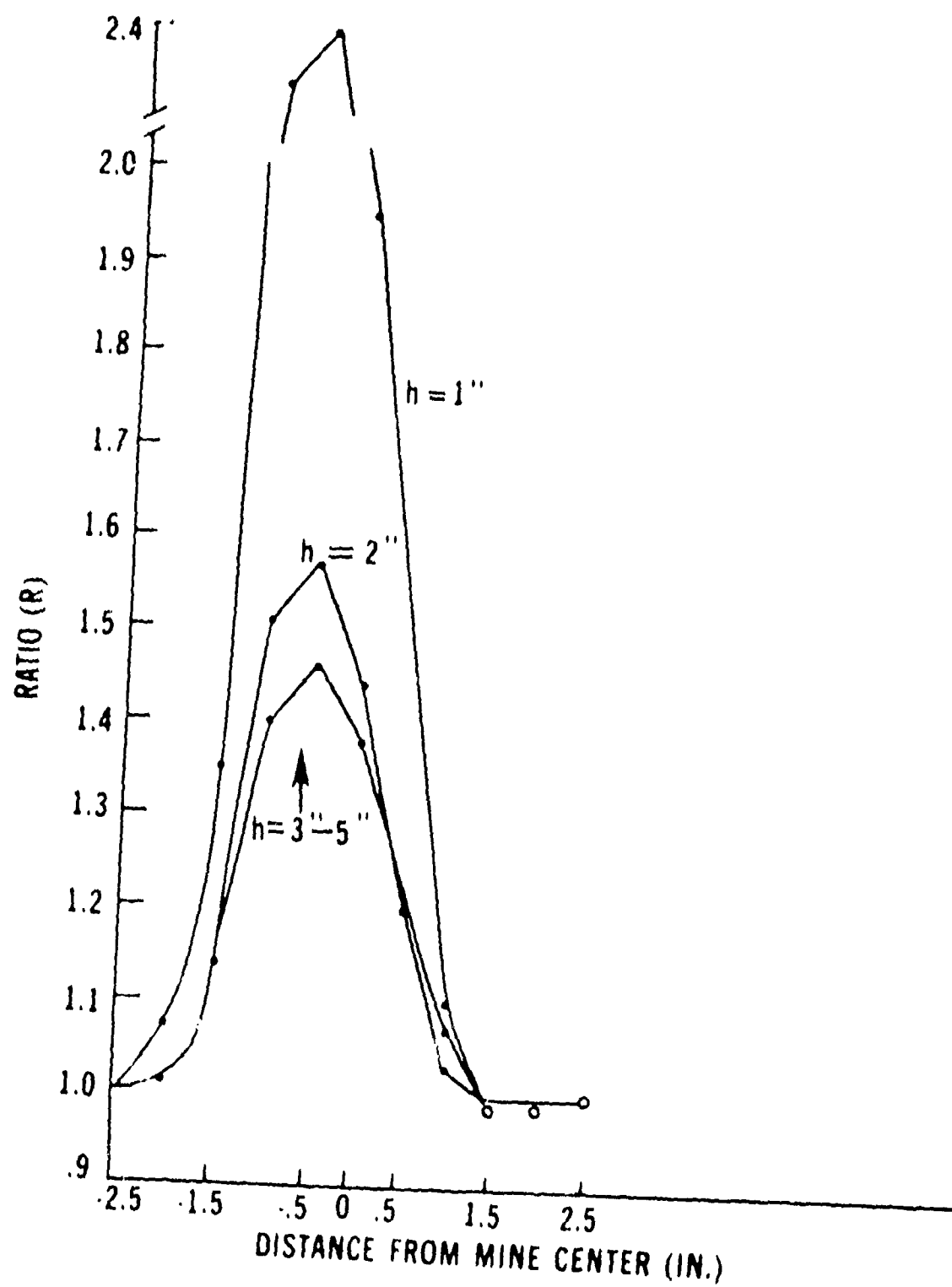


Figure 44. Sensor performance with multiaperture collimator as a function of position over mine. (After Thompson)

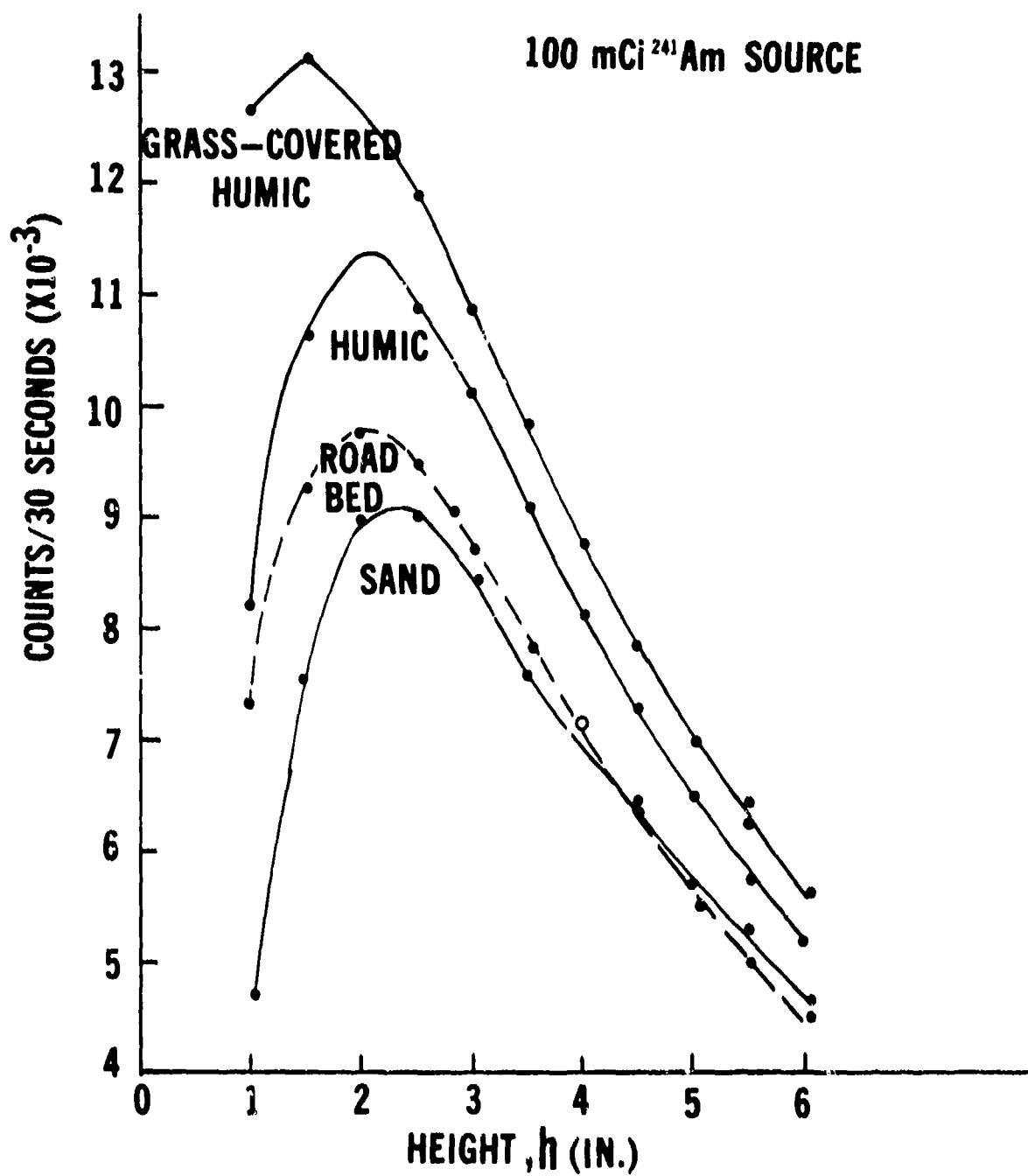


Figure 45. Dependence of count rate on height and soil type for  $^{241}\text{Am}$  gamma source.  
(After Thompson)



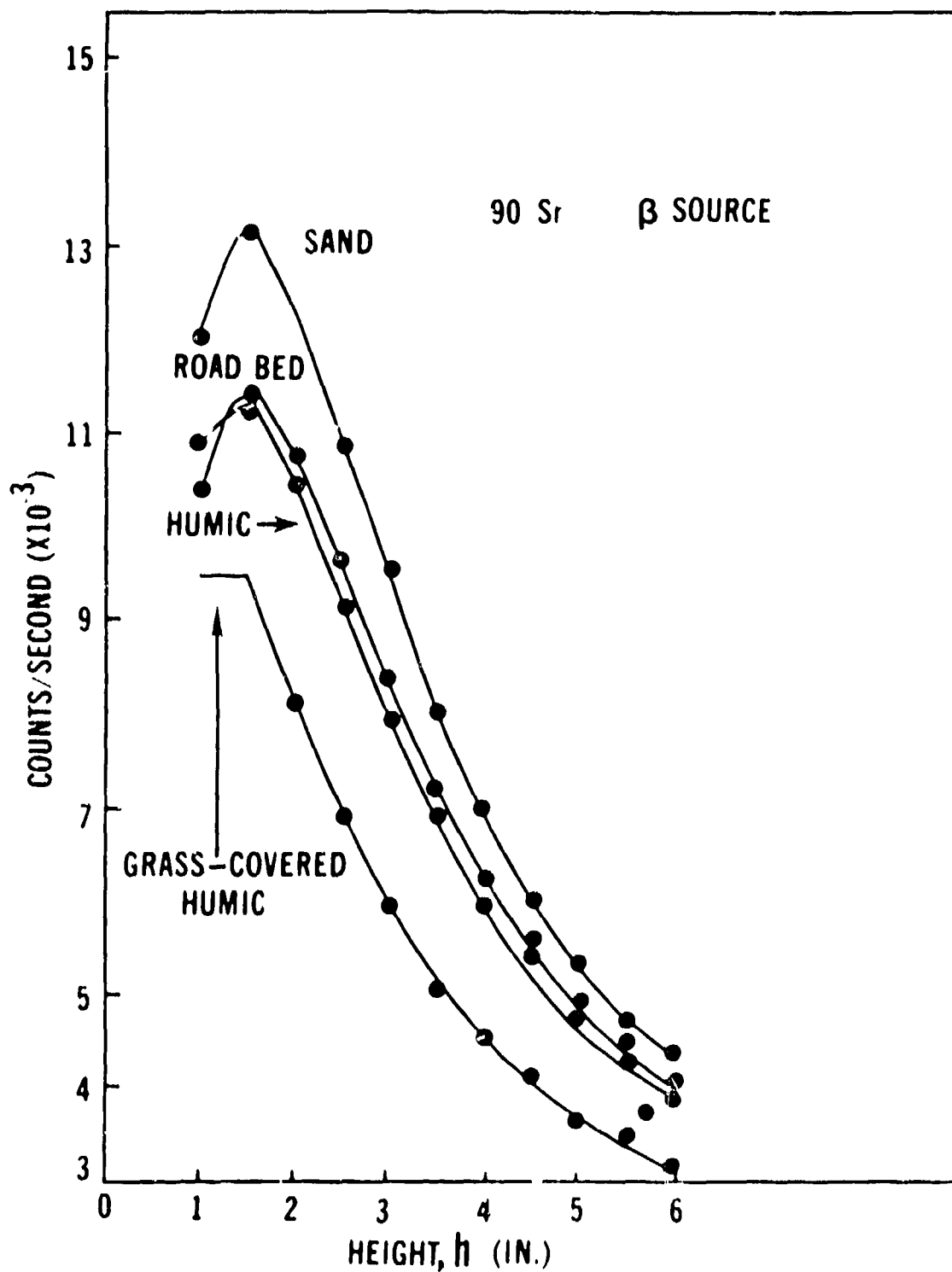


Figure 46. Dependence of count rate on height and soil type for  $^{90}\text{Sr}$  beta source.  
(After Thompson)

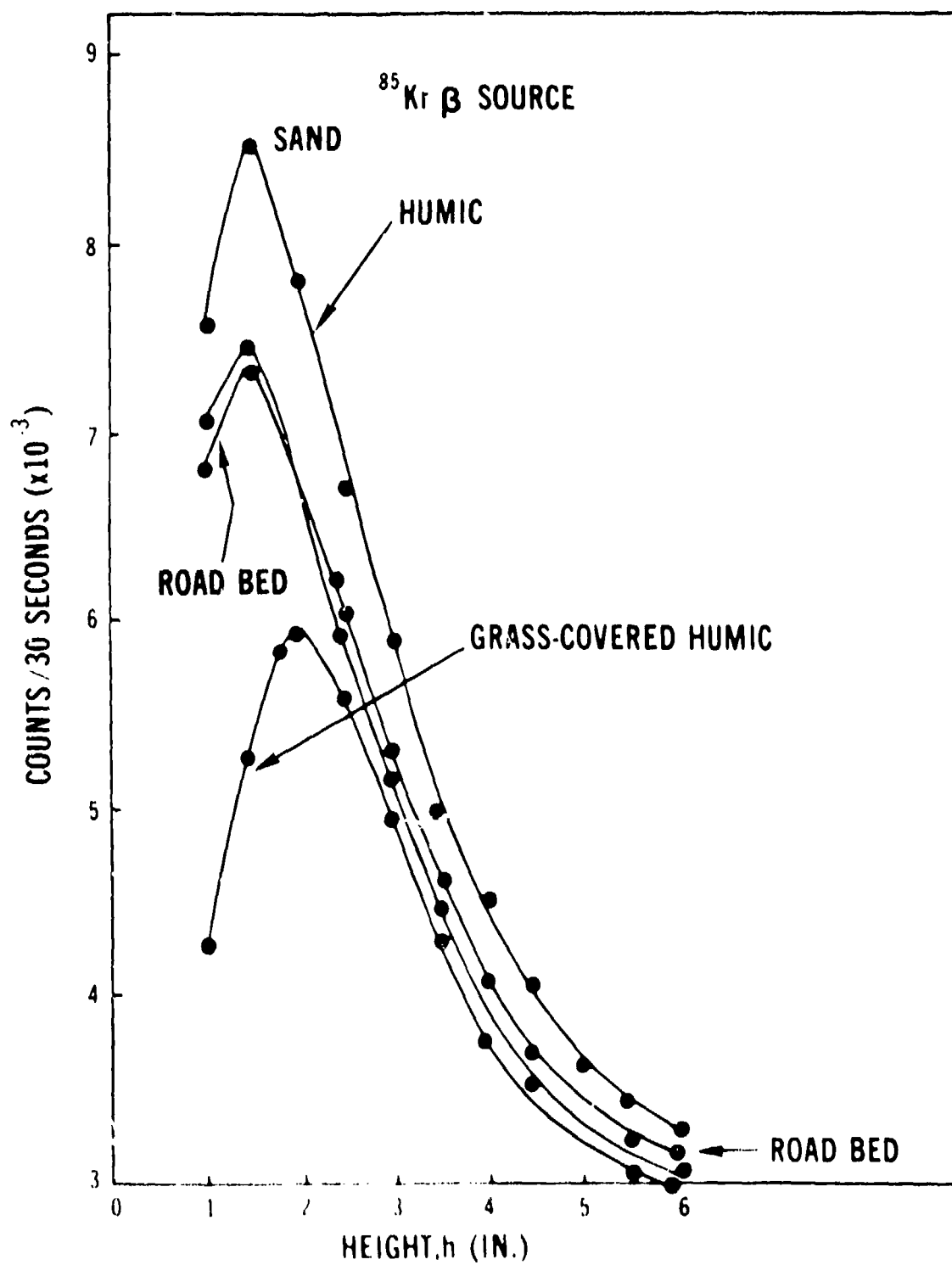


Figure 47. Dependence of countrate on height and soil type for  $^{85}\text{Kr}$  beta source. (After Thompson)

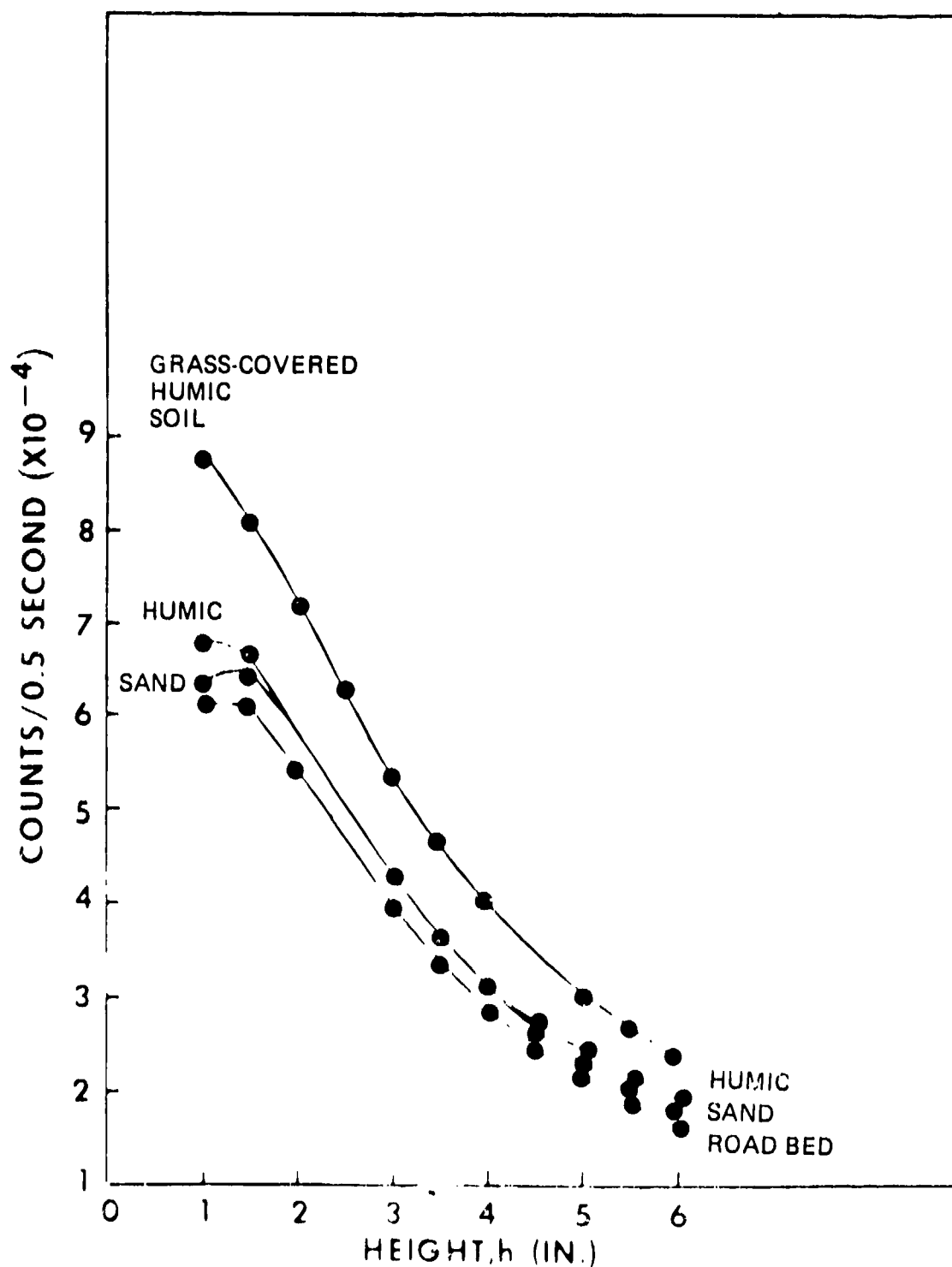


Figure 48. Dependence of count rate on height and soil type for  $^{241}\text{Am}$  source and uncollimated gamma detector. (After Thompson)

The final technique investigated involved the use of rare-earth filters. The theoretical explanation of this technique may be found in paragraph 11c and will not be repeated here. Three filters were tried: Sm, Eu, and Gd, which have K-edges at 46.8, 48.5, and 50.2 keV, respectively. However, since no attempt was made to optimize filter thickness, filter placement, or source/detector separation, and since optimization of all of these parameters would be required to fabricate a fieldable detector, the results of this investigation can be said to have established only concept feasibility.

Figures 49 through 51 show the change in detector countrate as a function of height with and without each of the three filters and with and without an M-14 mine in sand. If the addition of the filter achieved its desired result, a change in the slope of the countrate-versus-height curve was to be expected. As may be seen from the figures, significant change in slope was observed only for the Eu filter. Consequently, all further studies were conducted with this filter.

Figures 52 through 54 depict countrate-versus-height curves over the three remaining soil types (roadbed, humic, and grass-covered humic). Note that, as expected, the slopes of the filtered and unfiltered curves continue to differ for all the soil types. Unfortunately, the slopes of both the filtered and unfiltered curves do appear to vary slightly with soil type, which, in turn, makes this technique of height compensation less than ideal. Nevertheless, filtration was considered the most promising height-compensation technique and was, therefore, implemented in an experimental sensor head. Results of tests with this head will be found in section IV.

#### IV. DELIVERED HARDWARE

The purpose of this section is to briefly describe significant end items delivered under the contracts discussed in section III and to present, in an unclassified context, the capabilities and limitations of each.

**18. Experimental Vehicle-Mounted X-Ray Backscatter Detector of Antivehicular Mines.** This detector was designed and fabricated under Contract DAAK02-69-C-0263 with the Nuclear-Chicago Corporation. Minor modification and extensive testing of this detector were carried out under Contract DAAK02-72-C-0271, also with Nuclear-Chicago. Results reported here are extracted from the Final Report of this latter contract.<sup>39</sup>

**a. Description.** The detector employed geometry (b), utilizing two Dunlee Z-141 X-ray tubes as the source and four hermetically sealed CsI (Tl) scintillators

<sup>39</sup> W. D. Miller et al., *Test and Evaluation of a Vehicle-Mounted Experimental Explosive Sensor System Using X-Ray Backscatter Techniques*, Confidential Final Report, Contract DAAK02-72-C-0271 (July 1973).

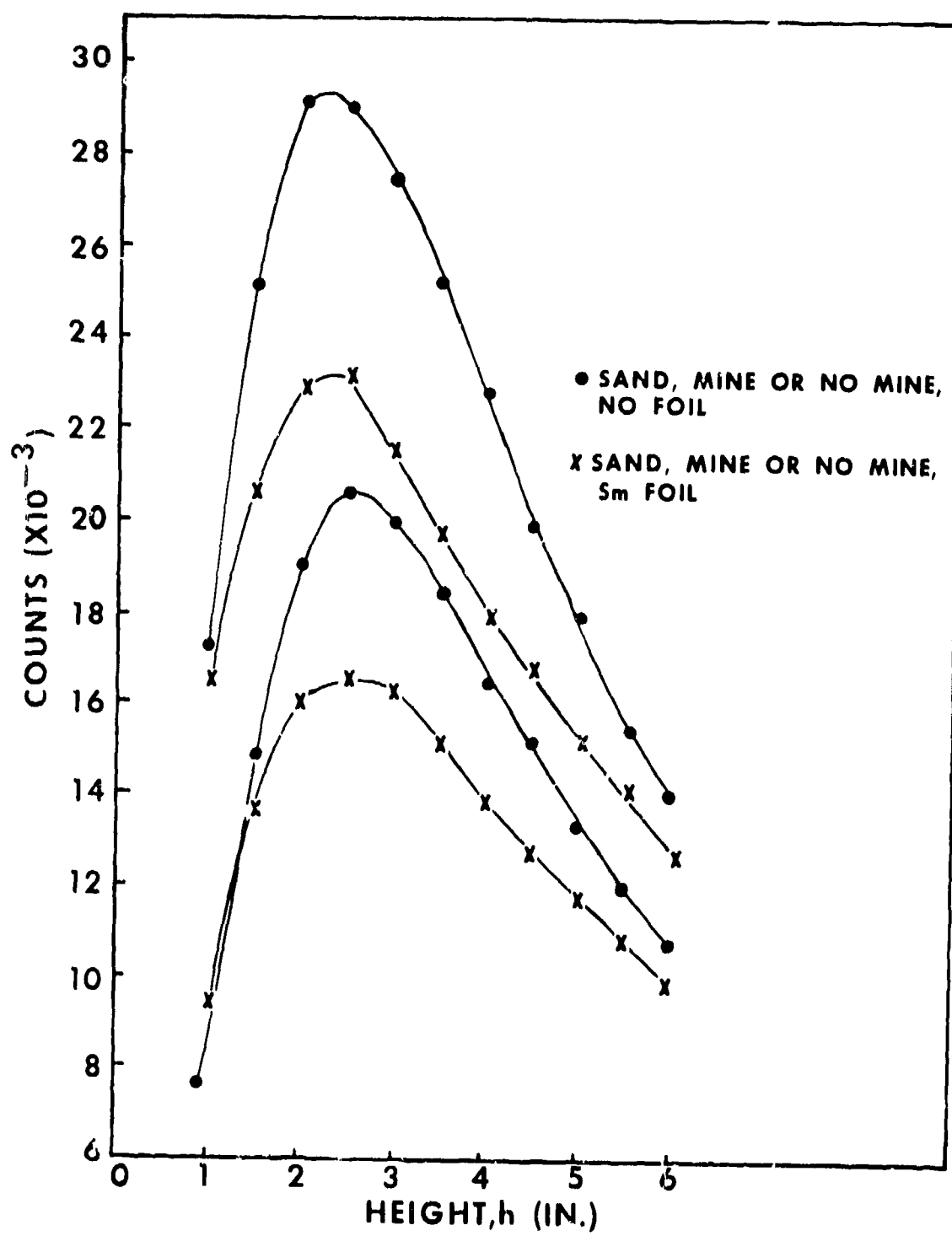


Figure 49. Dependence of countrate on height using Sm filter. (After Thompson)

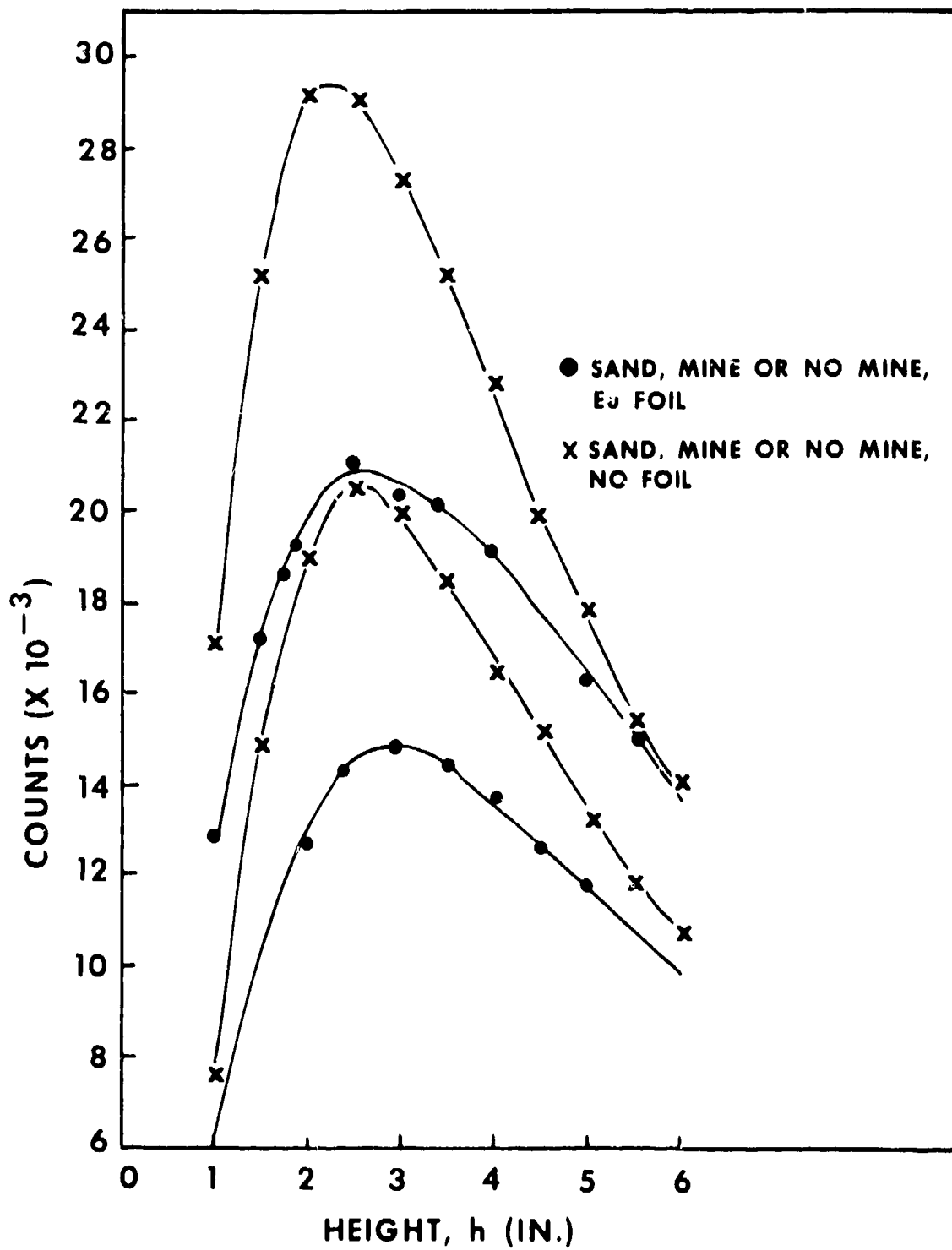


Figure 50. Dependence of countrate on height using Eu filter. (After Thompson)

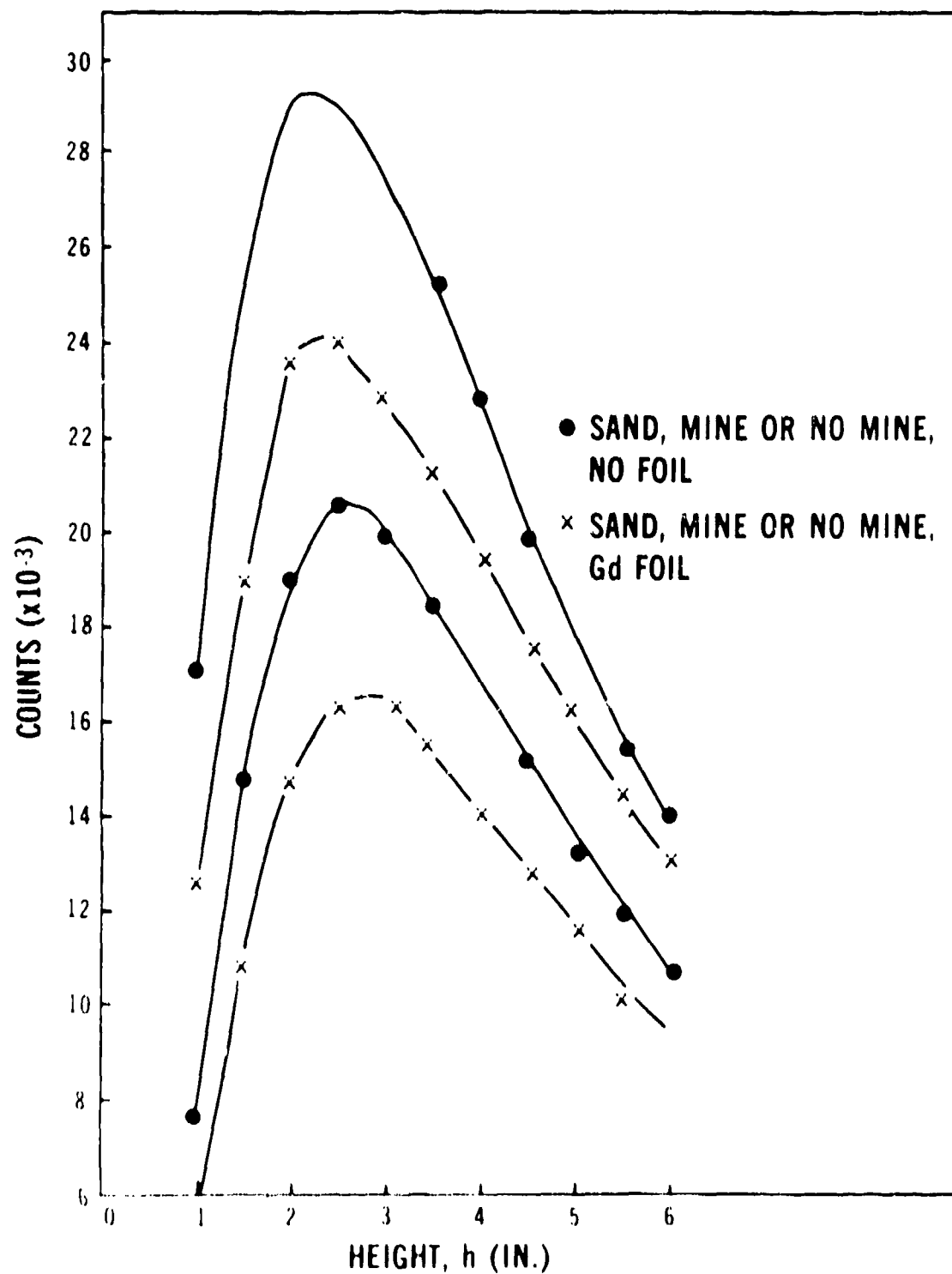


Figure 51. Dependence of count rate on height using Gd filter. (After Thompson)

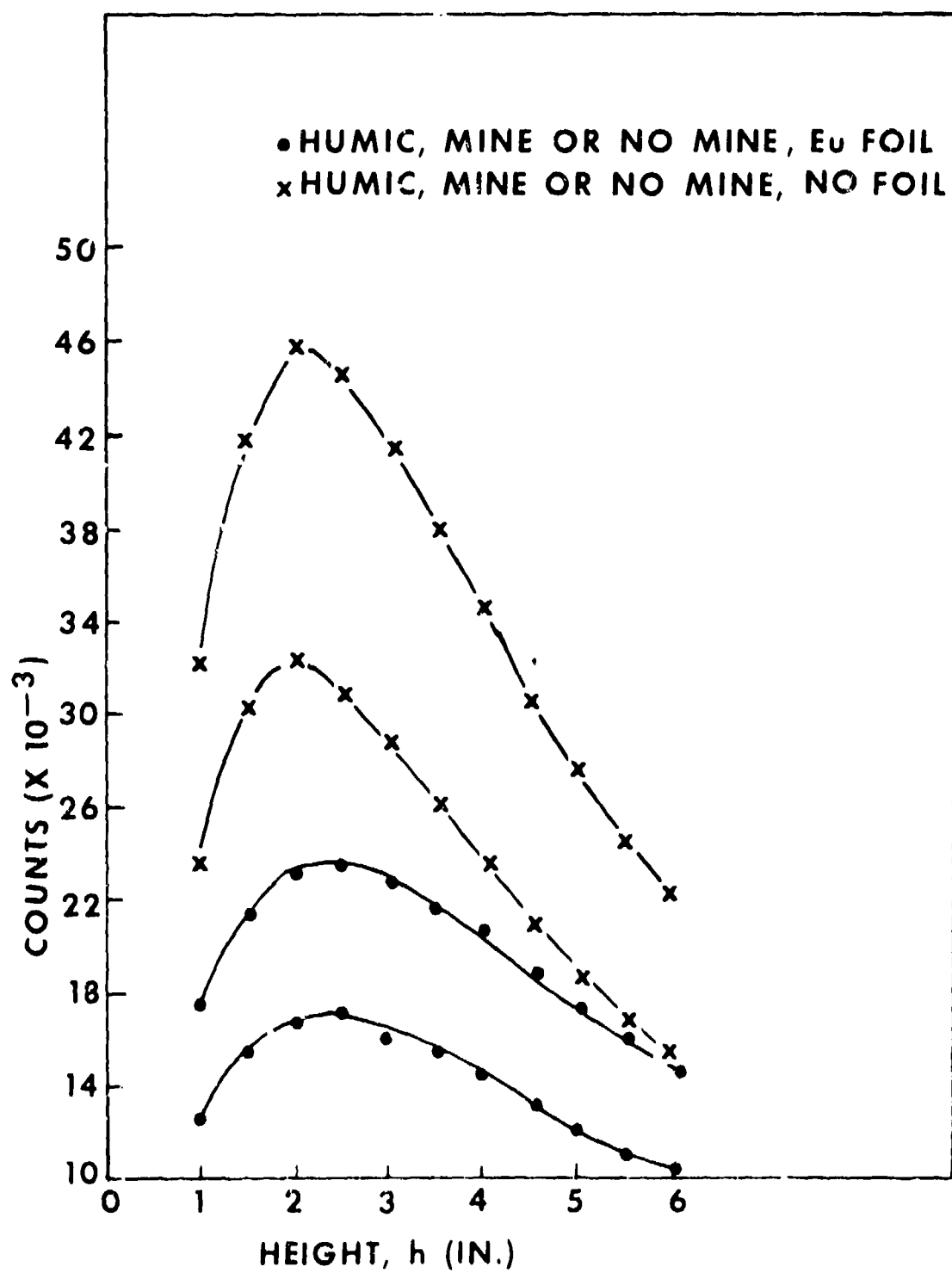


Figure 52. Dependence of count rate on height using Eu filter (humic). (After Thompson)



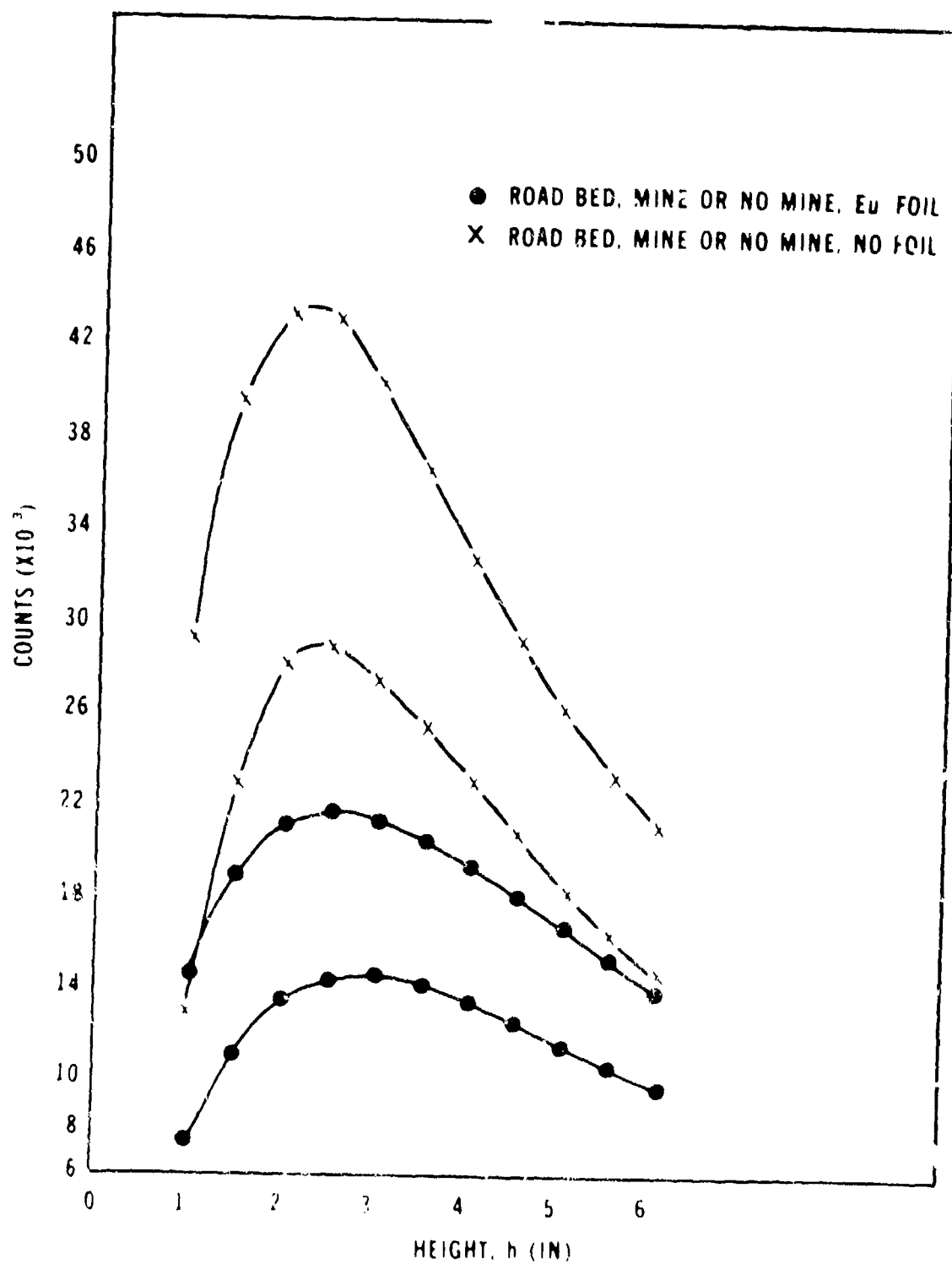


Figure 53. Dependence of countrate on height using Eu filter (roadbed). (After Thompson)

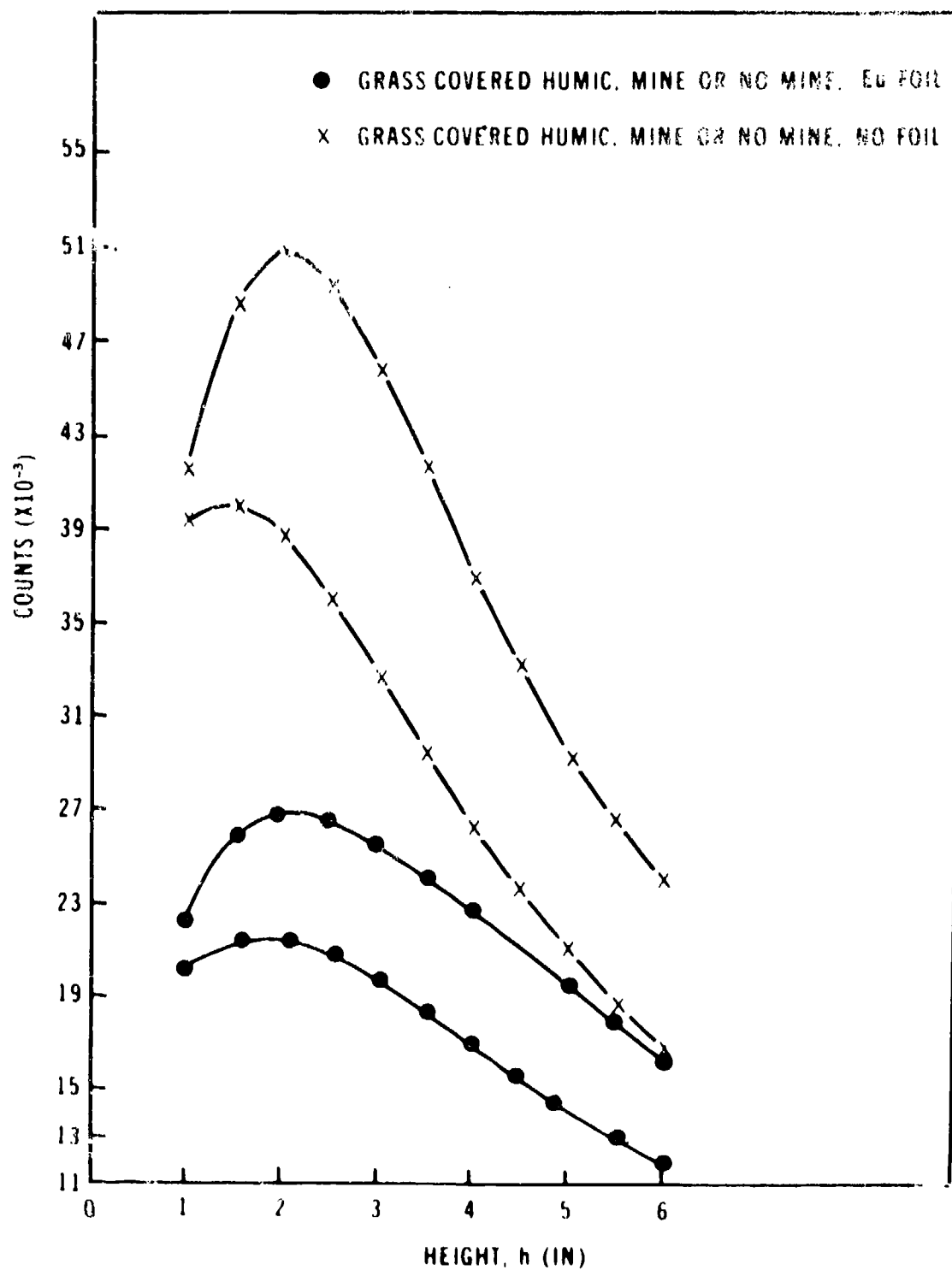
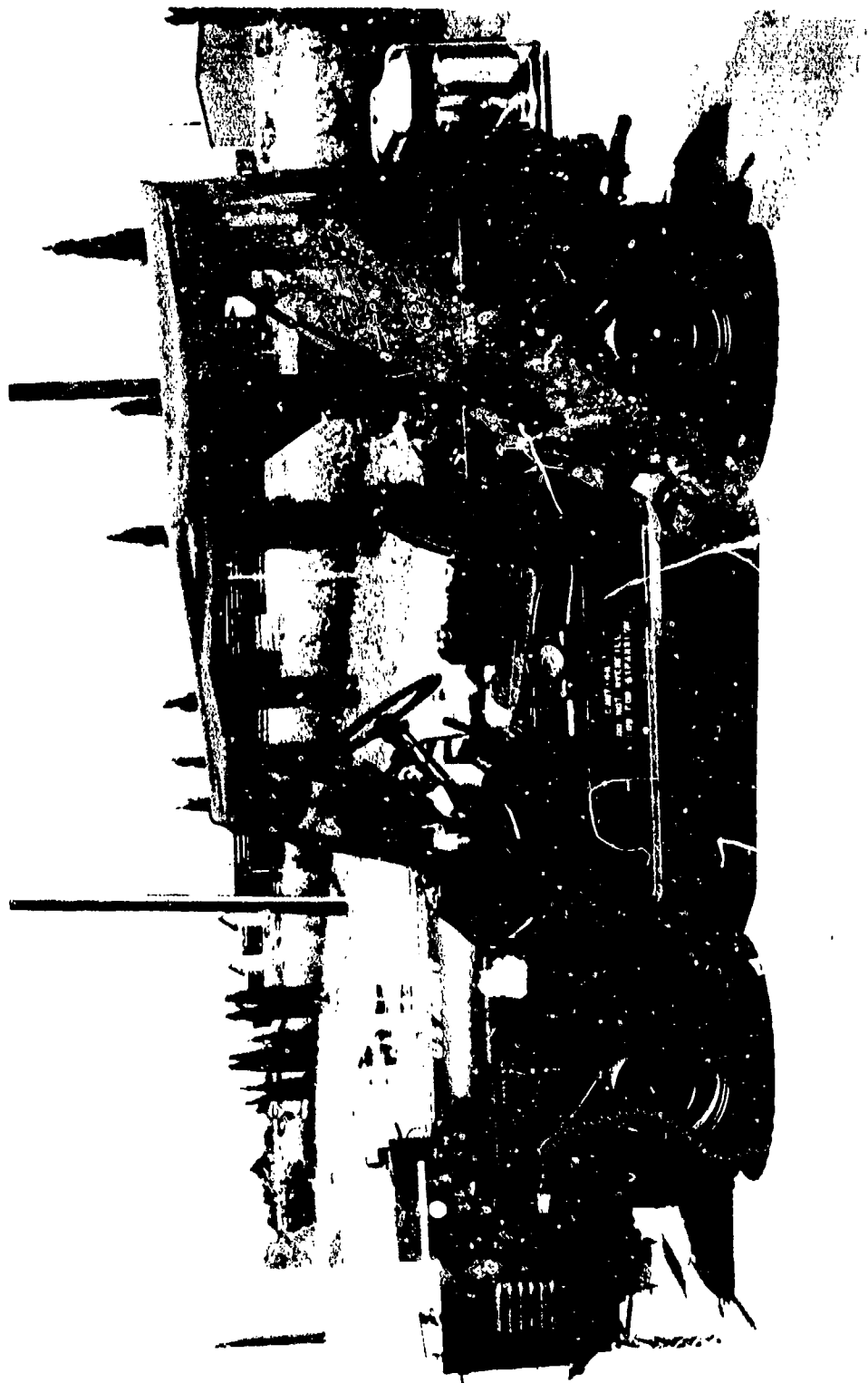


Figure 54. Dependence of countrate on height using Eu filter (grass-covered humic).  
(After Thompson)

coupled to RCA 6199 photomultiplier tubes as the radiation detectors. The system could be mounted either directly to the front bumper of a ¼-ton truck (Figure 55) or at the end of a 7-foot boom supported by a low-pressure tire. Power was supplied by a Honda Model 1500E motor/alternator set. For evaluation purposes, a Honeywell Model 2206 Visicorder Oscillograph was employed to record data from all four detectors and a tachometer simultaneously.

Figure 56 is a closeup of the searchhead. The X-ray tubes were mounted horizontally in the long aluminum tube visible below the support frame. Beam collimation was provided by internal litharge sections and by lead sheet wrapped around the outside of the housing. Positive high voltage was applied to the tube anodes by cables entering at each end, and negative high voltage to the cathode and filament power were supplied by a cable entering the housing from the top. The dielectric-oil coolant entered the tube housing from both ends, flowed around the tube anodes, and exited through the center top. The oil pump and cooling fan were housed in the aluminum box to the right of the searchhead shown in Figure 56. High-voltage (HV) power supplies (Hipotronics, Power Packs Models 80BP and 80BN) were contained in the aluminum box to the left of the searchhead, along with a small cooling fan. Each unit supplied up to 80 kV and 5 mA continuous. Since the X-ray tubes were operated in the center-grounded mode, each unit supplied half of the total high voltage. The emission control unit, the large aluminum can situated behind the X-ray tubes in Figure 56, later was replaced by an oil-filled unit situated on top of the HV power supplies. By sensing the current drawn by each tube from the negative HV supply, the control unit continuously adjusted filament power to give a constant X-ray-emission level (usually 1.2 mA at 135 kVp, continuous). The CsI (Tl) detectors, situated in front of the X-ray tubes, were mounted in lead shields to prevent the feedthrough of direct or single-scatter radiation. Collimation was provided by 1-inch-deep by 0.1-inch-square lead honeycombs and by a 4-inch-long annular shield mounted below the honeycombs. Each detector viewed a circular area, ~ 4.5 inches in diameter, on the soil surface at a nominal operating height of 15 inches. The rectangular object at the front of the searchhead was a mirror which permitted the vehicle operator to view the soil under the searchhead.

Figure 57 shows the service control section (behind driver's seat), the electronics section (to the right of the driver's seat), and the recorder as they were mounted in the ¼-ton truck. The service control section distributed power from the motor/alternator set (mounted on the rear bumper) to the remainder of the system. The electronics section contained the high-voltage supply for the photomultiplier tubes along with four independent data channels and the tachometer. Each data channel consisted of a low-noise, gain-controlled amplifier; a single-channel analyzer; and a variable-time-constant (25 to 1000-ms) ratemeter. Outputs from the ratemeters and tachometer were recorded on the strip-chart recorder mounted at the right rear.



T14729

Figure 55. Vehicle-mounted detector.

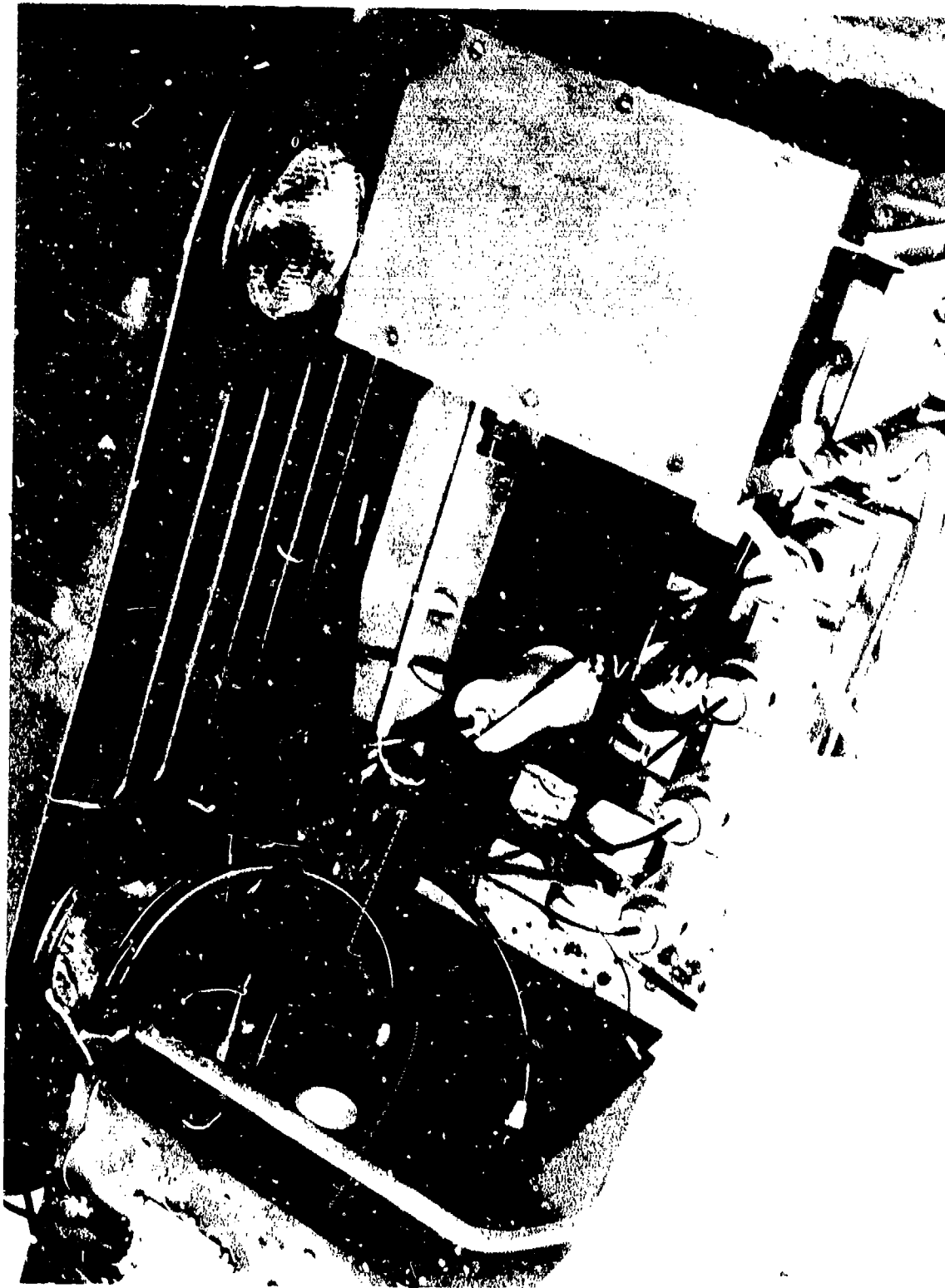


Figure 56. Closeup of searchhead.

T14726

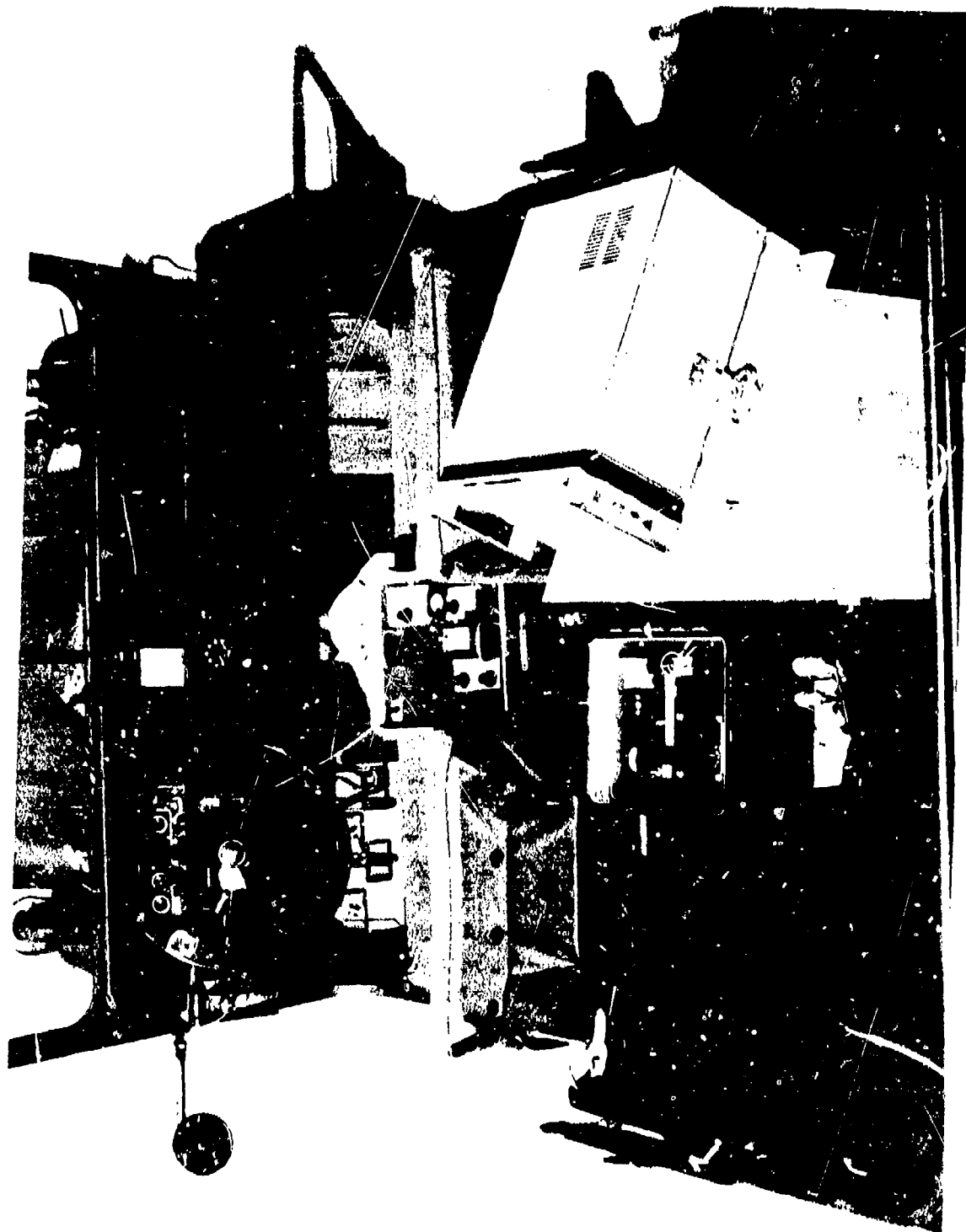


Figure 57. Service control section.

T14728

b. **Test Conditions.** In order to assess the performance of the vehicle-mounted system for various soil types under near-real-world conditions, tests were conducted along dirt roads at five Government facilities: Fort Hood, Texas; the Mississippi Test Facility; Eglin Air Force Base, Florida; the Jefferson Proving Ground, Indiana; and Fort Belvoir, Virginia. Tests were conducted over a 3-month period, from February through May 1973. Targets for these tests were simulated M-19, M-15, TMDB, and TM-60 antivehicular mines. (TM-60 mines were employed only at Jefferson Proving Ground and Fort Belvoir.) All targets were filled with DNT and emplaced in accordance with accepted military practices as outlined in FM 20-32 and TM 9-1345-200. Soil density, depth of emplacement, and the approximate density of the soil replaced over the target were recorded. In addition, runs were made along dirt roads in which no targets were buried in order to gauge the incidence of false alarms and to determine their origin. Source/detector separation ( $q$ ), search speed, and ratemeter time constant were parametrically varied in order to determine optimum parameters for field application. The range of variation of these parameters is shown below.

Range of Variables for Field Tests of Vehicular System

<u>Variable</u>	<u>Range</u>
$q$ (In.)	4.75; 5.75; 6.75
Time Constant $\tau$ (ms)	50; 100; 150
Search Speed $v$ (ft/s)	4; 10
Operating Potential (kV)	135

Based on this study, it was determined that  $q = 4.75$  inches,  $\tau = 50$  ms, and  $v = 4$  ft/s represented the best combination of parameters for field testing against antivehicular mines. Higher search speeds would require correspondingly lower values of  $\tau$  (see discussion in paragraph 19c).

c. **Test Results.** Figures 58-62 depict the results obtained at each of the five test locations, setting  $q = 4.75$  inches,  $\tau = 50$  ms, and  $v = 4$  ft/s, with the searchhead coupled directly to the front bumper of the  $\frac{1}{4}$ -ton truck. In each case, the peak value obtained as the searchhead passed over the target is the center of the crosshatched region at the top of the data bar. The width of the crosshatched area represents a  $\pm 2\sigma$  variation about this peak value. For comparison, the average background level, also with a  $\pm 2\sigma$  variation, is shown next to each target return. These figures show a rapid decrease in the target signal as emplacement depth is increased from 1 to 3 inches; there is a comparatively smaller decrease from 3 to 4 inches. At no time did a target disappear entirely. The Russian TMDB presented the strongest signature, and the Russian TM-60 the weakest.

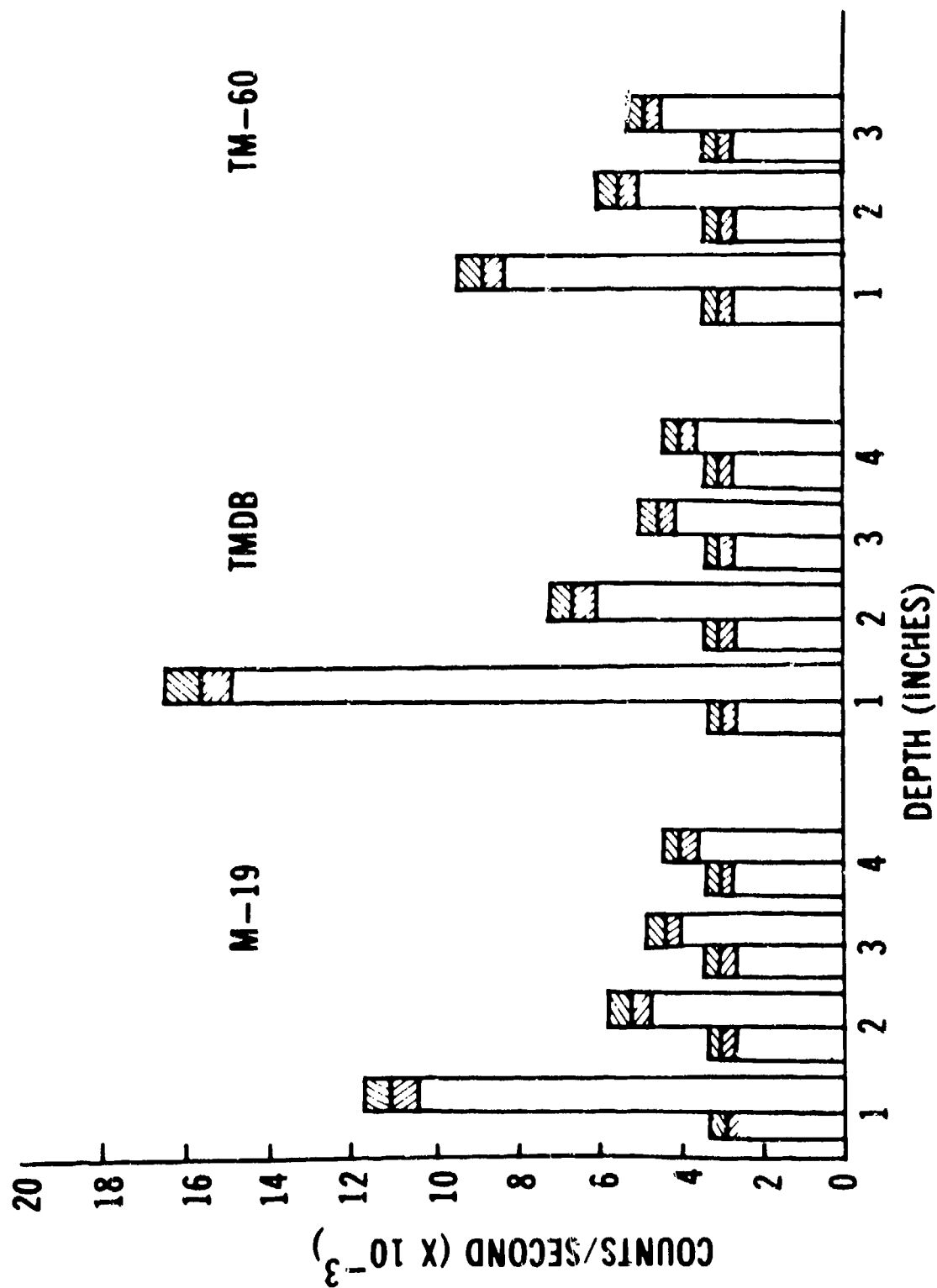


Figure 58. Jefferson Proving Ground results. (After Miller et al.)



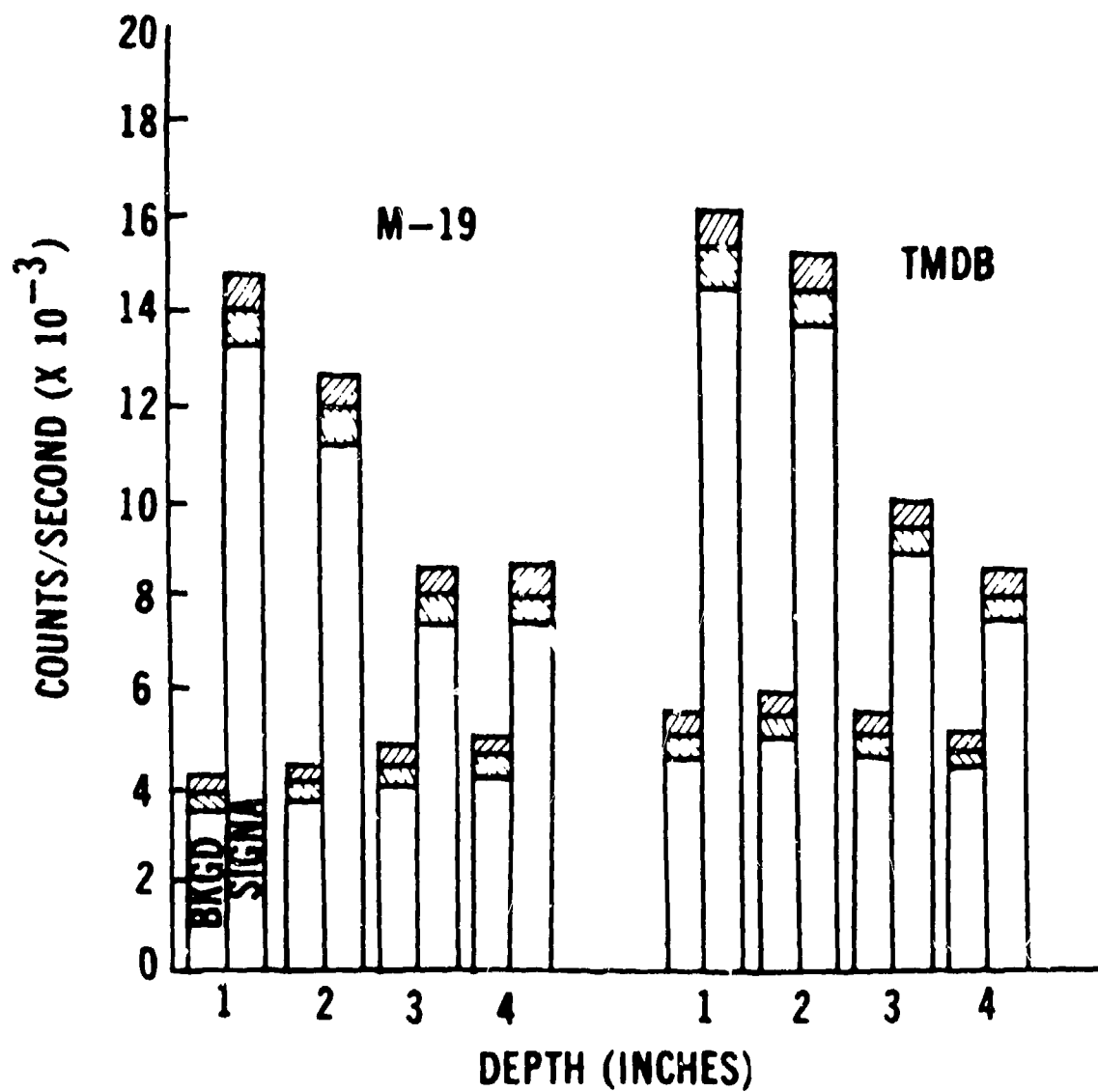


Figure 59. Fort Hood results. (After Miller et al.)

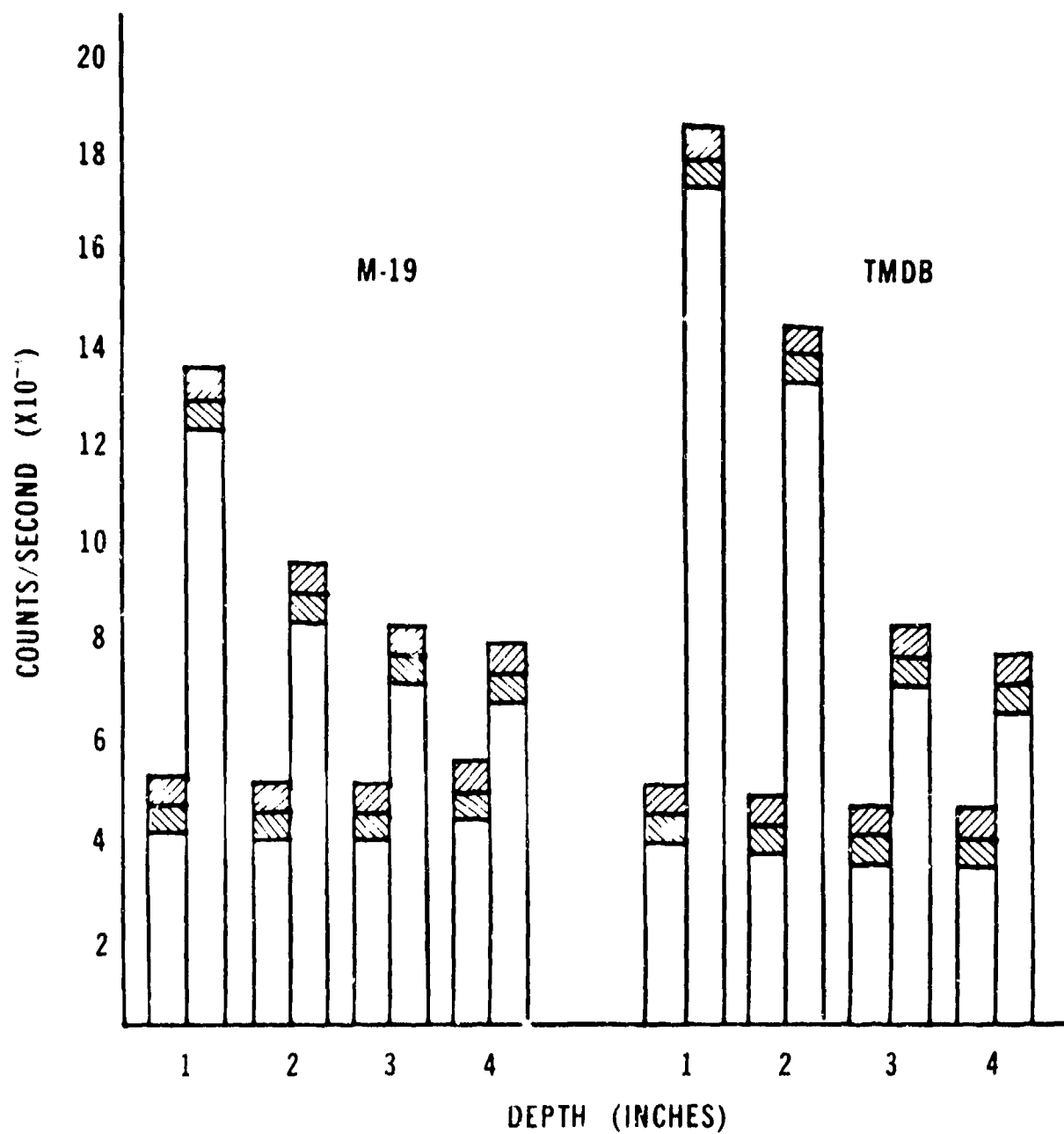


Figure 60. Mississippi Test Facility results. (After Miller et al.)

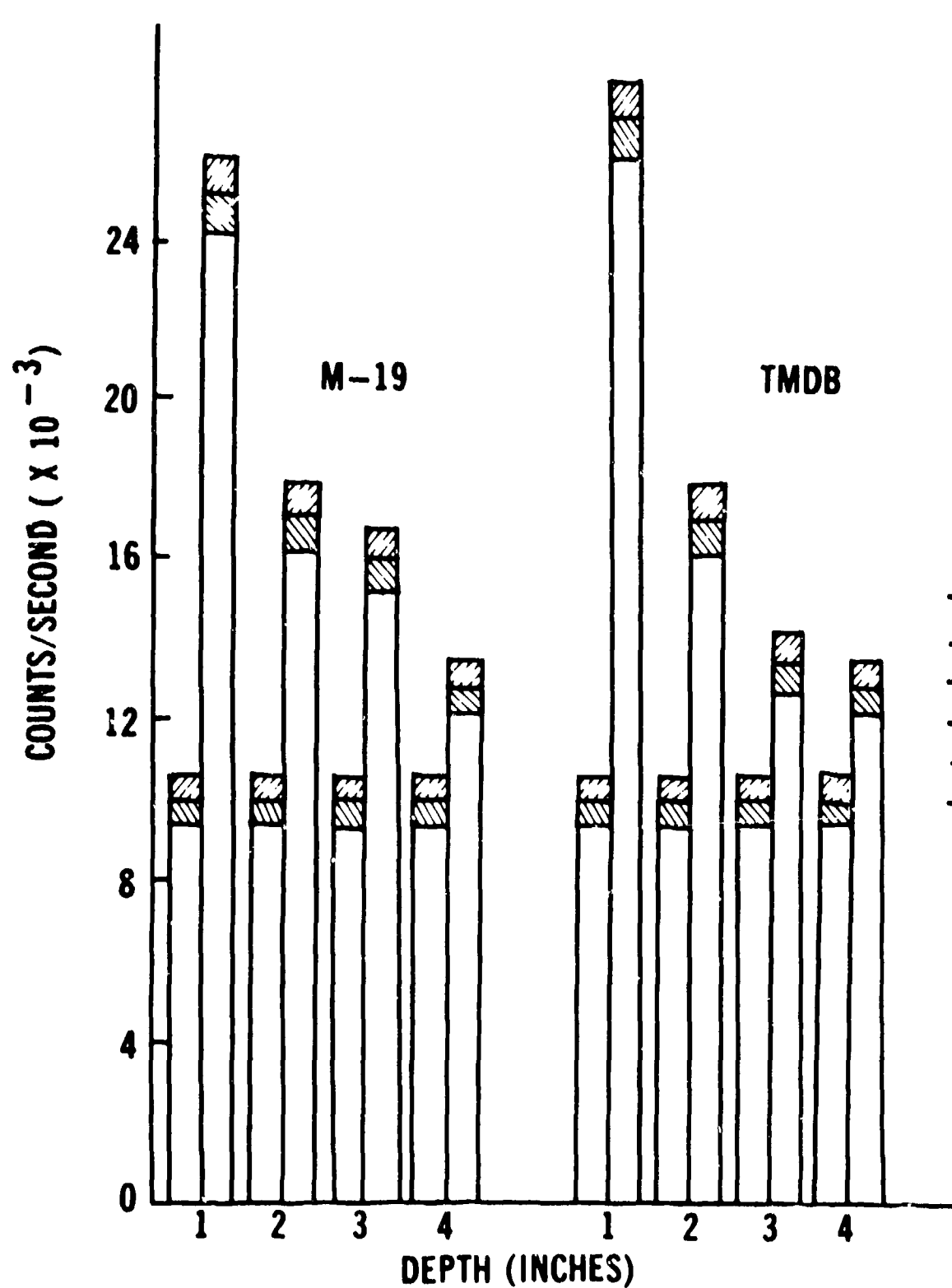


Figure 61. Eglin Air Force Base results. (After Miller et al.)

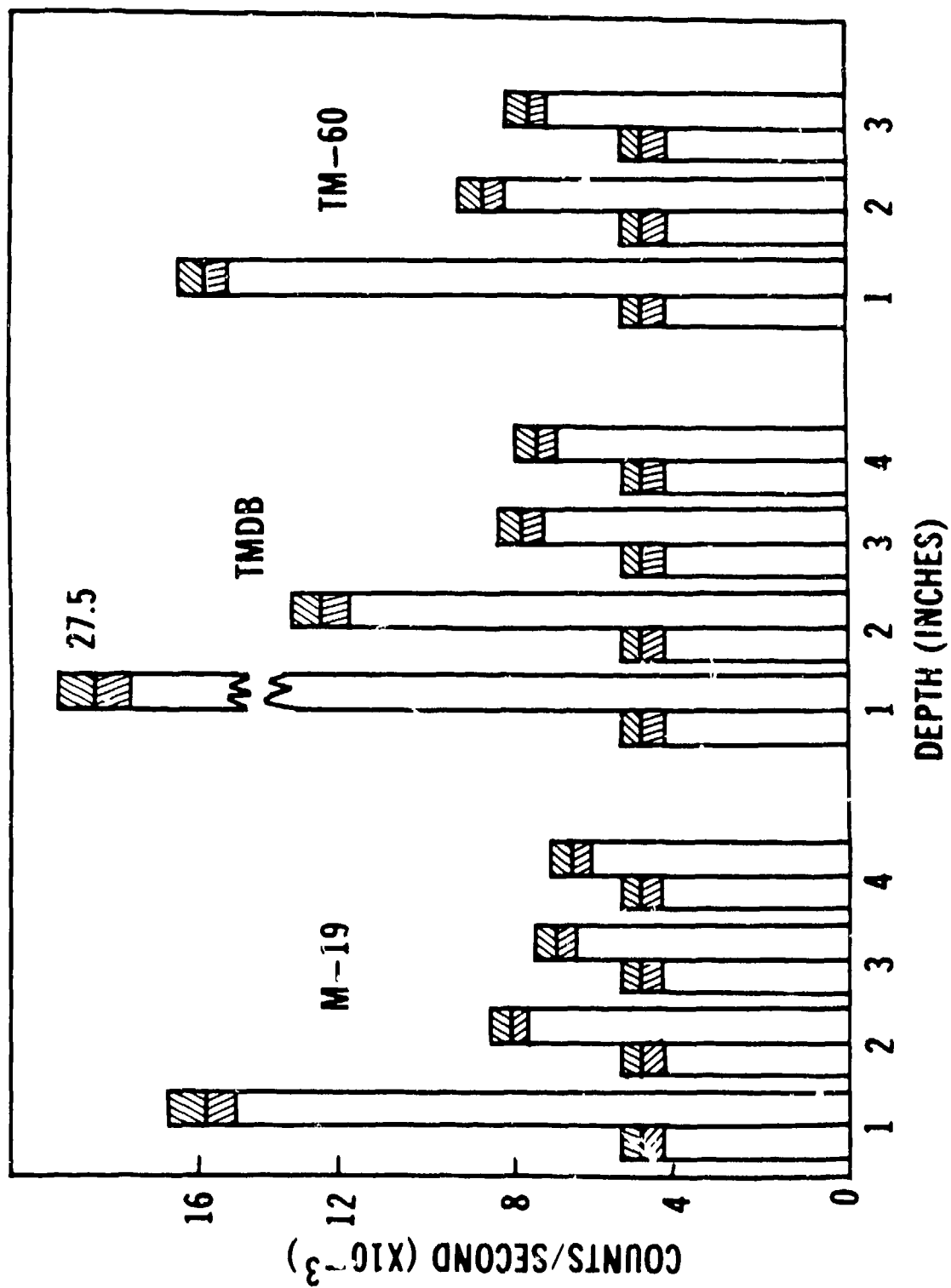


Figure 62. Fort Belvoir results. (After Miller et al.)

Although the test results, as presented here, appear to be extremely promising, they may be misleading in several important regards. First, the system was tested in areas known to be free of false alarms (e.g., buried organic artifacts, near-surface tree roots, etc.). Separate searches were made of roadways similar to and in the neighborhood of the test area in order to assess the expected incidence of false alarms. A false alarm was considered to be a point in the background (no target) trace which exceeded the normal background level by a certain ratio (R). Consequently, the number of false alarms encountered per mile of search was very much a function of the minimal R considered to represent an alarm. The higher the threshold, the fewer the number of false alarms but, also, the lower the probability of detecting a target. For example, Table 5 shows the probability of target detection and the number of false alarms per mile as a function of this threshold level for various targets and target-emplacement depths, given the same operating parameters used in obtaining the data shown in Figure 58. Thus, if 26 false alarms/mi are permissible, then antivehicular mines may be detected reliably when emplaced at a depth of 3 inches but not at a depth of 4 inches. If only 1 false alarm/mi is permissible, then mines may be detected reliably only up to 2 inches deep. It should be noted that the entries in Table 5 were arrived at by an inspection of the strip-chart recording. No attempt at signal processing was made. Since a mine produces a spike of characteristic duration (as a function of search speed), appropriate signal processing should significantly lower the false-alarm rate.

Table 5. False-Alarm Rate and Mine-Detection Probability as a Function of the Minimal R Value Required to Trigger an Alarm

Threshold R-Value	Probability of Mine Detection											False Alarms/Mile
	M-19 h-values				TMDB h-values				TM-60 h-values			
	(In.)				(In.)				(In.)			
	1	2	3	4	1	2	3	4	1	2	3	
1.1	1	1	1	1	1	1	1	1	1	1	1	$\infty$
1.2	1	1	1	1	1	1	1	1	1	1	1	277
1.3	1	1	1	0.7	1	1	1	0.7	1	1	1	26
1.4	1	1	0.8	0.2	1	1	0.9	0.2	1	1	1	1
1.5	1	1	0.4	0	1	1	0.5	0	1	1	0.8	1

NOTE: Data taken at Jefferson Proving Ground, Indiana, with  $q = 4.75$  inches,  $v = 4$  ft/s and  $\tau = 50$  ms.

Second, the test areas were comparatively level. Although geometry (b) is relatively height-insensitive (compared to geometries (a) and (c)), it is known that deep ruts (or other depressions) of width comparable to a mine diameter will produce false alarms. However, no tests were performed to quantitatively assess this problem.

Third, the test areas were either free of surface vegetation (Jefferson Proving Ground and Fort Belvoir) or covered with moderate vegetation (Fort Hood,

Mississippi Test Facility, and Eglin Air Force Base). Since it is known that dense vegetation will significantly lower R over a target and, if nonuniform, provide a potential source of false alarms, results obtained along roads cannot be extrapolated to operations across fields.

Finally, and perhaps most importantly, the signal obtained by the searchhead is partially a function of soil density. Data presented thus far were obtained by emplacing the targets according to standard, Army procedures; in this case, this resulted in the soil above the mine being recompacted to approximately 75 percent of its original density. Further tests by the contractor demonstrated that if the soil could be recompacted to its original density (which was not always possible), half the signal obtained from a mine emplaced at 3 inches was lost and that a mine emplaced at 4 inches disappeared entirely. (No significant signal loss was noted for targets emplaced at 1 and 2 inches.) Consequently, it must be concluded that mines emplaced at depths of 4 inches or more and which have "weathered in" will escape detection by this system. Further, in areas where mines have been freshly emplaced, the enemy could generate false alarms for harassment purposes by digging and refilling holes.

d. **Conclusions.** In these tests, the vehicle-mounted, X-ray backscatter system was demonstrated to be capable of becoming a practical field device capable of detecting nonmetallic antivehicular mines emplaced at depths of up to 2 inches along dirt roads maintained in reasonably good repair. It also was demonstrated that mines freshly emplaced in dirt roads at depths of 3 inches or more could be detected reliably with a reasonably low incidence of false alarms, provided that the mine emplacements are the only holes dug and refilled along the roadbed.

**19. Experimental Man-Portable Detector of Antipersonnel Mines (Coaxial Geometry).** This detector was designed and fabricated under Contract DAAK02-71-C-0359 with the Nuclear-Chicago Corporation. In total, three complete detectors were fabricated. The first such unit utilized 100 mCi of  $^{241}\text{Am}$  per detection element; the latter two units utilized 300 mCi of  $^{241}\text{Am}$  per detection element. Test results reported here were obtained at Fort Belvoir with the first-delivered detector.<sup>40</sup>

a. **Description.** Figure 63 shows the searchhead, electronics package, and associated hardware. Figure 64 shows the system in use at the Fort Belvoir Mine Lanes Test Facility. Note the three cylindrical housings mounted on the base plate of the searchhead. Each of these housings contained a 1.5-inch-diameter by 0.5-inch-thick

<sup>40</sup> Because of the degree of collimation required by the searchhead geometry, the source surface area could not be increased. Since  $^{241}\text{Am}$  has a low specific activity and a low gamma-ray energy, increasing the source activity by a factor of three increased the gamma flux at the aperture of the source collimator by less than 50 percent. Consequently, the performance manifested by the first searchhead was not significantly different from that manifested by the latter two searchheads.

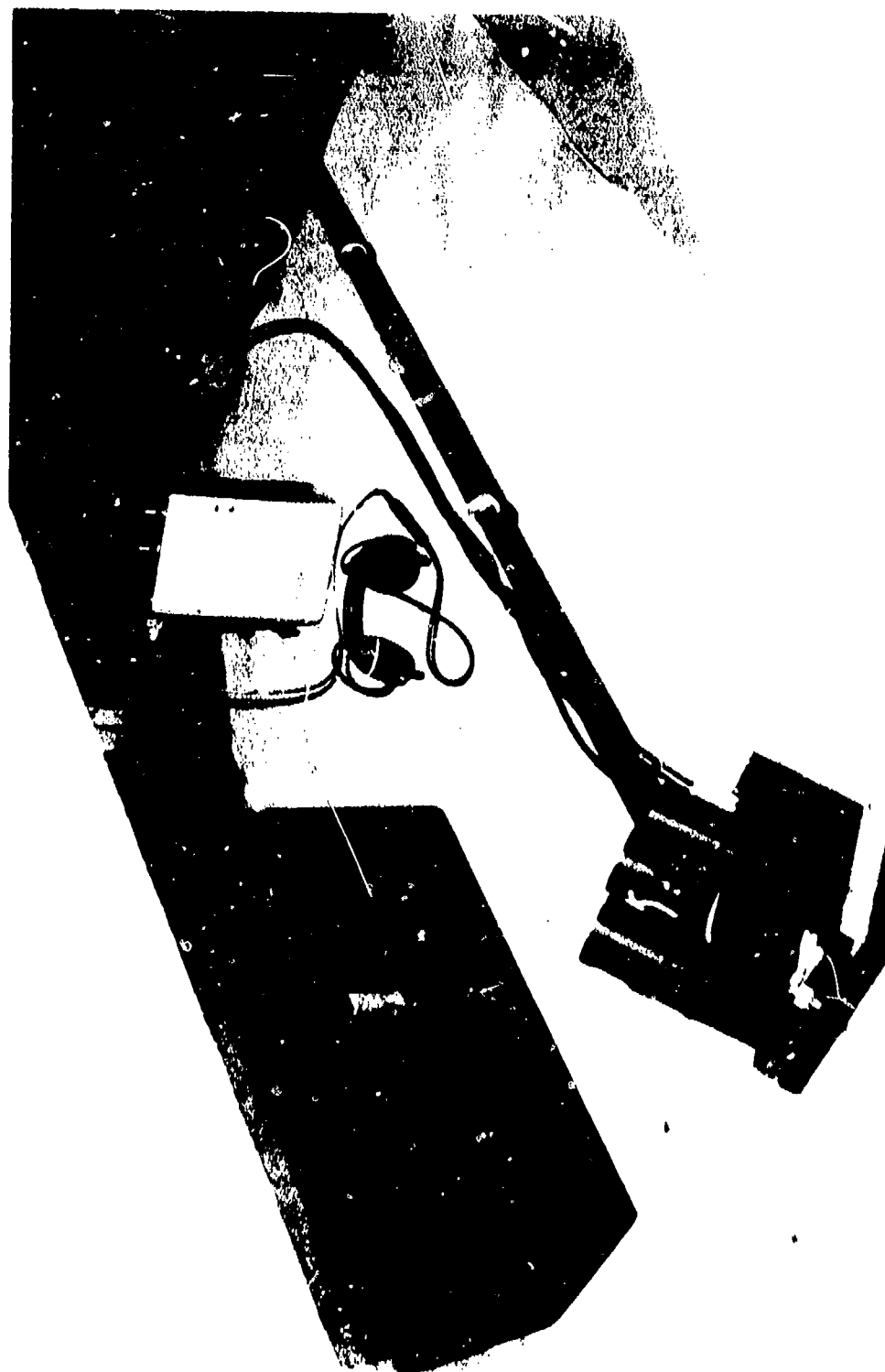


Figure 63. Experimental man-portable detector.

V3066



Figure 64. Experimental man-portable detector in use at Fort Belvoir.

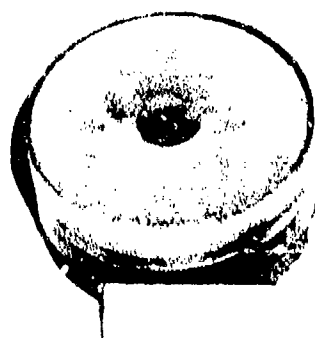
V3C60



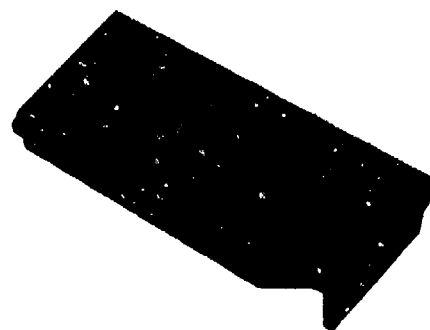
CsI (Tl) scintillator coupled to an RCA 31016F photomultiplier, an  $^{241}\text{Am}$  source (in this case, 100 mCi), and a combination collimator/scatter shield (see Figure 36). In addition, lead shields were positioned along part of the interior of the cylindrical housings to prevent crosstalk between detection elements. The meter, visible at the rear of the searchhead in Figure 64, was omitted from the latter two detectors, leaving only the aural readout. The searchhead was designed to operate at a height above the soil surface of from 1.5 to 3.5 inches, clearing a swath 6 inches wide (2 inches per detection element) with a lateral scan speed on the order of 1 ft/s.

The electronics package contained the batteries, the high-voltage supply for the photomultiplier tubes, three linear amplifiers, three discriminators, three variable-time-constant ratemeters, and the alarm subsystem. The alarm subsystem provided an audio signal to the earphones: the frequency of this signal increased with the output of the highest reading ratemeter. In addition, jacks were provided to enable the recording of the three ratemeter outputs directly.

**b. Test Conditions.** Tests were conducted in an inorganic clay test lane at the Fort Belvoir Mine Lanes Test Facility. The composition of the soil was 72 percent  $\text{SiO}_2$ , 20 percent  $\text{Fe}_2\text{O}_3$ , 5 percent organic, and 3 percent  $\text{H}_2\text{O}$ ;  $\langle Z \rangle \cong 12$  (see Table 2). For purposes of these tests, the detector searchhead was attached to a wooden dolly suspended on tracks above the test lane. Using the jacks provided on the electronics package, the ratemeter output from any one detection element was recorded on a Hewlett Packard Model 321 strip-chart recorder. Search speed was measured by dividing the distance traversed by the total time expended. However, because the speed of the dolly varied greatly from point to point for the same setting of the speed control, these figures should be considered only as average speeds. Similarly, although the surface of the test lane was nominally level, the figures given for detector height also should be considered to be averages. Targets for these tests consisted of M-14 antipersonnel-mine cases filled with 1 ounce of DNT and of mockups of PMN (USSR) and P-PMA-1 (Yugoslavian) antipersonnel mines. The foreign mines were fabricated in-house from drawings in TM 5-280 (Foreign Mine Warfare Equipment) and conformed to the originals in size, geometry, total weight, and weight of the high-explosive charge. DNT was used in place of TNT, and the balance of the mine was constructed of Lucite and epoxy. See Figure 65 and Table 6. All targets were emplaced in a straight line along the centerline of the path of one detection element. The M-14 mines were emplaced at 0 and 0.5 inch; the P-PMA-1 and PMN mines were emplaced at 0, 0.5, and 1.0 inch. In addition, mines with no DNT fill, emplaced flush with the surface, and an empty M-25, with its pressure plate above the surface, were inserted into the test line. The beginning and end of the test line were identified, respectively, by the signals produced by a DNB block and a bar mine (UK) emplaced flush with the surface.



MOCK-UP  
PMN NONMETALLIC  
ANTIPERSONNEL MINE  
(USSR)



MOCK-UP  
P-PMA-1 NONMETALLIC  
ANTIPERSONNEL MINE  
(YUGOSLAVIA)

Figure 65. Simulated foreign mines.

V3064

Table 6. Specifications Utilized in Preparing Mockups of Foreign Mines

Type	Shape	Dimensions	Weight (Ounces)	Main Charge (Ounces of TNT)
PMN (USSR)	Cylindrical	4.5 In. Diameter by 2.2 In. Deep	19	8.4
P-PMA-1 (Yugoslavia)	Rectangular Box	6 In. Long by 2.6 In. Wide by 1.3 In. Deep	9.8	7

c. **Test Results.** Figure 66 depicts a sample run made with the detection element centered on the test line at a height of 1.5 inch and the ratemeter time constant  $\tau = 100$  ms. The legend indicates the order and nature of the targets in the test line. The test results shown here are representative of the performance of this detector. Although the signal levels and signal-to-noise (S/N) ratio for specific targets could be increased or decreased by varying the test parameters, no target buried deep enough to escape detection in this trace could be discerned in any other test run. In each instance, the mines emplaced at 0 and 0.5 inch were detectable, as were the empty PMN and M-14 mine cases emplaced flush with the surface and the empty M-25 mine case. In each instance, the PMN mines yielded the strongest signal and the M-14 mines, the weakest. Neither for a mine emplaced at 1 inch could be detected.

Parameters varied for these tests were scan speed  $V$ , ratemeter time constant  $\tau$ , detector height  $h$ , and lateral displacement of the searchhead. Figure 67 illustrates the effects of varying  $\tau$ . The portion of each trace to the left of the heavy, vertical line was obtained with the detector stationary; consequently, the signal fluctuations shown are due almost entirely to statistical noise. Note that as  $\tau$  increases, the amplitude of these statistical variations decreases. By visually projecting these statistical variations across the traces, one may conclude that, given the ideal conditions of the test lane, no other source of noise is significant. From Figure 67 it also may be concluded that the S/N ratio for a target at a given scan speed varies with  $\tau$ . In general, the larger the target diameter, the higher the optimum value of  $\tau$ . From a visual inspection of the data, it was determined that  $\sim 100$  ms worked best for an M-14 and that  $\sim 150$  to 250 ms worked best for a PMN.<sup>41</sup> However, since in all cases the M-14 posed the more difficult detection problem, further tests were performed with  $\tau = 100$  ms.

<sup>41</sup> It can be shown that, in counting random events with a ratemeter, the optimum operating condition for detecting a transient increase in the mean counting rate is achieved when  $\tau \approx 0.8t$ , where  $t$  is the duration of the transient. However, it also can be shown that transient detection does not degrade rapidly as  $\tau$  is varied from this value. The reader may readily verify that agreement with this result was obtained in the present case. [K. G. Forges, *Detection of Transients in Nuclear Surveillance - Counting Channels*, Report No. ANL-7470, Argonne National Laboratory (Nov 1968).]



Figure 66. Sample test run.

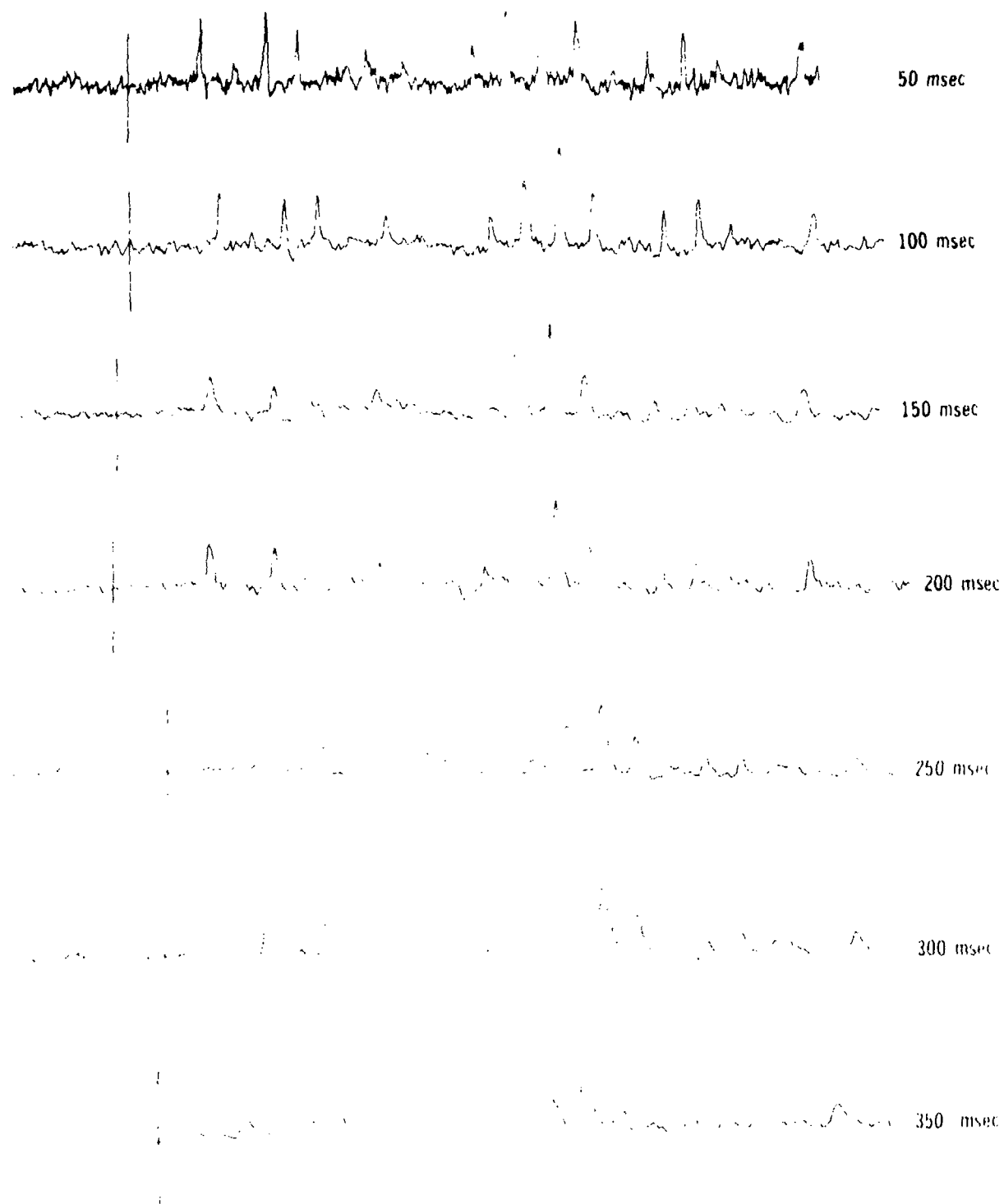


Figure 67. Effects of varying the ratemeter time constant.

Figure 68 illustrates the effect of varying detector height. Note that, as  $h$  increases, the S/N ratio decreases for all targets, although this effect is of greater importance for the smaller targets. Over the designated operating range of 1.5 to 3.0 inches, the S/N ratio for a PMN decreased by 20 percent; whereas, for an M-14 the S/N ratio decreased by 50 percent. The change in the no-mine signal over the soil as  $h$  was varied was far more stable: over the 1.5- to 3.0-inch operating range, the signal increased by less than 5 percent. This indicated that minor changes in soil microrelief would not produce false alarms.

Figure 69 illustrates the effects of displacing the sensor to the left or right of the test line. The larger targets (P-PMA-1 and PMN) showed essentially no decrease in S/N for left or right displacements of at least 1 inch. The M-14 and M-25, on the other hand, showed marked decreases for even 0.5-inch displacements. Since the design goal for each detection element of the searchhead was to cover a 2-inch-wide swath, the marked drop in S/N for an M-14 passing the detection element 1 inch off axis (50-percent drop for 1-inch-right displacement, 85-percent drop for 1-inch-left displacement) indicated that a target the size of an M-14 could pass readily under the searchhead and still not be detected.

In addition to the tests performed in the Mine Lanes, the detector was employed in tests along dirt roads and in grassy areas of Fort Belvoir in order to assess the detector's potential false-alarm rate under real-world conditions. Although no attempt was made to record or analyze the detector's performance under these conditions, it was clearly determined that operating the detector in areas with even moderate vegetation resulted in continuous false alarms: small clumps of grass always yielded signals as strong as those obtained for a surface-emplaced M-14. The PMN mine posed a better target, but even the signal from this mine could be lost in sufficiently lush vegetation. Only in areas with no visible vegetation did the false-alarm rate drop to a reasonable level. In this environment, the detector could reliably detect PMN mines buried at depths of up to 0.5 inch, although it could not reliably detect surface-emplaced M-14's due to the limited coverage of the detection elements.

**20. Breadboard Searchhead: Man-Portable Detector of Antipersonnel Mines (Geometry (b)).** This searchhead was designed and fabricated under a modification to contract DAAK02-71-C-0359 with the Nuclear-Chicago Corporation after preliminary testing of the previously fabricated coaxial searchhead had revealed its deficiencies. The design objectives of this latter searchhead were twofold: (1) to enable the detection of a surface-emplaced M-14 mine in a moderately vegetative environment and (2) to assure the detection of an M-14 mine passing anywhere beneath the searchhead. The searchhead employed a  $^{90}\text{Sr}/^{90}\text{Y}$  beta source and small Geiger-Mueller detectors to effect height compensation, along with  $^{241}\text{Am}$  gamma sources and  $\text{NaI}(\text{Na})$  scintillation detectors for target detection. (See paragraph 16)

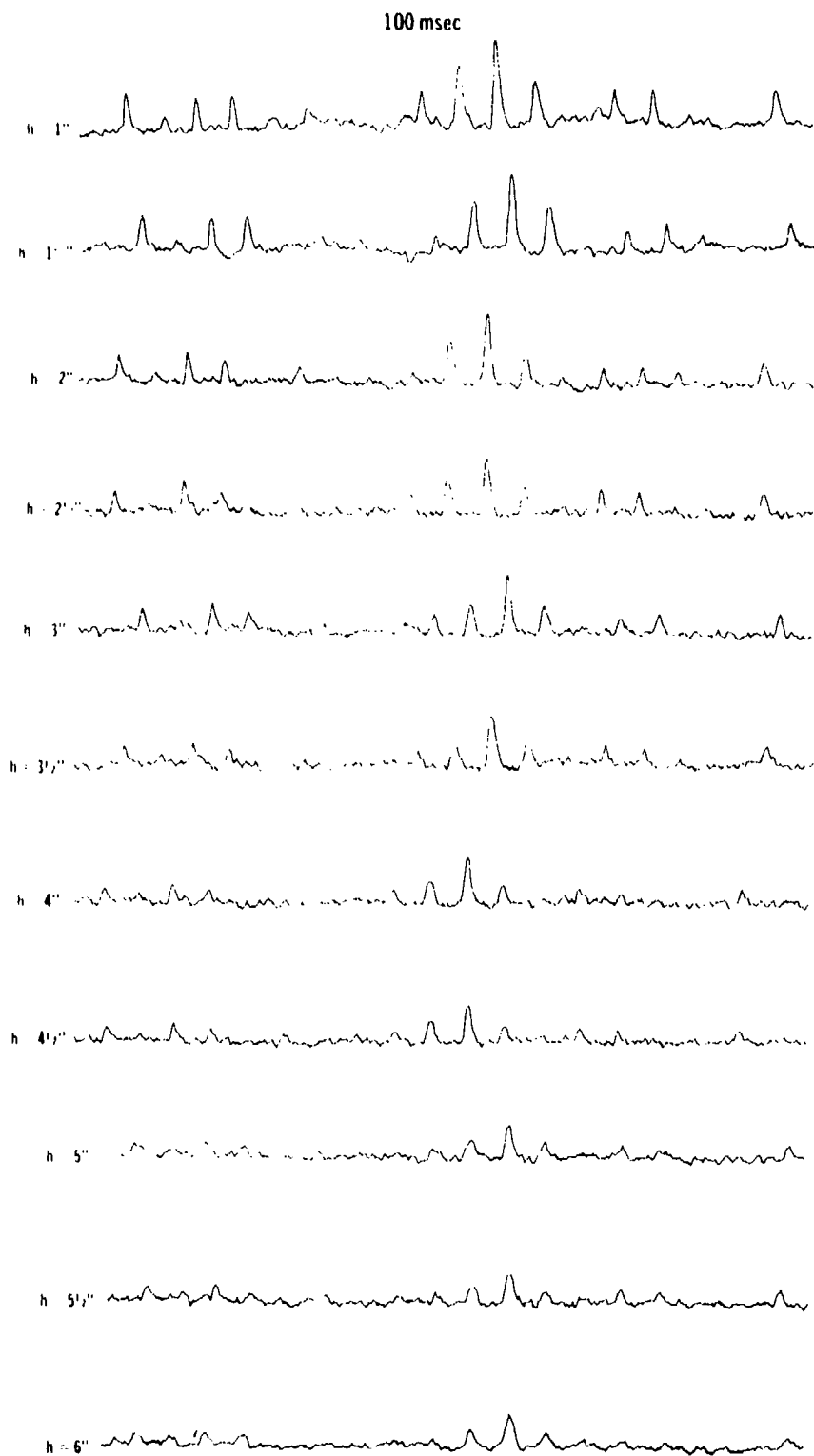


Figure 68. Effects of varying detector height.

# LEFT OFF SET

# RIGHT OFF SET

Offset	Left Off Set	Right Off Set
0	0	0
1.4	1.4	1.4
1.2	1.2	1.2
3.4	3.4	3.4
1	1	1
1.4	1.4	1.4
1.2	1.2	1.2

Figure 69. Effects of centerline offset.

107



a. **Description.** Figure 70 is a sketch of the breadboard searchhead. It consisted of six detection elements unequally spaced about a 4-inch-diameter circle and a single, cylindrical source collimator/shield placed at the center of that circle. Structural support was provided by two spaced, aluminum disks; a separate cover plate was provided to shield the exit port of the source cylinder when the searchhead was not in use.

The spacing of the detection elements was such that, when the searchhead was laterally scanned, each element viewed a nonoverlapping, 0.75-inch-wide swath. Each element consisted of a lead-shielded, 1-inch-diameter by 1/8-inch-thick CsI(Na) scintillator, coupled to an RCA C31016F photomultiplier and placed above a 1-inch-diameter by 1.5-inch-long, cylindrical lead collimator. An Amperex 18550 (623) GM tube was positioned in the collimator with the tube axis 0.5 inch below the lower face of the scintillator.

The lead source cylinder (positioned between the aluminum support disks), contained four 300-mCi  $^{241}\text{Am}$  gamma sources — each with its own collimator — and a 1-mCi  $^{90}\text{Sr}/^{90}\text{Y}$  beta source positioned at the bottom of the cylinder. In the electronics package, four external potentiometers were provided; these controlled beta offset, beta slope, gamma offset, and gamma slope. Before using the searchhead, it was necessary to follow a calibration procedure to adjust these potentiometers for the local soil conditions. (See paragraph 16, especially Figure 37, for explanation.) Output of the electronics section could be displayed on a meter or remotely recorded on a strip-chart recorder.

b. **Test Conditions.** By the time of delivery of the breadboard searchhead, it already had been determined that, given the theoretical limitations of the photon-backscatter approach, no mine detector utilizing this principle would find acceptance within the Army system. Consequently, only limited acceptance testing of the breadboard searchhead was performed.

Tests were performed in the Mine Lanes Test Facility in order to facilitate reproducible positioning of the searchhead and recording of the data. The soil sample used for these tests, however, was taken as a single block from a grassy area of Fort Belvoir. No attempt was made to quantitatively assess the organic and water content of this sample; qualitatively, it was moist and fully covered by grass and weeds. The only target used for these tests was an M-14 mine case, filled with 1 ounce of DNT and buried flush with the soil surface.

c. **Test Results.** After calibration of the searchhead over the soil sample, tests were run at three heights: 2, 2.5, and 3.5 inches. (See Figure 71.) Scans at heights below 2 inches were precluded by irregularities of the soil. Scan speed, although not

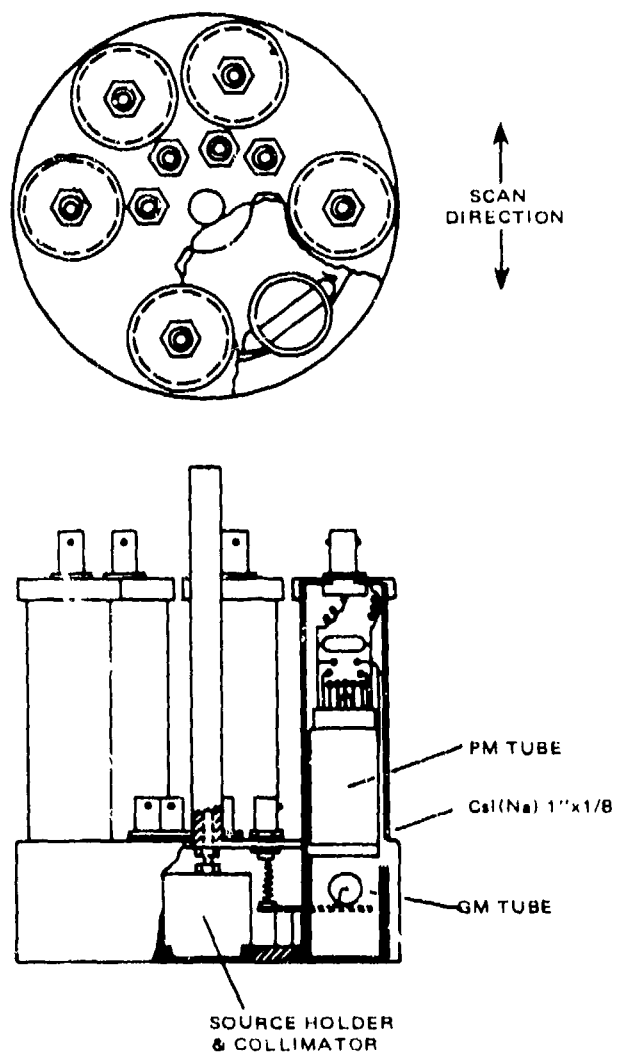


Figure 70. Sketch of beta-gamma breadboard searchhead.  
(After Miller, Anastasi, and Tucker)

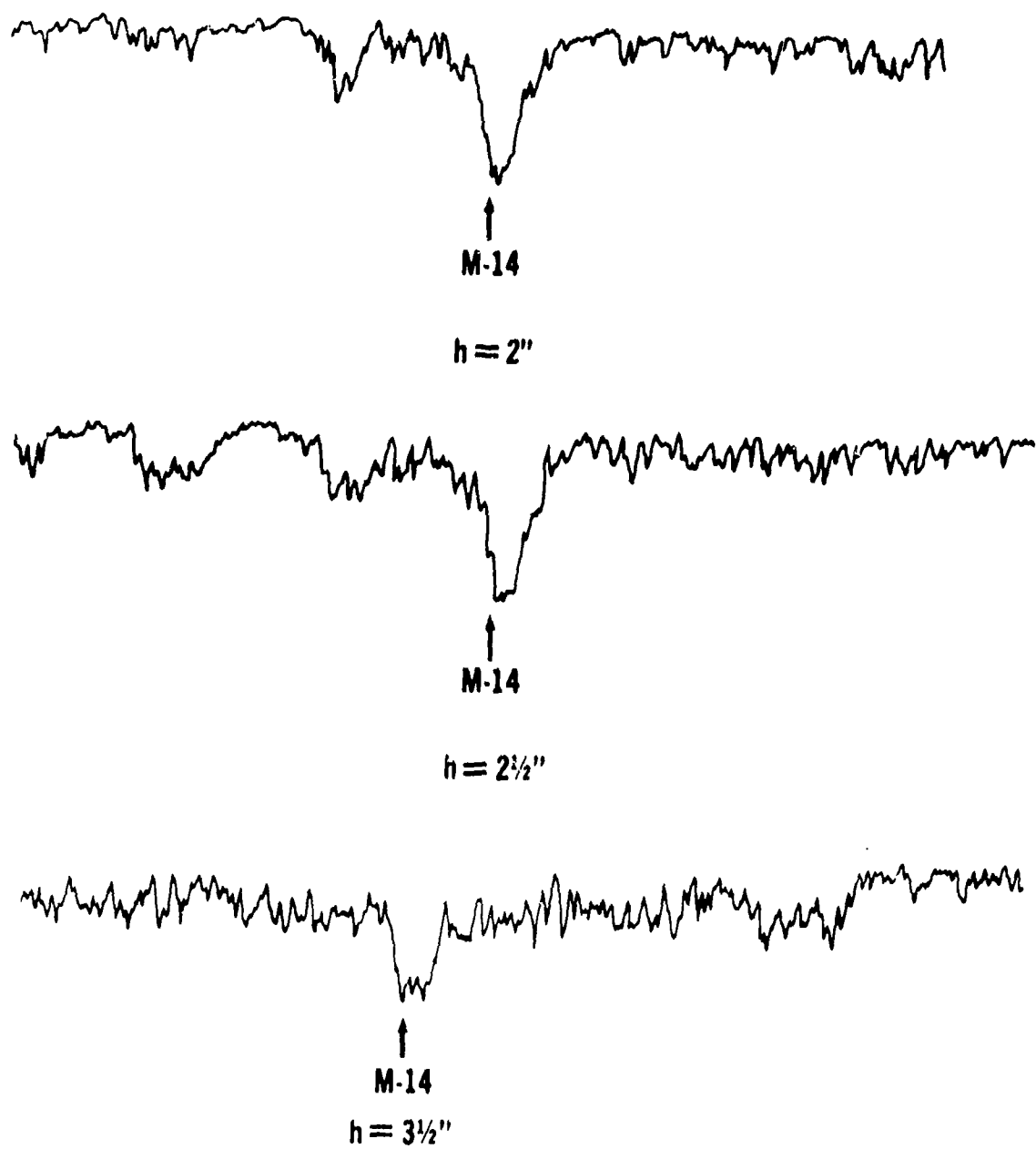


Figure 71. Test results for beta-gamma breadboard searchhead.

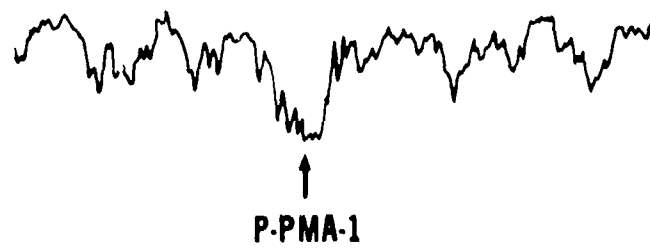
measured, was extremely low ( $< 0.5$  ft/s); data were recorded only for the detector element passing directly over the target.

The S/N ratio measured for the M-14 varied from a high of  $\sim 2$  at  $h = 2$  inches to a low of  $\sim 1.5$  at  $h = 3.5$  inches. It must be emphasized, however, that, unlike in the case of the coaxial detector, the "noise" we now refer to is due to surface irregularity and differences in organic and water content, as well as to statistical variations. Under identical conditions, the coaxial detector was totally unable to detect the M-14. On the negative side, it must be remembered that this searchhead must be calibrated for each type of soil encountered. Figure 72 shows the result of using the searchhead, while calibrated for grass, over a gravel test bed in which a P-PMA-1 mine has been emplaced. Clearly, variations in the background are prohibitively large.

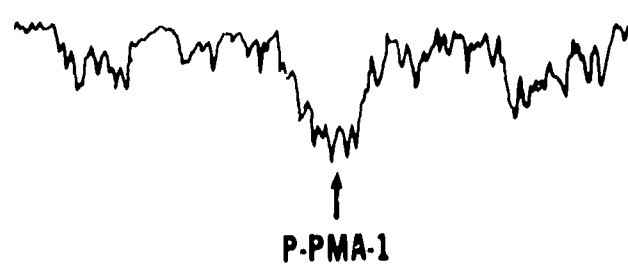
**d. Conclusions.** Tests of the breadboard-model searchhead demonstrated that it did meet its design goal of detecting surface-emplaced M-14 mines in moderately vegetative areas. No offset tests were performed to determine if this searchhead, like the coaxial searchhead, had a coverage problem. However, logic (and contractor-performed tests) indicate that the searchhead did not suffer from such problems (each detection element viewed a 0.75-inch-wide swath instead of the 2-inch-wide swath in the coaxial design). Principal deficiencies of this breadboard-model detector were its slow scan speed ( $\sim 0.5$  ft/s), narrow coverage (4-inch-wide swath), and need for calibration before use.

**21. Breadboard Searchhead: Man-Portable Detector of Antipersonnel Mines (Geometry (c)).** This searchhead was designed and fabricated by the Industrial Nucleonics Corporation under Contract DAAK02-72-C-0619. The searchhead was developed concurrently with the development of the geometry-(b) searchhead by TND. The major design objectives for this searchhead were identical to those for the geometry-(b) searchhead, namely: (1) to detect surface-emplaced M-14 mines in moderately vegetative media, and (2), to detect M-14 mines passing anywhere beneath the searchhead. As a secondary design objective, it was intended that the R values obtained by this searchhead for M-14 mines be essentially independent of searchhead height over the designated operating range  $h = 2$  to 5 inches. Height compensation of the searchhead was to be accomplished by the K-edge filter technique (see paragraphs 11c and 17), although the delivered breadboard detector was neither optimized for the implementation of this technique nor capable of the necessary real-time signal processing.

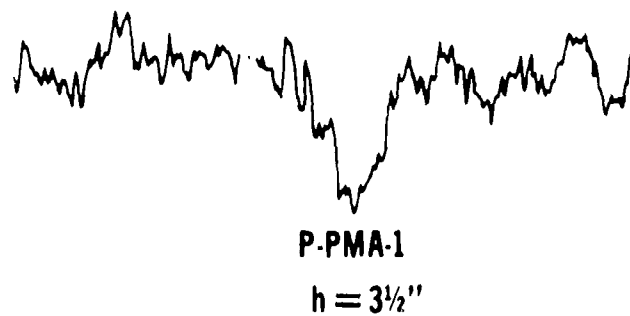
**a. Description.** The searchhead consisted of two 1-inch-diameter NaI (Tl) scintillators coupled to 2-inch-diameter photomultipliers. (Employment of 2-inch-diameter instead of 1-inch-diameter photomultipliers was a mistake on the part of the detector vendor. The performance schedule of the contract precluded rectification of this error.) Collimation was provided by 1.5 inch-long, variable-hole-diameter brass



$h = 2''$



$h = 2\frac{1}{2}''$



$h = 3\frac{1}{2}''$

Figure 72. Test results over gravel when the searchhead is calibrated for grass.

cylinders (see paragraph 17). The detector axes were tilted toward each other so that both detectors viewed the same area on the soil surface for  $h = 2.5$  inches. A thin Eu foil was placed in front of one of the cylinders. The source, 1 Ci of  $^{241}\text{Am}$ , was housed in a lead cylinder between the detectors and was shielded by a spring-loaded lead shutter when the searchhead was not in operation. When the shutter was open, the source irradiated the entire area below the searchhead. The electronics package for this searchhead was in the form of NIM modules: high-voltage supply, linear amplifier, single-channel analyzer, and printing scaler/timer. Output from both detectors could be processed and recorded simultaneously.

b. **Test Conditions.** Tests were performed by the contractor with the apparatus and under the conditions described in paragraph 17. In addition, some very limited tests were performed at the Fort Belvoir Mine Lanes Test Facility utilizing a level and essentially uniform piece of sod over a gravel base as the test medium. The target for all tests was an M-14-mine case filled with 1 ounce of DNT. All measurements for this searchhead were made in a static configuration and with long count times. Consequently, statistical variation in the data was not significant.

c. **Test Results.** It was empirically determined by the contractor that the quantity  $N_1^2/N_2$  (where  $N_1$  and  $N_2$  are the total number of counts obtained by the filtered and unfiltered detectors, respectively) represented a good figure of merit for target detection. It must be emphasized, however, that the searchhead was not optimized for height compensation and that this figure of merit was not the result of an analysis of signal-processing techniques. Figures 73 through 76 show  $N_1^2/N_2$  as a function of position for several values of  $h$  for each of the soil types considered (sand, road-bed, humic, and grass-covered humic). In each case, the axis of the target was at  $Y = 0$ . These figures indicate that an M-14 could be detected by a searchhead of this kind over the range of  $h$  values considered for all soil types except the grass-covered humic. In this last case, for constant values of  $h$ , the target was clearly discernible. However, the count-rate was found to vary too greatly with searchhead height to permit reliable detection in the field. Without additional effort, it cannot be determined if the target-masking effects of insufficient height compensation could be overcome by better sensor design or signal processing.

The tests performed at Fort Belvoir did not attempt to achieve height compensation: the sod employed was as uniform and level as possible, and only differences in the unfiltered countrate were considered. These tests showed that an R value of  $\sim 1.3$  was attainable for a surface-emplaced M-14 in moist sod.

d. **Conclusions.** Tests of the geometry-(c) breadboard-model searchhead demonstrated that an uncollimated-source - collimated-detector design can detect surface-emplaced M-14 mines in moderately vegetative areas. No attempt was made to

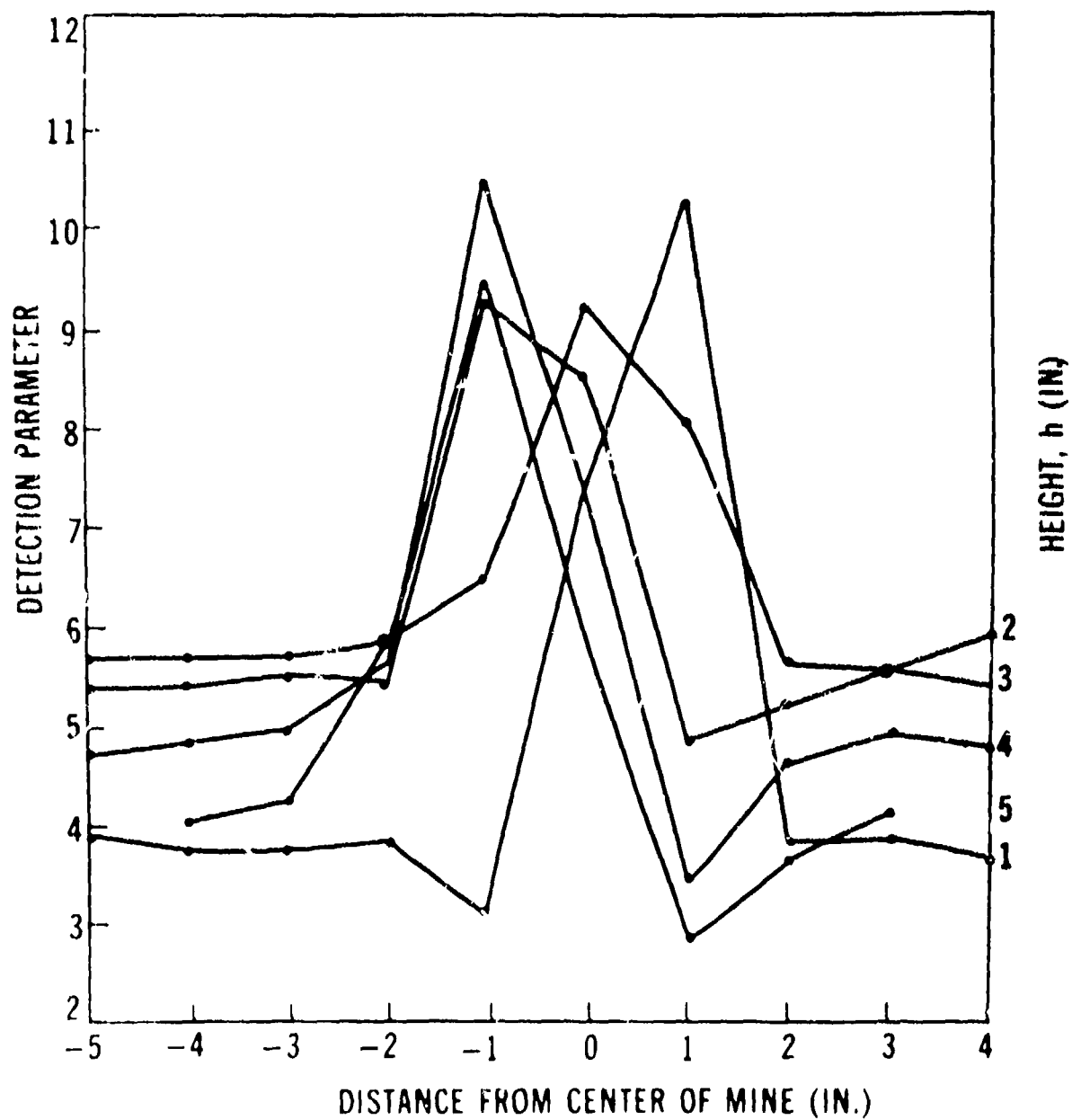


Figure 73. Performance of filter height-compensated searchhead (sand).  
(After Thompson)

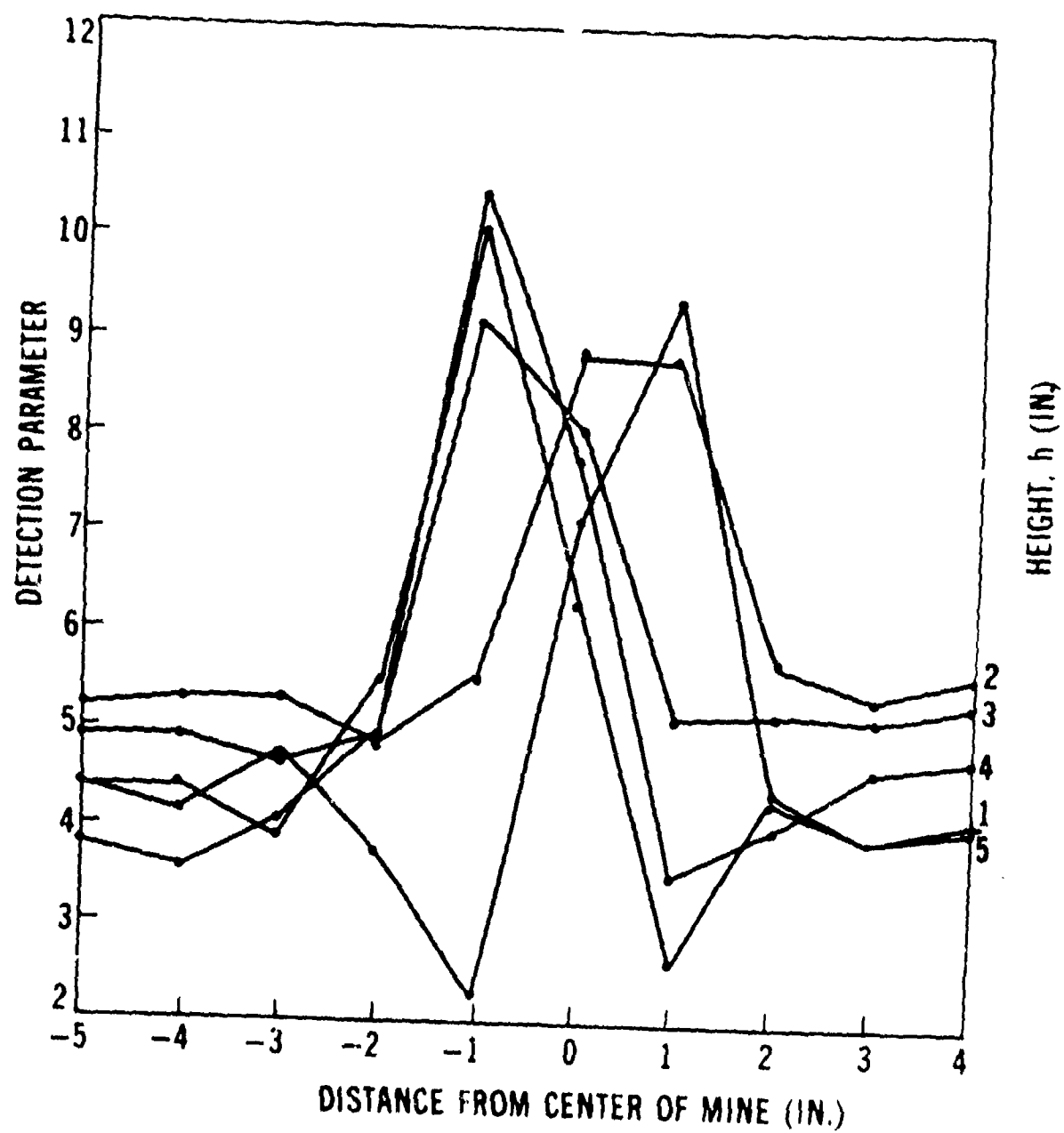


Figure 74. Performance of filter height compensated searchhead (roadbed).  
(After Thompson)



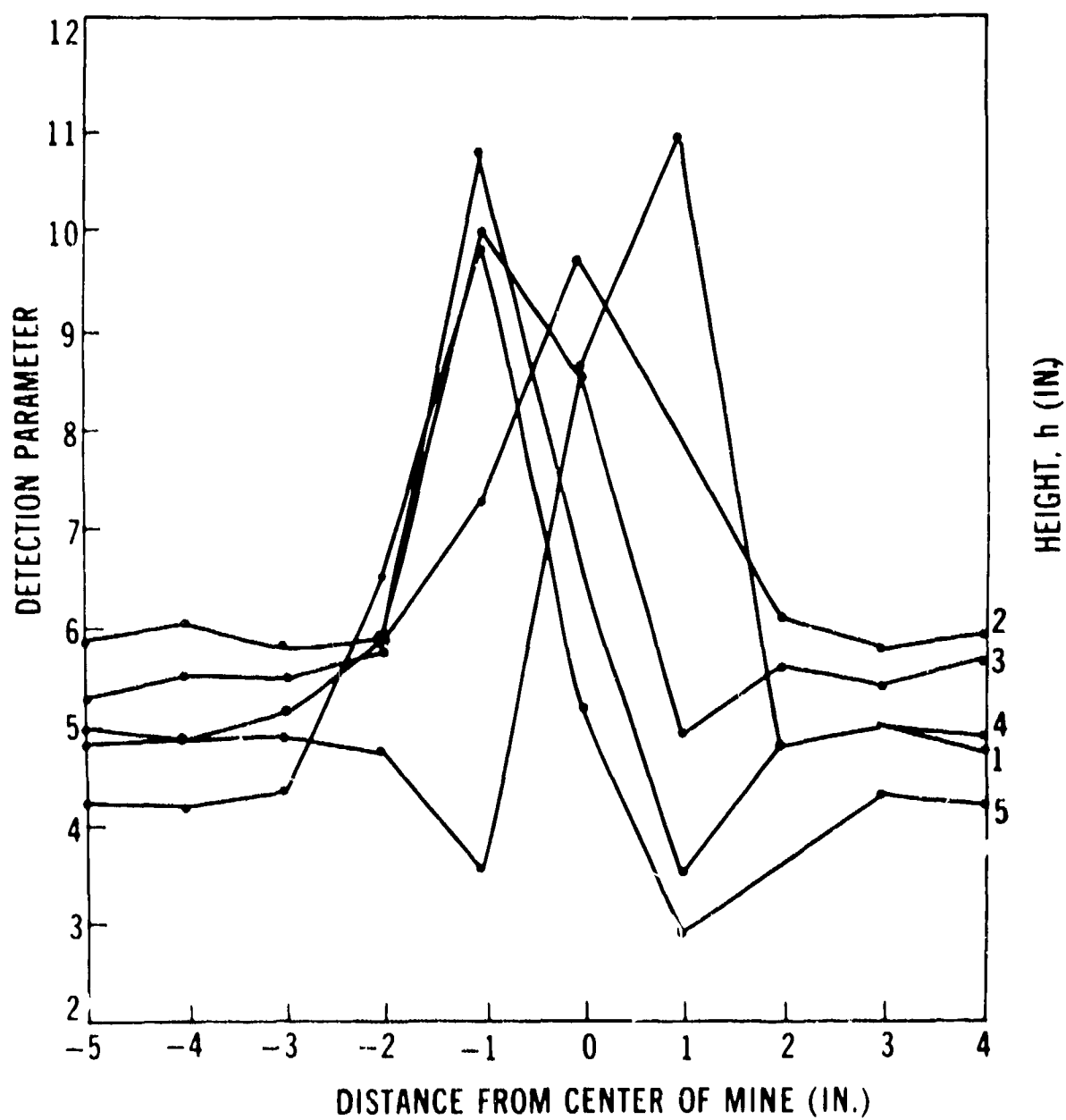


Figure 75. Performance of filter height-compensated searchhead (humic).  
(After Thompson)

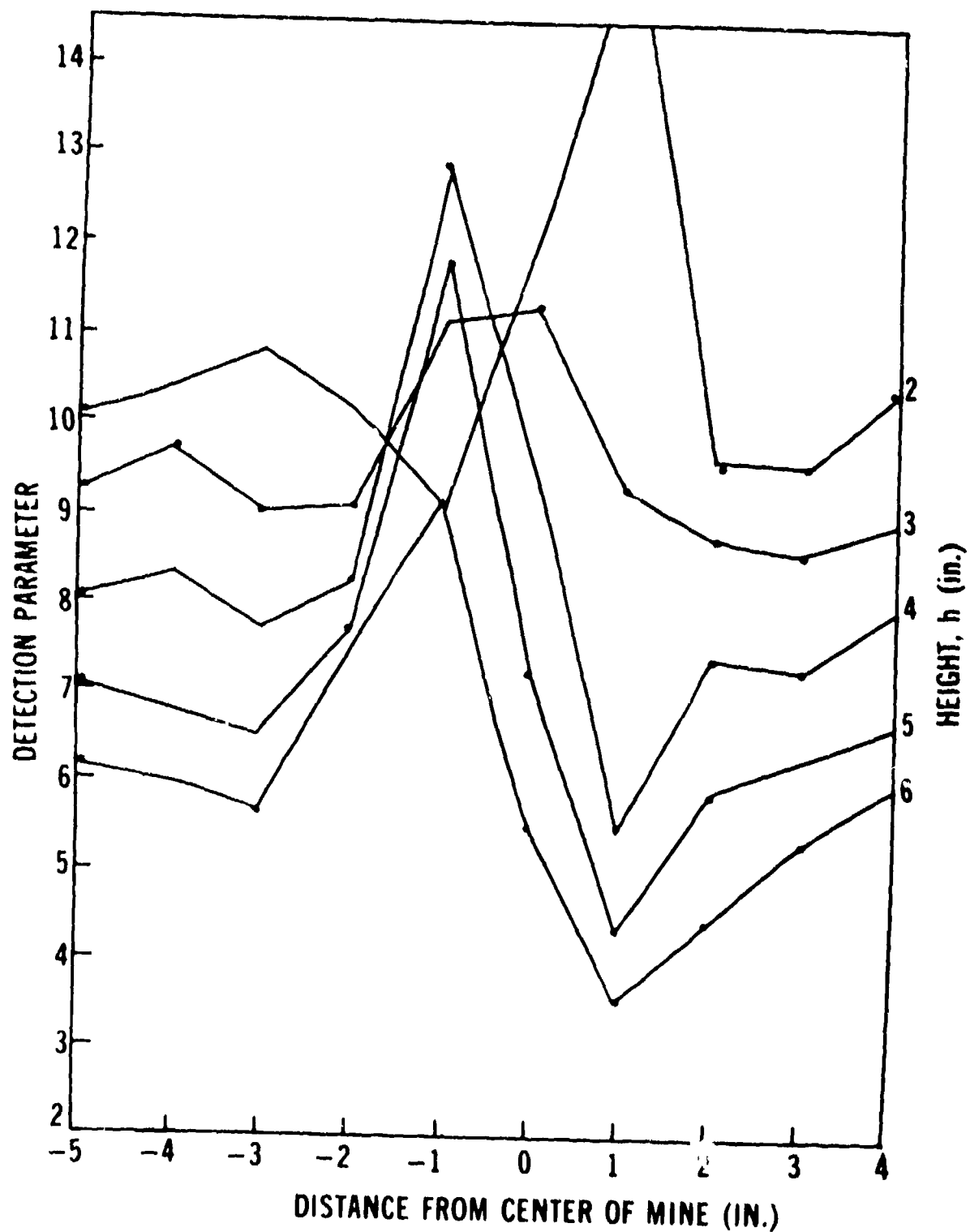


Figure 76. Performance of filter height-compensated searchhead (grass-covered humic).  
(After Thompson)

assess the coverage potential of this design, although there is no reason to expect this to be a problem. Unlike those for the TND searchhead, R values for the geometry-(c) searchhead remained essentially constant for  $h = 2$  to 5 inches. This however, was achieved at the expense of countrate; it was for this reason that only static measurements were made. Finally, the geometry-(c) searchhead demonstrated the potential feasibility of utilizing the K edge filter technique to achieve height compensation. Although by no means certain, this technique does look promising.

## V. SUMMARY AND CONCLUSIONS

**22. Summary and Conclusions.** X-ray and gamma-ray backscattering have been examined from theoretical and experimental viewpoints, and observed results have been explained. Development and testing of experimental detectors using these principles have been described. Inherent limitations of the backscatter approach have been identified. Principal among these limitations are the limited penetration depth of photons of useful energy and the sensitivity to naturally occurring low-Z materials (especially vegetation). It is concluded that these limitations outweigh the capabilities of the backscatter approach when viewed from a practical military standpoint.

## APPENDIX A

### MONTE CARLO CALCULATIONS

In June 1969, personnel of the Nuclear Effects Laboratory (NEL), Edgewood Arsenal (later part of the Ballistic Research Laboratories (BRL), Aberdeen Research and Development Center), undertook to perform certain Monte Carlo calculations in support of the photon-backscatter mine-detection program. It is the purpose of this appendix to discuss the nature and results of these calculations as they relate to that program. The basic Monte Carlo program utilized in performing these calculations is available from Oak Ridge National Laboratory.<sup>A1 A2</sup> A discussion of the correlated sampling technique employed by NEL may be found in a BRL report.<sup>A3</sup>

For purposes of these calculations, the following physical model was employed (see Figure A-1): A disk of dinitrobenzene (DNB), 9 inches in diameter by 3.5 inches thick, was emplaced at depths (d) of 2 and 4 inches in a dry, homogeneous soil medium. Chemical composition of both DNB and soil are shown in Table A-1. A monoenergetic photon flux at energies of 70,130, and 200 keV was assumed normally incident within a 1.75-inch-diameter circle on the soil surface, the center of the circle being on the axis of the buried DNB disk.

Given the above input parameters, the computer generated the following data for two cases (target present and target absent): the number and energy of photons (per incident photon per square centimeter) backscattered from the soil, normal to the soil surface, within the radial (R) intervals 0 to 2, 2 to 4, 4 to 6, 6 to 8, 8 to 12, 12 to 17, 17 to 22, and 22 to 28 cm. (R = 0 corresponded to the axis of the target.) Note that this model corresponds to a vertically collimated source and a vertically collimated

<sup>A1</sup> S. K. Penny, D. K. Trubey, and M. B. Emmett, *OGRE, A Monte Carlo System for Gamma-Ray Transport Studies Including an Example (OGRE-P1) for Transmission through Laminated Slabs*, Report ORNL-3805, Oak Ridge National Laboratory (1966).

<sup>A2</sup> D. K. Trubey and M. B. Emmett, *OGRE-G, An OGRE System Monte Carlo Code for the Calculation of Gamma-Ray Dose at Arbitrary Points in an Arbitrary Geometry*, Report ORNL-TM-1212, Oak Ridge National Laboratory (1966).

<sup>A3</sup> W. A. Coleman, *Calculations on the Sensitivity of the X-Ray Field Backscattered from Soil Due to Subterranean Material Differences*, Report BRL-R-1537, Ballistic Research Laboratories (1971).

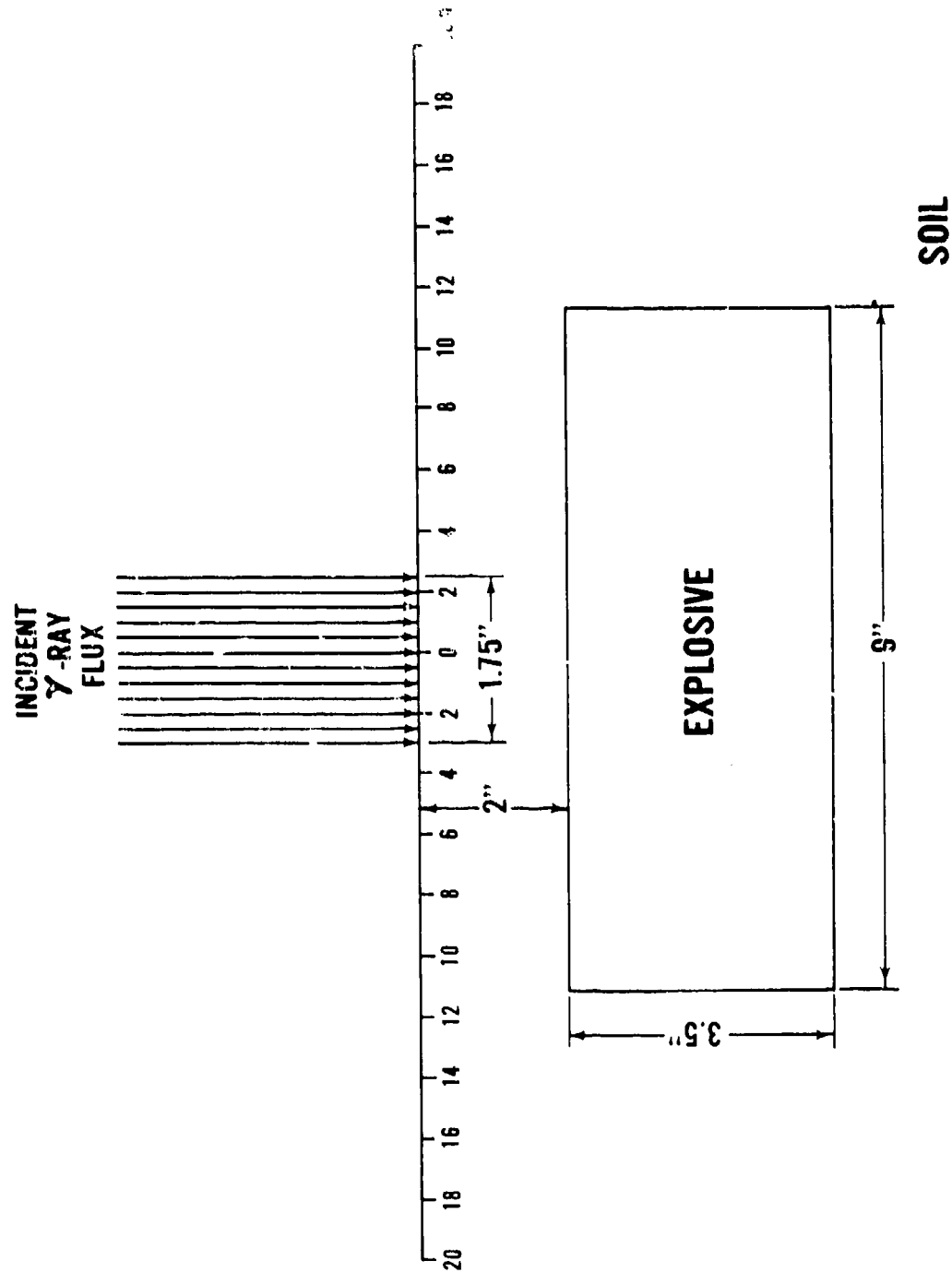


Figure A-1. Model for Monte Carlo calculations.

detector, i.e., geometry (b), (paragraph 6).<sup>A4</sup> (See Figure 7.) Results for  $E_0 = 130$  keV and  $d = 2$  inches are shown in Figure A-2; results for  $E_0 = 200$  keV and  $d = 4$  inches are shown in Figure A-3.<sup>A5 A6</sup>

Table A-1. Chemical Composition of DNB and Soil Used for Monte Carlo Calculations

Element	Soil (g/cm <sup>3</sup> )	DNB (g/cm <sup>3</sup> )
H	0.0195	0.0343
C	0.1378	0.6171
N	0	0.2400
O	0.5616	0.5486
Mg	0.0026	0
Al	0.1872	0
Si	0.2626	0
Ti	0.0091	0
Fe	0.1196	0
Total	1.3	1.44

In Figure A-2, a maximum may be seen to exist in the 80 to 90-keV energy bin for all values of  $R$ , the relative magnitude of this maximum decreasing as  $R$  increases. For  $R = 0$  to 2 centimeters, and probably for  $R = 2$  to 4 centimeters, the major contribution to this maximum comes from single scatter, which, for these small  $R$ -values, is not geometrically excluded. ( $E_{s.s.} = 86.16$  keV.) The continued presence of this maximum for larger values of  $R$  may be seen to be due to double scatter, since for this particular case ( $\theta = 180^\circ$ ) all double-scattered photons will exit the medium at the single-scatter energy. (The reader wishing clarification of this point is referred to USAMERDC Report 2097.<sup>A7</sup>) A similar situation may be seen to obtain for the 100 to 120-keV bin in

<sup>A4</sup> By requiring that the backscattered photons exit the medium normal to the surface, perfect detector collimation has been assumed. For real detectors, however, the solid angle subtended by the detector at the final scatter point in the medium will vary with the depth of that scatter point. As a result, some lack of agreement between computed and experimentally obtained results may be expected. Robert Genet, Raff Associates, Silver Spring, Maryland, private communication (1973).

<sup>A5</sup> Although it is customary to present data of this kind in the form of histograms, we have elected to connect the midpoints of the energy intervals to form simulated pulse-height spectra. This was done to emphasize the difference between spectra for the mine-present-mine absent cases.

<sup>A6</sup> No spectral data are shown for the  $E_0 = 70$ -keV,  $d = 2$ -inch case since the great majority of the backscattered photons was found to fall within two 10-keV-wide energy bins.

<sup>A7</sup> F. L. Roder and D. G. Conley, *Computed Energy Distribution of Double-Scattered Photons. Obtained for Purposes of Mine Detector Design Analysis*, USAMERDC Report 2097 (1974).

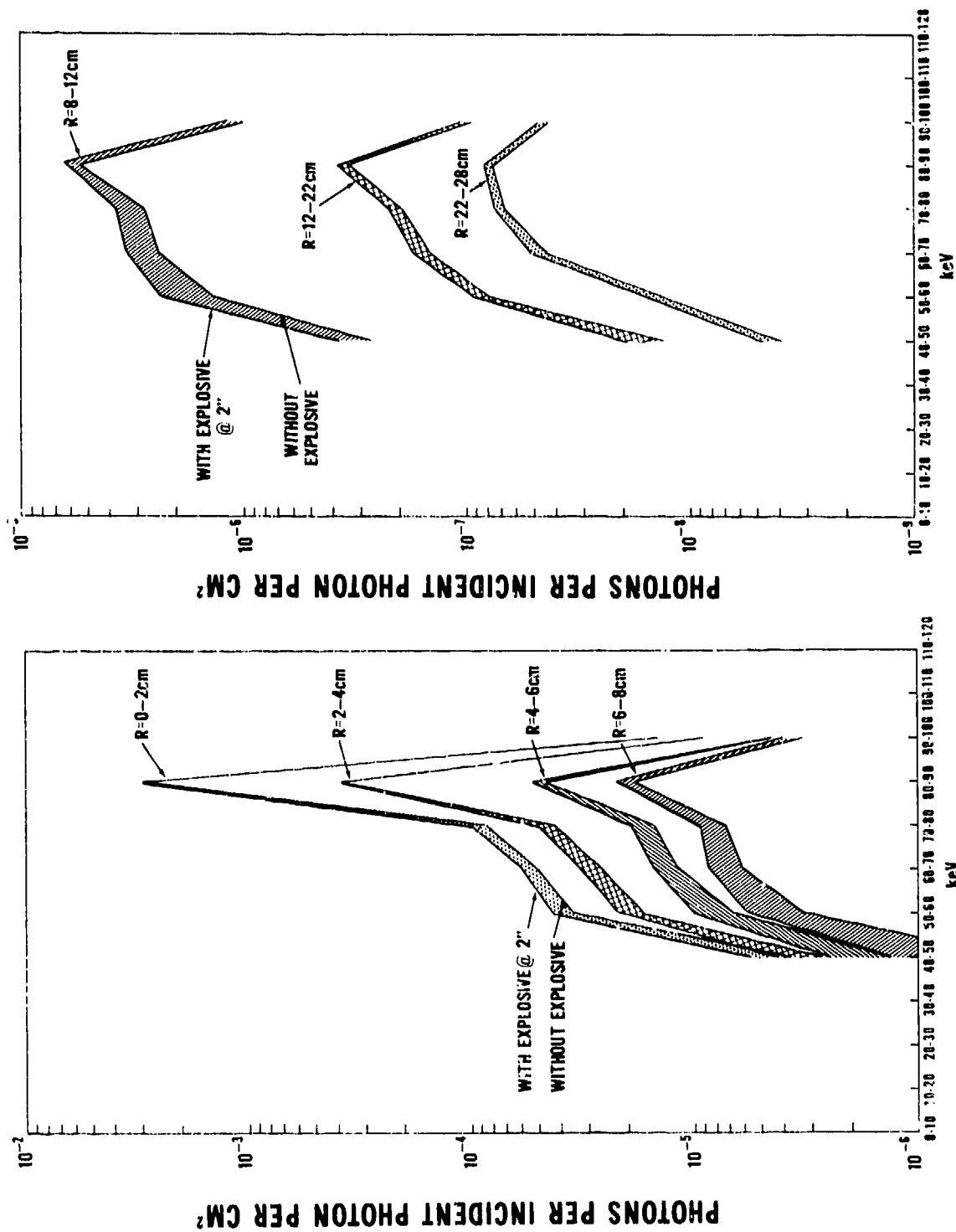


Figure A-2. Results for  $E_0 = 130$  keV and  $d = 2$  inches.

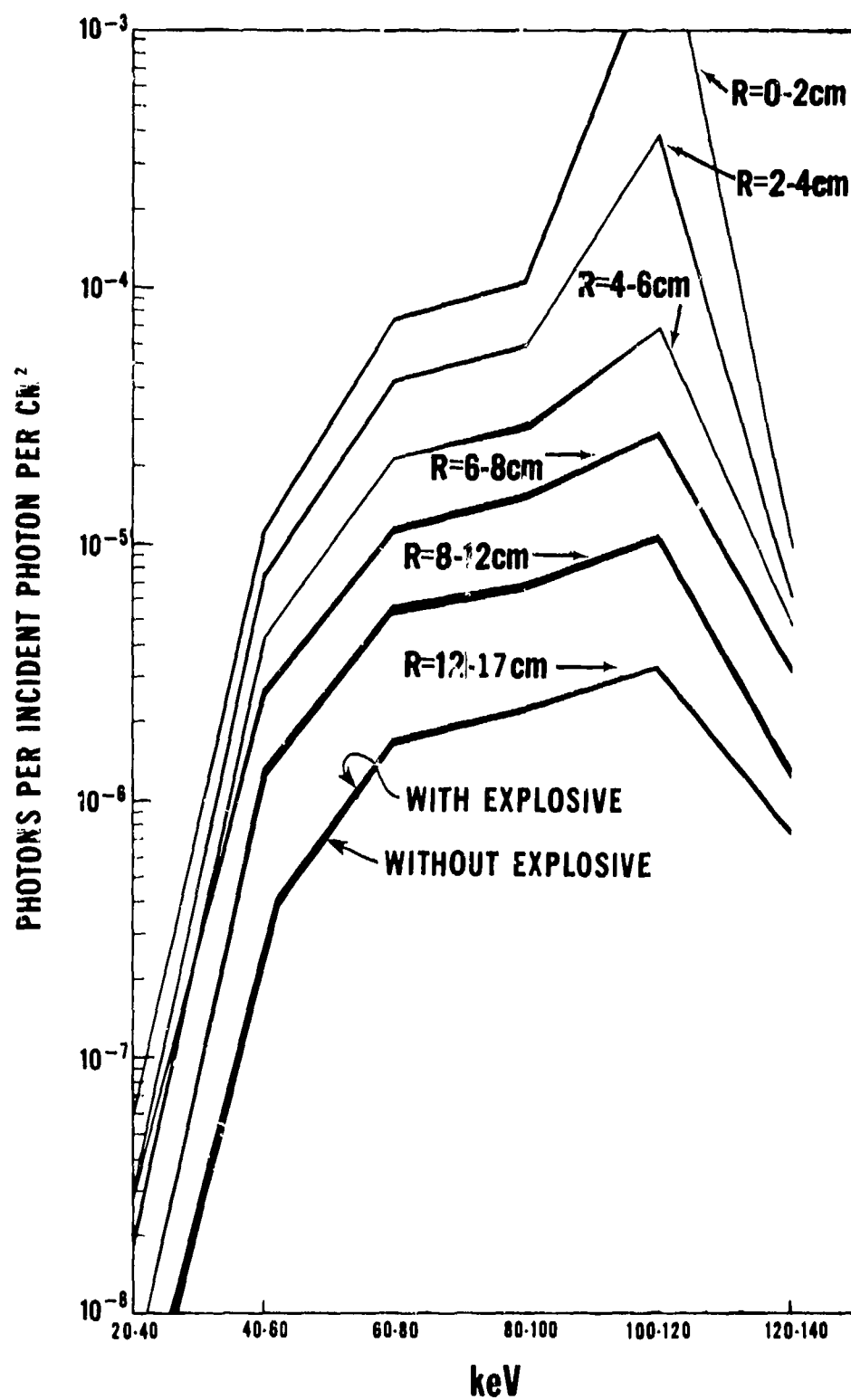


Figure A-3. Results for  $E_0 = 200$  keV and  $d = 4$  inches.



Figure A-3. Note that Figures A-2 and A-3 demonstrate a very rapid decrease in the number of normally backscattered photons as R increases.

Figures A-4 through A-6, respectively, show the increase in backscatter flux ( $\Delta \phi/\phi$ ), with the target present versus target absent, integrated over energy, for three cases:  $E_0 = 70$  keV,  $d = 2$  inches;  $E_0 = 130$  keV,  $d = 2$  inches; and  $E_0 = 200$  keV,  $d = 4$  inches. Figure A-5 also shows  $\Delta \phi/\phi$  for each of two energy components of the backscatter flux: 40 to 80 keV and 80 to 110 keV.

Figure A-5 appears to reflect experimental results the most accurately:  $\Delta \phi/\phi$  is seen to increase with R until  $R \cong$  target radius ( $\sim 11.4$  cm in this case). Beyond this point,  $\Delta \phi/\phi$  decreases but does not drop immediately to zero. The lower energy component of the target signal decreases considerably more abruptly at the target/soil interface than does the higher energy (80 to 110-keV) component, as might be expected due to the sudden increase in photoelectric cross section at this point. Figures A-4 and A-6 also show decreases in  $\Delta \phi/\phi$  as R increases past the edge of the target; although these changes are not as pronounced as in the  $E_0 = 130$ -keV case.<sup>A8</sup>

Finally, Figures A-7 through A-14 depict computed backscatter spectra obtained for the same source and target/soil conditions specified above (for  $E_0 = 130$  keV,  $d = 2$  inches), but relaxing the constraint that only photons backscattered normal to the surface shall contribute. Note that the ordinate values shown in these figures are no longer in photons/cm<sup>2</sup>, but are, rather, the total number of photons backscattered within rings specified by their respective radial intervals. Since the area of these rings increases as R increases, the fluence is actually a decreasing function of R. Physically, the spectra shown would correspond to those obtained by uncollimated ring scintillators with 100-percent efficiency. As a result, detector response is no longer independent of height, and each figure corresponds to one ring detector varied in height from 0 to 18 inches. These figures demonstrate that, for this geometry, (1) count rate varies as a function of detector height, and (2)  $\Delta \phi/\phi$  values are very low compared to those obtainable with geometry (b) and vary with detector height. It should be noted that the collimated-source-uncollimated-detector geometry was never investigated for mine detection and that these computational results only reinforced our intuitively reached conclusions.

<sup>A8</sup> A word of caution is in order in interpreting these results: because Monte Carlo computations consist of following the histories of individual photons, statistical errors are often significant. (Each of the cases discussed resulted from the compilation of 10,000 photon histories.) As a result, the lower the total number of photons scattered to a given radial interval, the higher the statistical error in that number. Thus, for example, the percent relative standard error for  $\phi$  for  $E_0 = 130$  keV is 1.6 percent for  $R = 2.4$  cm and 8.1 percent for  $R = 17.22$  cm. The number of recorded events also affects the statistical certainty of the  $\Delta \phi/\phi$  values; but, because of the correlated-sampling technique employed, the percent relative standard errors generated for this quantity are still not unreasonable. For example, for  $E_0 = 130$  keV, the error is 2.5 percent for  $R = 2.4$  cm and 10.6 percent for  $R = 17$  to 22 cm.

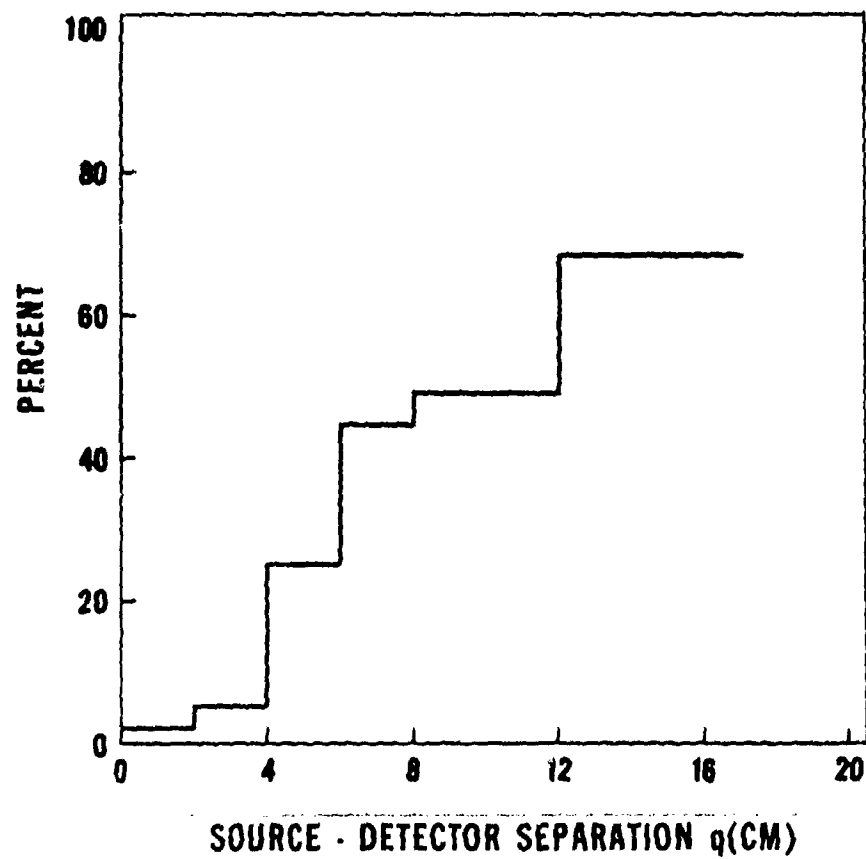


Figure A-4. Percent increase in  $\phi$  for  $E_0 = 70$  keV and  $d = 2$  inches.

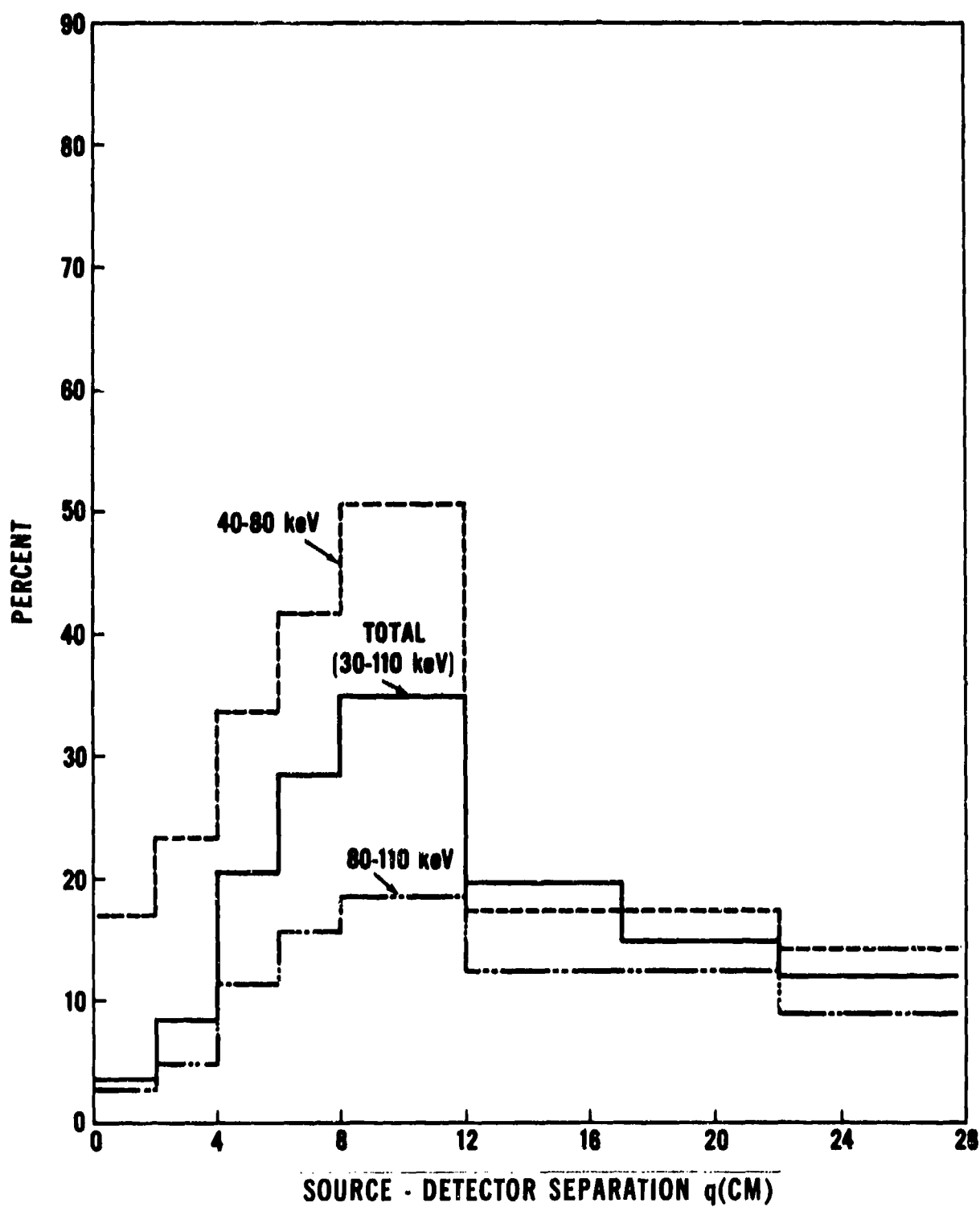


Figure A-5. Percent increase in  $\phi$  for  $E_o = 130$  keV and  $d = 2$  inches.

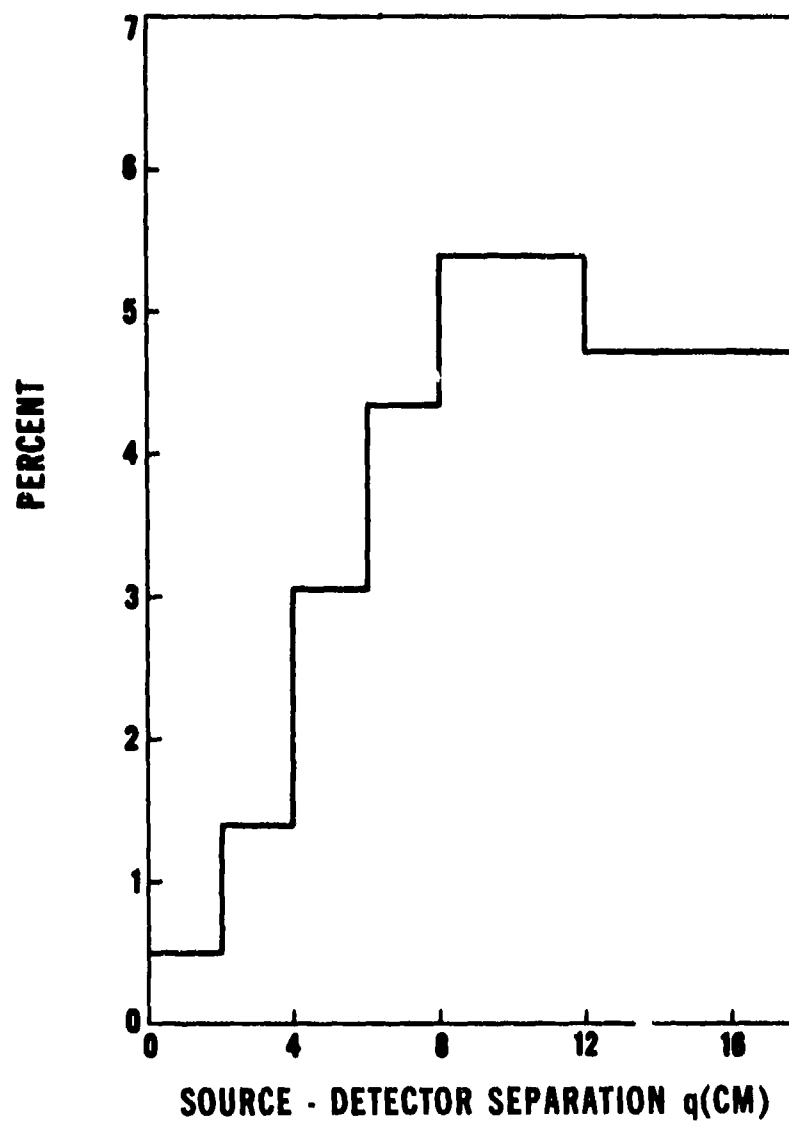


Figure A-6. Percent increase in  $\phi$  for  $E_0 = 200$  keV and  $d = 4$  inches.

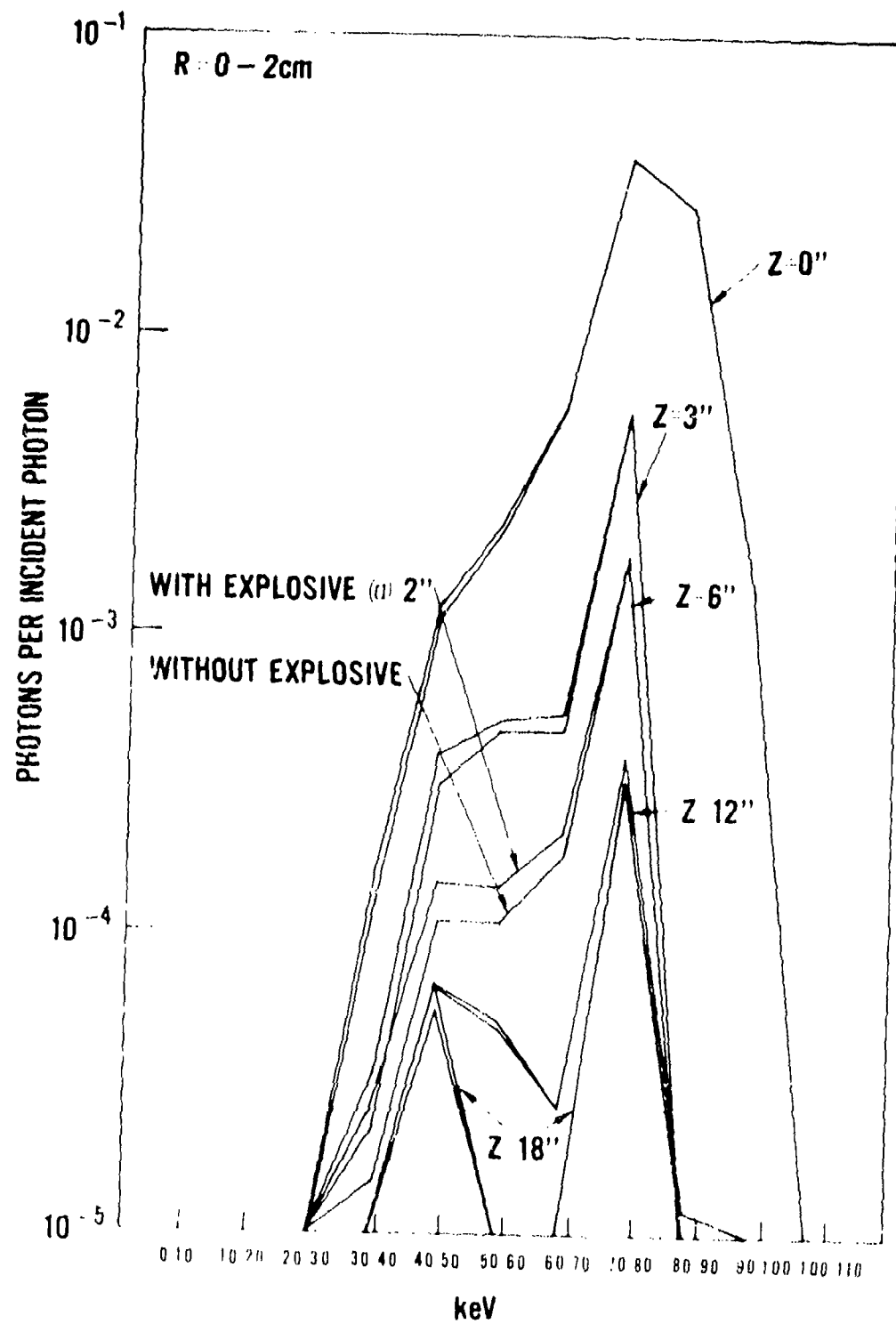


Figure A 7. No detector collimation,  $R = 0$  to 2 centimeters.

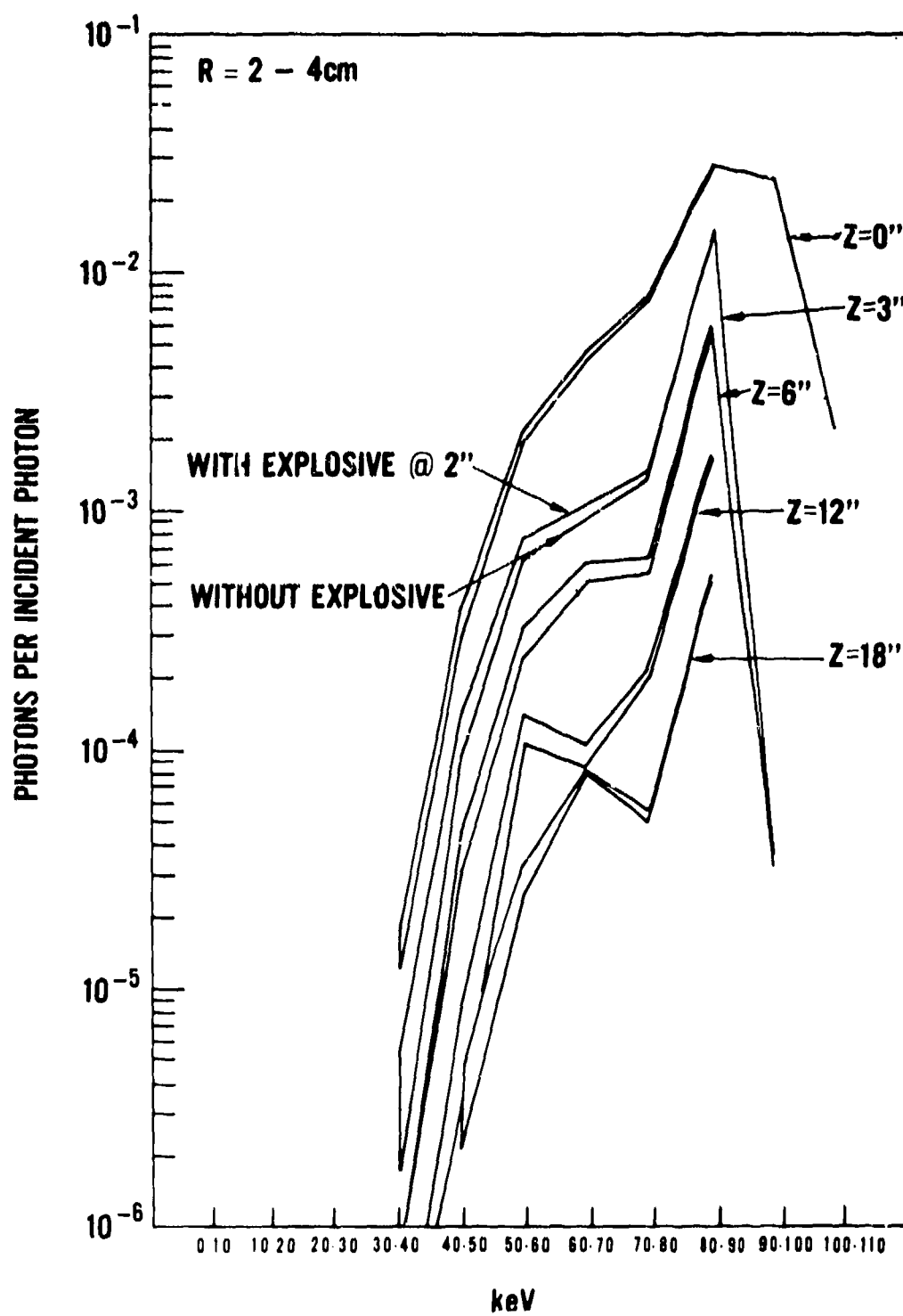


Figure A-8. No detector collimation, R = 2 to 4 centimeters.

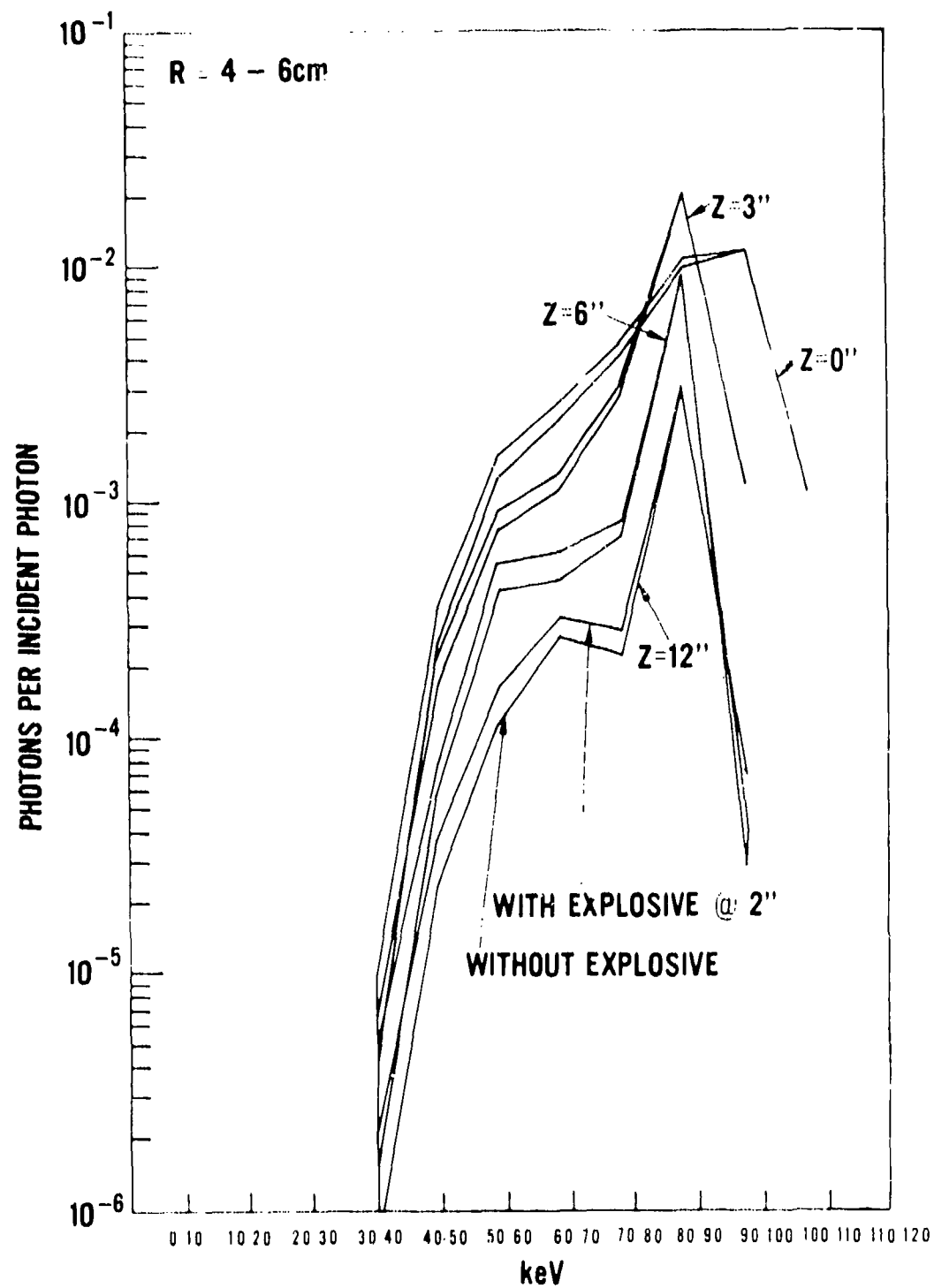


Figure A-9. No detector collimation,  $R = 4$  to 6 centimeters.

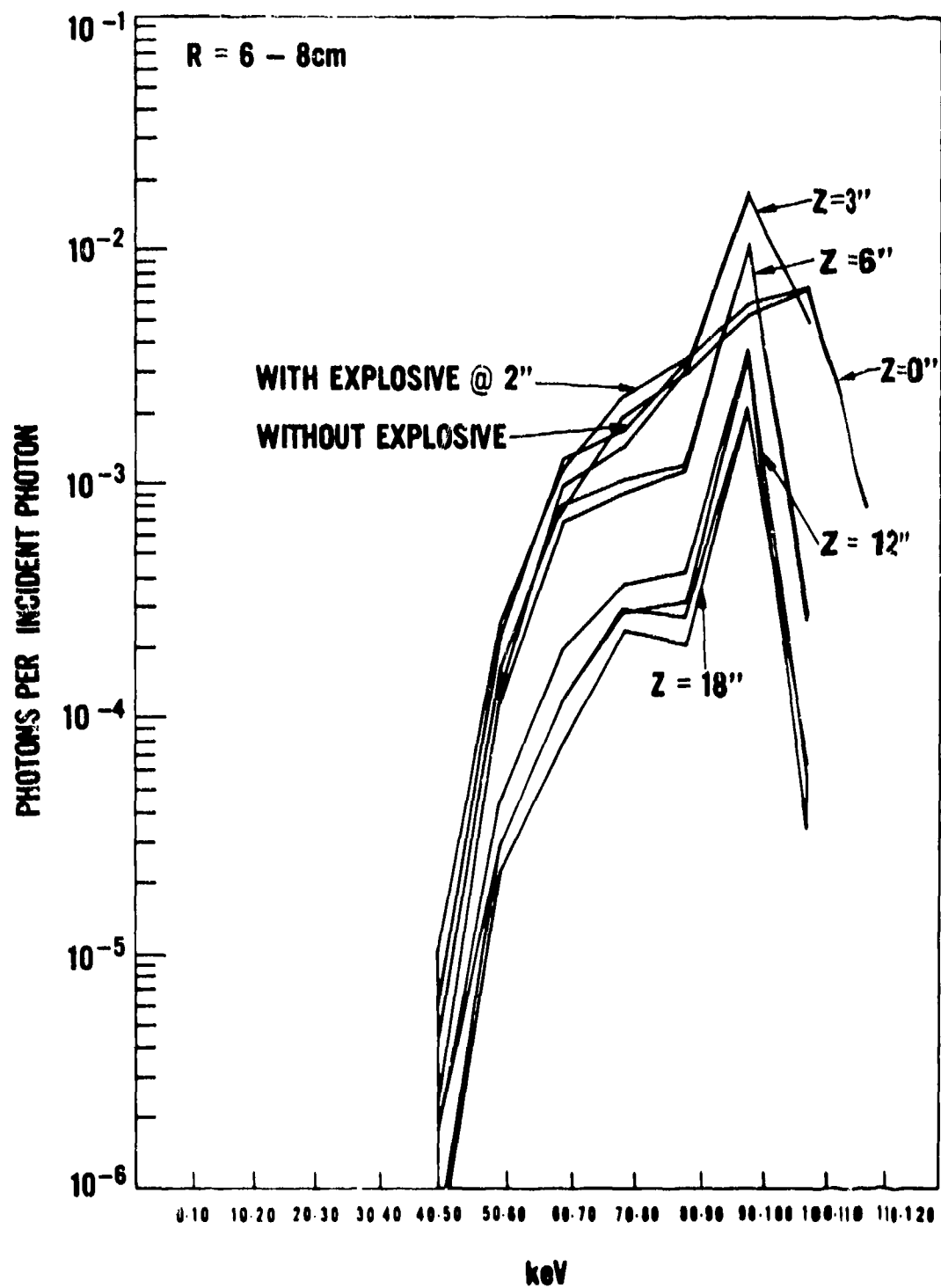


Figure A-10. No detector collimation, R = 6 to 8 centimeters.



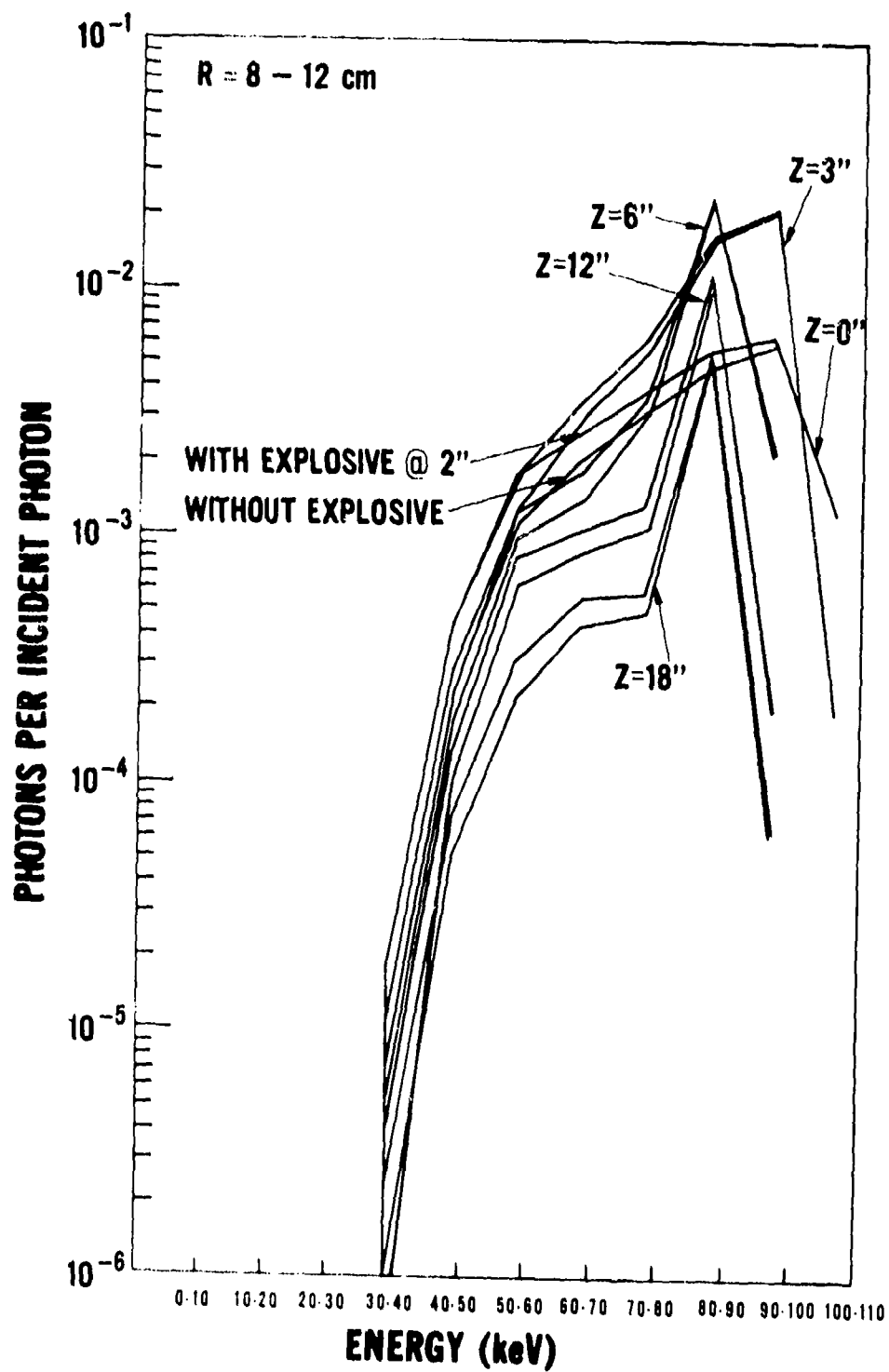


Figure A-11. No detector collimation,  $R = 8$  to 12 centimeters.

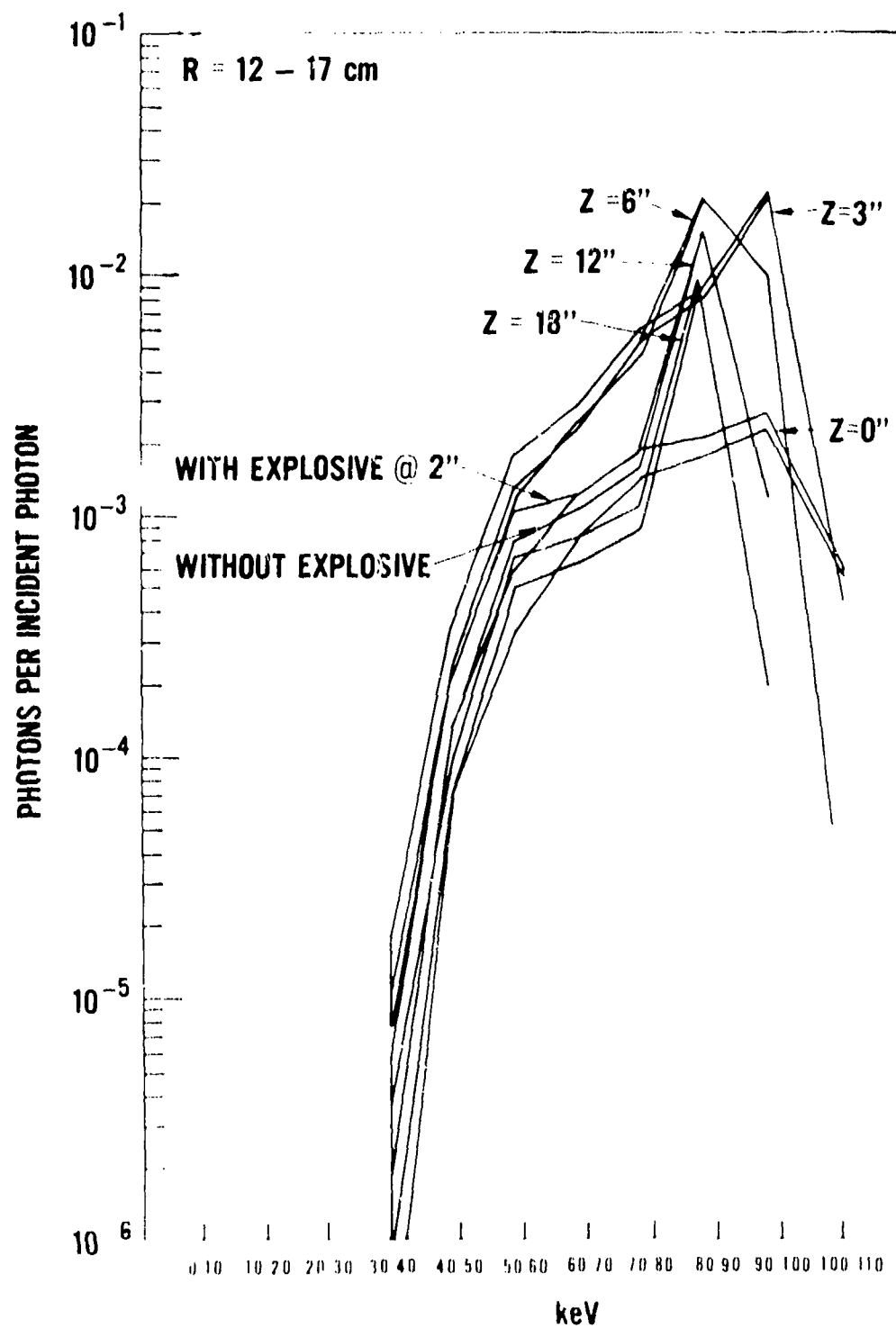


Figure A-12. No detector collimation, R = 12 to 17 centimeters.

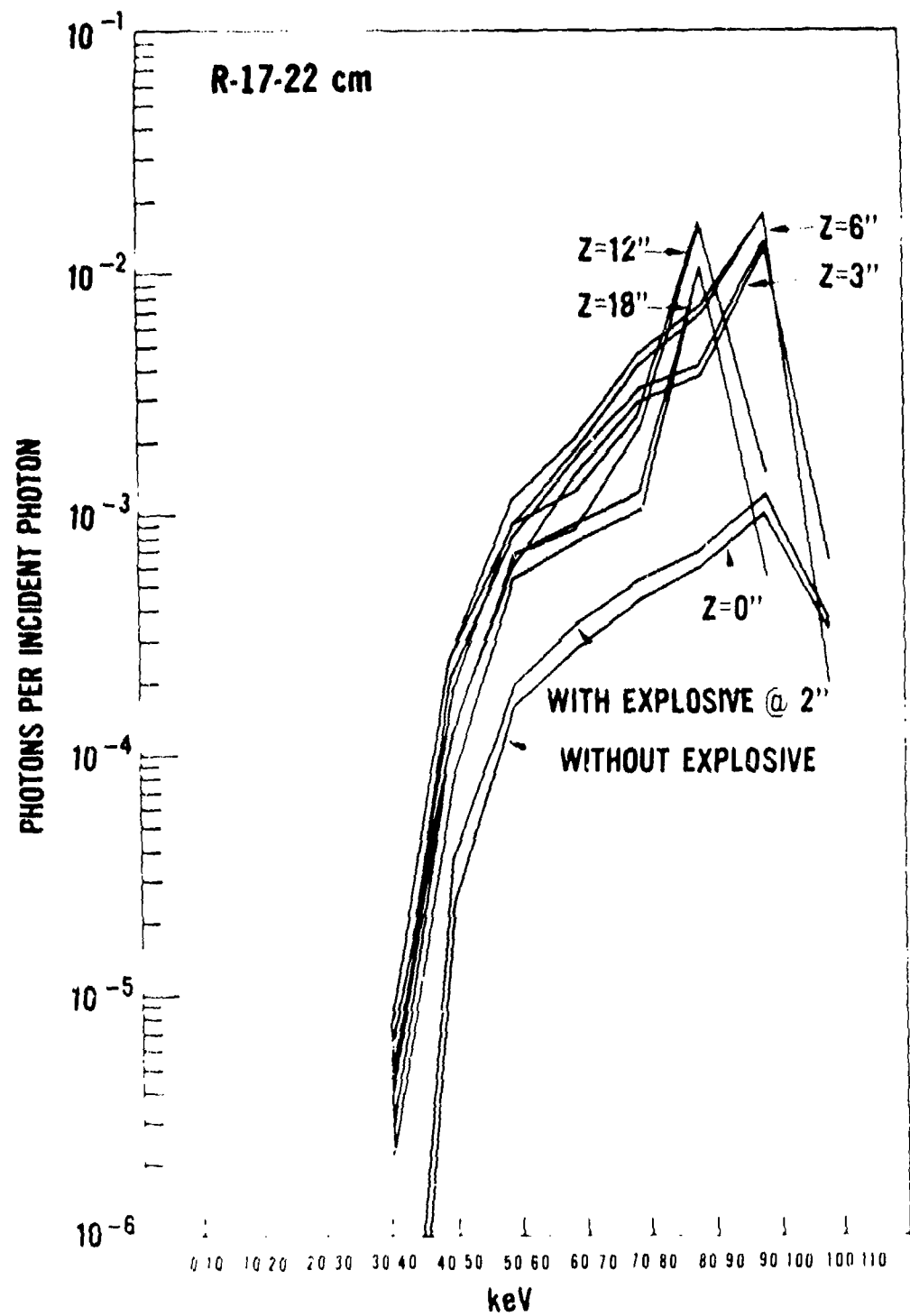


Figure A-13. No detector collimation,  $R = 17$  to 22 centimeters.

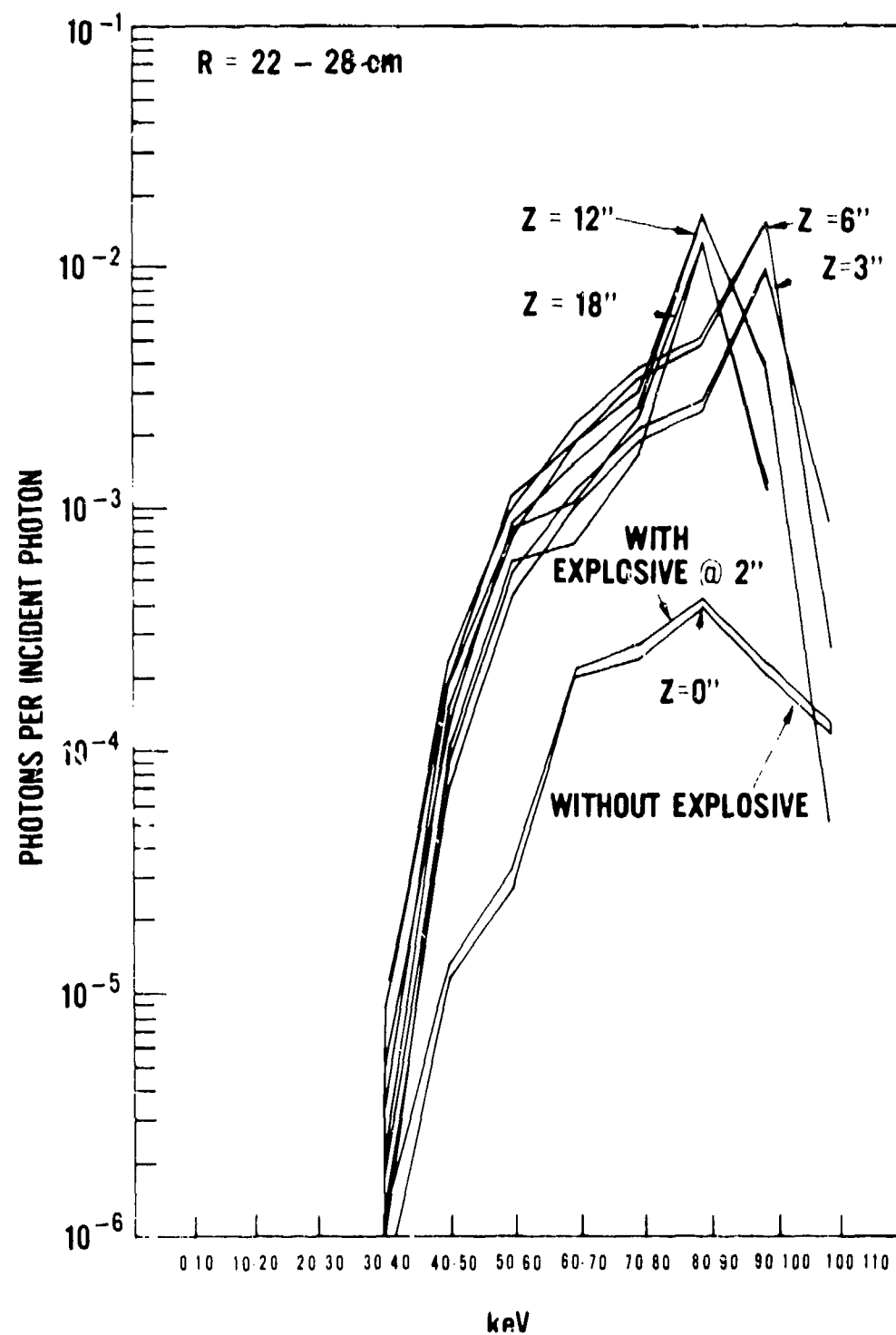


Figure A-14. No detector collimation,  $R = 22$  to 28 centimeters.

## APPENDIX B

### STATISTICAL ANALYSIS OF BACKSCATTER MINE DETECTION

Since the emission and scattering of radiation are both random processes, the number of counts observed by a backscatter detector during an interval  $T$  can be represented by a Poisson distribution. For a sufficiently large count, this can be approximated by a Gaussian distribution, which is continuous rather than discrete:

$$P(N) = \frac{1}{\sigma \sqrt{2\pi}} \exp \left[ -\frac{1}{2} \left( \frac{N - \bar{N}}{\sigma} \right)^2 \right],$$

where  $P(N)$  is the probability that  $N$  counts will be observed in the interval  $T$  if  $\bar{N}$  is the mean number observed in many such intervals. The standard deviation  $\sigma$  of the distribution is given by:

$$\sigma = \sqrt{\bar{N}} \cong \sqrt{N}$$

for sufficiently large  $N$ .

In the case of mine detection, let  $\bar{N}$  be the mean number of counts observed during a time  $T$  over unmined soil, and let  $\bar{M}$  be the corresponding value over a buried mine. The distribution of counts in each case is shown in Figure B-1. Note that  $\bar{M}$  is larger than  $\bar{N}$  because the backscattered flux is greater over the mine. The standard deviation of the "mine-present" count is then  $\sqrt{\bar{M}}$ , and the standard deviation of the "mine-absent" count is  $\sqrt{\bar{N}}$ . In order to detect the mine, it is necessary to establish, at some number of counts  $L$ , an alarm threshold which lies between  $\bar{M}$  and  $\bar{N}$ . Whenever an individual count exceeds  $L$ , an alarm is given. It can be seen from Figure B-1 that a portion of the "mine-present" distribution lies below  $L$  and that a portion of the "mine-absent" distribution lies above  $L$ . These facts will lead to undetected mines and false alarms, respectively. For reliable detection, it is desired to minimize these overlapping portions of the distribution curves. Since the ratio  $R = \bar{M}/\bar{N}$  is fixed for a given detection situation, and since the *relative* widths of the distributions can be narrowed by increasing  $\bar{M}$  and  $\bar{N}$ , it is possible to obtain any desired confidence level by the use of sufficiently large counts. Such a procedure is limited in practice, however, by the maximum counting rate of the detector and by the required speed of search, as well as by the allowable source size.

It is of interest to determine the value of  $\bar{N}$ , the mean number of counts over unmined soil in the interval  $T$ , which is necessary to provide the required degree of

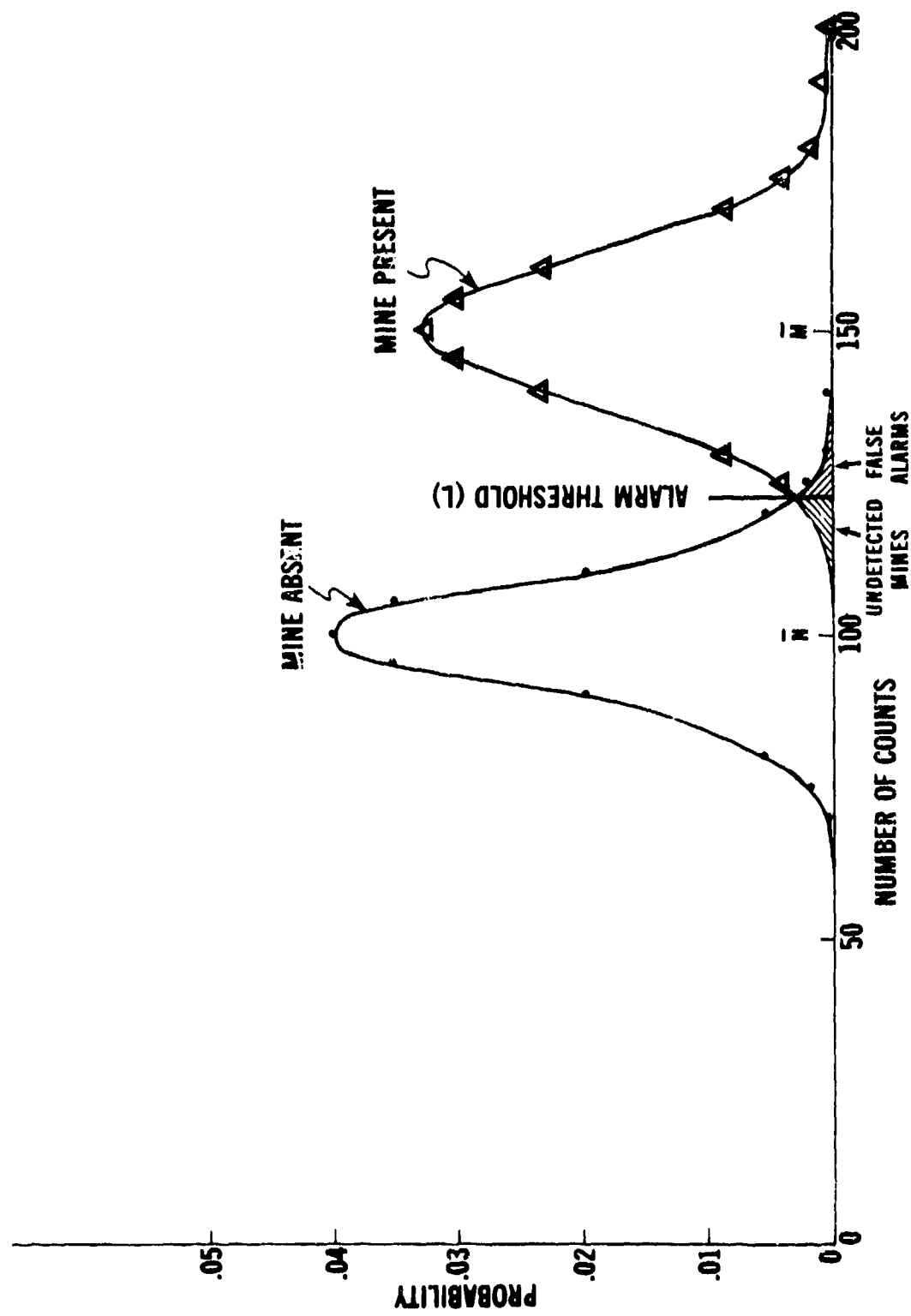


Figure B-1. Probability distributions of count with mine present and mine absent for the case:  $N = 100$ ,  $R = 1.5$ .

certainty of detection and certainty against false alarms.

The probability  $P_D$  of detecting a mine which is present is given by

$$P_D = \frac{1}{\sqrt{2\pi\bar{M}}} \int_L^{\infty} \exp \left[ -\frac{1}{2} \frac{(M - \bar{M})^2}{\bar{M}} \right] dM,$$

which is simply the integral of the portion of the "mine-present" distribution lying above the threshold  $L$ . This integral can be reduced to

$$P_D = \frac{1}{2} \left[ 1 + H \left( \frac{\bar{M} - L}{\sqrt{2\bar{M}}} \right) \right],$$

where  $H$  is defined as the error function and is tabulated in standard mathematical tables.

Similarly, the probability  $P_F$  that a count of duration  $T$  (which is sufficient to produce an average count  $\bar{N}$ ) over unmined soil will result in a statistically induced false alarm is given by

$$P_F = \frac{1}{\sqrt{2\pi\bar{N}}} \int_L^{\infty} \exp \left[ -\frac{1}{2} \frac{(N - \bar{N})^2}{\bar{N}} \right] dN,$$

which reduces to

$$P_F = \frac{1}{2} \left[ 1 - H \left( \frac{L - \bar{N}}{\sqrt{2\bar{N}}} \right) \right],$$

where  $H$  is again the tabulated error function.

For a given value of  $R = \bar{M}/\bar{N}$ , it now is possible to determine the lowest value of  $\bar{N}$  which will simultaneously produce any values of  $P_D$  and  $P_F$  desired. Calculations have been carried out for values of  $R$  ranging between 1.1 and 2 and for values of  $P_D$  and  $P_F$  from 0.90 to 0.9999 and from 0.10 to 0.0001, respectively. The results are shown in Figure B-2. Note that complementary  $P_D$  and  $P_F$  values have been coupled for simplification, although this is not necessary (i.e., curves are shown for  $P_D = 0.90$  while  $P_F = 0.10$ , for  $P_D = 0.99$  while  $P_F = 0.01$ , etc.). Using these results, it is possible to obtain an estimate of the counting rate required for a given ratio ( $R$ ), forward speed ( $V$ ), mine size ( $Q$ ), and degree of confidence desired. The necessary counting rate  $C$  is given by

$$C \text{ (cps)} = \frac{1.47 \text{ (ft/s / mi/h)} \bar{N} \text{ (counts)} V \text{ (mi/h)}}{Q \text{ (ft)}}.$$

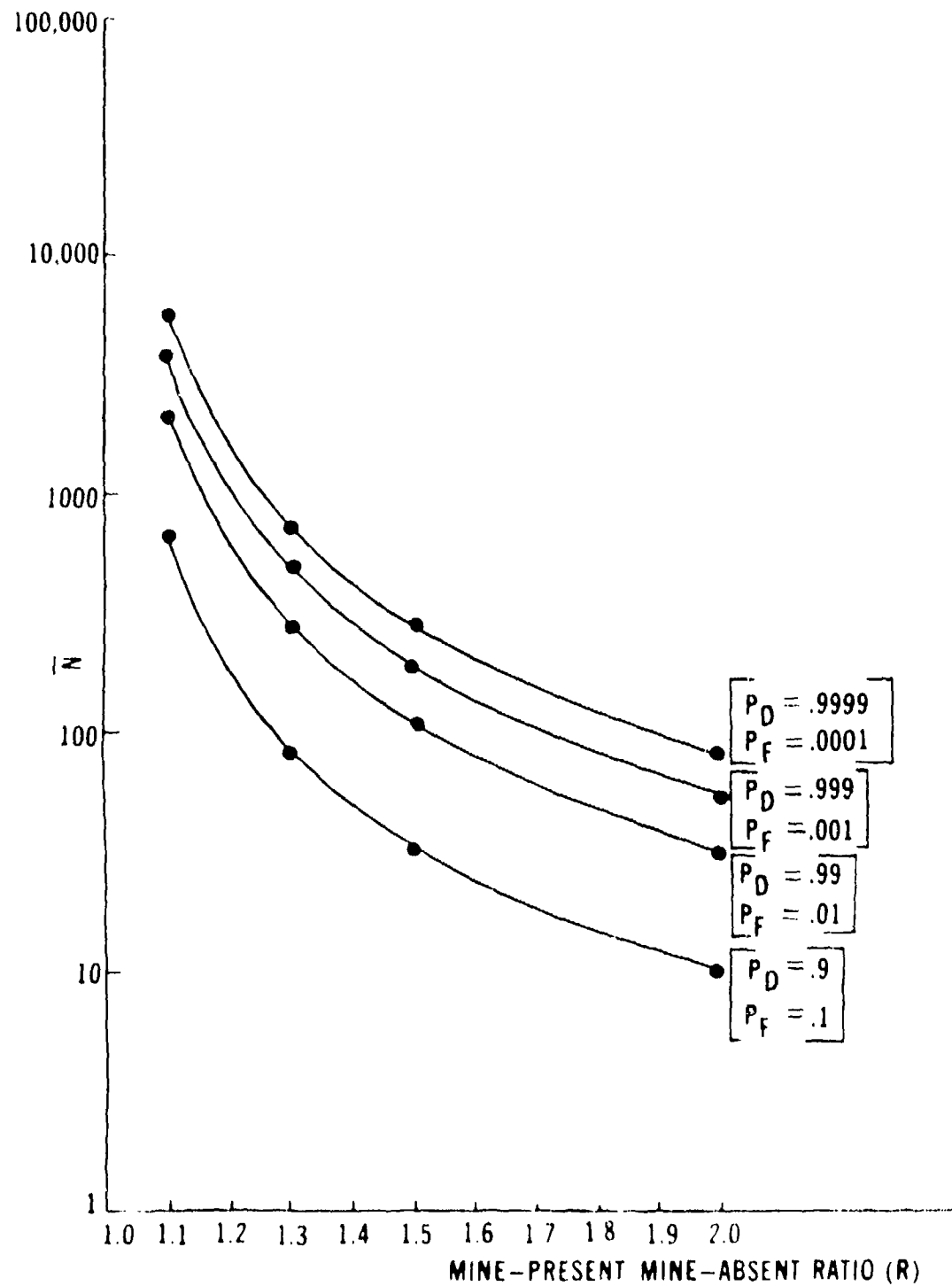


Figure B-2. Required mean count as a function of the mine-present -- mine-absent count ratio for various degrees of certainty.



For example, consider the case of a vehicle-mounted detector: The ratio  $R$  for a mine buried 2 inches below the surface has been determined to be about 1.3, neglecting disturbed-soil effects. If the mine is 1 foot across, the desired forward speed 3 mi/h, the degree of certainty of detection 0.999, and the allowable false alarm rate 1 per 1,000 feet of forward travel, the value of  $C$  can be seen to be about 2,200 cps. For a single scanning lane, if the confidence levels were reduced to  $P_D = 0.99$  and  $P_F = 1$  per 100 feet, the required counting rate would be about 1,200 cps.

Other desired values could be chosen for the parameters, and the resulting required countrate could be found; but, the general result of this analysis is that the countrate probably should be at least several thousand per second for a vehicular-mine detector. It must be noted that although a high countrate has obvious advantages, it also carries penalties: Higher source strength is required, which leads to greater power requirements, increased weight, and higher radiation exposure to operating personnel. In addition, faster detectors and counting circuitry are required. Clearly, a compromise is necessary, and the final design must be determined by experiment.

It should be noted that this analysis has considered only statistical fluctuations in the countrate. The effect of height variations and differences in soil composition and density will be to increase or decrease the countrate from its average value. For the purpose of considering  $P_D$ , it should be assumed that such effects will decrease the countrate just at the time when the detector is over a mine, thus tending to mask the mine's presence. In considering  $P_F$ , it should be assumed that the countrate will be increased over "innocent" ground, tending to create false alarms. The net effect is, therefore, a broadening of the "Mine-present" and "Mine-absent" distributions toward the threshold (i.e., toward each other) and a consequent degradation of detector performance. The extent of these effects could be determined only by field testing.